

Washington University in St. Louis

Washington University Open Scholarship

All Theses and Dissertations (ETDs)

8-15-2011

Dynamic Characterization of the IKK: κ B α :NF κ B Negative Feedback Loop Using Real-Time Bioluminescence Imaging

Britney Moss

Washington University in St. Louis

Follow this and additional works at: <https://openscholarship.wustl.edu/etd>



Part of the [Biology Commons](#)

Recommended Citation

Moss, Britney, "Dynamic Characterization of the IKK: κ B α :NF κ B Negative Feedback Loop Using Real-Time Bioluminescence Imaging" (2011). *All Theses and Dissertations (ETDs)*. 622.
<https://openscholarship.wustl.edu/etd/622>

This Dissertation is brought to you for free and open access by Washington University Open Scholarship. It has been accepted for inclusion in All Theses and Dissertations (ETDs) by an authorized administrator of Washington University Open Scholarship. For more information, please contact digital@wumail.wustl.edu.

Washington University

Division of Biology and Biomedical Sciences

Program in Molecular Cell Biology

Dissertation Examination Committee

David Piwnica-Worms, Chair

William Harbour

Erik Herzog

Raphael Kopan

Deborah Novack

Jason Weber

“Dynamic Characterization of the IKK:IkB α :NF- κ B Negative Feedback Loop

Using Real-Time Bioluminescence Imaging”

by

Britney Lane Moss

A dissertation presented to the

Graduate School of Arts and Sciences of Washington University

in partial fulfillment of the requirements for the degree of

Doctor of Philosophy

August, 2011

St. Louis, Missouri

ABSTRACT OF THE DISSERTATION

Dynamic Characterization of the IKK:I κ B α :NF- κ B Negative Feedback Loop

Using Real-Time Bioluminescence Imaging

by

Britney Lane Moss

Doctor of Philosophy in Molecular Cell Biology

Washington University in St Louis, 2011

Dr. David Piwnica-Worms, Chairperson

The transcription factor NF- κ B is a pivotal regulator of mammalian cell function, modulating genes implicated in cellular stress responses, proliferation, differentiation, cell survival and apoptosis, as well as immune and inflammatory responses. Improper regulation of NF- κ B signaling has been implicated in a myriad of human pathological disorders, including cardiovascular and neurodegenerative diseases, chronic inflammation, and various cancers. A key regulatory node within canonical NF- κ B signaling is the IKK:NF- κ B:I κ B α negative feedback loop that plays a major role in regulating the strength and duration of NF- κ B transcriptional activity. We have developed and characterized a unique bioluminescent reporter (κ B₅→I κ B α -FLuc) that recapitulates this transcriptionally coupled negative feedback loop, and have extensively utilized this reporter to interrogate how diverse stimuli (i.e., ligand type, duration, concentration, sequential stimulation, etc.) impact the IKK:NF- κ B:I κ B α negative feedback loop *in cellulo* and *in vivo*. We found that the negative feedback loop

exhibits differential and reproducible dynamic patterns in response to modulation of TNF α concentration or pulse duration, and that responses to TNF α exhibited a remarkable degree of synchronicity at the level of single cells, cell populations, and *in vivo*. Furthermore, we discovered a TNF α -induced transient refractory period (lasting up to 120 min) during which cells were unable to fully degrade I κ B α following a second TNF α challenge, and identified nuclear export of NF- κ B:I κ B α complexes as a rate-limiting step that may impact this refractory period. A high-throughput RNAi screen to identify new phosphatase and kinase regulators of TNF α -induced IKK:NF- κ B:I κ B α negative feedback loop dynamics revealed a vast array of different I κ B α -FLuc dynamic profiles, highlighting the large number and diverse activities of kinases and phosphatases regulating the NF- κ B pathway. Two of these hits, PTPRJ and DAPK3, have been validated and are the subjects of current investigations to understand the physiological and/or pathophysiological relevance in NF- κ B, especially in the context of TNF α signaling during cancer and inflammation in the liver. In conclusion, our studies using dynamic, real-time bioluminescence imaging have demonstrated the utility of employing bioluminescent reporters alongside traditional biochemical assays, *in silico* modeling, and cell/molecular biology techniques to rigorously interrogate how diverse stimuli impact the IKK:NF- κ B:I κ B α negative feedback loop in single cells, cell populations, and at the organ- and tissue-level *in vivo*.

ACKNOWLEDGEMENTS

Thank you to all of the past and present members of the Piwnica-Worms lab, to my colleagues at Washington University, to my Thesis Committee, and to my advisor, David Piwnica-Worms, for showing me what it means to be a scientist and a seeker of truth; these are lessons and skills that I carry with me into my career and into all aspects of my life. I am also gratefully indebted to all of my wonderful friends and family in Montana, Idaho, Washington, Missouri, and Illinois who have supported and encouraged my love of science from childhood to the present day.

TABLE OF CONTENTS

Abstract	ii
Acknowledgements	iv
Table of Contents.....	v
List of Figures	viii
List of Tables.....	xi
Chapter One – Introduction	1
1.1 NF- κ B Signaling : An Historical Perspective	1
1.2 Canonical NF- κ B Signaling & The IKK:I κ Ba:NF- κ B Negative Feedback Loop.....	2
1.3 Clinical Relevance of NF- κ B Signaling in the Liver	5
1.4 The NF- κ B Signaling Pathway as an Exemplary Proving Ground for Systems Biology Approaches in Mammalian Cells	6
1.5 Bioluminescence Imaging & The NF- κ B Pathway.....	8
1.6 Figures	12
1.7 References	13
Chapter Two – Identification of a Ligand-Induced Transient Refractory Period in Nuclear Factor-κB Signaling.....	17
2.1 Introduction	17
2.2 Results	21
2.3 Discussion.....	33

2.4 Methods	38
2.5 Figures	45
2.6 Tables	52
2.7 References	53
Chapter Three – Synchronicity of the IκBα:NF-κB Negative Feedback Loop <i>In Cellulo</i> and <i>In Vivo</i>	56
3.1 Introduction	56
3.2 Results	59
3.3 Discussion.....	72
3.4 Methods	77
3.5 Figures	83
3.6 Supplementary Figures.....	93
3.7 References	99
Chapter Four – High-Throughput Phosphatase RNA Interference Screen Identifies Novel Regulators of TNFα-Induced IKK:IκBα:NF-κB Negative Feedback Loop Dynamics.....	102
4.1 Introduction	102
4.2 Results	103
4.3 Discussion.....	117
4.4 Methods	121
4.5 Figures	129
4.6 Supplemental Figures.....	147

4.7 Tables	158
4.8 Supplementary Tables	162
4.9 References	163
Chapter Five – High-Throughput Kinase RNA Interference Screen Identifies Novel Regulators of TNFα-Induced IKK:IκBα:NF-κB Negative Feedback Loop Dynamics.....	165
5.1 Introduction	165
5.2 Results	167
5.3 Discussion.....	171
5.4 Methods	176
5.5 Figures	181
5.6 Supplementary Figures.....	184
5.7 References	190
Chapter Six – Conclusions and Future Directions.....	193
6.1 Identification of a Ligand-Induced Transient Refractory Period in Nuclear Factor- κ B Signaling.....	194
6.2 Synchronicity of the I κ B α :NF- κ B Negative Feedback Loop <i>In Cellulo</i> and <i>In Vivo</i>	196
6.3 High-Throughput Phosphatase and Kinase RNA Interference Screens Identify Novel Regulators of TNF α -Induced IKK:I κ B α :NF- κ B Negative Feedback Loop Dynamics	199
6.4 References	203

LIST OF FIGURES

Chapter One – Introduction

Figure 1.1	13
------------------	----

Chapter Two – Identification of a Ligand-Induced Transient Refractory Period in Nuclear Factor- κ B Signaling

Figure 2.1	45
Figure 2.2	47
Figure 2.3	48
Figure 2.4	49
Figure 2.5	50
Figure 2.6	51

Chapter Three – Synchronicity of the I κ B α :NF- κ B Negative Feedback Loop *In Cellulo* and *In Vivo*

Figure 3.1	83
Figure 3.2	85
Figure 3.3	87
Figure 3.4	89
Figure 3.5	91
Supplementary Figure S3.1	93
Supplementary Figure S3.2	95
Supplementary Figure S3.3	97

Chapter Four – High-Throughput Phosphatase RNA Interference Screen Identifies Novel Regulators of TNF α -Induced IKK: $\text{I}\kappa\text{B}\alpha$:NF- κB Negative Feedback Loop Dynamics

Figure 4.1.....	129
Figure 4.2.....	130
Figure 4.3.....	131
Figure 4.4.....	132
Figure 4.5.....	135
Figure 4.6.....	136
Figure 4.7.....	138
Figure 4.8.....	139
Figure 4.9.....	140
Figure 4.10.....	143
Figure 4.11.....	144
Figure 4.12.....	145
Figure 4.13.....	146
Supplementary Figure S4.1.....	147
Supplementary Figure S4.2.....	154

Chapter Five – High-Throughput Kinase RNA Interference Screen Identifies Novel Regulators of TNF α -Induced IKK: $\text{I}\kappa\text{B}\alpha$:NF- κB Negative Feedback Loop Dynamics

Figure 5.1.....	181
Figure 5.2.....	182
Figure 5.3.....	183

Supplementary Figure S5.1	184
Supplementary Figure S5.2	186
Supplementary Figure S5.3	188

LIST OF TABLES

Chapter Two – Identification of a Ligand-Induced Transient Refractory Period in Nuclear Factor- κ B Signaling

Table 2.1	52
-----------------	----

Chapter Four – High-Throughput Phosphatase RNA Interference Screen Identifies Novel Regulators of TNF α -Induced IKK: $\text{I}\kappa\text{B}\alpha$:NF- κ B Negative Feedback Loop Dynamics

Table 4.1	158
Table 4.2	159
Table 4.3	161
Supplementary Table ST4.1	162

CHAPTER ONE

Introduction

The transcription factor NF- κ B is a pivotal regulator of mammalian cell function, modulating genes implicated in cellular stress responses, proliferation, differentiation, cell survival and apoptosis, as well as immune and inflammatory responses [1]. Improper regulation of NF- κ B signaling has been implicated in a myriad of human pathological disorders, including chronic inflammation, various cancers, as well as cardiovascular and neurodegenerative diseases [2, 3]. In recent years, bioluminescence imaging has proven an invaluable tool to probe the complex dynamics of NF- κ B signaling both *in vitro* and *in vivo*.

1.1 NF- κ B SIGNALING : A HISTORICAL PERSPECTIVE

The NF- κ B transcription factor was originally identified by Sen and Baltimore as a protein bound only to the κ light-chain enhancer DNA at the sequence GGGACTTTCC and was called NF- κ B because it was a nuclear factor that bound selectively to the κ enhancer and was originally found in extracts of B-cell tumors but not other cell lines [4, 5]. Soon after they also showed that NF- κ B is a factor that pre-exists in an apparently inhibited state, is released from that inhibition by LPS treatment, and that inhibited NF- κ B is not specific to B-lineage cells as it was evident in T cells and even HeLa cells [6]. Furthermore, work in the Baltimore lab established that the inactive form of NF- κ B is in the cytoplasm and can be liberated from its inhibited form by treatment of cytoplasmic extracts with a detergent [7]. This discovery led to purification of the

inhibitor, which was named I κ B [8]. Years of intense research that followed demonstrated that NF- κ B is expressed in almost all cell types and tissues, and specific NF- κ B binding sites are present in the promoters/enhancers of a large number of genes, especially those involved in inflammation, innate immune responses, adaptive immune responses, secondary lymphoid organ development and osteoclastogenesis [9, 10]. Concurrent to the discovery and elucidation of NF- κ B transcription factors and NF- κ B signaling pathways, other researchers were investigating two proteins, v-Rel and Dorsal, that also exhibited variable nucleo-cytoplasmic subcellular localization. Along with NF- κ B, these proteins were eventually recognized as members of the same family, and the biological processes investigated in these original studies – immunity (NF- κ B), oncogenesis (v-Rel), and development (Dorsal) – continue to be areas that provoke much of the interest in NF- κ B [11].

1.2 CANONICAL NF- κ B SIGNALING & THE IKK:I κ B α :NF- κ B NEGATIVE FEEDBACK LOOP

The vertebrate NF- κ B transcription factor family consists of five members: p50/p105, p52/p100, c-Rel, RelA (aka p65), and RelB; different NF- κ B complexes are formed from homo- and heterodimers of these family members [12]. These proteins are related via a highly conserved N-terminal DNA binding/dimerization domain called the Rel homology domain (RHD) and bind to 9-10 base pair DNA sites (κ B sites) which have a remarkably loose consensus sequence (5'-GGGRNWYYCC-3'; R, A or G; N, any nucleotide; W, A or T; Y, C or T) [13]. The vertebrate NF- κ B family proteins can form both homo- and heterodimers *in vivo*, except for RelB which only forms homodimers *in vivo*. Interestingly, use of cell lines null for various NF- κ B family members has shown that there is little correlation between the sequence of the κ B DNA-

binding site and the function/subunit specificity of NF- κ B dimers, indicating that NF- κ B family member specificity for endogenous promoters is not solely encoded by the κ B site sequence itself [14].

NF- κ B transcription factors are rapidly activated in response to numerous stimuli allowing quick regulation of a few hundred genes [15-17] that can be divided into four major families [2, 17]: (1) pro-inflammatory genes (e.g., COX 2, IL-1, TNF α , iNOS, ICAM-1, E-selectin, etc.), (2) pro-proliferative genes (e.g., Cyclin D, c-Myc), (3) anti-apoptotic genes (Bcl2, Bcl_{XL}, XIAPs, cIAPs), and (4) auto-inhibitory genes (e.g., A20, CYLD, SOCS-1 and I κ B α). This rapid response system requires the sequestration of NF- κ B dimers in the cytoplasm through interaction with inhibitory I κ B proteins. As with the NF- κ B transcription factors, there are several I κ B proteins (I κ B α , I κ B β , BCL-3, I κ B ϵ , I κ B λ , and the NF- κ B precursor proteins p100 and p105) that are characterized by five to seven ankyrin repeats that assemble into long cylinders capable of interacting with the nuclear localization signal (NLS) of the given NF- κ B dimer and of interfering with sequences involved in DNA binding [13, 18]. For I κ B α , this NLS masking is only partially effective and thus NF- κ B–I κ B α complexes shuttle into the nucleus even in the absence of cellular stimulation; however, I κ B α also contains a nuclear export sequence (NES), which causes the rapid export of NF- κ B–I κ B α complexes back to the cytoplasm, resulting in steady state population within the cytosol [19-21].

In resting cells, NF- κ B dimers are sequestered in the cytoplasm through binding to isoforms of the I κ B family. Canonical activation of NF- κ B (Fig 1.1) relies on ligand-dependent stimulation of IKK, a large heterotrimeric kinase complex containing two catalytic subunits (IKK α and IKK β) and a regulatory subunit (IKK γ , NEMO) [20, 22]. Many different surface receptors signal to IKK through multiprotein complexes containing TRAFs (TNF receptor

associated factors which seem to serve as adaptors and may mediate K63-linked regulatory ubiquitination events) and a multitude of other adaptor proteins (with specific receptors interacting with specific subsets of TRAFs and other adaptors; Fig 1.1) that recruit and activate the IKK complex [22, 23]. Activation of IKK requires phosphorylation of T loop serines, however, the precise mechanism by which this occurs (trans-autophosphorylation or through phosphorylation by an upstream kinase) remains a major unanswered question, and adaptor protein mediated multimerization also seems to significantly contribute to IKK activation [23]. Upon activation, IKK phosphorylates I κ B α (on Ser 32/36), thus rendering I κ B α a substrate for poly-ubiquitination and proteasomal degradation. This series of events releases NF- κ B to freely translocate to the nucleus where it can modulate expression of its target genes, including I κ B α , thus forming a transcriptionally-coupled negative feedback loop [24]. This newly synthesized I κ B α enters the nucleus and binds to NF- κ B which dissociates from the DNA and the complex translocates back to the cytoplasm [24-26], and, along with the activity of I κ B ϵ , drive NF- κ B nuclear:cytoplasmic oscillations [24, 27, 28]. Thus, this negative feedback loop plays a major role in regulating the strength and duration of NF- κ B transcriptional activity [29-32]. With respect to the negative feedback, other transcriptionally-*independent* processes, aimed at auto-inhibition of NF- κ B activity, do exist. Such mechanisms down-regulate NF- κ B signaling on a much shorter timeframe (sec-min). These include homologous receptor desensitization [33, 34], asymmetric heterologous receptor desensitization [34, 35], autocatalytic C-terminal IKK hyperphosphorylation [36] and protein phosphatase 2 β (PP2 β)-dependent dephosphorylation of IKK [37].

1.3 CLINICAL RELEVANCE OF NF- κ B SIGNALING IN THE LIVER

NF- κ B is well established as a regulator of a large number of genes involved in the different aspects of oncogenesis defined by Hanahan and Weinberg [38], and in the last few years, constitutive activation of NF- κ B has been causally linked to liver neoplastic progression via the transcriptional activation of genes involved in oncogenesis (reviewed in [39]). In hepatocytes, inappropriate and persistent NF- κ B activation can occur as a result of viral infection, carcinogen exposure, growth factor stimulation, and chronic inflammation (which can result from viral hepatitis and eventually lead to cirrhosis and hepatocellular carcinoma (HCC) development). Furthermore, it has been posited that chronic inflammation may actually account for approximately 20% of all human cancers [40]. Because NF- κ B is a central regulator of inflammatory processes, it has been proposed that NF- κ B activation during inflammation may represent a mechanism of protection against pro-apoptotic signals from the immune system [41-43]. To this end, Pikarsky and colleagues employed an Mdr2-knockout mouse model of hepatitis-induced HCC formation to show that the inflammatory process triggered hepatocyte NF- κ B activation through upregulation of TNF α in adjacent endothelial and inflammatory cells [43]. They further found that suppressing NF- κ B through anti-TNF α therapy or induction of an I κ B-superrepressor during the late stages of tumor development induced apoptosis and blocked progression of HCC. However, recent mouse models utilizing an inducible, hepatocyte-specific NEMO knockout have indicated that loss of NF- κ B activity can actually promote HCC tumor development [41, 44], showing increased rates of both apoptosis and proliferation. Thus, a more in-depth understanding of the complexities and intricacies of NF- κ B signaling in the liver is required to appropriately translate the use of NF- κ B-targeted therapeutics to liver pathologies.

1.4 THE NF- κ B SIGNALING PATHWAY AS AN EXEMPLARY PROVING GROUND FOR SYSTEMS BIOLOGY APPROACHES IN MAMMALIAN CELLS

Cells have evolved complex molecular networks to sense cues from the environment and transmit them throughout the cell to elicit appropriate biological responses. These signaling pathways require certain elemental properties (such as sensitivity, reversibility, a capacity to be regulated, and robustness) that are crucial to reliably maintaining the organization and function of cells within organisms. In addition, these networks equip cells with the ability to distinguish often weak signals from background noise with high precision and selectivity [45, 46]. These molecular networks are made up of sets of recurring regulation patterns, network motifs, that link together in a variety of combinations to create a web of connectivity within a given signaling cascade or between multiple cascades [47]. Feedback loops, processes that connect output signals back to their input, represent one of the most frequently observed biological network motifs and are now appreciated as a useful framework for understanding how signaling networks elicit specific cellular responses. In particular, negative feedback loops, defined as sequential regulatory steps that feed the output signal (inverted) back to the input, represent a single motif that is capable of generating many distinct signaling functions, including stabilizing basal signaling levels, limiting maximal signaling output, enabling adaptive response, and creating transient signal responses [46].

In the past, much of the work elucidating these complex molecular networks focused on identifying the key molecules within the network and biochemically defining their individual interactions [45, 48]. Additionally, the techniques typically employed to define these networks were static, destructive, semi-quantitative, *in vitro* biochemical methodologies that lack spatiotemporal resolution and average information from a large number of cells. Recently, the focus of attention is shifting towards experimental and computational modeling approaches that

address the question of how biological networks operate as a system to perform biological functions, specifically within the context of a single cell. Recent developments in optical imaging and biophysical methods have enabled significant advances in the ability to capture spatiotemporal signaling information in a single cell, leading to the development and refinement of mathematical and dynamical models of molecular networks [49].

One cellular signaling pathway that has emerged as an exemplary illustration of how molecular network topology can be probed through the coupled use of live-cell imaging and computational simulation is the NF- κ B pathway. Because of its biological importance, the NF- κ B pathway has been extensively studied and has emerged as an exemplary proving ground for systems biology approaches that couple computational modeling and cellular imaging with conventional cell biology methods to study dynamic NF- κ B responses to cytokines.

Recent studies have shown that continuous stimulation or sequential pulsing of TNF α can induce oscillations in NF- κ B nuclear translocation that are dependent upon cycles of degradation and re-synthesis of I κ B proteins (i.e., negative feedback loops), and that the frequency of these NF- κ B oscillations encode distinct gene expression profiles [27, 28, 31, 50, 51]. Additional work has suggested that the amplitude of NF- κ B activity, but not the temporal profile, is particularly sensitive to changes in TNF α concentration and is crucially dependent on the transient nature of IKK activity [52]. Recently, single cell imaging has emerged as a paradigm-of-choice to study the dynamics of NF- κ B nuclear localization as monitored by nuclear:cytoplasmic shuttling of NF- κ B proteins fused to fluorescent protein reporters. Coupled with computational modeling, these single cell studies have revealed stochastic, heterogeneous, and paracrine NF- κ B responses at the single cell level, especially in response to low concentrations of TNF α [53-56]. A key unresolved issue in the field relates to how biological robustness is achieved within cell populations displaying heterogeneous and dynamic single-cell

behavior [49, 55, 56], and the physiologic relevancy of these single-cell phenomena to tissue- and organ-level biological responses *in vivo*. And if these asynchronous and oscillatory NF- κ B signaling behaviors are relevant *in vivo*, what impact do they have on responses to chronic and/or acute waves of TNF α (or a variety of other cytokines), and what are the implications for therapeutic targeting of NF- κ B? As has been posited by others [57], "...it may be necessary to develop a new generation of biomarkers that predict "healthy" asynchronised oscillatory NF- κ B activity versus "unhealthy" synchronised oscillatory NF- κ B. Distinguishing between these variables may enable us to effectively target NF- κ B to promote resolution of inflammation and wound-healing in the context of ongoing injury."

1.5 BIOLUMINESCENCE IMAGING AND THE NF- κ B PATHWAY

One goal of molecular imaging is to advance the understanding of biology and medicine through noninvasive *in vivo* investigation of the cellular and molecular events mediating normal physiology and pathologic processes [58, 59]. While some aspects of molecular imaging relate to clinical applications, a great deal of basic research is performed with cellular and animal models of development, normal physiology, and disease. In practice, molecular imaging can complement and, in some cases, replace conventional laboratory techniques. Routinely used methodologies in the laboratory and *in vitro* settings are based on destructive sampling of cells or tissues which yield only a static snapshot at a given experimental endpoint. New molecular imaging technologies now allow for noninvasive, repetitive, real-time *in vivo* imaging of dynamic biological processes.

One of these molecular imaging strategies, genetically-encoded imaging reporters, can be introduced into cells and transgenic animals to enable noninvasive, longitudinal studies of

dynamic biological processes in intact cells and living animals [58, 59]. These reporters can produce signal intrinsically (e.g., fluorescent proteins), through enzymatic activation of an inactive substrate (luciferases), by enzymatic modification of an imagable (e.g., optical) substrate with selective retention in reporter cells, or by direct binding or import of an active (e.g., radiolabeled) reporter substrate or probe. Except in the context of gene therapy, genetically-encoded reporters are less likely to be used in humans, but possess a fundamental advantage in basic and pre-clinical research in that once validated, a single genetically-encoded reporter can theoretically be cloned into a variety of vectors to interrogate a broad array of regulatory pathways. Compared to injectable radiopharmaceuticals, for example, this eliminates constraints inherent to traditional routes of synthesizing, labeling and validating a new and different radioligand for every new receptor or protein of interest.

The most common reporters include firefly luciferase (bioluminescence imaging), green fluorescence protein (fluorescence imaging), transferrin receptor (magnetic resonance imaging), Herpes Simplex Virus-1 thymidine kinase (positron emission tomography) and variants with enhanced spectral and kinetic properties optimized for use *in vivo* [58, 60]. When cloned into promoter/enhancer sequences or engineered into fusion proteins, imaging reporters enable fundamental processes such as transcriptional regulation, signal transduction cascades, protein-protein interactions, protein degradation, oncogenic transformation, cell trafficking and targeted drug action to be temporally and spatially recorded *in vivo*. Ideally, the magnitude and time course of reporter gene activity should parallel the strength and duration of endogenous target gene expression. Genetically-encoded imaging reporters also provide the potential for a stable source of signal enabling longitudinal studies in living organisms with high temporal and, in some cases, high spatial resolution.

Bioluminescence imaging (BLI) assays rely on the use of luciferase enzymes that catalyze the oxidation of a specific substrate, luciferin, into an oxyluciferin (in the presence of molecular oxygen and ATP), with the concurrent emission of one photon of light [61]. There are many naturally-occurring luciferases with matching substrates available, though most are blue/green and therefore less suitable for deep tissue imaging. The luciferases that have been found to be most useful for molecular imaging are firefly luciferase (550-570 nm peak emission), *Renilla* luciferase (480 nm), green or red click beetle luciferases (537 nm, 613 nm) and *Gaussia* luciferase (460 nm) [62-65]. Nonetheless, the favorable attributes of luciferin-based imaging provide a versatile platform for studying biology *in vivo*.

BLI of luciferase reporters provides a relatively simple, robust, and cost-effective means to image fundamental biological processes in live cells and *in vivo*. Luciferases exhibit exceptionally high signal-to-noise levels (almost no background noise sources exist, save for food-derived phosphorescence), provide an extremely quantitative read-out, are active immediately after translation (a favorable property as compared to many fluorescent proteins), and have a relatively short half-life ($t^{1/2} \sim 3\text{--}6$ h, and even shorter when artificially modified with degradation sequences) allowing for dynamic measurements with high temporal sensitivity [66]. Nevertheless, bioluminescence remains dependent on substrate pharmacokinetics, except in the case of bacterial *lux* operons, and relies upon ultrasensitive CCD cameras for detection due to the extremely dim light output of luciferases. BLI has also traditionally been subject to restricted spatial resolution, but recent advances in low-light microscopy are enabling microscopic analysis of bioluminescent reporters in single cells and sub-cellular compartments [49, 59, 67-69], making it possible to use a single bioluminescent reporter for microscopic and macroscopic studies.

In particular, BLI has proven useful to study NF- κ B transcriptional activity *in vivo*. Recently, a transgenic mouse expressing a luciferase driven by an NF- κ B responsive promoter

has been used to examine prostate NF- κ B activity in response to acute and chronic cytokine exposure [70], an approach that may be amenable to the *in vivo* study of pharmacological NF- κ B modulators. In another study, Ma et al used NF- κ B-Luc mice as donors or recipients in mouse models of cardiac transplantation and tissue ischemia-reperfusion injury (IRI) [71]. They showed elevated NF- κ B activity in both the cardiac allografts and the IRI cardiac grafts, and used mAbs and ligands to examine inhibition of NF- κ B signaling *in vivo*.

Imaging post-transcriptional events in the NF- κ B signaling pathways, such as translational regulation, protein-protein interactions (PPI), protein processing or protein degradation, can be accomplished by fusing the reporter gene to the protein of interest, thereby generating a molecular sensor that activates (or deactivates) the reporter in response to a given protein interaction or modification. For example, we have previously shown that an I κ B α -firefly luciferase (I κ B α -FLuc) fusion reporter driven by a constitutive CMV promoter enables quantitative monitoring of I κ B α degradation (which can be directly correlated to IKK activity) and can be used in cultured cells to provide a continuous, noninvasive readout of the kinetics and dynamics of ligand-induced IKK activation [72]. This reporter was additionally used *in vivo* to monitor the real-time activity of IKK in response to LPS-mediated activation. Applying this approach to a tumor xenograft model expressing the I κ B α -FLuc fusion reporter, robust time- and dose-dependent pharmacodynamic characterization of a novel IKK inhibitor (PS-1145) was characterized using a minimal number of animals. Thus, bioluminescence imaging provides a unique toolkit that is well-suited to rigorously interrogate the real-time dynamics of NF- κ B signaling in live cells and live animals.

1.6 FIGURES

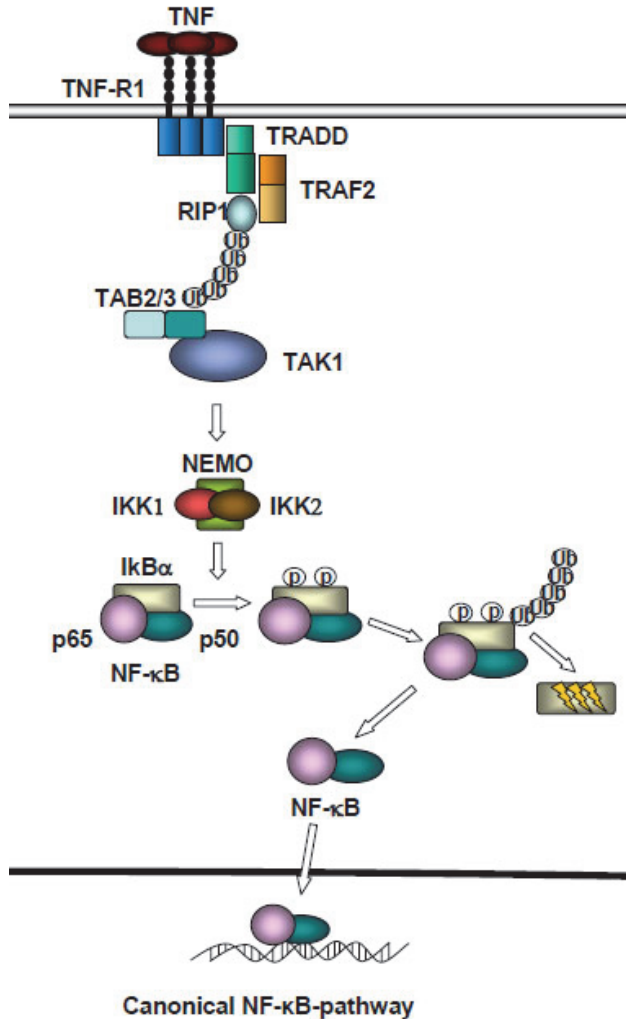


Figure 1.1: Activation of Canonical NF-κB Signaling by TNF-α. Binding of homotrimeric TNF α ligands drives trimerization of TNF-R1 and results in TRADD-dependent TRAF2 and RIP1 recruitment. TRAF2 mediates K63-linked ubiquitination of RIP1 and recruits the IKK complex via the catalytic subunit NEMO. Autoubiquitination of TRAF2 causes TAK1 activation by interaction via TAB2/3. In consequence, TAK1 phosphorylates and activates IKK β (IKK2), which in turn phosphorylates I κ B α , leading to proteasomal degradation and release of NF- κ B which can then translocate into the nucleus and modulate transcription. Modified from Vucur, et al [73].

1.7 REFERENCES

1. Li, Q. and I.M. Verma, *NF-kappaB regulation in the immune system*. Nat Rev Immunol, 2002. **2**(10): p. 725-34.
2. Karin, M., et al., *NF-kappaB in cancer: from innocent bystander to major culprit*. Nat Rev Cancer, 2002. **2**: p. 301-310.
3. Karin, M., *Nuclear factor-kappaB in cancer development and progression*. Nature, 2006. **441**(7092): p. 431-6.
4. Sen, R. and D. Baltimore, *Multiple nuclear factors interact with the immunoglobulin enhancer sequences*. Cell, 1986. **46**(5): p. 705-16.
5. Baltimore, D., *Discovering NF-kappaB*. Cold Spring Harb Perspect Biol, 2009. **1**(1): p. a000026.
6. Sen, R. and D. Baltimore, *Inducibility of kappa immunoglobulin enhancer-binding protein Nf-kappa B by a posttranslational mechanism*. Cell, 1986. **47**(6): p. 921-8.
7. Baeuerle, P.A. and D. Baltimore, *Activation of DNA-binding activity in an apparently cytoplasmic precursor of the NF-kappa B transcription factor*. Cell, 1988. **53**(2): p. 211-7.
8. Baeuerle, P.A. and D. Baltimore, *I kappa B: a specific inhibitor of the NF-kappa B transcription factor*. Science, 1988. **242**(4878): p. 540-6.
9. Oeckinghaus, A. and S. Ghosh, *The NF-kappaB family of transcription factors and its regulation*. Cold Spring Harb Perspect Biol, 2009. **1**(4): p. a000034.
10. Hoffmann, A., G. Natoli, and G. Ghosh, *Transcriptional regulation via the NF-kappaB signaling module*. Oncogene, 2006. **25**(51): p. 6706-16.
11. Gilmore, T.D., *NF-kappa B, KBF1, dorsal, and related matters*. Cell, 1990. **62**(5): p. 841-3.
12. Courtois, G. and T.D. Gilmore, *Mutations in the NF-kappaB signaling pathway: implications for human disease*. Oncogene, 2006. **25**(51): p. 6831-43.
13. Gilmore, T.D., *Introduction to NF-kappaB: players, pathways, perspectives*. Oncogene, 2006. **25**(51): p. 6680-4.
14. Hoffmann, A., T.H. Leung, and D. Baltimore, *Genetic analysis of NF-kappaB/Rel transcription factors defines functional specificities*. Embo J, 2003. **22**(20): p. 5530-9.
15. Bunting, K., et al., *Genome-Wide Analysis of Gene Expression in T Cells to Identify Targets of the NF- κ B Transcription Factor c-Rel*. J Immunol, 2007. **178**(11): p. 7097-109.
16. Naamane, N., J. van Helden, and D.L. Eizirik, *In silico identification of NF-kappaB-regulated genes in pancreatic beta-cells*. BMC Bioinformatics, 2007. **8**: p. 55.
17. Kim, H.J., N. Hawke, and A.S. Baldwin, *NF-kappaB and IKK as therapeutic targets in cancer*. Cell Death Differ, 2006. **13**(5): p. 738-47.
18. Hayden, M.S. and S. Ghosh, *Signaling to NF-kappaB*. Genes Dev, 2004. **18**(18): p. 2195-224.
19. Johnson, C., D. Van Antwerp, and T.J. Hope, *An N-terminal nuclear export signal is required for the nucleocytoplasmic shuttling of IkappaBalpha*. Embo J, 1999. **18**(23): p. 6682-93.

20. Perkins, N.D., *Integrating cell-signalling pathways with NF-kappaB and IKK function*. Nat Rev Mol Cell Biol, 2007. **8**(1): p. 49-62.
21. Huang, T.T., et al., *A nuclear export signal in the N-terminal regulatory domain of IkappaBalpha controls cytoplasmic localization of inactive NF-kappaB/IkappaBalpha complexes*. Proc Natl Acad Sci U S A, 2000. **97**(3): p. 1014-9.
22. Hacker, H. and M. Karin, *Regulation and function of IKK and IKK-related kinases*. Sci STKE, 2006. **2006**(357): p. re13.
23. Hayden, M.S. and S. Ghosh, *Shared principles in NF-kappaB signaling*. Cell, 2008. **132**(3): p. 344-62.
24. Hoffmann, A., et al., *The IkappaB-NF-kappaB signaling module: temporal control and selective gene activation*. Science, 2002. **298**(5596): p. 1241-5.
25. Arenzana-Seisdedos, F., et al., *Nuclear localization of I kappa B alpha promotes active transport of NF-kappa B from the nucleus to the cytoplasm*. Journal of Cell Science, 1997. **110**(3): p. 369-378.
26. Bergqvist, S., et al., *Kinetic enhancement of NF-Î°BÁ·DNA dissociation by Î°BÎ±*. Proceedings of the National Academy of Sciences, 2009. **106**(46): p. 19328-19333.
27. Nelson, D.E., et al., *Oscillations in NF-kappaB signaling control the dynamics of gene expression*. Science, 2004. **306**(5696): p. 704-8.
28. Kearns, J.D., et al., *IkappaBepsilon provides negative feedback to control NF-kappaB oscillations, signaling dynamics, and inflammatory gene expression*. J Cell Biol, 2006. **173**(5): p. 659-64.
29. Werner, S.L., D. Barken, and A. Hoffmann, *Stimulus specificity of gene expression programs determined by temporal control of IKK activity*. Science, 2005. **309**(5742): p. 1857-61.
30. Werner, S.L., et al., *Encoding NF-kappaB temporal control in response to TNF: distinct roles for the negative regulators IkappaBalpha and A20*. Genes Dev, 2008. **22**(15): p. 2093-101.
31. Ashall, L., et al., *Pulsatile stimulation determines timing and specificity of NF-kappaB-dependent transcription*. Science, 2009. **324**(5924): p. 242-6.
32. Barken, D., et al., *Comment on "Oscillations in NF-kappaB signaling control the dynamics of gene expression"*. Science, 2005. **308**(5718): p. 52.
33. Karmann, K., et al., *Activation and homologous desensitization of human endothelial cells by CD40 ligand, tumor necrosis factor, and interleukin 1*. J Exp Med, 1996. **184**(1): p. 173-82.
34. Alberts, B., Bray, D., Lewis, J., Raff, M., Roberts, K. and Watson, J.D., *Target-Cell Adaptation*, in *Molecular Biology of the Cell*. 1994, Garland Publishing: New-York. p. 771-785.
35. Holtmann, H. and D. Wallach, *Down regulation of the receptors for tumor necrosis factor by interleukin 1 and 4 beta-phorbol-12-myristate-13-acetate*. J Immunol, 1987. **139**(4): p. 1161-7.
36. Delhase, M., et al., *Positive and negative regulation of IkappaB kinase activity through IKKbeta subunit phosphorylation*. Science, 1999. **284**(5412): p. 309-13.

37. Prajapati, S., et al., *Protein phosphatase 2Cbeta association with the IkappaB kinase complex is involved in regulating NF-kappaB activity*. J Biol Chem, 2004. **279**(3): p. 1739-46.
38. Hanahan, D. and R.A. Weinberg, *The hallmarks of cancer*. Cell, 2000. **100**(1): p. 57-70.
39. Arsur, M. and L.G. Cavin, *Nuclear factor-kappaB and liver carcinogenesis*. Cancer Lett, 2005. **229**(2): p. 157-69.
40. Coussens, L.M. and Z. Werb, *Inflammation and cancer*. Nature, 2002. **420**(6917): p. 860-7.
41. Elsharkawy, A.M. and D.A. Mann, *Nuclear factor-kappaB and the hepatic inflammation-fibrosis-cancer axis*. Hepatology, 2007. **46**(2): p. 590-7.
42. Maeda, S., et al., *IKKbeta couples hepatocyte death to cytokine-driven compensatory proliferation that promotes chemical hepatocarcinogenesis*. Cell, 2005. **121**(7): p. 977-90.
43. Pikarsky, E., et al., *NF kB functions as a tumor promote in inflammation-associated cancer*. Nature, 2004. **431**: p. 461-466.
44. Luedde, T., et al., *Deletion of NEMO/IKKgamma in liver parenchymal cells causes steatohepatitis and hepatocellular carcinoma*. Cancer Cell, 2007. **11**(2): p. 119-32.
45. Cebecauer, M., et al., *Signalling complexes and clusters: functional advantages and methodological hurdles*. J Cell Sci, 2010. **123**(Pt 3): p. 309-20.
46. Brandman, O. and T. Meyer, *Feedback loops shape cellular signals in space and time*. Science, 2008. **322**(5900): p. 390-5.
47. Alon, U., *Simplicity in biology*. Nature, 2007. **446**(7135): p. 497.
48. Sung, M.H. and J.G. McNally, *Live cell imaging and systems biology*. Wiley Interdiscip Rev Syst Biol Med, 2011. **3**(2): p. 167-82.
49. Spiller, D.G., et al., *Measurement of single-cell dynamics*. Nature, 2010. **465**(7299): p. 736-45.
50. Sung, M.H., et al., *Sustained oscillations of NF-kappaB produce distinct genome scanning and gene expression profiles*. PLoS One, 2009. **4**(9): p. e7163.
51. Tian, B., D.E. Nowak, and A.R. Brasier, *A TNF-induced gene expression program under oscillatory NF-kappaB control*. BMC Genomics, 2005. **6**: p. 137.
52. Cheong, R., et al., *Transient IkappaB kinase activity mediates temporal NF-kappaB dynamics in response to a wide range of tumor necrosis factor-alpha doses*. J Biol Chem, 2006. **281**(5): p. 2945-50.
53. Turner, D.A., et al., *Physiological levels of TNFalpha stimulation induce stochastic dynamics of NF-kappaB responses in single living cells*. J Cell Sci, 2010. **123**(Pt 16): p. 2834-43.
54. Tay, S., et al., *Single-cell NF-kappaB dynamics reveal digital activation and analogue information processing*. Nature, 2010. **466**(7303): p. 267-71.
55. Lee, T.K., et al., *A noisy paracrine signal determines the cellular NF-kappaB response to lipopolysaccharide*. Sci Signal, 2009. **2**(93): p. ra65.
56. Paszek, P., et al., *Population robustness arising from cellular heterogeneity*. Proc Natl Acad Sci U S A, 2010. **107**(25): p. 11644-9.
57. Chakraborty, J.B. and D.A. Mann, *NF-kappaB signalling: embracing complexity to achieve translation*. J Hepatol, 2010. **52**(2): p. 285-91.

58. Gross, S. and D. Piwnica-Worms, *Spying on cancer: molecular imaging in vivo with genetically encoded reporters*. *Cancer Cell*, 2005. **7**(1): p. 5-15.
59. Dothager, R., et al., *Advances in bioluminescence imaging of live animal models*. *Curr Opin Biotechnol*, 2009. **20**: p. 45-53.
60. Prescher, J.A. and C.H. Contag, *Guided by the light: visualizing biomolecular processes in living animals with bioluminescence*. *Curr Opin Chem Biol*, 2010. **14**(1): p. 80-9.
61. Marques, S.M. and J.C.G. Esteves da Silva, *Firefly bioluminescence: A mechanistic approach of luciferase catalyzed reactions*. *IUBMB Life*, 2009. **61**(1): p. 6-17.
62. Thorne, N., J. Inglese, and D.S. Auld, *Illuminating Insights into Firefly Luciferase and Other Bioluminescent Reporters Used in Chemical Biology*. *Chemistry & Biology*. **17**(6): p. 646-657.
63. Contag, C.H. and M.H. Bachmann, *Advances in in vivo bioluminescence imaging of gene expression*. *Annu Rev Biomed Eng*, 2002. **4**: p. 235-260.
64. Zhao, H., et al., *Spectral characterization of firefly, click beetle and Renilla luciferases in mammalian cells and living mice*. *Mol Imaging*, 2004. **3**(3): p. 229.
65. Tannous, B., D. Kim, and R. Weissleder, *Novel luciferases for in vitro and in vivo imaging*. *Mol Imaging*, 2004. **3**(3): p. 227.
66. Gross, S., B. Moss, and D. Piwnica-Worms, *Veni, vidi, vici: in vivo molecular imaging of immune response*. *Immunity*, 2007. **27**: p. 533-538.
67. Harper, C.V., et al., *Dynamic organisation of prolactin gene expression in living pituitary tissue*. *J Cell Sci*, 2010. **123**(Pt 3): p. 424-30.
68. Webb, A.B., et al., *Intrinsic, nondeterministic circadian rhythm generation in identified mammalian neurons*. *Proc Natl Acad Sci U S A*, 2009. **106**(38): p. 16493-8.
69. Nelson, G., et al., *Multi-parameter analysis of the kinetics of NF-kappaB signalling and transcription in single living cells*. *J Cell Sci*, 2002. **115**(Pt 6): p. 1137-48.
70. Vykhovanets, E.V., et al., *Molecular imaging of NF-kappaB in prostate tissue after systemic administration of IL-1 beta*. *Prostate*, 2008. **68**(1): p. 34-41.
71. Ma, L., et al., *Bioluminescence imaging visualizes activation of nuclear factor-kappaB in mouse cardiac transplantation*. *Transplantation*, 2008. **85**(6): p. 903-10.
72. Gross, S. and D. Piwnica-Worms, *Real-time imaging of ligand-induced IKK activation in intact cells and in living mice*. *Nat Methods*, 2005. **2**: p. 607-614.
73. Vucur, M., et al., *Mouse models of hepatocarcinogenesis: what can we learn for the prevention of human hepatocellular carcinoma?* *Oncotarget*, 2010. **1**(5): p. 373-8.

CHAPTER TWO

Identification of a Ligand-Induced Transient Refractory Period in Nuclear Factor- κ B Signaling

2.1 INTRODUCTION

Adequate resolution of an inflammatory reaction is as equally important as initiation. Persistent or fulminant responses can cause detrimental consequences both locally and systemically [1], and resolution of inflammation is important for both termination of an acute response as well as for prevention of destructive chronic responses. It is therefore not surprising that mechanisms aimed at rapid and specific initiation of pro-inflammatory reactions have co-evolved with mechanisms that provide timely termination of such processes. From a systems biology perspective, such “switchability” can be achieved by intracellular feedback loops that permit ligand-induced desensitization and re-sensitization of pro-inflammatory signaling cascades [2].

In this regard, recent studies have shown that nuclear factor- κ B (NF- κ B) signaling plays a critical role in both initiation and resolution of inflammation [2, 3]. The transcription factor NF- κ B is a key regulator of innate and adaptive immune responses, as well as a mediator of cell survival and proliferation [4]. Improper regulation of NF- κ B contributes to induction and progression of a wide range of human disorders, including a variety of pathological inflammatory conditions, neurodegenerative diseases as well as

many types of cancer [5, 6]. In resting cells, inactive NF- κ B is sequestered in the cytoplasm by binding to members of the inhibitor of NF- κ B (I κ B) family. Canonical activation of NF- κ B depends on I κ B kinase (IKK)-regulated proteasomal degradation of I κ B α , an event that frees NF- κ B for nuclear translocation within minutes [4, 7]. Upon nuclear transport, NF- κ B regulates the transcription of a few hundred genes [8-10] that can be divided into four major families [10, 11]: (1) pro-inflammatory genes (e.g., COX 2, IL-1, TNF α , iNOS, ICAM-1, E-selectin, etc.), (2) pro-proliferative genes (e.g., Cyclin D, c-Myc), (3) anti-apoptotic genes (Bcl2, Bcl_{XL}, xIAPs, cIAPs), and (4) auto-inhibitory genes (e.g., A20, CYLD, SOCS-1 and I κ B α).

With respect to the latter, other transcriptionally-independent processes, aimed at auto-inhibition of NF- κ B activity, do exist. Such mechanisms down-regulate NF- κ B signaling on a much shorter timeframe (sec-min). These include homologous receptor desensitization [12, 13], asymmetric heterologous receptor desensitization [13, 14], autocatalytic C-terminal IKK hyperphosphorylation [15] and protein phosphatase 2 β (PP2 β)-dependent dephosphorylation of IKK [16].

Considering the complex nature of the inflammatory milieu, one would expect that stationary tissue-residing cells are exposed to a myriad of temporally-distinct NF- κ B-stimulating cues. For instance, cells can be directly stimulated by pathogen-derived products (e.g., LPS through TLR4 receptors [17]), exposed to numerous soluble pro-inflammatory stimuli produced by circulating effector cells (e.g., cytokines, chemokines, etc.), and/or experience inflammation-induced oxidative stress [18]. These signals can occur simultaneously or sequentially to one another. For example, systemic

administration of bacterial LPS to mice was shown to induce transient production of TNF α (serum levels peaking at ~1.5 h and quickly returning to baseline), but IL-1 β production was delayed and prolonged (first detected at 2 h, but lasting >5-6 h) [19]. Thus, cells co-expressing TLR4, IL-1 and TNF α receptors would sequentially interrogate signals arising from LPS, TNF α and IL-1 β , each of which could independently activate NF- κ B.

Central to any signaling desensitization mechanism is a refractory period during which cells cannot fully respond to a second insult (autologous or heterologous desensitization). Therefore, consideration of the dynamic pattern of stimulus exposure described above begs the immediate question of whether cells can instantly initiate an NF- κ B response to a second activating stimulus, and if not, when will such cells be able to remount a full response again? Specifically, are ligand-preconditioned cells capable of eliciting NF- κ B activation to the same extent as naïve cells?

Little is known about the capacity of cells to activate NF- κ B in response to a second activating challenge since the highly dynamic nature of this process presents many technical difficulties. These include low temporal resolution of conventional transcriptionally-dependent NF- κ B reporter gene assays, low throughput, inability to acquire longitudinal data and the semi-quantitative nature of traditional biochemical assays (e.g., EMSA, immunoblotting, etc.). Such limitations render these assays incapable of accurate analysis of the early, ligand-induced dynamic changes in the capacity of cells to elicit a response to a second challenge.

To efficiently address this question, we generated an improved, transcriptionally-coupled version of a previously published genetically-encoded I κ B α -firefly luciferase (I κ B α -FLuc) fusion reporter [20] in conjunction with dynamic, live-cell bioluminescence imaging of cultured cells. We chose to focus on HepG2 human hepatoma cells as a model system because, (1) NF- κ B signaling has been extensively studied in these cells, (2) HepG2 cells have been shown to activate NF- κ B in response to a variety of pro-inflammatory ligands [21], (3) these cells can be easily transfected with readily-available reagents, and most importantly, (4) the pivotal role that NF- κ B signaling plays in hepatocytes to regulate inflammation, apoptosis and carcinogenesis [22].

Using bioluminescence imaging of live cells in conjunction with a variety of biochemical assays, we demonstrate herein that a 30 sec preconditioning exposure to TNF α is sufficient to robustly activate IKK, culminating in I κ B α degradation, NF- κ B nuclear translocation, and strong transcriptional up-regulation of I κ B α . Furthermore, the capacity of preconditioned cells to degrade I κ B α in response to a second TNF α challenge is transiently refractory, regaining full responsiveness approximately 120 min later. Finally, both IKK regulation and possibly NF- κ B nuclear export, but not receptor dynamics, govern this transient refractory period. This study highlights the interlocking layers of NF- κ B regulation, ensuring efficient and timely propagation as well as termination of pro-inflammatory signals.

2.2 RESULTS

Real-time bioluminescence imaging of $\kappa\text{B}_5 \rightarrow \text{I}\kappa\text{B}\alpha$ -FLuc-expressing cells recapitulated IKK-induced dynamics of endogenous $\text{I}\kappa\text{B}\alpha$. To monitor ligand-induced $\text{I}\kappa\text{B}\alpha$ rapid dynamics as well as physiologic transcriptionally-coupled behavior, we modified our previous $\text{I}\kappa\text{B}\alpha$ -FLuc fusion reporter [20] to be driven by a synthetic promoter comprised of 5 tandem κB response elements (TGGGGACTTTCCGC) followed by a minimal TATA-box. We hypothesized that this reporter would allow quantitative measurements of IKK-induced degradation as well as NF- κB -induced re-synthesis and post-translational stabilization of $\text{I}\kappa\text{B}\alpha$ from intact living cells (Fig. 2.1A). To validate use of this reporter, HepG2 cells were transiently transfected with a plasmid encoding the reporter and allowed to recover for two days before stimulation with a continuous or 30 sec pulse of $\text{TNF}\alpha$ (20 ng/mL) to induce IKK activation. Upon addition of $\text{TNF}\alpha$, a rapid and dramatic decrease in bioluminescence was observed when readouts were normalized to untreated controls [20] under both continuous (C) and 30 sec pulse (P) regimens (Fig. 2. 1B, C). This decrease in normalized bioluminescence, reflecting IKK-induced reporter degradation was followed by a sharp increase in bioluminescence, reflecting NF- κB -dependent reporter re-synthesis, reaching maximum values at ~120 min and then gradually declining toward baseline. Note that the rate at which $\text{I}\kappa\text{B}\alpha$ levels return to baseline is steeper under continuous $\text{TNF}\alpha$ treatment compared to the 30 sec pulse, providing evidence for reactivation of ligand-induced $\text{I}\kappa\text{B}\alpha$ degradation during continuous stimulation [23]. The magnitude of the initial decrease in bioluminescence was greater in continuously-treated cells than in 30 sec-pulsed cells (70% vs. 40% of

initial, respectively), indicating that a 30 sec pulse of TNF α leads to approximately 50% depletion of the I κ B α -NF- κ B pool compared to continuous TNF α exposure (Fig. 2.1C, 120 min). These data suggested that, (a) this reporter construct could report on both IKK-induced I κ B α degradation and successive re-synthesis of I κ B α , (b) a 30 sec pulse of TNF α at a saturating concentration (20 mg/mL) elicited robust IKK activity, culminating in I κ B α degradation and a full I κ B α transcriptional up-regulation, and (c) with the current κ B₅ synthetic promoter system, there was a non-linear relationship between I κ B α degradation and NF- κ B-dependent re-synthesis of I κ B α (i.e., saturation of I κ B α re-synthesis even at sub-maximal I κ B α degradation levels).

Strikingly, Western blot analysis revealed that endogenous I κ B α behaved exactly as the reporter under both C and P conditions, recapitulating the degree of degradation, recovery, and return to baseline (Fig. 2.1D). Pretreating p κ B₅→I κ B α -FLuc-expressing HepG2 cells with cycloheximide did not affect degradation of I κ B α -FLuc, but abolished signal recovery, indicating that this phase was totally dependent upon transcription and translation of new I κ B α -FLuc (Fig. 2.1E).

TNF α preconditioning induces a transient refractory period of I κ B α processing.

Upon a pro-inflammatory insult *in vivo*, effector cells (e.g., circulating macrophages) release TNF α and other activating cytokines in a temporally- and spatially-discrete manner. As a consequence, stationary target cells (e.g., epithelial cells, endothelial cells, hepatocytes, etc.) will sense a stochastic rise in the levels of such pro-inflammatory

ligands. In such a dynamic environment, as ligand-secreting cells continuously migrate to sites of inflammation, it is anticipated that over time, target cells will experience multiple pulses of activating ligands.

We therefore aimed to elucidate the effects of such ligand pulses on the capacity of hepatocytes to respond to a subsequent challenge of the same ligand. Having shown that, (a) $\text{p}\kappa\text{B}_5 \rightarrow \text{I}\kappa\text{B}\alpha\text{-FLuc}$ provided an accurate readout of $\text{I}\kappa\text{B}\alpha$ processing in intact cells and that, (b) a 30 sec pulse was sufficient to induce robust IKK activity, we next sought to investigate whether a short 30 sec preconditioning pulse with $\text{TNF}\alpha$ had a substantial effect on the capacity of cells to process $\text{I}\kappa\text{B}\alpha$ upon a subsequent continuous $\text{TNF}\alpha$ challenge.

HepG2 cells transiently expressing $\text{p}\kappa\text{B}_5 \rightarrow \text{I}\kappa\text{B}\alpha\text{-FLuc}$ were given a 30 sec pulse of $\text{TNF}\alpha$ (20 ng/mL) or vehicle at t_0 , washed, replaced in media containing D-luciferin and repeatedly imaged (every 5 min) prior to a $\text{TNF}\alpha$ challenge. At t_{30} , t_{60} , t_{120} , or t_{240} (min) after pulsing, cells were then challenged with a second continuous concentration of $\text{TNF}\alpha$ (20 ng/mL), and live-cell imaging was continued up to 360 min. To compare the processing dynamics of $\text{I}\kappa\text{B}\alpha\text{-FLuc}$ in naïve (un-preconditioned) cells with that of preconditioned cells, the resulting bioluminescence profiles of preconditioned cells (black lines, Figure 2.2A) were plotted along with the bioluminescence profile of un-preconditioned cells (i.e., only treated with continuous $\text{TNF}\alpha$ at t_0 , red line, Figure 2.2A). The different graph panels represent the differential dynamics of $\text{I}\kappa\text{B}\alpha\text{-FLuc}$ processing as the preconditioning pulse-challenge (P-C) intervals temporally increased (0-240 min).

We observed that challenging preconditioned cells with a continuous exposure to TNF α near the time that they had achieved maximal degradation from the preconditioning pulse (i.e., 30 min post preconditioning) resulted in a small amount of additional I κ B α degradation. As the interval between preconditioning and challenge increased, the magnitude of challenge-induced I κ B α degradation also increased. These data suggested that the TNF α -NF- κ B system possessed a built-in refractory period following TNF α treatment that prevented cells from fully responding to a second exposure to ligand. To quantify this phenomenon independent of confounding factors that may affect dynamic bioluminescence readouts (e.g., D-luciferin, ATP, O $_2$ or pH dynamics), and to verify its existence for endogenous I κ B α , we performed a similar experiment, but instead of live-cell imaging, we harvested whole-cell lysates at $t_{X+25 \text{ min}}$ (time of maximal I κ B α degradation after a ligand challenge given at t_X (Fig. 2.1C); for a schematic timeline see Fig. 2.2B). I κ B α -FLuc reporter levels in these lysates were analyzed by bioluminescence imaging (upon addition of saturating D-luciferin and ATP), and endogenous I κ B α levels were determined by Western blot analysis and semi-quantitative densitometric analysis (Fig. 2.2C). From these data, we were then able to calculate responsiveness levels for both I κ B α and I κ B α -FLuc as a function of time after TNF α preconditioning. Responsiveness at each challenge time was calculated by determining the magnitude of I κ B α degradation induced by TNF α challenge divided by the magnitude of I κ B α degradation in un-preconditioned cells from the same plate. Specifically, the ratio at $t_{X+25 \text{ min}}$ of I κ B α in preconditioned cells challenged with TNF α over preconditioned cells challenged with vehicle was divided by the ratio at t_{X+25

min of $\text{I}\kappa\text{B}\alpha$ in un-preconditioned cells challenged with $\text{TNF}\alpha$ over un-preconditioned cells challenged with vehicle, the latter ratio representing the maximal possible response. We observed a strong correlation ($r=0.95$) between levels of responsiveness for endogenous $\text{I}\kappa\text{B}\alpha$ and $\text{I}\kappa\text{B}\alpha\text{-FLuc}$ (Table 2.1). Consistent with our earlier observations derived from live-cell dynamic bioluminescence imaging experiments (Fig. 2.2A), we observed that at 30 min post-preconditioning, cells were approximately half as responsive as naïve (i.e., un-preconditioned) cells to a $\text{TNF}\alpha$ challenge, and had gained full responsiveness by 120 min. Thus, a transient refractory period seemed to exist from 30-120 min post $\text{TNF}\alpha$ preconditioning that rendered the cells unable to fully respond (as measured via $\text{I}\kappa\text{B}\alpha$ degradation) to a second challenge of $\text{TNF}\alpha$, and beyond this period, the cells were able to mount a full response to a second $\text{TNF}\alpha$ challenge. Notably, similar experiments performed with HeLa cells stably expressing $\text{pCMV}\rightarrow\text{I}\kappa\text{B}\alpha\text{-FLuc}$ (HeLa ^{$\text{I}\kappa\text{B}\alpha\text{-FLuc}$} [20]), yielded almost identical results (data not shown), suggesting that, (1) the $\text{TNF}\alpha$ -induced transient refractory period was not limited to hepatocytes, and (2) this effect was independent of both $\text{NF-}\kappa\text{B}$ -induced $\text{I}\kappa\text{B}\alpha$ transcription and the initial levels of $\text{I}\kappa\text{B}\alpha\text{-FLuc}$ (substantially higher in HeLa ^{$\text{I}\kappa\text{B}\alpha\text{-FLuc}$} [20]).

The ligand-induced transient refractory period for $\text{I}\kappa\text{B}\alpha$ processing correlated in part with temporal down-regulation of IKK, but not receptor dynamics.

Hypothetically, this loss and regain of the capacity of cells to process $\text{I}\kappa\text{B}\alpha$ can be explained by, (1) internalization or shedding of $\text{TNF}\alpha$ receptors (TNFR), followed by

their recycling to the cell membrane [24, 25], (2) transient down-regulation of IKK activity as previously reported [15, 26], or alternatively, (3) by a yet unknown mechanism of regulation, downstream of IKK. We therefore sought to establish the relative contributions of receptor dynamics and IKK regulation to this refractory period.

To determine the extent of receptor dynamics in governing the observed loss and regain of I κ B α processing, we took advantage of a discovery, made 20 years ago [14], that IL-1 β induces transient down-regulation of TNF α receptors, but not *vice versa* (i.e., TNF α has no effect on either the affinity or the number of IL-1 β surface receptors), as tested in a variety of cell lines and primary cells. Hence, we aimed to determine I κ B α responsiveness to an IL-1 β challenge as a function of time after TNF α preconditioning in HepG2 cells. Cells expressing p κ B α →I κ B α -FLuc were treated with a 30 sec pulse of TNF α (20 ng/mL) followed by a continuous challenge with IL-1 β , initiated at increasing P-C intervals (0-240 min). I κ B α processing was analyzed by live-cell dynamic bioluminescence imaging (Fig. 2.3A). Using this experimental setup, we again observed a transient refractory period (from 30-120 min post-TNF α preconditioning) during which HepG2 cells exhibited decreased I κ B α responsiveness. The magnitude of the ligand-induced degradation increased as the interval to the IL-1 β challenge increased, becoming fully responsive again by 120 min (Fig. 2.3A). These data suggested that even in the absence of ligand-induced receptor desensitization or cross-regulation, the capacity of cells to process I κ B α was compromised within the first two hours after a short TNF α stimulation.

We next aimed at deciphering whether transient down-regulation of IKK activity could explain the observed loss and regain in I κ B α responsiveness. We therefore performed a series of IKK kinase assays in order to directly measure the temporal activity profile of IKK, a central junction of the TNF α and IL-1 β pathways that integrates signals from a myriad of upstream regulators (e.g., TRAFs, MEKK, TAB, TAK, NIK, RIP, A20, PKC ζ , etc. [2, 7, 27]). HepG2 cells were treated with TNF α (20 ng/mL) either as a 30 sec pulse or continuously. At the indicated time points, cells were harvested, IKK complexes were immunoprecipitated and assayed for their capacity to phosphorylate exogenous GST-I κ B α (1-54) [23]. We found that for both 30 sec pulses and continuous TNF α exposure, temporal profiles of IKK activity were almost identical, with both peaking at 10 min. However, consistent with our earlier findings that continuous TNF α treatment elicits greater I κ B α degradation than a 30 sec pulse (Fig. 2.1C), continuous TNF α treatment exhibited slightly elevated and more sustained levels of IKK activity compared to pulsed TNF α treatment (Fig. 2.3B). Importantly, Western blot analysis showed that IKK complex levels (as determined by IKK α protein) did not change over the experimental time course (Fig. 2.3C), confirming that the increase in net kinase activity was due specifically to IKK activation.

IKK-KA data were also collected from preconditioned cells, 10 minutes post-challenge (at the time of maximal IKK activity, see Fig. 2.3B) at increasing P-C intervals (0-240 min). Using these data together with the IKK activity profiles generated for 30 sec pulse and continuous TNF α treatment regimens (Fig. 2.3B), we were able to calculate the net capacity of IKK to phosphorylate I κ B α as a function of time after TNF α .

preconditioning (i.e., IKK responsiveness, Table 2.1, see methods section for details on this calculation). Based on this calculation, we noted that the capacity of IKK to respond to a second challenge of TNF α was significantly compromised at 30 min post TNF α preconditioning and then gradually increased, reaching ~75% responsiveness by 120 min. Up to 240 min, IKK activity did not fully recover to initial levels, consistent with other reports indicating that upon TNF α stimulation, IKK activity rapidly and transiently declines due to autocatalytic C-terminal hyperphosphorylation [15] and PP2C β -dependent dephosphorylation [16], followed by late NF- κ B-dependent down regulation, a process attributed, in part, to A20, an IKK-inhibitory protein [27]. Hence, these data suggested that, (1) the observed ligand-induced transient refractory period of I κ B α processing (Figs. 2.2 and 2.3, Table 2.1) correlated only in part with ligand-induced transient down-regulation of IKK activity, and that, (2) the level to which cells are able to degrade I κ B α was not linear with the capacity of IKK to phosphorylate I κ B α , i.e., full I κ B α responsiveness was observed as soon as 120 min post TNF α preconditioning (Figs. 2.2 and 2.3A), a time point where IKK responsiveness was still compromised (Table 2.1). These data indicated that either submaximal IKK activity could now fully support ligand-induced I κ B α degradation following the refractory period, or that additional ligand-responsive elements existed that converged on I κ B α to induce a full response.

Computational modeling of NF- κ B signaling suggested an additional layer of regulation, downstream of IKK, governing the observed refractory period for I κ B α processing. The NF- κ B pathway provides an excellent example of a complex signaling

system employing numerous temporally distinct auto-regulatory mechanisms and negative feedback loops. IKK enzymatic activity, which is both endogenously and exogenously regulated, controls the degradation of its own substrate (I κ B α), which is later strongly up-regulated in an NF- κ B-dependent manner (Fig. 2.1A). Rapid changes in substrate availability, conformation and sub-cellular localization imply that alternative mechanisms of regulation might exist, other than changes in enzymatic activity. Although a ligand-induced transient refractory period of I κ B α processing could be explained in part by down-regulation of IKK activity, we were intrigued to examine whether an alternative regulatory mechanism, based on substrate (I κ B α) dynamics, might exist to complement or "back up" IKK regulation. Obviously, inhibition of IKK was not a viable option for analyzing downstream regulation, since such inhibition will result in complete loss of responsiveness in the absence or presence of preconditioning. We therefore decided to undertake a computational approach and explore I κ B α dynamics *in silico*, assuming no down-regulation of IKK activity. We used a well-accepted computational model that used experimentally- or hypothetically-driven IKK activity profiles as inputs and in return, calculated ligand-induced dynamics of 24 different sub-populations of mediators on the IKK-NF- κ B axis.

As a first step, to test the robustness of the model, we sought to compare our I κ B α -FLuc bioluminescence imaging data for 30 sec pulsing and continuous TNF α treatments (Fig. 2.1C) with the dynamics of I κ B α , as predicted by the computational model. To accomplish this, we used as inputs the IKK activity profiles generated for 30 sec pulse and continuous TNF α treatment regimens (Fig. 2.4A, left panel; see methods section for

details on numerical processing of the raw data to fit the model). The dynamics of six different free and complexed I κ B α sub-populations could be predicted by the model (i.e., free I κ B α _{cyt}, I κ B α :IKK_{cyt}, I κ B α :NF- κ B_{cyt}, I κ B α :IKK:NF- κ B_{cyt}, free I κ B α _{nuc} and I κ B α :NF- κ B_{nuc}). Since live-cell bioluminescence imaging of I κ B α -FLuc could not distinguish between these populations, we summed up the predicted concentrations of all I κ B α sub-populations and plotted the predicted total I κ B α levels as a function of time (Fig. 2.4A, right panel). For both treatment regimens, we noted an excellent correlation between the predicted profiles of I κ B α and the experimentally-generated profiles of I κ B α -FLuc (Fig. 2.1C). The timing and extent of I κ B α degradation as well as the overall dynamic behavior were highly similar. However, differences in the amplitude and timing of re-synthesis (experimental: \sim 8 fold-initial at \sim 120 min; computational: 1.2-1.5 fold-initial at \sim 90 min) were observed and could be explained by dynamic differences between the endogenous I κ B α promoter and the synthetic κ B₅-TATA promoter driving I κ B α -FLuc (i.e., differences in binding affinity and cooperativity towards NF- κ B).

We next generated hypothetical IKK profiles representing IKK activities from preconditioned/challenged cells, assuming no upstream receptor or IKK regulation (i.e., experimentally-derived challenge-specific IKK activity were overlaid on top of experimentally-derived precondition-specific residual IKK activity). These hypothetical IKK activity profiles (Fig. 2.4B-E, left panels, each generated with a different P-C interval) were used as inputs for computing total I κ B α dynamics (Fig. 2.4B-E, right panels). Surprisingly, the computational model predicted that even in the absence of receptor dynamics or IKK regulation, I κ B α processing would be transiently

compromised (compare for example the second, challenge-induced degradation phase at 120 or 240 min with the ones at 30 or 60 min). These data suggested that although IKK down-regulation partially correlated with the ligand-induced transient refractory period for I κ B α processing, an additional regulatory mechanism was present downstream of IKK. Importantly, I κ B α availability *per se* was not sufficient to explain changes in I κ B α responsiveness because, as confirmed experimentally and computationally, at 60 min post-preconditioning, the I κ B α concentration had already recovered, while degradation potential was still low (compare Figs. 2.2A, 2.2C, Table 2.1 and 2.4C).

Nuclear export of I κ B α :NF- κ B complexes may also control the capacity of cells to process I κ B α . Having demonstrated experimentally the phenomenon of a ligand-induced transient refractory period for I κ B α processing and after dissecting biochemically and computationally the origins of this observation, we next sought to more closely examine the components of the computational model in order to identify candidates, downstream of IKK, capable of regulating I κ B α responsiveness. While examining the rate constants of a variety of reactions used by the model, we noticed that free vs. NF- κ B-bound I κ B α differed tremendously in their capacity to associate with IKK (1.35 vs. 11.1 $\mu\text{M}^{-1} \text{min}^{-1}$, respectively) and to be degraded in an IKK-dependant manner (0.12 vs. 0.00006 min^{-1} , respectively). These differences in IKK association and ligand-induced degradation were experimentally established by Zandi *et al.* [28].

This led us to put forward the following model (Fig. 2.5A): (1) free I κ B α and NF- κ B-bound I κ B α represent “protected” and “unprotected” populations with respect to ligand-induced, IKK-dependent proteasomal degradation. (2) Under steady-state conditions, there is a stoichiometric excess of I κ B α over NF- κ B in the cytoplasm (~ 0.7 NF- κ B per I κ B α according to the model). This may explain our observations that even at saturating concentrations of TNF α or IL-1 β , I κ B α degradation never exceeded 70-80% of initial (e.g., Fig. 2.1C). (3) Upon ligand stimulation, NF- κ B-bound I κ B α is degraded, NF- κ B translocates to the nucleus and I κ B α is resynthesized. (4) At this point, although I κ B α is highly abundant, its capacity to be degraded in response to a second stimulus is still severely compromised because NF- κ B is in the nucleus. (5) I κ B α can freely shuttle between the cytoplasm and the nucleus, pulling NF- κ B molecules (that lack nuclear export signals [29]) back to the cytoplasm. This step may be the rate limiting step for acquisition of full responsiveness. (6) Newly-synthesized I κ B α molecules uncomplexed with NF- κ B are rapidly degraded [30], and only after all NF- κ B molecules are recovered back to the cytosol and the NF- κ B-bound-I κ B α over free-I κ B α ratio returns to pre-stimulation levels (~ 0.7), are cells able to mount a full response again.

To experimentally examine the nuclear export hypothesis, we sought to analyze ligand-induced changes in cytoplasmic I κ B α :NF- κ B complexes. However, the computational model predicted that ligand-induced changes of cytoplasmic I κ B α :NF- κ B and total cytoplasmic NF- κ B were essentially the same (i.e., at any given time, virtually all cytoplasmic NF- κ B was bound to I κ B α , Fig. 2.5B), suggesting that monitoring

cytoplasmic total NF- κ B was an excellent approximation for following cytoplasmic I κ B α :NF- κ B complexes. We therefore pulsed HepG2 cells for 30 sec with TNF α (20 ng/mL) and at various times after stimulation, we fixed, permeabilized and immunostained the cells for p65 NF- κ B (Fig. 2.5C). We found that upon a 30 sec TNF α pulse, p65 rapidly translocated to the nucleus (maximal by 30 min), but by 60-120 min was back in the cytoplasm. The excellent temporal correlation between the levels of cytoplasmic NF- κ B (as derived computationally or experimentally, Fig. 2.5B and 5C, respectively) and the competence of cells to degrade I κ B α in response to a pro-inflammatory ligand (i.e., Table 2.1) strongly suggested that nuclear transport of NF- κ B provided a potential alternative mechanism to transiently desensitize I κ B α processing (refractory period), in addition to the mechanism of IKK down-regulation (Fig. 2.3B, C; Table 2.1).

2.3 DISCUSSION

Ligand-induced desensitization is a common theme in many biological systems [13], thereby allowing cells to mount an appropriate response independently of ligand exposure time. Thus, prolonged exposures will not result in excessive responses, but instead, cells are enabled to build up a downstream response, while being unable to perceive a second activating cue. Desensitization and re-sensitization are traditionally perceived to be linked to receptor dynamics (internalization, shedding and recycling),

however, any mediator or regulator along a signaling pathway can be hypothetically desensitized, therefore transiently blocking signal transduction [13].

In this work, we demonstrated that while cells can efficiently activate NF- κ B in response to a TNF α exposure as short as 30 sec, such stimulation was followed by a refractory period during which the capacity of cells to respond to a second homologous or heterologous stimulus was severely compromised. We further found that this transient refractory period correlated in part with a temporal down-regulation of IKK activity, but not with receptor desensitization. Computational modeling enabled us to identify an additional layer of regulation, downstream of IKK, controlling the capacity of cells to respond to a second challenge. Ligand-induced dynamic changes in substrate (I κ B α) availability, conformation and sub-cellular localization form the basis for this mechanism. Further analysis led us to conclude that nuclear export of NF- κ B may be a rate limiting step in controlling I κ B α homeostatic metabolism, a term recently coined by O'Dea et al. [31].

Our study highlights the multifaceted regulation of NF- κ B signaling (Fig. 2.6) and sheds light on the refractory nature of I κ B α processing as a route to transiently desensitize NF- κ B activity upon subsequent rounds of stimulation. Rapid and transient deactivation of IKK activity as well as temporal reduction in its capacity to respond to a subsequent challenge (IKK responsiveness) seems to play a crucial role in this process. Previous studies indicated that both the amplitude and the timing of IKK activation affect not only the intensity of NF- κ B-dependent transcription, but also the specificity of the transcriptional response [23, 32]. This indicated that besides resolution of the

inflammatory response and induction of a refractory period (temporally preventing subsequent rounds of I κ B α degradation upon re-stimulation), rapid down-regulation of IKK activity [26] plays a pivotal role in determining the type of elicited transcriptional program.

In addition to IKK regulation, our work demonstrated that nuclear export of I κ B α :NF- κ B complexes may have also regulated I κ B α responsiveness (Figs. 2.4 and 2.5). This suggested that NF- κ B positively controls I κ B α both transcriptionally and post-translationally. Such double-layered feedback regulation ensures that NF- κ B transcriptional activity will fully resume only after reconstitution of the cytosolic pool of NF- κ B. Two other I κ B isoforms, I κ B β and I κ B ϵ , are degraded more slowly under both TNF α -induced and unstimulated conditions [23, 33] and have been implicated in dampening I κ B α -mediated oscillations of NF- κ B activity [33-35]. I κ B ϵ has been shown to be highly NF- κ B inducible in MEFs, and contribute to nuclear export of NF- κ B, but only at times greater than 3 hrs post-stimulation [36]. Thus, it is seems unlikely that I κ B ϵ contributes substantially to the export of NF- κ B over the 2 hrs of the refractory period observed in the present study. It may be interesting to determine whether similar transient refractory periods exist for processing of other I κ B isoforms.

While TNF α -induced re-synthesis of endogenous I κ B α peaks at ~60-90 min post onset of stimulation (as validated both experimentally and computationally, Figs. 2.1D and 2.4A, respectively), maximum levels of newly-synthesized I κ B α -FLuc reporter were observed ~120 min after TNF α stimulation (Figs. 2.1C, 2.1E, and 2.2A). This

discrepancy may be explained by differences likely to be present in affinity and cooperativity of binding of NF- κ B to endogenous vs. synthetic promoters (the endogenous promoter contains 3 distant κ B sites, while the synthetic promoter contains 5 tandem high affinity κ B sites). Nevertheless, since both endogenous I κ B α and I κ B α -FLuc exhibit similar half-life times [20], differences in the timing of re-synthesis cannot be explained by differences in turnover rate. Following the peak of I κ B α re-synthesis, both endogenous I κ B α and our I κ B α -Fluc reporter begin returning to baseline levels faster under continuous TNF α treatment, suggesting that ligand-induced reactivation of I κ B α degradation is occurring under continuous TNF α exposure, as expected [23].

In the present and previous studies [20], we demonstrated that dynamic bioluminescence imaging of I κ B α -FLuc reporters in live cells provides robust and accurate readouts of ligand-induced I κ B α dynamics. In effect, real time bioluminescence imaging was equivalent to performing continuous on-line Western blots of I κ B α at five minute intervals. An analogous transcriptionally-coupled reporter (κ B $_5$ \rightarrow I κ B α -EGFP) was generated by Nelson *et al.* [34] for monitoring I κ B α dynamics in single cells by live-cell fluorescence microscopy. While such a system provides the means to monitor ligand-induced translocations and oscillations in I κ B α levels, temporal resolution of this reporter is limited by the long maturation time of EGFP (>1 h, [37, 38]). This notion, and the fact that Nelson *et al.* co-overexpressed p65-DsRed [34, 35] may explain the vast difference between the observed period of I κ B α -EGFP oscillations (~300 min) and the period of endogenous I κ B α oscillations, as predicted computationally (~90-120 min, [33]). While longer term I κ B α oscillatory behavior was not the focus of the present study,

we did observe single oscillations within ~150-180 min. Because FLuc is active immediately upon translation, our reporter should afford greater temporal resolution, enabling accurate readouts of I κ B α dynamics and oscillations in live cells for such studies as well as the multi-stimulation protocols as described herein.

Of note, a previous study aimed at analysis of I κ B α stabilization indicated a role for p38 in I κ B α stabilization, and in some cell lines, in prevention of sequential degradation of I κ B α upon concurrent exposure to TNF α following continuous pretreatment with IL-1 β [39]. However, since IL-1 β has been shown to induce rapid and dramatic down-regulation of TNF α receptors (but not *vice versa*) [14], inhibition of TNF α -induced I κ B α processing, as observed by Place *et al.*, could be attributed directly to receptor dynamics rather than I κ B α stabilization. This confounding factor highlights the importance of asymmetric receptor cross-desensitization, a phenomenon that remains poorly understood, but has far-reaching physiological consequences.

In conclusion, TNF α preconditioning protocols and dynamic imaging revealed a transient suppression of the capacity of cells to process I κ B α . This refractory period for I κ B α processing was controlled both by IKK activity and NF- κ B distribution. In particular, the data suggested that nuclear export of NF- κ B may provide additional rate-limiting regulation governing the refractory period machinery. These regulatory mechanisms provide a "molecular timer" controlling the amplitude, timing and specificity of the NF- κ B-mediated transcriptional program.

2.4 METHODS

Materials- D-luciferin (potassium salt) was from Biosynth (Naperville, IL). Human tumor necrosis factor α (TNF α) and interleukin-1 β (IL-1 β) were from R&D systems (Minneapolis, MN). Complete protease inhibitors cocktail was from Roche (Basel, Switzerland). ^{32}P - $5'$ -adenosine triphosphate (^{32}P -ATP) was from Perkin-Elmer (Waltham, MA). Carbenicillin, isopropyl β -D-1-thiogalactopyranoside (IPTG), ampicillin, kanamycin, glutathione S-transferase (GST), β -glycerolphosphate, NaCl, NaF, Na_3VO_4 , KOH, MgCl_2 , ethylenediaminetetraacetic acid (EDTA), phenylmethylsulfonyl fluoride (PMSF), NP-40, Tween-20, Triton X-100, ATP, dithiothreitol (DTT), paraformaldehyde, cycloheximide (CHX) and HEPES were from Sigma-Aldrich (St. Louis, MO).

Plasmids- p $\kappa\text{B}_5 \rightarrow \text{FLuc}$ (Stratagene, La Jolla, CA) contains five repeats of a κB motif upstream of a minimal TATA box controlling expression of firefly luciferase. p $\kappa\text{B}_5 \rightarrow \text{I}\kappa\text{B}\alpha\text{-FLuc}$ was produced by cloning an *EcoRI* – *HpaI* (blunt) fragment from pCMV $\rightarrow \text{I}\kappa\text{B}\alpha\text{-FLuc}$ [20] into the *EcoRI* and *EcoRV* (blunt) sites of p $\kappa\text{B}_5 \rightarrow \text{FLuc}$. p $\kappa\text{B}_5 \rightarrow \text{FLuc}$, pCMV $\rightarrow \text{I}\kappa\text{B}\alpha\text{-FLuc}$ and p $\kappa\text{B}_5 \rightarrow \text{I}\kappa\text{B}\alpha\text{-FLuc}$ were propagated in TOP10 electrocompetent *E. Coli* (Invitrogen, Carlsbad, CA) and purified using Qiagen HiSpeed Maxi Kits (Qiagen, Valencia, CA). pGST-I $\kappa\text{B}\alpha\text{N}$ (encoding for GST fused to the N-terminal fragment of human I $\kappa\text{B}\alpha$ (1-54)) was a kind gift from Prof. Alexander Hoffmann (UCSD, San Diego, CA). pGST-I $\kappa\text{B}\alpha\text{N}$ was propagated in BL21 codon⁺ *E. Coli* cells (Stratagene).

Cells and Transfections- HepG2 human hepatoma cells were from the American Type Culture Collection (ATCC, Manassas, VA). Cells were cultured in DMEM supplemented with heat-inactivated FBS (10%) and L-glutamine (2 mM). Cell cultures were grown at 37°C in a

humidified atmosphere of 5% CO₂. HepG2 cells (10⁵) were transiently transfected (Fugene 6, Roche) with pκB₅→IκBα-FLuc (200 ng/well) and plated in black-coated 24-well plates (*In Vitro* Systems GmbH, Gottingen, Germany). Cells were then allowed to recover for 48 h prior to imaging.

Dynamic Bioluminescence live-cell imaging- Prior to imaging, cells were washed with pre-warmed phosphate-buffered saline (PBS, pH 7.4) and placed into 900 μL of colorless HEPES-buffered DMEM, supplemented as above and with D-luciferin (150 μg/mL). Cells were allowed to equilibrate for 1 hour (37°C) before proceeding with ligand stimulation and imaging. Four different stimulation regimens were included in this study:

(1) **Continuous TNFα (C):** TNFα (final concentration 20 ng/mL) or vehicle (colorless DMEM) was added (100 μL) to D-luciferin-containing DMEM and imaging was performed before, and at the indicated time points after addition of TNFα.

(2) **TNFα Pulse (30 sec, P):** cells were pulsed for 30 sec with TNFα (20 ng/mL) or vehicle, washed with PBS, returned to D-luciferin-containing DMEM and imaged before, and at the indicated time points after the pulse of TNFα.

(3) **TNFα Preconditioning (30 sec pulse) followed by Continuous TNFα challenge (P+C):** At t₀ cells were pulsed for 30 sec with TNFα (20 ng/mL) or vehicle, washed with PBS, returned to D-luciferin-containing DMEM (900 μL) and imaged before, and at the indicated time points after the pulse of TNFα. At t_x, TNFα (final concentration 20 ng/mL) or vehicle (colorless DMEM) were again added (100 μL) and imaging was performed before, and at the indicated time points after addition of TNFα.

(4) TNF α Preconditioning (30 sec pulse) followed by Continuous IL-1 β challenge (P+C): As in (3), but continuous challenge was performed with IL-1 β (10 ng/mL).

TNF α or IL-1 β challenge was performed at the following time points: $t_x = 0$ (no preconditioning), 30, 60, 120 and 240 min post preconditioning. Assay plates were imaged using an IVIS-100 imaging system (Xenogen Caliper, Alameda, CA). Acquisition parameters were as follows: acquisition time, 60 sec; binning, 4; FOV, 10 cm; f/stop, 1; filter, open; image-image interval, 5 min; number of acquisitions, 73 (360 min).

To analyze ligand-induced regulation of *de novo* reporter re-synthesis, cells were pretreated with cycloheximide (100 μ g/mL) for 1 hour before continuous stimulation with TNF α and bioluminescence imaging (as above).

I κ B α Responsiveness Assays- HepG2 cells, transfected with p κ B $_5$ →I κ B α -FLuc (as above) or HeLa cells, stably expressing pCMV→I κ B α -FLuc [20], were plated in 4 wells of a six-well plate (one plate per time point) and grown for 48 hours. At t_0 , all wells were washed with pre-warmed PBS, pulsed for 30 sec with TNF α (20 ng/mL, 1 mL) or vehicle (PBS), washed again with PBS, returned to regular medium (1 mL) and placed in a 37°C incubator. This procedure was defined as TNF α preconditioning (P). At t_x , two wells were treated (continuously) with TNF α (20 ng/mL) and two wells were treated with vehicle only (PBS). This procedure was defined as TNF α challenge (C). Following this TNF α challenge, cells were returned to the incubator. At $t_x + 25$ min (time of maximal I κ B α degradation [20]; see Fig. 2.2A for schematic timeline), cells were harvested (by scraping) in reporter lysis buffer (Promega, Madison, WI). Cell lysates were normalized for protein content by bicinchoninic acid (BCA) protein assay (Promega), aliquoted and frozen (-80 °C) for *in vitro* bioluminescence and Western blot analyses (see below). For *in*

in vitro bioluminescence assays, lysates (10 μ L, in triplicate) were mixed with luciferase assay buffer (190 μ L; HEPES, 25 mM; NaCl, 154 mM; MgSO₄, 5.4mM; DTT, 10 mM; ATP, 5 mM; D-luciferin, 150 μ g/mL; pH 8.0) in a 96-well plate immediately prior to imaging. Assay plates were imaged using the IVIS-100 (acquisition time, 10 sec; binning, 4; FOV, 10 cm; f/stop, 1; filter, open).

Western Blot Analyses- Whole-cell lysates were resolved by 10% or 7.5% SDS-PAGE, transferred to a PVDF membrane and probed for the indicated proteins using standard immunoblotting techniques. Primary antibodies against total human I κ B α , β -actin and IKK α were from Santa Cruz Biosciences (Santa Cruz, CA). Anti-phospho-I κ B α (Ser 32/36) was from Cell Signaling Technologies (Danvers, MA). Secondary horseradish peroxidase-labeled anti-mouse and anti-rabbit IgG antibodies were from GE Healthcare Biosciences (Piscataway, NJ).

IKK Kinase Assay (IKK-KA)- IKK-KA reactions were carried out as per Werner *et al* [23] and quantified in a medium-throughput manner as per Hastie *et al* [40]. Briefly, HepG2 cells were grown in 10 cm tissue culture dishes to confluency. Cells were then washed in PBS (once) and treated with 20 ng/mL TNF α using three different treatment regimens: P, C or P+C (see above). To capture the full IKK activity profiles of cells treated with continuous (C) or pulse (P) regimens, cytosolic extracts were prepared at t = 0 (before), 5, 10, 15, 30, 60, 120, or 240 min post TNF α treatment. To capture maximal IKK activity of P+C-treated cells, cytosolic extracts were prepared 10 min post TNF α challenge (given at 10, 30, 60, 120 and 240 min post preconditioning). Cells were harvested by removing media, washing in ice-cold PBS + EDTA (1 mM), scraping, and pelleting at 2000 g. To prepare cytosolic extracts, cell pellets were resuspended in 200 μ L of CE Buffer (10 mM HEPES-KOH, pH 7.9, 250 mM NaCl, 1 mM

EDTA, 0.5% NP-40, 0.2% Tween 20, 2 mM DTT, 20 mM β -glycerophosphate, 10 mM NaF, and 0.1 mM Na_3VO_4 supplemented with complete protease inhibitor cocktail), incubated on ice (2 min), vortexed (1 min), and pelleted at 2000 g. Supernatants were collected, normalized for protein content by Bradford Assay (Pierce, Rockford, IL) and stored at -80°C . To immunoprecipitate IKK complexes, cytoplasmic extracts (100 μL) were incubated with anti-IKK γ antibody (15 μL , overnight, 4°C with rotation) and then with Protein G 4FF bead slurry (20 μL , 50% (v/v)). Beads were pelleted at 4600 RPM, washed twice with CE Buffer (500 μL) and once with Kinase Buffer (500 μL , 20 mM HEPES, pH 7.7, 20 mM β -glycerophosphate, 100 mM NaCl, 0.1 mM Na_3VO_4 , 10 mM MgCl_2 , 2 mM DTT supplemented with complete protease inhibitor cocktail). For the IKK kinase reaction, beads were incubated for 30 min at 30°C in Kinase Buffer (20 μL) containing 20 μM ATP, 10 μCi ^{32}P -ATP, and 0.5 μg GST-I κ B α (1–54). Beads were removed by centrifugation (4600 RPM) and 15 μL of each reaction supernatant was spotted onto a 1 cm^2 square of P81 phosphocellulose paper (Millipore, Billerica, MA) and immediately immersed into phosphoric acid (75 mM) for 5 min. Phosphoric acid washes were performed two more times, papers were rinsed in acetone, and then allowed to dry. Each paper was transferred to a scintillation vial and radioactivity was determined on a beta counter (Beckman Coulter, Fullerton, CA). Blank and no-lysate controls were subtracted from the experimental samples. Data were represented as fold-initial (untreated controls).

Calculating Ligand-Dependent IKK Responsiveness- IKK responsiveness profiles (i.e., the net kinase capacity of IKK in response to a second challenge of $\text{TNF}\alpha$, as a function of time after initial 30 sec preconditioning) were calculated numerically from IKK-KA data using the following formula:

$$IKK \text{ Responsiveness} = \frac{PC_{x+10} - P_{x+10}}{PC_0 \left(\frac{C_{10}}{C_0}\right)}$$

where PC_{x+10} is IKK activity of preconditioned+challenged cells, as recorded 10 minutes post challenge. P_{x+10} is the residual IKK activity of preconditioned, but un-challenged cells at this exact time point. C_0 and PC_0 are initial IKK activities of challenged but un-preconditioned, and fully preconditioned and challenged cells, respectively. C_{10} is the maximal IKK activity of challenged but un-preconditioned cells (recorded 10 minutes post challenge). Note that while all parameter units in the nominator and denominator are in c.p.m., IKK responsiveness is dimensionless, similar to $I\kappa B\alpha$ responsiveness.

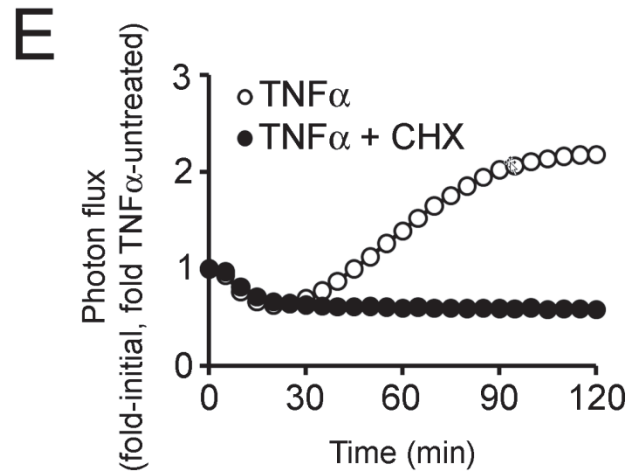
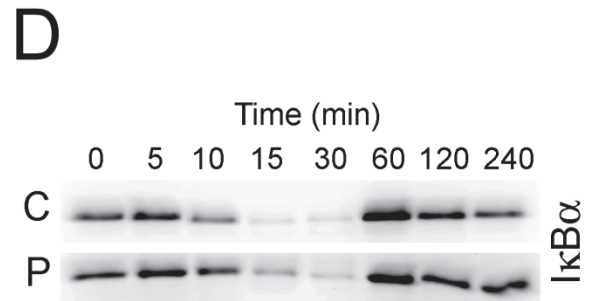
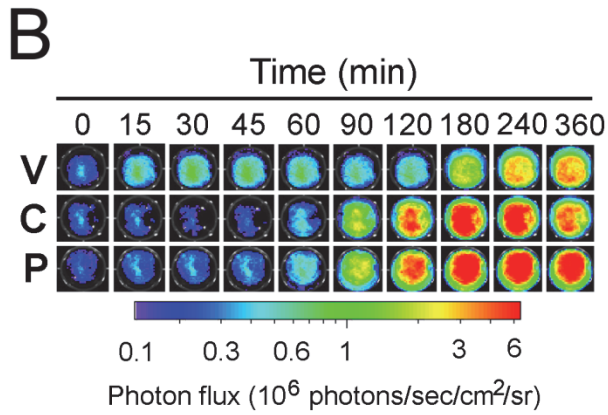
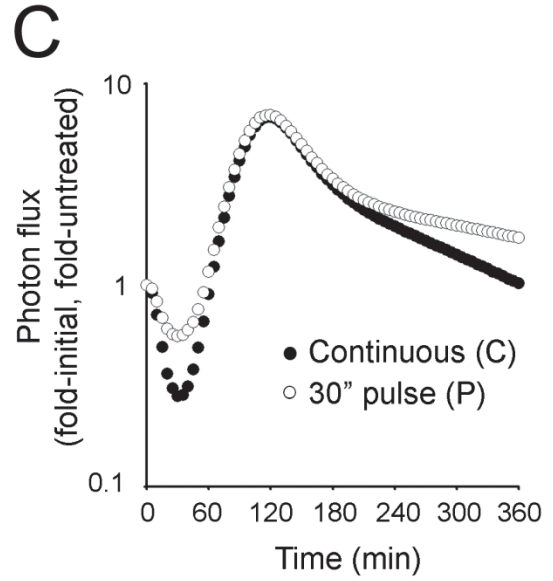
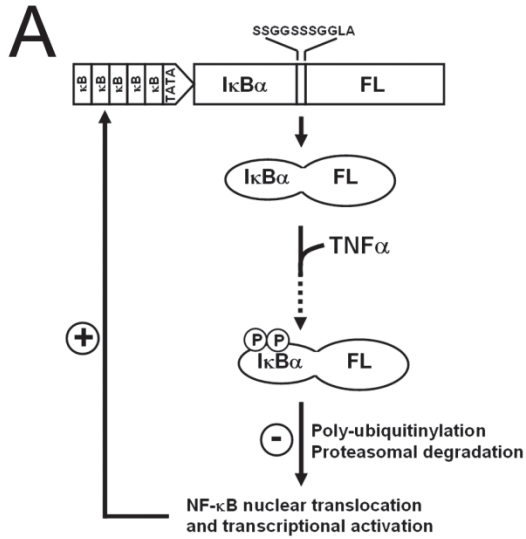
Computational Simulations- To simulate the dynamics of major regulators on the IKK-NF- κ B axis, we used a well-established computational model generated by Hoffmann et al. [33] and refined by Werner et al. [23]. Briefly, an experimentally- or hypothetically-derived IKK activity profile was fed into the program as an input. Embedded in the model were 24 components, 70 reactions and 70 parameters or rate constants for these reactions. Differential equations were solved numerically using Matlab 7.0 (Mathworks, Natick, MA) with subroutine *Ode15*. Interpolated and extrapolated (0-360 min at 5 min intervals) IKK activity profiles were calculated (Origin version 7.5, OriginLab, Northhampton, MA) from experimental IKK-KA data (see above). To fit the model, initial steady-state IKK activity (i.e., intracellular concentration of active IKK) was set to be 1 nM. To computationally simulate $I\kappa B\alpha$ dynamics of cells challenged at different times after initial preconditioning, when assuming no upstream IKK or receptor

regulation, we used hypothetical IKK activity profiles as inputs, derived from superimposing experimentally-acquired IKK activity profiles of 30 sec-pulsed and continuously-treated cells, at increasing intervals (30, 60, 120 and 240 min, see Fig 4, black lines).

Immunofluorescence Microscopy- HepG2 cells were seeded into 35 mm glass bottom culture dishes (MatTek Corp.; Ashland, MA) and grown to ~40% confluency. Cells were pulsed for 30 sec with TNF α as above and fixed at the indicated time points (by washing once with PBS, followed by fixation (4% paraformaldehyde for at least 15 min) and permeabilization (ice cold methanol, 10 min at -20°C)). Cells were washed in PBS, blocked in 5% normal goat serum in 0.3% Triton X-100/PBS (1 hour), and then incubated with anti-p65 antibody (Santa Cruz, 1:200 in 0.3% Triton X-100/PBS at 4°C, overnight with rocking). Cells were next incubated with AlexaFluor 635-conjugated goat anti-rabbit antibody (Invitrogen, 1:200 in 0.3% Triton X-100/PBS, 90 min, at room temperature with rocking). Cells were washed three times with PBS before being mounted with VECTASHIELD Mounting Media (Vector Laboratories; Burlingame, CA). Confocal images were captured using the 40x objective (water immersion) on a Zeiss Axiovert 200 (Zeiss, Thornwood, NY) laser scanning microscope equipped with the appropriate filter sets and analyzed using Zeiss LSM Image Browser and Adobe Photoshop CS2.

2.5 FIGURES

Figure 2.1: $\text{p}\kappa\text{B}_5 \rightarrow \text{I}\kappa\text{B}\alpha\text{-FLuc}$: a transcriptionally-coupled reporter for monitoring $\text{I}\kappa\text{B}\alpha$ dynamics in live cells. *A.* A schematic representing ligand-induced degradation and transcriptionally-coupled re-synthesis of the reporter. *B.* Raw bioluminescence images of HepG2 cells transiently expressing $\text{p}\kappa\text{B}_5 \rightarrow \text{I}\kappa\text{B}\alpha\text{-FLuc}$ treated with $\text{TNF}\alpha$ (20 ng/mL) continuously (C) or as a 30 sec pulse (P) or with vehicle only (V) and imaged for 360 min. Images show pseudocolor-coded photon flux maps superimposed on black-and-white photographs of the assay plate. *C.* Graphical representation of the changes in photon flux from (b) as a function of time after $\text{TNF}\alpha$ addition. Data are plotted as fold-initial, fold-vehicle-treated ($n=3$ for all points; s.e.m. $\leq 5\%$; representative of 3 independent experiments). *D.* Western blot analysis of endogenous $\text{I}\kappa\text{B}\alpha$ from HepG2 cell lysates prepared at the indicated times after a 30 sec-pulse or continuous treatment with $\text{TNF}\alpha$ (20 ng/mL). *E.* Pretreatment with cycloheximide (CHX, 1 h, 100 $\mu\text{g}/\text{mL}$) totally abrogated $\text{TNF}\alpha$ -induced $\text{I}\kappa\text{B}\alpha\text{-FLuc}$ re-synthesis, but had no effect on reporter degradation.



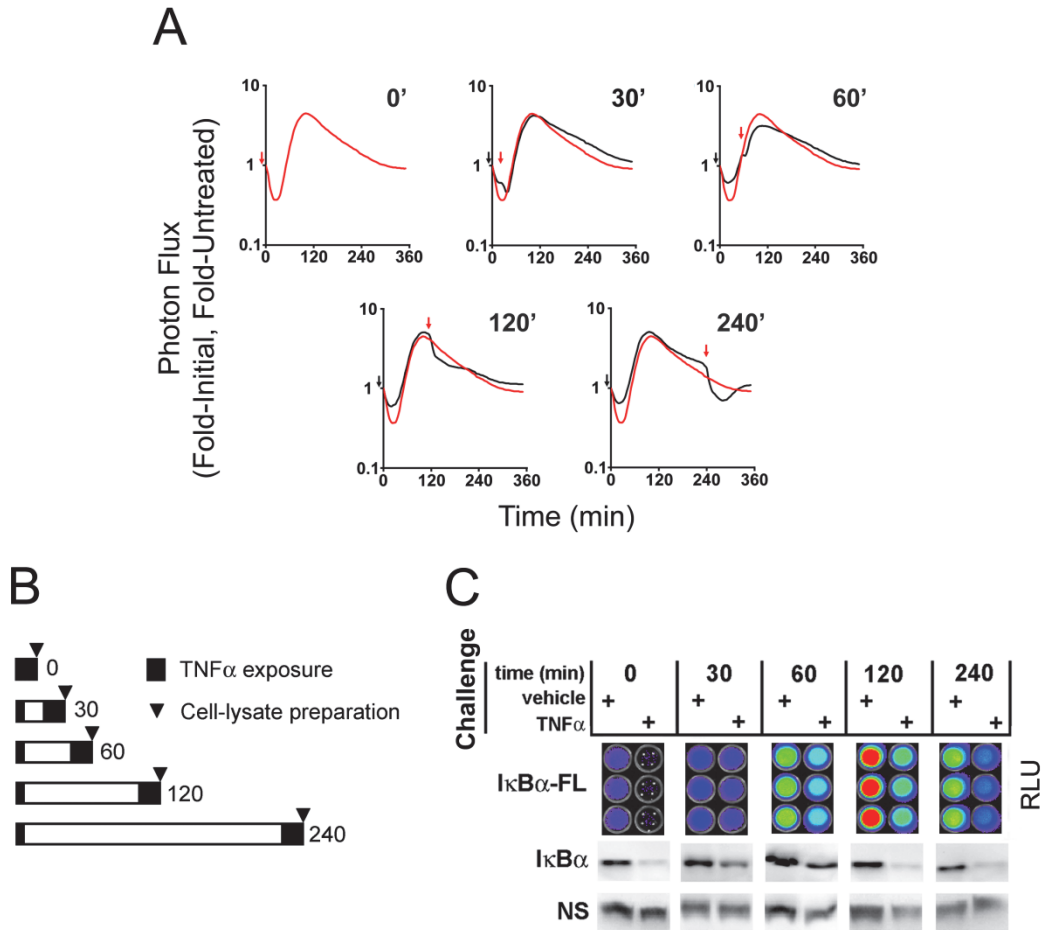


Figure 2.2: TNF α -induced a transient refractory period for I κ B α processing. *A.* Dynamic live-cell bioluminescence imaging profiles of I κ B α -FLuc from TNF α preconditioning+challenge experiments. Black arrows denote 30 sec preconditioning pulse; red arrows denote the beginning of continuous TNF α challenge; black profiles represent cells pre-conditioned and then challenged at the indicated time points; red profiles represent cells treated at time 0 with continuous TNF α (denoting the maximal possible degradation response of I κ B α upon continuous TNF α treatment). Data are presented as fold-initial, fold-TNF α -untreated. *B.* Schematic representation of the experimental timeline as used in *c.* Cells were preconditioned with TNF α for 30 sec and then, at increasing intervals (0-240 min), were continuously challenged with TNF α . Arrowheads represent when cells were harvested and lysates prepared (25 min post challenge for quantitative bioluminescence imaging and Western blot analysis). *C.* I κ B α -Fluc and endogenous I κ B α levels, 25 min post TNF α or vehicle challenge, as measured by bioluminescence imaging and Western blot, respectively.

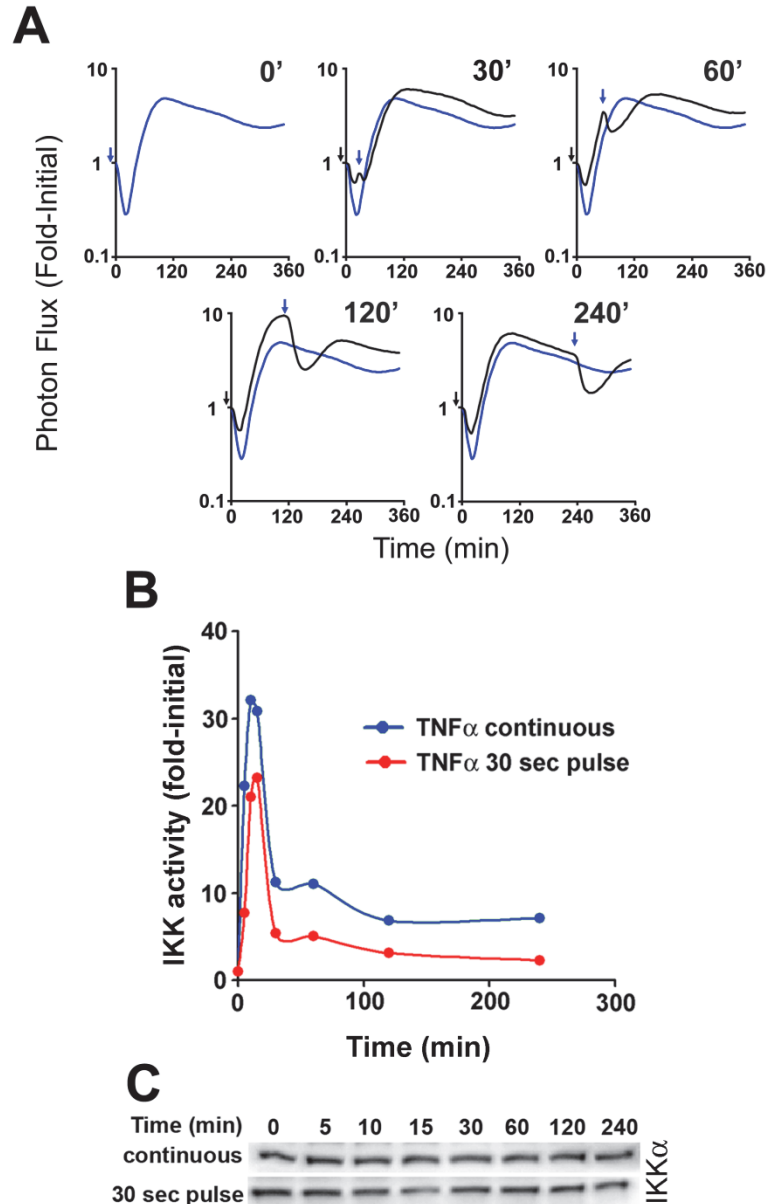


Figure 2.3: Impact of receptor dynamics and IKK regulation on I κ B α responsiveness. *A.* Dynamic live-cell bioluminescence imaging profiles of I κ B α -FLuc from TNF α preconditioning, IL-1 β challenge experiments. Black arrows denote 30 sec preconditioning pulse of TNF α ; blue arrows denote the beginning of continuous IL-1 β (10 ng/mL) challenge; black profiles represent cells pre-conditioned and then challenged with IL-1 β at the indicated time points; blue profiles represent cells treated at time 0 with continuous IL-1 β (denoting the maximal possible degradation response of I κ B α upon continuous IL-1 β treatment). Data are presented as fold-initial. *B.* IKK kinase activity was measured at the indicated time points after initiation of a continuous (blue curve) or a 30 sec pulse (red curve) of TNF α (20 ng/mL). Results are presented as background-normalized, fold-initial (untreated) controls. *C.* Western blot analysis of IKK α in cytoplasmic fractions, used as inputs for immunoprecipitation and kinase reactions presented in (b).

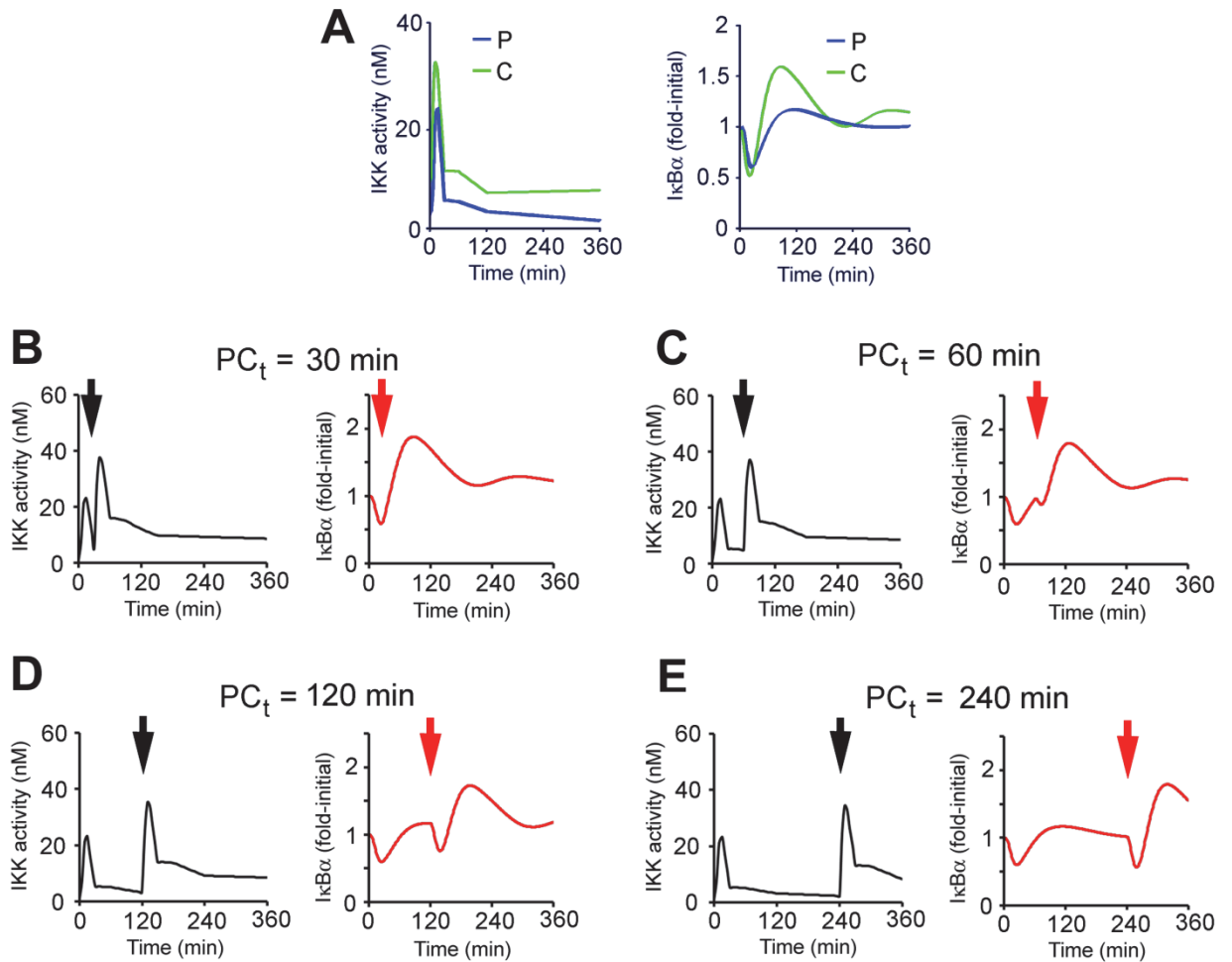


Figure 2.4: Computational simulation of IκBα responsiveness in the absence of upstream receptor or IKK regulation. *A.* Interpolated and extrapolated (0-360 min, at 5 min intervals) IKK activity profiles (right panel) of cells treated continuously (C, green curve) or by a 30 sec pulse (P, blue curve) of TNFα (20 ng/mL) were used as inputs to computationally simulate total IκBα dynamics (right panel). *B-E.* Left panels: Hypothetical IKK activity profiles of preconditioned cells, challenged at the indicated times (denoted by black arrowheads) with a second, continuous dose of TNFα were generated by superimposing the continuous TNFα-induced IKK profiles at increasing intervals after the 30 sec pulse TNFα-induced IKK profile. For generating these hypothetical profiles, we assume no preconditioning-induced receptor or IKK regulation. Right panels: The hypothetical IKK profiles were used as inputs into the model to predict IκBα dynamics. Note that challenge-induced IκBα degradation (initiated at the red arrowhead) is recovered in a time-dependent manner.

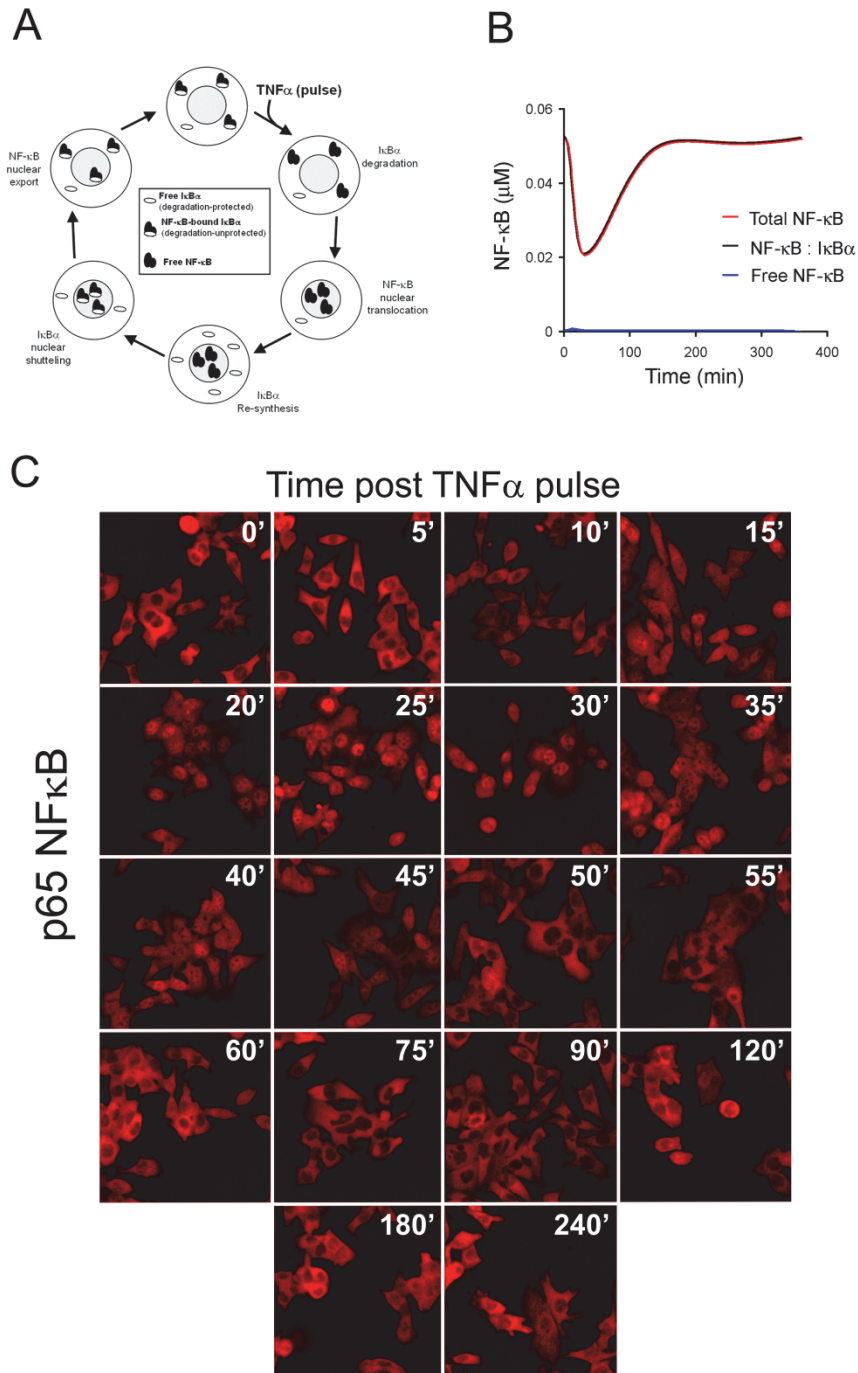


Figure 2.5: Nuclear export of NF- κ B may regulate I κ B α sensitivity to ligand-induced degradation. *A.* A schematic illustrating sub-cellular localization and levels of free I κ B α , free NF- κ B, and NF- κ B-bound I κ B α in response to a pulse of TNF α . *B.* Computationally-predicted profile of all *cytoplasmic* populations of NF- κ B following a pulse of TNF α . Note the exceeding small free NF- κ B population. *C.* HepG2 cells were stimulated with a 30 sec TNF α pulse. At the indicated time points, cells were fixed, permeabilized and immunostained for p65 NF- κ B. Shown are representative immunofluorescence confocal photomicrographs.

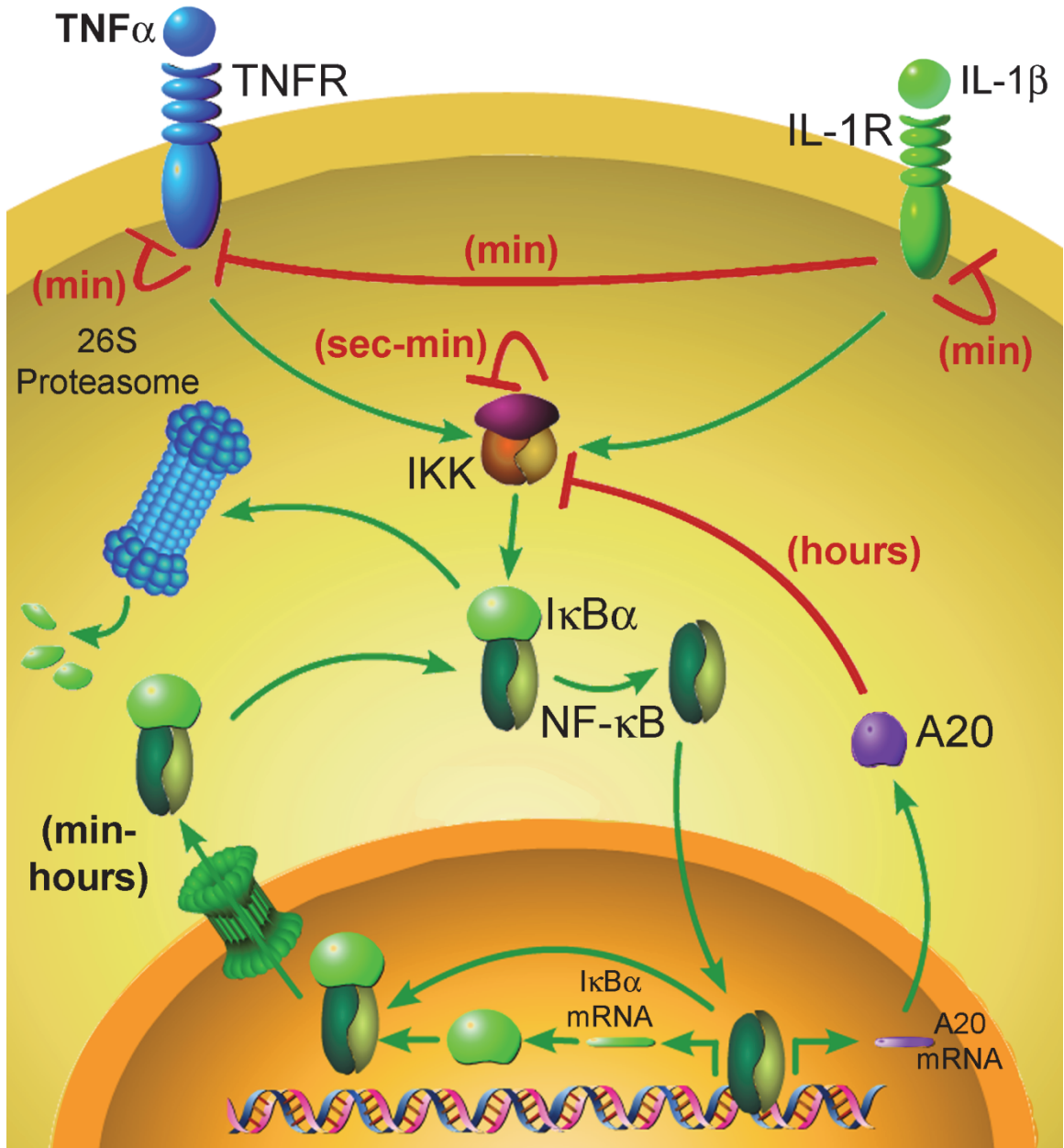


Figure 2.6: Refractory period in NF- κ B signaling. Schematic representation of the different ligand-induced autoregulatory mechanisms that control responsiveness in the NF- κ B signaling pathway.

2.6 TABLES

	Time after TNFα Preconditioning (min)			
	30'	60'	120'	240'
I κ B α (Western blot)	49%	80%	100%	82%
I κ B α -FLuc (bioluminescence)	43%	74%	90%	94%
IKK Activity	35%	56%	75%	69%

Table 2.1: Percent Responsiveness of I κ B α Processing

Quantification of I κ B α -FLuc and I κ B α responsiveness to a second continuous challenge of TNF α at the indicated interval following a 30 sec preconditioning pulse of TNF α was determined from the bioluminescence imaging and Western blot data shown in Figure 2C. Responsiveness at each challenge time was calculated by determining the percent of challenge-specific I κ B α degradation divided by the percent of I κ B α degradation in unpreconditioned cells from the same plate. The responsiveness of IKK was determined by IKK kinase assay.

2.7 REFERENCES

1. Han, J. and R.J. Ulevitch, *Limiting inflammatory responses during activation of innate immunity*. Nat Immunol, 2005. **6**(12): p. 1198-205.
2. Winsauer, G. and R. de Martin, *Resolution of inflammation: intracellular feedback loops in the endothelium*. Thromb Haemost, 2007. **97**(3): p. 364-9.
3. Hoffmann, A. and D. Baltimore, *Circuitry of nuclear factor kappaB signaling*. Immunol Rev, 2006. **210**: p. 171-86.
4. Perkins, N.D., *Integrating cell-signalling pathways with NF-kappaB and IKK function*. Nat Rev Mol Cell Biol, 2007. **8**(1): p. 49-62.
5. Karin, M. and F.R. Greten, *NF-kappaB: linking inflammation and immunity to cancer development and progression*. Nat Rev Immunol, 2005. **5**(10): p. 749-59.
6. Karin, M., *Nuclear factor-kappaB in cancer development and progression*. Nature, 2006. **441**(7092): p. 431-6.
7. Hayden, M.S. and S. Ghosh, *Signaling to NF-kappaB*. Genes Dev, 2004. **18**(18): p. 2195-224.
8. Bunting, K., et al., *Genome-Wide Analysis of Gene Expression in T Cells to Identify Targets of the NF- κ B Transcription Factor c-Rel*. J Immunol, 2007. **178**(11): p. 7097-109.
9. Naamane, N., J. van Helden, and D.L. Eizirik, *In silico identification of NF-kappaB-regulated genes in pancreatic beta-cells*. BMC Bioinformatics, 2007. **8**: p. 55.
10. Kim, H.J., N. Hawke, and A.S. Baldwin, *NF-kappaB and IKK as therapeutic targets in cancer*. Cell Death Differ, 2006. **13**(5): p. 738-47.
11. Karin, M., et al., *NF-kappaB in cancer: from innocent bystander to major culprit*. Nat Rev Cancer, 2002. **2**: p. 301-310.
12. Karmann, K., et al., *Activation and homologous desensitization of human endothelial cells by CD40 ligand, tumor necrosis factor, and interleukin 1*. J Exp Med, 1996. **184**(1): p. 173-82.
13. Alberts, B., Bray, D., Lewis, J., Raff, M., Roberts, K. and Watson, J.D., *Target-Cell Adaptation*, in *Molecular Biology of the Cell*. 1994, Garland Publishing: New-York. p. 771-785.
14. Holtmann, H. and D. Wallach, *Down regulation of the receptors for tumor necrosis factor by interleukin 1 and 4 beta-phorbol-12-myristate-13-acetate*. J Immunol, 1987. **139**(4): p. 1161-7.
15. Delhase, M., et al., *Positive and negative regulation of IkappaB kinase activity through IKKbeta subunit phosphorylation*. Science, 1999. **284**(5412): p. 309-13.
16. Prajapati, S., et al., *Protein phosphatase 2Cbeta association with the IkappaB kinase complex is involved in regulating NF-kappaB activity*. J Biol Chem, 2004. **279**(3): p. 1739-46.
17. Trinchieri, G. and A. Sher, *Cooperation of Toll-like receptor signals in innate immune defence*. Nat Rev Immunol, 2007. **7**(3): p. 179-90.
18. Gloire, G., S. Legrand-Poels, and J. Piette, *NF-kappaB activation by reactive oxygen species: fifteen years later*. Biochem Pharmacol, 2006. **72**(11): p. 1493-505.

19. Blanque, R., et al., *Selective enhancement of LPS-induced serum TNF-alpha production by carrageenan pretreatment in mice*. Gen Pharmacol, 1998. **31**(2): p. 301-6.
20. Gross, S. and D. Piwnica-Worms, *Real-time imaging of ligand-induced IKK activation in intact cells and in living mice*. Nat Methods, 2005. **2**: p. 607-614.
21. Nejjari, M., et al., *alpha6beta1 integrin expression in hepatocarcinoma cells: regulation and role in cell adhesion and migration*. Int J Cancer, 1999. **83**(4): p. 518-25.
22. Wullaert, A., et al., *Hepatic tumor necrosis factor signaling and nuclear factor- κ B: effects on liver homeostasis and beyond*. Endocr Rev, 2007. **28**(4): p. 365-86.
23. Werner, S.L., D. Barken, and A. Hoffmann, *Stimulus specificity of gene expression programs determined by temporal control of IKK activity*. Science, 2005. **309**(5742): p. 1857-61.
24. Higuchi, M. and B.B. Aggarwal, *TNF induces internalization of the p60 receptor and shedding of the p80 receptor*. J Immunol, 1994. **152**(7): p. 3550-8.
25. Dri, P., et al., *TNF-Induced shedding of TNF receptors in human polymorphonuclear leukocytes: role of the 55-kDa TNF receptor and involvement of a membrane-bound and non-matrix metalloproteinase*. J Immunol, 2000. **165**(4): p. 2165-72.
26. Cheong, R., et al., *Transient IkappaB kinase activity mediates temporal NF-kappaB dynamics in response to a wide range of tumor necrosis factor-alpha doses*. J Biol Chem, 2006. **281**(5): p. 2945-50.
27. Liu, Y.C., J. Penninger, and M. Karin, *Immunity by ubiquitylation: a reversible process of modification*. Nat Rev Immunol, 2005. **5**(12): p. 941-52.
28. Zandi, E., Y. Chen, and M. Karin, *Direct phosphorylation of IkappaB by IKKalpha and IKKbeta: discrimination between free and NF-kappaB-bound substrate*. Science, 1998. **281**(5381): p. 1360-3.
29. Huxford, T., et al., *The crystal structure of the IkappaBalpha/NF-kappaB complex reveals mechanisms of NF-kappaB inactivation*. Cell, 1998. **95**(6): p. 759-70.
30. Pando, M.P. and I.M. Verma, *Signal-dependent and -independent degradation of free and NF-kappa B-bound IkappaBalpha*. J Biol Chem, 2000. **275**(28): p. 21278-86.
31. O'Dea, E.L., et al., *A homeostatic model of IkappaB metabolism to control constitutive NF-kappaB activity*. Mol Syst Biol, 2007. **3**: p. 111.
32. Covert, M.W., et al., *Achieving stability of lipopolysaccharide-induced NF-kappaB activation*. Science, 2005. **309**(5742): p. 1854-7.
33. Hoffmann, A., et al., *The IkappaB-NF-kappaB signaling module: temporal control and selective gene activation*. Science, 2002. **298**(5596): p. 1241-5.
34. Nelson, D.E., et al., *Oscillations in NF-kappaB signaling control the dynamics of gene expression*. Science, 2004. **306**(5696): p. 704-8.
35. Barken, D., et al., *Comment on "Oscillations in NF-kappaB signaling control the dynamics of gene expression"*. Science, 2005. **308**(5718): p. 52.
36. Kearns, J.D., et al., *IkappaBepsilon provides negative feedback to control NF-kappaB oscillations, signaling dynamics, and inflammatory gene expression*. J Cell Biol, 2006. **173**(5): p. 659-64.

37. Sniegowski, J.A., et al., *Base catalysis of chromophore formation in Arg96 and Glu222 variants of green fluorescent protein*. J Biol Chem, 2005. **280**(28): p. 26248-55.
38. Zhang, L., et al., *Reaction progress of chromophore biogenesis in green fluorescent protein*. J Am Chem Soc, 2006. **128**(14): p. 4766-72.
39. Place, R.F., D. Haspeslagh, and C. Giardina, *Induced stabilization of IkappaBalpha can facilitate its re-synthesis and prevent sequential degradation*. J Cell Physiol, 2003. **195**(3): p. 470-8.
40. Hastie, C.J., H.J. McLauchlan, and P. Cohen, *Assay of protein kinases using radiolabeled ATP: a protocol*. Nat Protoc, 2006. **1**(2): p. 968-71.

CHAPTER THREE

Synchronicity of the $\text{I}\kappa\text{B}\alpha$:NF- κB Negative Feedback Loop *In Cellulo* and *In Vivo*

3.1 INTRODUCTION

Cells have evolved complex signaling networks that sense cues from the environment and transduce this information to elicit appropriate biological responses [1]. These networks equip cells with sensitive, reversible, regulated, and robust responses to a variety of signaling activators; in particular, these networks can confer on cells the ability to distinguish weak signals from background noise with high precision and selectivity [2, 3]. The NF- κB signaling pathway and its downstream transcriptional targets are responsive to a large number of different stimuli [4], and recent work has focused on NF- κB pathway responsiveness to the *mode* of stimulation (i.e., stimulus concentration, pulse duration, or pulse interval). Particularly relevant during cellular responses are inflammatory cytokines, such as TNF α , which are likely perceived as transient pulses or waves of TNF α occurring over a wide range of concentrations [5-10].

The transcription factor NF- κB is a pivotal regulator of innate immunity and inflammation, and is active in both immune cells and non-immune tissues [11, 12]. In this capacity, the NF- κB pathway must rapidly decode signals and integrate intracellular information to control individual cell fate decisions (proliferation, apoptosis, differentiation, etc.) and regulate the production and secretion of cytokines that can

amplify and propagate the inflammatory response [13, 14]. NF- κ B dimers are typically sequestered and held inactive in the cytoplasm through binding to isoforms of the I κ B family, with I κ B α representing the prototypical member and major regulator of canonical NF- κ B activity. TNF α -induced stimulation of NF- κ B relies on activation of the I κ B kinase complex (IKK), which phosphorylates I κ B α , marking it for subsequent ubiquitination and proteasomal degradation [4]. This series of events liberates NF- κ B, allowing it to undergo nuclear translocation and activation of target gene expression, including the I κ B α gene itself [15], thus establishing a critical transcriptionally-coupled negative feedback loop (Fig. 1A, [16]). Recently, NF- κ B has emerged as a mechanistic link between inflammation and cancer [17, 18]. This has been extensively studied in the liver where hepatocellular carcinoma (HCC) slowly unfolds on a background of chronic inflammation (often triggered by exposure to infectious agents or toxic compounds) [19]. TNF α -induced activation of NF- κ B signaling plays a pivotal role in liver homeostasis and pathophysiology due to its capacity to induce both hepatocyte cell death and proliferation [20, 21]. In the liver, NF- κ B signaling can have both tumor promoting and tumor suppressing effects that are dependent upon the type of cells (i.e., liver resident macrophages vs. hepatocytes), the stimuli, and cell context [19, 22, 23]. Thus, a more in-depth understanding of the complexities and intricacies of NF- κ B signaling in the liver is required to appropriately translate the use of NF- κ B-targeted therapeutics to liver pathologies.

Because of its biological importance, the NF- κ B pathway has emerged as an exemplary proving ground for systems biology approaches that couple computational modeling and cellular imaging with conventional cell biology methods to study dynamic

NF- κ B responses to cytokines. These studies have shown that continuous stimulation or sequential pulsing of TNF α can induce oscillations in NF- κ B nuclear translocation that are dependent upon cycles of degradation and re-synthesis of I κ B proteins (i.e., negative feedback loops), and that the frequency of these NF- κ B oscillations encode distinct gene expression profiles [8, 24-27]. Additional work has suggested that the amplitude of NF- κ B activity, but not the temporal profile, is particularly sensitive to changes in TNF α concentration and is crucially dependent on the transient nature of IKK activity [28]. Recently, single cell imaging has emerged as a paradigm-of-choice to study the dynamics of NF- κ B nuclear localization as monitored by nuclear:cytoplasmic shuttling of NF- κ B proteins fused to fluorescent protein reporters. Coupled with computational modeling, these single cell studies have revealed stochastic, heterogeneous, and paracrine NF- κ B responses at the single cell level, especially in response to low concentrations of TNF α [9, 10, 13, 29]. A key unresolved issue in the field relates to how biological robustness is achieved within cell populations displaying heterogeneous and dynamic single-cell behavior [13, 29, 30], and the physiologic relevancy of these single-cell phenomena to tissue- and organ-level biological responses *in vivo*.

To this end, we have developed, characterized, and utilized a dynamic bioluminescent reporter for quantitative interrogation of NF- κ B:I κ B α negative feedback loop regulation in live cells and at the tissue-level in live animals. Previously we demonstrated that fusing I κ B α to the firefly luciferase gene (I κ B α -FLuc) enables quantitative monitoring of I κ B α degradation (which can be directly correlated to IKK activity) *in vitro* and *in vivo* [31]. We then placed the fusion reporter under the control of an NF- κ B responsive promoter (κ B $_5$ →I κ B α -FLuc) and showed that it recapitulates the

endogenous I κ B α negative feedback loop (i.e., IKK-directed I κ B α degradation and subsequent NF- κ B driven re-synthesis of the I κ B α gene; Fig. 1A) and complements *in silico* experiments conducted with a robust computational model of the NF- κ B pathway [5, 6, 16]. This reporter offers the advantage of monitoring protein *activity* within different subcellular compartments as opposed to simply measuring changes in total protein levels or localization. For example, κ B₅→I κ B α -FLuc reports both TNF α -induced degradation of I κ B α (which is dependent on the activity of IKK, β -TrCP, and the proteasome) and subsequent NF- κ B-dependent transcriptional up-regulation of I κ B α (which is dependent upon NF- κ B nuclear translocation as well as additional post-translational modifications and co-activator associations in the nucleus). Additionally, the synthetic κ B₅ promoter has enhanced sensitivity that enables measurement of subtle changes in transcriptional dynamics. In the present work, we have exploited the unique characteristics of this negative feedback loop reporter to rigorously characterize dynamic I κ B α responses in single cells, populations of cell, and *in vivo* upon stimulation with a range of TNF α concentrations and pulses, revealing surprisingly synchronous responses.

3.2 RESULTS

Characterization of the Effect of Modulating TNF α Pulse Duration or Concentration on the I κ B α :NF- κ B Negative Feedback Loop in Cell Populations.

The I κ B α :NF- κ B negative feedback loop represents a major regulatory node within the NF- κ B pathway and is a critical determinant of NF- κ B oscillatory behaviors

that encode stimulus-specific gene expression programs [8, 24-27, 29]. To temporally resolve the dynamics of I κ B α degradation and subsequent NF- κ B-driven re-synthesis in living cells, we used our previously validated κ B₅→I κ B α -FLuc fusion-protein reporter in HepG2 (human hepatocellular carcinoma) cells [5, 31] (Fig. 1A). Western blot analysis of HepG2 cells transiently transfected with the κ B₅→I κ B α -FLuc reporter and exposed to 170 pM (3 ng/mL) TNF α indicated that the reporter was expressed at sub-endogenous levels and that the kinetics and degree of endogenous I κ B α and chimeric I κ B α -FLuc degradation were similar (Fig. 1B). However, the quantitative kinetics of reporter re-synthesis were delayed compared to endogenous I κ B α , a trend noted previously [5] and likely due to promoter differences (synthetic κ B₅ vs. endogenous I κ B α promoter).

With this real-time bioluminescent reporter system, we systematically evaluated the impact of short duration TNF α pulses on the dynamic regulation of the I κ B α :NF- κ B negative feedback loop within populations of cells in culture. HepG2 cells transfected with κ B₅→I κ B α -FLuc were stimulated with the pro-inflammatory cytokine TNF α (1.2 nM, 20 ng/ml) either continuously or as a pulse (5 sec, 15 sec, 30 sec, 5 min or 15 min) and images of cells were captured sequentially every 5 min for 6 hr. Generally, the normalized I κ B α -FLuc photon flux (Fig. 2A) rapidly decreased to a transient minimum (due to TNF α -induced degradation of I κ B α) and then strongly rebounded above initial levels (due to NF- κ B-induced re-synthesis of I κ B α). This rebound was previously shown to be consistent with *de novo* transcription and translation of I κ B α [5] and with the previously-reported ligand-induced stabilization of newly-synthesized I κ B α [32, 33].

Surprisingly, a TNF α pulse as short as 5 sec in duration was capable of inducing substantial I κ B α degradation ($35 \pm 9\%$, mean \pm SEM unless noted otherwise), suggesting

that extremely brief exposure can induce significant IKK-dependent activation of canonical NF- κ B signaling (Fig. 2A). This was confirmed by Western blot analysis, which exhibited substantial I κ B α degradation in response to a 5 sec TNF α pulse (Fig. 2B). As TNF α pulse duration was lengthened from 5 sec to 15 min, the degree of I κ B α degradation increased, and when pulsed for 5 min or longer I κ B α degradation saturated at levels (~70%) equivalent to continuous TNF α stimulation (Fig. 2A, inset; Fig. 2C). The time at which maximal degradation occurred did not change as TNF α pulse duration was modulated (Fig. 2D).

Examination of the degree of I κ B α re-synthesis (measured as percent of maximum re-synthesis) in response to TNF α pulse duration revealed increasing levels of I κ B α re-synthesis that eventually peaked and leveled-off when pulsed for 5 min or longer (Fig. 2E). Interestingly, TNF α pulses elicited a broader I κ B α re-synthesis phase with a less defined peak when compared to continuous TNF α stimulation. Furthermore, maximal I κ B α re-synthesis in response to a 15 min TNF α pulse was higher ($97 \pm 3\%$ of maximum) than observed for continuous TNF α stimulation ($65 \pm 8\%$ of maximum). As had been observed for I κ B α degradation, modulating TNF α pulse duration did not greatly affect the timing of the re-synthesis peak (Fig. 2F), suggesting that these cell populations were responding synchronously. Additionally, peak I κ B α re-synthesis occurred later (164 ± 16 min vs. 137 ± 5 min) for a 15 min TNF α pulse when compared to continuous.

We next investigated the impact of TNF α concentration on the dynamic regulation of the I κ B α :NF- κ B negative feedback loop *in cellulo* by treating HepG2 cells with a range of TNF α concentrations (0.1 - 10 ng/mL, 0.57 - 570 pM) under *continuous*

exposure conditions (Fig. 2G). The degree of I κ B α degradation increased with increasing TNF α concentration, eventually saturating ($68 \pm 2\%$) at the highest concentrations tested (Fig. 2G, inset; Fig. 2H), yielding a degradation EC₅₀ value of 6.7 pM TNF α (5.7 to 7.9 pM, 95% confidence interval). Moreover, examination of I κ B α degradation kinetics (Fig. 2I) showed that increasing TNF α concentration resulted in faster degradation, with the time of maximal degradation shifting from 53 ± 4 min to 29 ± 2 min.

The relationship between TNF α concentration and I κ B α re-synthesis was more complex than was seen for degradation. Increasing the TNF α concentration elicited increasing levels of I κ B α re-synthesis up to a maximum (corresponding to 57 pM; 1 ng/mL TNF α) beyond which higher amounts of TNF α actually elicited lower levels of re-synthesis (i.e., a “roll-over” back down to $74 \pm 3\%$ of maximum levels; Fig. 2G, J). Furthermore, increasing TNF α concentration resulted in faster I κ B α re-synthesis kinetics, with the maximal re-synthesis time shifting from 278 ± 39 min to 148 ± 3 min and eventually leveling off at this time between 57 pM and 171 pM (Fig. 2K).

Thus, we found that the κ B₅→I κ B α -FLuc reporter enabled quantitative comparison of the effects of modulating TNF α pulse duration versus concentration in real-time in live cells. This systematic analysis revealed that I κ B α degradation was highly sensitive to both stimulation regimens and in each case eventually saturated at approximately 70% degradation. Modulation of TNF α pulse duration had little effect on the kinetics of I κ B α degradation, while increasing TNF α concentration resulted in faster degradation. Both stimulation regimens elicited biphasic patterns in the degree of I κ B α .

re-synthesis, but only modulation of TNF α concentration had a strong effect on re-synthesis kinetics.

Characterization of TNF α -Induced Regulation of the I κ B α :NF- κ B Negative Feedback Loop in Single Cells.

Having discovered complex and reproducible patterns of I κ B α dynamics in response to modulating TNF α pulse duration and concentration in live cultured cell populations, we next utilized the κ B β →I κ B α -FLuc reporter to investigate whether the I κ B α :NF- κ B negative feedback loop exhibits similar dynamic response patterns at the level of single cells, or whether single cell responses are less reproducible, and more heterogeneous and asynchronous. In other words, are broad peaks and complex kinetics measured within cell populations the sum of heterogeneous single cell behaviors rather than the synchronous behavior of cells residing in a population?

We first verified that we could image single bioluminescent cells in the IVIS100 imaging system by transiently transfecting HepG2 cells with a dual bioluminescent/fluorescent reporter construct, FUW-FLG, comprising pGL3 firefly luciferase fused through a flexible linker to EGFP and driven by a constitutive ubiquitin promoter [34]. HepG2 cells were transfected with this plasmid as described above for the κ B β →I κ B α -FLuc reporter; however, 36 hr after transfection the cells were trypsinized into a single cell suspension, counted, diluted, and plated at a density of 60 cells/well on top of pre-plated, untransfected HepG2 cells in a black 24 well plate (to best simulate the same conditions used in the earlier cell population studies). After a 12 hr recovery period, cells were imaged first for bioluminescence and then for fluorescence on an

InCell 1000 imager (Fig. 3A). We found an excellent correlation between single bioluminescent foci and single cell fluorescence (a small number of foci corresponded to two or three cells). Thus, single HepG2 cells expressing a dual-imaging reporter could be imaged in a lawn of otherwise isogenic cells, establishing the principle for studying the TNF α -induced responses of single HepG2 cells expressing $\kappa B_5 \rightarrow I\kappa B\alpha$ -FLuc.

Using this same procedure with HepG2 cells expressing $\kappa B_5 \rightarrow I\kappa B\alpha$ -FLuc, we carried out both continuous- and 30 sec pulse-TNF α stimulations. Under continuous stimulation, the I $\kappa B\alpha$ -FLuc profiles of individual cells (Fig 3B) remarkably resembled those observed for cell populations (Fig. 2). Interestingly, while single cells exhibited substantial heterogeneity in the *amplitude* of degradation and re-synthesis, collective analysis of the I $\kappa B\alpha$ -FLuc re-synthesis peaks of individual cells strongly resembled the trends observed in cell populations (Fig. 2A), each peaking at almost the exact same times (133 ± 4 min vs. 137 ± 5 min, respectively), indicating that this pattern is a property of single cell responses to continuous TNF α . On the other hand, a 30'' pulse of TNF α yielded much broader I $\kappa B\alpha$ -FLuc re-synthesis peaks for single cells (Fig. 3C), which strongly resembled the broad peaks observed for population studies (Fig. 2A) also peaking at very similar times (154 ± 2 min for single cells vs. 170 ± 23 min for populations) and similarly showing a delayed peak compared to continuous treatment (Fig. 2F and Fig. 3G). Again, strong heterogeneity was noted in the *amplitude* of I $\kappa B\alpha$ -FLuc re-synthesis (Fig 3C), though the amplitudes of the average I $\kappa B\alpha$ -FLuc profile for all individual cells combined and the I $\kappa B\alpha$ -FLuc profile observed for a population of cells are nearly the same (Fig. 3C black line versus Fig. 2A red line). The degree of I $\kappa B\alpha$ degradation observed in TNF α pulsed cells was less than that observed under

continuous TNF α , recapitulating another trend noted in the population studies (Fig. 2). Interestingly, 18% of continuously stimulated cells exhibited I κ B α -FLuc oscillatory behavior, peaking once at 109 min (102.9 to 114.6, 95% CI) and again at 244 min (227.4 to 261.3, 95 % CI) (Fig 3E); this phenomenon was never observed in cells given a 30 sec TNF α .

We next investigated individual cell responses to a range of TNF α concentrations under continuous stimulation as described previously for cell population studies (Fig. 2G-K). While heterogeneous I κ B α -FLuc amplitudes were again observed, an obvious general trend emerged with most cells exhibiting increased levels of degradation and re-synthesis as the TNF α concentration increased (Fig. 3F). At the lowest doses tested, 0.57 and 1.7 pM, many cells (62%) did not respond to TNF α stimulation (as defined by falling within the 95% CI of vehicle stimulated cells and not exhibiting a local maximum; Fig. 3F, 0 pM panel). For each higher TNF α concentration, less than 7% of cells were non-responders. When all cells that did respond were considered, increasing TNF α concentration resulted in faster I κ B α -FLuc degradation, with the time of maximal degradation shifting from 65 ± 8 min to 20 ± 1 min, a trend similar to that seen in our population studies (Fig. 2). However, we did not observe a strong pattern of shifting I κ B α -FLuc maximum re-synthesis times in relation to altering TNF α , though the lowest concentrations did exhibit a higher degree of variance in peak times (Fig. 3I). This heterogeneity in re-synthesis times at low doses could account for the broad peaks and variability in peak timing observed at 0.57 pM and 1.7 pM in cell populations (Fig. 2G, K). Thus, single cell I κ B α dynamic profiles showed highly synchronous kinetics and

remarkable similarity to I κ B α dynamic profiles observed in cell populations, especially with regard to profile shape under different conditions.

Experimental Investigation of Complex I κ B α Re-Synthesis Patterns.

Having observed novel and complex patterns in the dynamics of I κ B α degradation and re-synthesis in single cells and cell populations (hereafter combined into the term *in cellulo*) in response to modulation of TNF α pulse duration and concentration, we next sought to investigate potential mechanisms behind these highly-reproducible behaviors. We first examined whether the experimentally observed patterns of I κ B α dynamics could be recapitulated in an existing computational model of TNF α -induced NF- κ B signaling [6, 16]. We reasoned that if mathematical modeling could reproduce the TNF α -driven complexities observed for I κ B α degradation and re-synthesis, it may offer insight into the fundamental processes driving these patterns and assist in the development of experimentally-testable hypotheses.

The computational model utilizes experimentally-derived IKK kinase activity input profiles, of which we employed a previously determined IKK input derived from HepG2 cells stimulated continuously with 20 ng/mL TNF α [5]. The IKK activity input profile (Fig. 4A) was fitted with a shape-preserving interpolating polynomial in MatLab (function `pchip`) simulating the duration of the IKK activation phase (a), peak IKK activity (p), and the duration of the IKK deactivation phase (d). In an effort to simulate the complex patterns in I κ B α dynamics seen *in cellulo* in response to altering TNF α pulse duration and concentration, the IKK input profile was modified in the following ways: 1) alteration of IKK activation phase duration (a: 5, 10, 20, 40, and 80 min from 0

to peak activity), 2) alteration of IKK deactivation phase duration (d: 20, 30, 50, and 100 min post peak activity), or 3) alteration of IKK peak activity magnitude (p: 0.5-, 1-, 3-, 6, and 10-fold over the previous experimentally-determined IKK activity peak). These modifications resulted in a collection of 80 IKK activity profiles that could be used as input functions into the model (Fig. 4A, Fig. S1) to generate predicted I κ B α dynamic profile plots (Fig. 4B,C; S2). Generally, there was a remarkable correlation between the computationally-predicted I κ B α profiles and the experimentally-generated I κ B α -FLuc profiles (Fig. 2, 3), with the timing and extent of I κ B α degradation as well as the overall dynamic behavior being highly similar. However, as noted previously [5], the computationally-predicted amplitude of I κ B α re-synthesis was lower than seen for I κ B α -FLuc and the kinetics of re-synthesis were faster, discrepancies that may stem from the amplified sensitivity of the concatenated κ B₅ promoter driving I κ B α -FLuc.

Interestingly, we found that when the time required for IKK to deactivate was prolonged from 20 min to 100 min (Fig. 4B, S2), no effect was observed upon I κ B α degradation, but the magnitude of I κ B α re-synthesis increased with little effect on the kinetics, resembling the I κ B α re-synthesis patterns observed upon stimulation with TNF α pulses (Fig. 2, 3). On the other hand, increasing the magnitude of peak IKK activity (Fig. 4C, S2) yielded computational I κ B α plots in which *both* I κ B α degradation and re-synthesis were enhanced and exhibited faster kinetics, strongly resembling the I κ B α dynamics observed when TNF α concentration was modulated (Fig. 2, 3). However, modifying IKK magnitude did *not* recapitulate I κ B α re-synthesis roll-over, even though I κ B α degradation had saturated.

Thus far we had observed that (1) pulses of TNF α *in cellulo* strongly affected the level of I κ B α re-synthesis without impacting the kinetics or shape of I κ B α re-synthesis profiles and could be modeled *in silico* by altering the timing of IKK deactivation, and (2) modulating TNF α concentration *in cellulo* affected the amplitude, kinetics, and shape of I κ B α re-synthesis and could be accurately recapitulated *in silico* (with the exception of re-synthesis roll-over) by modulating IKK peak magnitude. We hypothesized that many of these complex patterns in I κ B α re-synthesis are a consequence of the continuous presence of TNF α driving subsequent rounds of IKK-activation (i.e., possibly mimicking prolonging the IKK deactivation phase *in silico*) and I κ B α degradation during the re-synthesis phase. This hypothesis was supported by our previous finding that HepG2 cells given a 30 sec pulse of TNF α regain the capacity to fully re-initiate a second TNF α -induced I κ B α degradation only after 60-120 min, the approximate time frame during which maximal I κ B α re-synthesis and roll-over occur [5].

To assess the impact of TNF α presence at various time points before and during I κ B α re-synthesis, HepG2 cells were treated with increasing concentrations of TNF α that was then washed out after 1, 5, 10, 15, 30, 60, 90, 120, and 180 min to remove the effect of continuous TNF α driving subsequent rounds of IKK-mediated I κ B α degradation. Two representative I κ B α plots are shown in Fig. 4D, E (un-normalized photon flux data and additional TNF α and mock wash-out plots are shown in Fig. S3). The removal of TNF α at any time before I κ B α re-synthesis had peaked (i.e., up to 120 min), resulted in broadly shaped I κ B α re-synthesis profiles (Fig. 4D, S3), rather than the narrower peaks seen under continuous TNF α (Fig. 2, 3) or mock TNF α wash-out stimulation (Fig. S3). TNF α wash-outs performed at 120 min (Fig. S3) and 180 min (Fig. 4E) exhibited the

expected primary I κ B α re-synthesis peak observed at 120 min under continuous TNF α , followed by a *second* I κ B α peak (occurring at approximately 240 min and 300 min, respectively), more similar to the peaks observed for earlier TNF α wash-out times (Fig. 4D, S3). When high concentrations of TNF α (170-570 pm) were washed out, cells exhibited significantly higher levels of I κ B α re-synthesis compared to continuous TNF α stimulation (Fig. 4F). Furthermore, TNF α wash-out resulted in I κ B α re-synthesis peaking later than continuously stimulated cells and nearly abolished the pattern of faster I κ B α re-synthesis observed in response to increasing TNF α concentration (Fig. 4G). Additionally, I κ B α re-synthesis roll-over was still observed when TNF α was washed out (Fig. 4F).

To further address the role of secondary (i.e., later time point) TNF α -induced I κ B α degradation in governing I κ B α -FLuc re-synthesis phase dynamics, we utilized a modified bioluminescent reporter, κ B $_5$ →I κ B α (S32,36A)-FLuc [35]. The serine-to-alanine substitutions render I κ B α unresponsive to IKK-directed phosphorylation and subsequent proteasomal degradation; however, the reporter is still responsive to the NF- κ B transcriptional activity elicited once endogenous I κ B α is degraded and NF- κ B translocates into the nucleus. If re-initiation of I κ B α degradation is critical in governing the timing, magnitude and overall shape of I κ B α re-synthesis, or the re-synthesis roll-over effect, then we would *not* expect to observe these phenomena with the κ B $_5$ →I κ B α (S32,36A)-FLuc reporter under continuous TNF α stimulation. As anticipated, TNF α stimulation did not cause any I κ B α degradation (Fig. 4H), but did exhibit subsequent NF- κ B-directed re-synthesis of the reporter. Strikingly, these I κ B α profiles

strongly resembled the TNF α wash-out experiments (Fig. 4D, E, S3): the I κ B α re-synthesis phases were broad (regardless of TNF α concentration), the peak magnitude increased (Fig. 4F), and the re-synthesis kinetics were more synchronized and delayed (Fig. 4G) compared to wild type reporter, indicating that these patterns were indeed affected by secondary IKK-driven degradation of wild-type I κ B α . Similarly, continuous TNF α stimulation in *single* HepG2 cells transfected with the I κ B α (S32,36A)-FLuc mutant reporter also exhibited broad I κ B α re-synthesis peaks with synchronized and delayed kinetics compared to wild-type reporter (Fig 3D, G), further highlighting the cell-autonomous nature of these trends in I κ B α dynamics.

Characterization of TNF α -Induced Regulation of the I κ B α :NF- κ B Negative Feedback Loop In Vivo.

Having discovered complex and synchronous patterns of I κ B α dynamics in response to modulating TNF α pulse duration and concentration in single cells and in cell populations in culture, we then utilized the κ B α \rightarrow I κ B α -FLuc reporter to investigate whether the I κ B α :NF- κ B negative feedback loop exhibits similar patterns in response to varying TNF α doses *in vivo*. Somatic gene transfer by hydrodynamic transfection was employed to express the κ B α \rightarrow I κ B α -FLuc plasmid in murine livers [36]. Three to twelve weeks post plasmid injection, sufficient time for hepatocellular recovery and stable integration of reporter plasmids into a subpopulation of hepatocytes, animals were administered vehicle (PBS) or TNF α (1, 10, or 30 ng/mouse) by bolus tail vein injection and imaged at 5 min intervals for 3 hr to capture full I κ B α -FLuc dynamic profiles (Fig.

5A, B). Strikingly, the general dynamics of the *in vivo* I κ B α profiles were highly synchronous and strongly resembled the profiles observed *in cellulo* in response to TNF α pulses (Fig. 2,3). Of the three TNF α doses used, the lowest (1 ng/mouse) appeared to induce little or no I κ B α -FLuc reporter degradation, whereas the two higher doses showed increasing amounts of degradation (Fig. 5C; 10 ng/mouse: 30% \pm 7%; 30 ng/mouse: 59% \pm 7%). Interestingly, the time of maximal degradation appeared to occur slightly earlier *in vivo* (no later than 20 min, Fig. 5D) than was seen *in cellulo* (no earlier than 25 min for the highest TNF α concentrations, Fig. 2D). Increasing the TNF α dose resulted in higher levels of maximal re-synthesis (Fig. 5E) that peaked at nearly 20-fold over vehicle treated animals. The re-synthesis phase was broad in shape (similar to the *in cellulo* I κ B α profiles in response to TNF α pulses), and peaked and leveled off at approximately 100 min for both the 10 and 30 ng/mouse doses (Fig. 5F). This is in contrast to the highest TNF α concentrations used *in cellulo* that did not achieve maximal re-synthesis until \sim 150 min (Fig. 2). Thus, even though TNF α was administered at varying doses *in vivo*, the resultant I κ B α dynamic profiles exhibited kinetics that were highly synchronous, suggesting uniform cellular responses within the liver. These *in vivo* patterns of I κ B α dynamics closely resembled the patterns observed upon modulating TNF α pulse duration *in cellulo* (Fig. 2, 4), and suggested that circulating TNF α is perceived by hepatocytes *in vivo* as a pulse.

3.3 DISCUSSION

Cells have evolved complex molecular networks to sense signals from the environment and translate them into a wide variety of biological responses. The NF- κ B pathway is responsive to a variety of stimuli and to the *mode* of stimulation, which is of critical importance during responses to inflammatory cytokines, such as TNF α , which are likely perceived as transient pulses/waves occurring over a wide range of concentrations [5, 7-10, 28]. Of particular interest is understanding how these diverse TNF α stimulation modes impact the NF- κ B:I κ B α negative feedback loop in single cells and within populations of cells *in vivo*, providing insight into a key cellular regulatory loop that directs NF- κ B nuclear localization dynamics and transcriptional responses.

To this end, we have developed, characterized, and utilized a dynamic bioluminescent reporter (κ B₅→I κ B α -FLuc) for quantitative interrogation of NF- κ B:I κ B α negative feedback loop regulation in single cells, cell populations, and *in vivo*. These non-destructive assays are based on luciferase reporters and as such, do not rely on antibodies, have high temporal resolution, are amenable to high-throughput platforms, are readily translatable to *in vivo* systems, and have potential for low-light microscopic analysis of single cell and sub-cellular compartments [30, 37-40]. We have employed the unique capabilities of our NF- κ B:I κ B α negative feedback loop reporter, coupled with *in silico* modeling, to systematically interrogate the impact of modulating TNF α pulse duration and concentration. We demonstrated that cells are sensitive to pulses of TNF α stimulation as short as 5 sec (Fig. 2A, B), highlighting that the NF- κ B network is remarkably sensitive and tuned to elicit responses to very short bursts of ligand [7]. Increasing TNF α *pulse duration* did not strongly impact the kinetics or shape of I κ B α re-

synthesis or generate re-synthesis roll-over, but did exhibit I κ B α re-synthesis levels that tended to be higher and broader in shape than seen for continuous TNF α stimulation (Fig. 2). At the single cell level, continuous and 30 sec TNF α pulses (Fig 3B, C) yielded I κ B α -FLuc dynamic profiles that remarkably resembled the shape of the cell population data (Fig. 2). Thus, the broad peaks observed in cell populations upon stimulation with pulsatile TNF α are *not* a result of heterogeneous responses from individual cells generating a broad average, but are an intrinsic property of single cell responses. Additionally, most of the cells exhibited synchronous responses, as evidenced by the tight 95% confidence intervals (Fig. 3G) on the kinetics of peak re-synthesis. In the future, it will be interesting to determine the impact of a wide range of TNF α pulses on the heterogeneity of single cell responses, especially since our data indicate that the kinetics of I κ B α degradation and re-synthesis do not significantly change as pulse duration increases (Fig. 2). A similar trend in invariant temporal NF- κ B nuclear localization was observed by Werner et al. [7] in response to TNF α pulses; however, they did not observe changes in the amplitude of NF- κ B activity (as measured by EMSA and computational prediction), while our reporter measured definitive pulse-dependent changes in the amplitude of I κ B α re-synthesis, a process that is dependent upon NF- κ B transcriptional activity.

Additionally, real-time measurements indicated that the I κ B α :NF- κ B negative feedback loop is responsive to a wide range of TNF α concentrations, even as low as 0.57 pM (0.01 ng/mL), affirming what has been observed previously by NF- κ B EMSA [28] and single cell microscopy [9, 10]. Both of these TNF α stimulation paradigms (pulsing cells or varying concentration) elicited increasing levels of I κ B α degradation that

eventually saturated at ~70% degradation. However, only changes in TNF α concentration exhibited robust alteration of the temporal dynamics of degradation, with degradation rates increasing as TNF α concentration increased (Fig. 2I). Interestingly, this same trend held true at the single cell level, indicating that it is an inherent property of TNF α responses in single cells (Fig. 3H). Whereas Paszek et al. [29] looked at the time to I κ B α degradation following TNF α stimulation using RelA-dsRedxp and I κ B α -EGFP fusion reporters and observed very degradation heterogeneous start times at 1.7 pM (0.03 ng/mL) TNF α (sometimes 100+ minutes post-TNF α), we observed that most cells exhibited degradation of the κ B β →I κ B α -FLuc reporter within 0-60 min and showed re-synthesis peaks between 120-18 min TNF α (Fig. 3H, I). And while both Tay et al. [10] and Paszek et al. [29] noted that the time to peak nuclear NF- κ B in individual cells tended to increase and became more variable at lower TNF α concentrations, we observed very little change in the average peak re-synthesis time of the κ B β →I κ B α -FLuc reporter (a functional read-out of nuclear NF- κ B activity), but it did exhibit greater heterogeneity at the lowest concentrations tested (Fig. 3I).

Having observed novel and complex patterns in I κ B α dynamics in response to modulation of TNF α pulse duration and concentration in single cells and cell populations, we next sought to investigate potential mechanisms behind these highly-reproducible behaviors. We discovered that these complex I κ B α re-synthesis patterns (with the exception of re-synthesis roll-over) resulted from the continuous presence of TNF α initiating re-activation of IKK and driving secondary rounds of I κ B α degradation (Fig. 3D, 4). Previously, we and others discovered a TNF α -induced transient refractory period during which TNF α -preconditioned cells are unable to fully respond (i.e., degrade I κ B α)

upon a second TNF α challenge until 60-120 min post preconditioning [5, 8, 41]. This refractory period is likely governed by the rate of I κ B α :NF- κ B nuclear export that repopulates the cytoplasm with IKK-degradable complexes [5, 40, 42, 43]. Thus, we suggest that the observed patterns in I κ B α re-synthesis dynamics are a manifestation of this transient refractory period, whereby continuous TNF α is unable to induce a subsequent round(s) of I κ B α degradation until the passage of this refractory period.

Interestingly, the single cell imaging experiments also revealed that 18% of cells continuously stimulated with TNF α exhibited I κ B α -FLuc oscillatory behavior, with an approximate period of 130 min (Fig. 3B, E). This may correlate to the NF- κ B nuclear:cytoplasmic oscillations observed by others with a period of \sim 100 min [8-10, 24-27], and may be slightly longer due to the time required to transcribe and translate new I κ B α -FLuc. This oscillation phenomenon was never observed in cells given a 30 sec TNF α (Fig. 3C) or cells expressing the I κ B α (S32,36A)-FLuc mutant reporter (Fig 3D), highlighting the critical role that secondary I κ B α degradation plays in the oscillation phenotype.

After rigorous characterization of the TNF α -induced response patterns of the κ B α \rightarrow I κ B α -FLuc reporter in single cells and cell populations in culture, we took advantage of the amenability of luciferase reporter imaging *in vivo* to interrogate TNF α -induced activation of the I κ B α :NF- κ B negative feedback loop within mouse livers. Our data indicated that circulating TNF α , administered at varying doses, produced I κ B α dynamic behaviors *in vivo* (Fig. 5) with synchronized kinetics and very high levels of I κ B α re-synthesis, patterns that were consistent with *in cellulo* experiments in which TNF α pulse duration was varied (Figs. 2, 3, 4). This strongly suggested that circulating

TNF α is perceived by liver cells as a pulse, also plausible given the dual re-circulation physiology of the liver (hepatic arterial and portal venous) as well as hemodilution effects. This finding underscores the importance of studying cytokine signaling pathways under conditions of pulsatile exposure (rather than just continuously bathing cells in ligand) that may better reproduce physiologic cytokine stimulation paradigms. Furthermore, while several *in silico* and *in vitro* studies have demonstrated highly heterogeneous and/or asynchronous NF- κ B responses to TNF α at the single cell level that are largely masked when individual cells are averaged together into populations [8-10, 24, 26, 29], our single cell, cell population, and *in vivo* data indicated that I κ B α degradation and re-synthesis is surprisingly robust and synchronous. These data, coupled with the low frequency at which we observed I κ B α -FLuc oscillatory behavior, place reservations on the physiologic relevance of the highly heterogeneous and oscillatory NF- κ B behaviors observed during *continuous* TNF α stimulation of single cells. On the other hand, our data do support the relevancy of the synchronous NF- κ B oscillatory behaviors that are observed upon sequential TNF α *pulsing* and that drive frequency-encoded transcriptional programs [8, 10].

Thus, our work revealed that the NF- κ B:I κ B α negative feedback loop exhibits differential and reproducible dynamic patterns in response to modulating TNF α concentration or pulse duration, and that responses to TNF α exhibited a remarkable degree of synchronicity at the level of single cells, cell populations, and *in vivo*. Interestingly, administration of TNF α at varying doses *in vivo* resulted in hepatocyte responses that were most consistent with perception of TNF α as a single concentration administered with increasing pulse duration.

3.4 METHODS

Plasmids. The $\kappa B_5 \rightarrow I\kappa B\alpha$ -FLuc plasmid was produced by cloning an *EcoRI* – *HpaI* (blunt) fragment from CMV $\rightarrow I\kappa B\alpha$ -FLuc [31] into the *EcoRI* and *EcoRV* (blunt) sites of $\kappa B_5 \rightarrow FLuc$ [5]. The $\kappa B_5 \rightarrow I\kappa B\alpha(S32,36A)$ -FLuc mutant plasmid was prepared by Quikchange mutagenesis (Stratagene, San Diego, CA, USA) following the protocol provided by the manufacturer [35]. The FUW-FLG plasmid encoding a fusion of FLuc and EGFP proteins driven by the human ubiquitin C promoter within an established lentiviral backbone has been previously described [34]. All plasmids were propagated in TOP10 electrocompetent *E. Coli* (Invitrogen, Carlsbad, CA) and purified using Hi-Speed Plasmid Maxi kits (Qiagen, Valencia, CA).

Cell culture and transfection. HepG2 human hepatoma cells were from the American Type Culture Collection (ATCC, Manassas, VA). Cells were cultured in DMEM supplemented with heat-inactivated FBS (10%) and L-glutamine (2 mM). Cell cultures were grown at 37°C in a humidified 5% CO₂ atmosphere. HepG2 cells (3 X 10⁵) were transiently transfected (Fugene 6, Roche, Indianapolis, IN) with $\kappa B_5 \rightarrow I\kappa B\alpha$ -FLuc (100 to 200 ng/well) and plated in black-coated 24-well plates (*In Vitro* Systems GmbH, Gottingen, Germany). Cells were then allowed to recover for 48 hr prior to imaging.

Dynamic bioluminescence imaging measurements in live-cell. Prior to analysis by bioluminescence imaging, HepG2 cells transiently expressing $\kappa B_5 \rightarrow I\kappa B\alpha$ -FLuc were washed with pre-warmed phosphate-buffered saline (PBS, pH 7.4) and incubated in 900 μ L of assay buffer (colorless sodium bicarbonate-buffered DMEM supplemented with

heat-inactivated FBS (10%), L-glutamine (2 mM), and D-luciferin (150 $\mu\text{g}/\text{mL}$). Cells were allowed to equilibrate for 30 min (at 37°C in a 5% CO_2 atmosphere) before stimulation with 100 μL of pre-warmed assay buffer with or without $\text{TNF}\alpha$ (#210-TA-050, R & D Systems, Minneapolis, MN). Bioluminescence measurements were acquired in IVIS 100 imaging system (Caliper Life Sciences, Hopkinton, MA) at 37°C under 5% CO_2 flow. Typical acquisition parameters were as follows: acquisition time, 30-60 sec; binning, 8 or 16; FOV, 10 or 23 cm; f/stop, 1; filter, open; image-image interval, 5 min; total number of acquisitions, 73. Where indicated, cells were transiently exposed to $\text{TNF}\alpha$ for the specified durations and concentrations, washed with pre-warmed PBS, returned to pre-warmed assay buffer (with or without $\text{TNF}\alpha$) and imaged as above. Bioluminescence photon flux (photons/sec) data were analyzed by region of interest (ROI) measurements in Living Image 3.2 (Caliper Life Sciences); this raw data was imported into Excel (Microsoft Corp., Redmond, WA) or Sigma Plot 8.0 (Systat Software Inc., San Jose, CA) and averaged, normalized to initial ($t = 0$) values (fold-initial), and normalized to vehicle-treated controls (fold-vehicle) to generate $\text{I}\kappa\text{B}\alpha$ dynamic plots (for an example of unnormalized photon flux data, refer to Fig. S4A). Quantification of the amplitude and timing of $\text{I}\kappa\text{B}\alpha$ degradation and re-synthesis was carried out in Excel; in the few instances of noisy $\text{I}\kappa\text{B}\alpha$ data, a moving-average smoothing function was applied to ease determination of true maximum $\text{I}\kappa\text{B}\alpha$ amplitudes and kinetics.

Single-cell bioluminescence imaging measurements. Cells were transfected as described above with either the $\kappa\text{B}_5 \rightarrow \text{I}\kappa\text{B}\alpha\text{-FLuc}$ plasmid or the FUW-FLG construct, but at 36 hr post-transfection were trypsinized, counted, diluted, and plated at 60

cells/well onto pre-plated, untransfected HepG2 cells (3×10^5 cells/well plated at the same time as initial transfection) in a black 24 well plate. Proof of principle bioluminescence and fluorescence measurements were acquired 12 hr later in gridded black 24 well plates. Bioluminescence was imaged on an IVIS50 with the following acquisition settings: acquisition time, 5 min; binning, 8; FOV, 4 cm; f/stop, 1; filter, open; instrument, IVIS50. GFP expression was then analyzed on the InCell Analyzer 1000 using a 10X objective and by collecting 300 fluorescent and brightfield images with a 10% overlap to allow image stitching. This large format image of the entire well, coupled with the visible grid on both the fluorescent and bioluminescent image overlays (Figure 3A), allowed easy correlation of bioluminescent foci with fluorescent cells. Additional image processing and overlays were performed in ImageJ.

Full single-cell bioluminescence imaging sequences were acquired by stimulating the cells exactly as described previously for cell populations with the following changes to image acquisition settings on the IVIS100: acquisition time, 5 min; binning, 8; FOV, 10 cm; f/stop, 1; filter, open; image-image interval, 0 min; total number of acquisitions, 73. Bioluminescence photon flux (photons/sec) data were analyzed by region of interest ROI measurements in ImageJ by drawing circular ROIs around each distinct glowing foci visible at $t = 0$ min. This raw photon flux data was then imported into MatLab and fitted with a fifth-degree polynomial to find the time of the first re-synthesis peak. Cells falling within the 95% CI of the signal of vehicle stimulated cells were labeled non-responders and excluded from time of min and max determinations.

Western blot analysis. HepG2 cells were cultured in 35 mm dishes and stimulated with TNF α (at the indicated concentrations) either continuously or as a 30 sec pulse. At the indicated time points, cells were harvested and lysed in RIPA buffer (150 mM NaCl, 50 mM Tris, 5 mM EDTA, 1% NP-40, 0.1% SDS, 0.5% sodium deoxycholate, pH 7.4), supplemented with protease inhibitor cocktail (Roche, Basel, Switzerland), sodium orthovanadate (1 mM), and PMSF (1 mM). Whole-cell lysates were normalized for protein content by BCA assay (Pierce, Rockford, IL). Proteins were resolved by SDS-PAGE (7.5% Biorad Precast Tris HCl or 4%-15%, Biorad Criterion Tris-HCl, Hercules, CA), transferred to a PVDF membrane and probed with I κ B α antibody (#9242, Cell Signaling Technology, Inc., Danvers, MA), GAPDH antibody(#G9545, Sigma, St. Louis, MO), and γ -Tubulin antibody (#sc-17787, Santa Cruz Biotechnology, Inc., Santa Cruz, CA). Secondary horseradish peroxidase-IgG antibodies were from GE Healthcare Biosciences (Piscataway, NJ), and blots were exposed on the IVIS 100 imaging system. Densitometric analysis was performed with Living Image 3.2 (Caliper Life Sciences) and Excel software.

Hydrodynamic injections and in vivo imaging. *In vivo* transfection of mouse hepatocytes was performed using the hydrodynamic somatic gene transfer method as described [44, 45]. Briefly, κ B5 \rightarrow I κ B α -FLuc (3 μ g) was diluted in PBS (pH 7.4) in a volume of 1 ml per 10 g of body weight and rapidly injected into tail veins of mice (FVB/N, 6-week-old males) [45]. Imaging for luciferase activity was performed 3-12 weeks after somatic gene transfer; mice used more than once were allowed to recover for 8 weeks before use in another round of imaging. Cohorts of 4 mice were injected with D-

luciferin (150 $\mu\text{g/g}$ of body weight, i.p.), anesthetized under 2.5% isoflurane, and imaged 10 min later in the IVIS 100 (acquisition, 4 min; binning, 8; FOV, 23 cm; f/stop, 1; filter, open) to obtain a pre-TNF α stimulation image. Following this, the mice were then quickly administered 100 μL of vehicle (sterile PBS) or TNF α (at the indicated concentrations) by tail vein i.v., placed back in the IVIS, and imaged every 5 min for 3 hr under anesthesia. Uniform ROI's were drawn around the liver, and total photon flux was measured and normalized to the pre-TNF α stimulation levels (fold-initial) and to a vehicle-treated animal (fold-vehicle).

Computational Concentration-Response Analysis. A well established computational model generated by Hoffman et al. [16] and modified by Werner et al. [6] was used to simulate I κ B α dynamics in response to varying IKK activity profiles.

A physiologic IKK activity profile in HepG2 cells was generated by kinase assay following continuous TNF α (20 ng/ μL) treatment and then interpolated and extrapolated in 5 min intervals to a total time of 360 min by Moss, et al. [5]. To allow manipulation, this experimentally obtained profile was reduced to three components of IKK activity: activation phase duration (a), peak activity magnitude (p), and deactivation phase duration (d) (Fig. 4A). The following values were used for each parameter: a = [5, 10, 20, 40, 80] min, p = [0.5, 1, 3, 6, 10] fold initial, d = [20, 30, 50, 100] min. A simple algorithm was then developed to generate 80 unique parameter combinations (with the constraint that the sum of (a) and (d) does not exceed 120 min), each defined by four points that were then interpolated using MatLab function pchip, a shape preserving interpolant (Fig. S1). These 80 IKK activity profiles were used as inputs into the

computational model and the differential equations were solved numerically using MatLab R2010b (Mathworks, Natick, MA) with subroutine *Ode15*. From these IKK inputs, the model predicted the dynamics of six different free and bound I κ B α subpopulations (free I κ B α _{cyt}, I κ B α :IKK_{cyt}, I κ B α :NF- κ B_{cyt}, I κ B α :IKK:NF- κ B_{cyt}, free I κ B α _{nuc}, and I κ B α :NF- κ B_{nuc}). Because live cell bioluminescence imaging of B₅-I κ B α -FLuc could not distinguish between these distinct I κ B α subpopulations, we summed the concentrations of the six predicted subpopulations and plotted the 80 predicted total I κ B α profiles as a function of time (Fig. S2).

Statistical Analysis. Statistical significance was evaluated using Student's *t* test for I κ B α -FLuc re-synthesis patterns (Fig. 4F,G).

3.5 FIGURES

Figure 3.1: $\kappa B_5 \rightarrow I\kappa B\alpha$ -FLuc Bioluminescent Reporter System. (A) The $\kappa B_5 \rightarrow I\kappa B\alpha$ -FLuc bioluminescent reporter utilizes an $I\kappa B\alpha$ gene fused by a flexible linker to a firefly luciferase (FLuc) gene under the control of a synthetic NF- κB promoter (κB_5), thus recapitulating the endogenous negative feedback loop. (B) HepG2 cells were transiently transfected with $\kappa B_5 \rightarrow I\kappa B\alpha$ -FLuc and stimulated continuously with $TNF\alpha$ (170 pM; 3 ng/mL). Lysates were collected at the indicated time points, resolved on a 7.5% SDS-PAGE gel, and blotted for $I\kappa B\alpha$ and GAPDH (loading control).

Figure 1

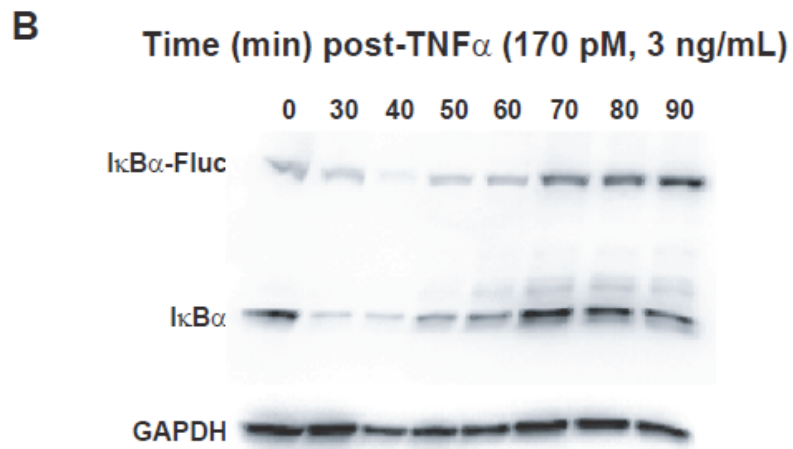
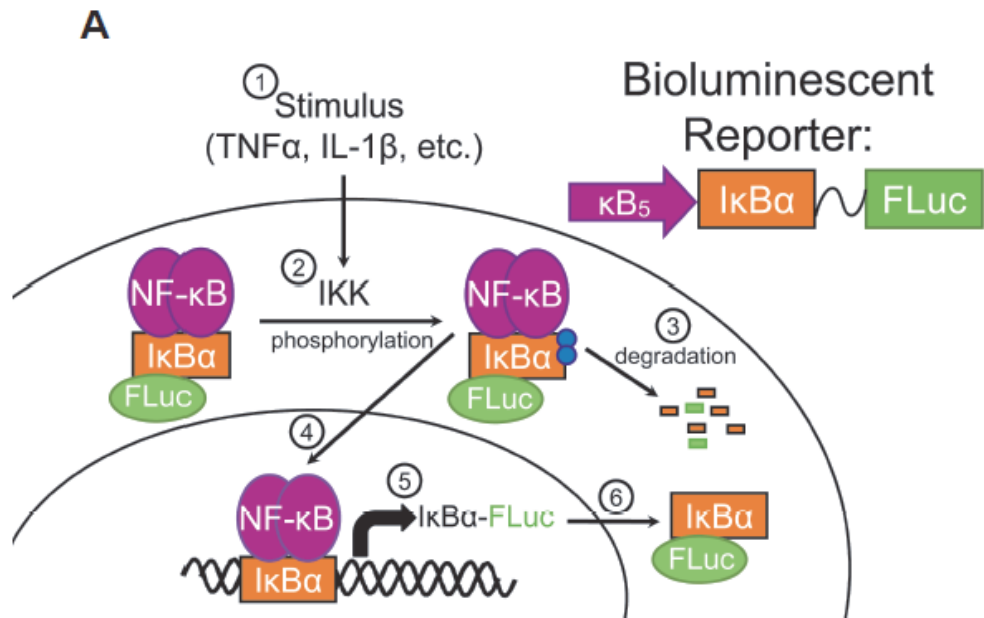


Figure 3.2: I κ B α Dynamics as a Function of TNF α Pulse Duration & Concentration.

(A) HepG2 cells transiently expressing $\kappa B_5 \rightarrow I\kappa B\alpha$ -FLuc were pulsed with a saturating concentration of TNF α (1.2 nM; 20 ng/mL) or vehicle for the indicated durations with data acquisition over a period of 360 min. Data were normalized as fold-initial and fold-vehicle (relative to cells pulsed with vehicle for the same duration), and represent the mean of three independent TNF α exposure experiments, each performed in duplicate and averaged. **(B)** HepG2 cells were stimulated with a 5 sec pulse of TNF α (1.2 nM; 20 ng/mL) and lysates were collected to capture I κ B α degradation and re-synthesis. Lysates were resolved together on a 4-15% gradient gel and blotted for endogenous I κ B α and γ -Tubulin (loading control). **(C,D)** Plots representing the extent of maximal I κ B α degradation **(C)**, and the time at which maximal I κ B α degradation occurred **(D)**, as functions of TNF α pulse duration. **(E, F)** Plots representing the extent of maximal I κ B α re-synthesis (expressed as a percentage of the maximum level of re-synthesis achieved in a given experiment) **(E)**, and the time at which maximal I κ B α re-synthesis occurred **(F)**, as functions of TNF α pulse duration. Note that the x-axis is plotted on a log scale (min) in (C-F). **(G)** HepG2 cells expressing $\kappa B_5 \rightarrow I\kappa B\alpha$ -FLuc were continuously treated with TNF α or vehicle at the indicated concentrations and bioluminescent data were acquired for 360 min. Data were normalized as before and represent three independent experiments, performed in triplicate and averaged. **(H, I)** Plots representing the extent of maximal I κ B α degradation **(H)**, and the time at which maximal I κ B α degradation occurred **(I)**, as functions of TNF α concentration. **(J, K)** Plots representing the extent of maximal I κ B α re-synthesis **(J)**, and the time at which maximal I κ B α re-synthesis occurred **(K)**, as functions of TNF α concentration. The x-axis is plotted on a log scale ([TNF α] pM) in panels H-K.

Figure 2

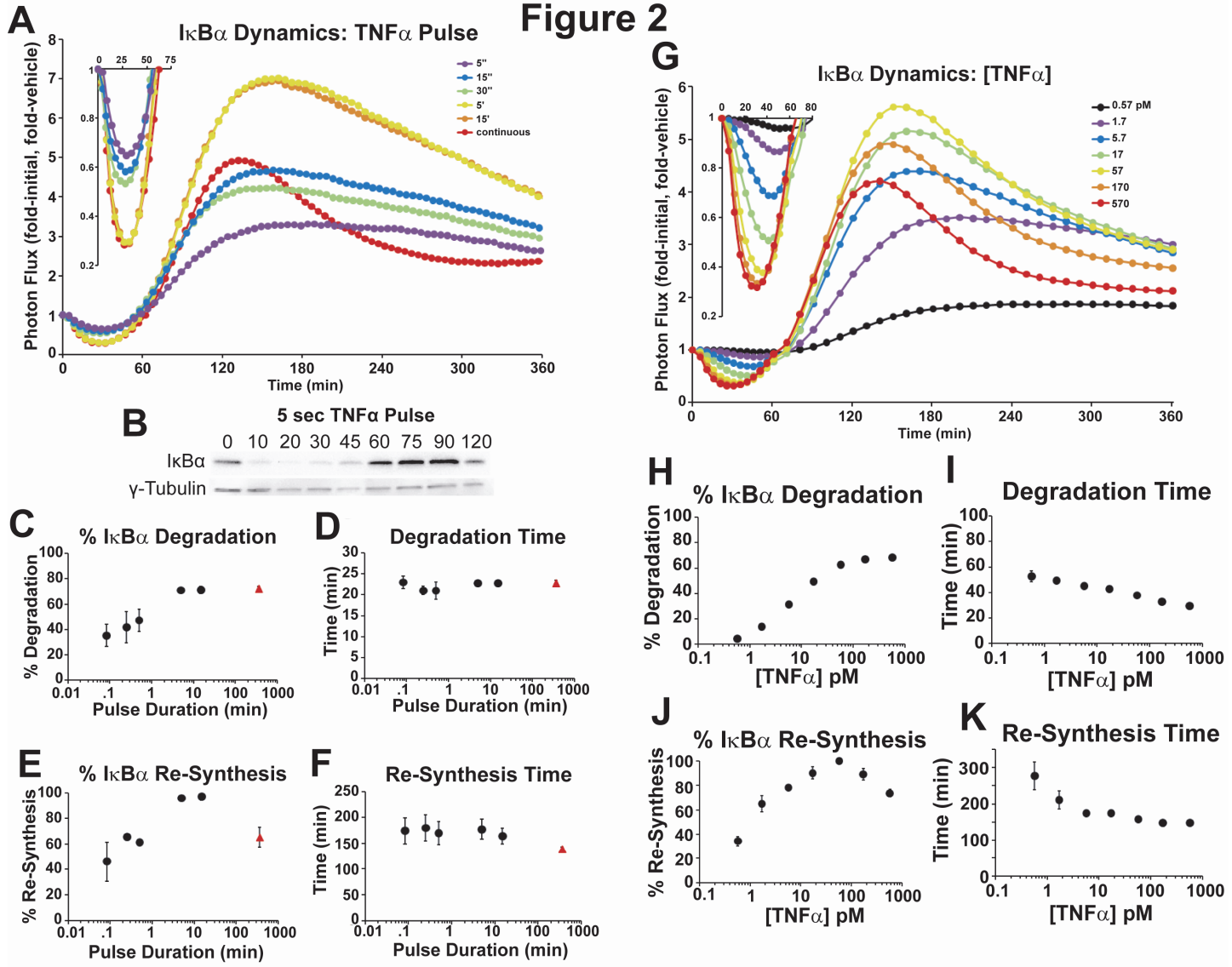


Figure 3.3: Characterization of I κ B α Dynamics in Single Cells. (A) Image of a single well of a 24 well plate with bioluminescent foci representing sparsely plated HepG2 cells transiently expressing the FUW-FLG luciferase-EGFP fusion reporter. Insets represent 10X fluorescent micrographs of the indicated bioluminescent foci, demonstrating that most foci represent a single transfected cell, and occasionally a small group of 2-3 cells. (B-E) Single HepG2 cells transiently expressing κ B $_5$ →I κ B α -FLuc (B,C) or κ B $_5$ →I κ B α (S32,36A)-Fluc (D) were given continuous (B, D) or a 30 sec pulse (C) of TNF α (1.2 nM; 20 ng/mL). Data were normalized as fold-initial, and data from two independent experiments are plotted together. Black lines represent the mean and red dashed lines represent the 95% confidence interval of the vehicle-treated controls. (E) Select examples of I κ B α -Fluc oscillations observed in some of the cells from (B). (F) Single HepG2 cells transiently expressing κ B $_5$ →I κ B α -FLuc were continuously treated with TNF α or vehicle at the indicated concentrations. (G-I) Scatter plots representing the time of maximum re-synthesis (G) calculated from data in (B-D), and the time of minimum degradation (H) and re-synthesis (I) from data in (F).

Figure 3

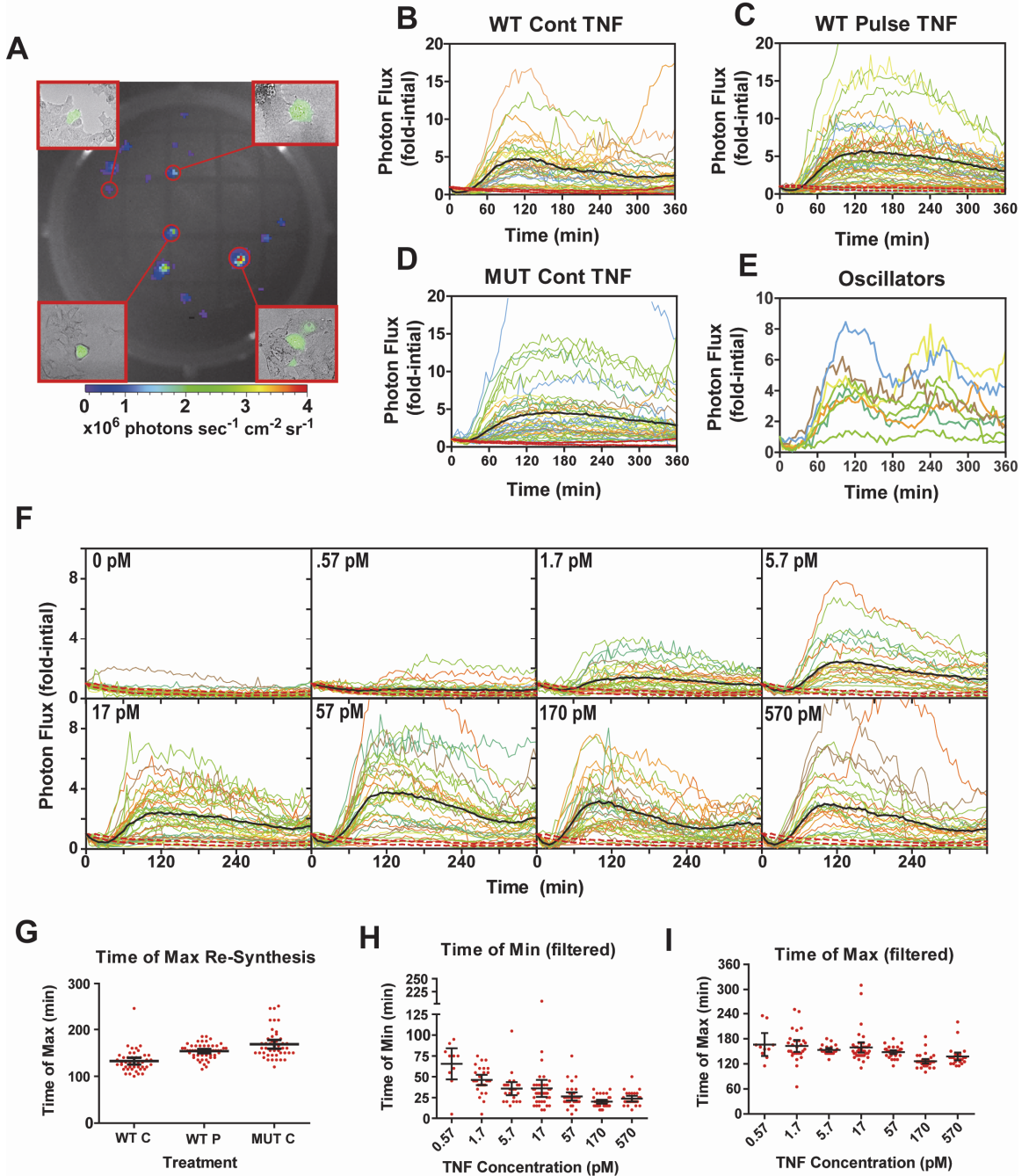


Figure 3.4: Experimental Investigation of Complex I κ B α Re-Synthesis Patterns.

(A) A physiologic IKK time-activity plot obtained by Moss & Gross et al. shown in red was reduced to four points capturing three components of IKK activity: activation rate (activation time parameter a), peak magnitude (parameter p), and deactivation rate (deactivation time parameter d). Each of the three IKK activity parameters described in (A) were modified to generate a total of 80 IKK input profiles (inset). (B) Effect of IKK deactivation (d) on I κ B α dynamics when a and p were held constant at 10 min and 1X fold-initial, respectively. (C) Effect of IKK peak magnitude (p) on I κ B α dynamics when a and d were held constant at 10 min and 30 min, respectively. (D, E) HepG2 cells expressing κ B $_5$ →I κ B α -FLuc were treated with the indicated TNF α concentrations or vehicle at $t = 0$ min. At 60 or 180 min, the cells were washed and replenished with fresh, TNF α -free media (wash-out conditions) or media containing TNF α at the initial concentration (a mock wash-out). Data were acquired every 5 min for 360 min and normalized as before to represent the mean of three or four independent TNF α exposure experiments, each performed in triplicate and averaged. (F) Plot representing the effect of washout time and TNF α concentration (5.7 pM or higher) on maximum I κ B α re-synthesis magnitude. All 180 min data represent parameters calculated from the second I κ B α re-synthesis peak. Data are mean \pm SEM. * indicates $p < 0.05$ for TNF α (170 or 570 pM) wash-out or mutant I κ B α (S32,36A)-FLuc versus continuous TNF α wild-type I κ B α -FLuc. The 30 min and 60 min data were $n = 2$ and thus were excluded from statistical analysis. (G) Plot representing the effect of wash-out time and TNF α concentration on the timing of maximum I κ B α re-synthesis. # indicates $p < 0.05$ for lowest vs. highest TNF α concentration within a given TNF α treatment. (H) HepG2 cells expressing κ B $_5$ →I κ B α (S32,36A)-FLuc were treated continuously with TNF α at the indicated concentrations or with vehicle and imaged every 5 min for 360 min; data were normalized as described previously and represent three independent experiments, each performed in triplicate and averaged.

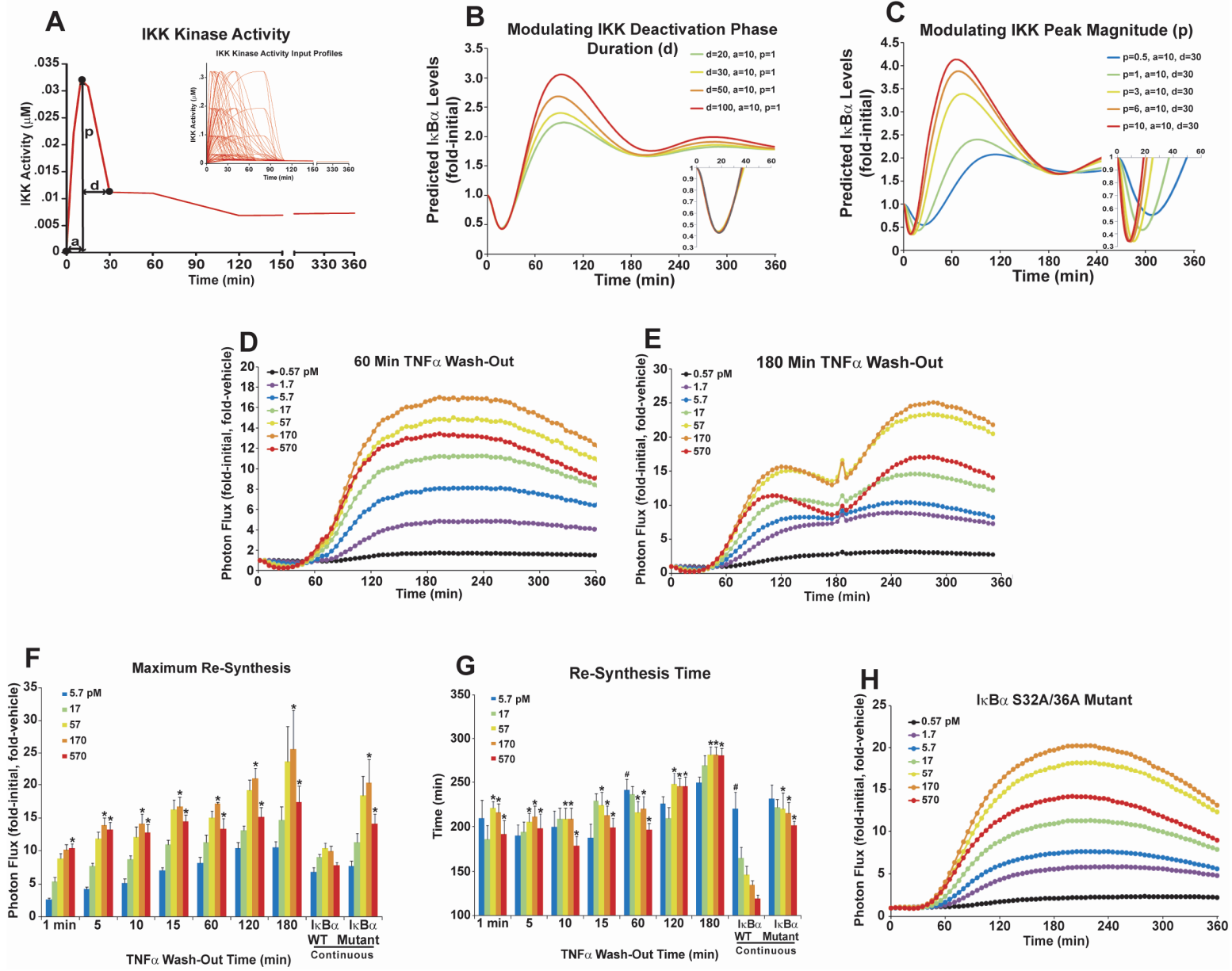
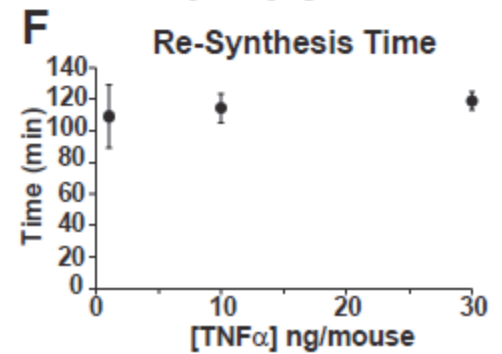
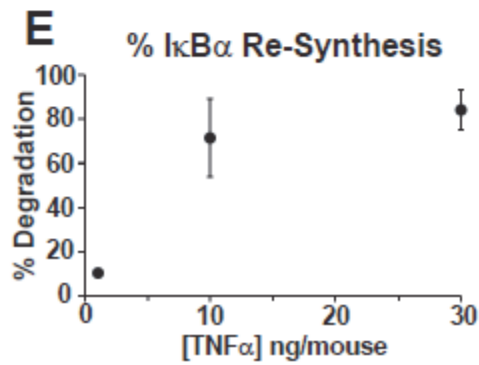
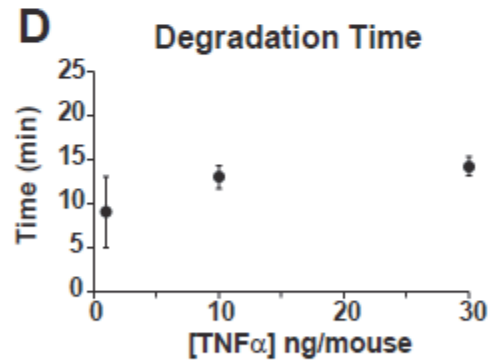
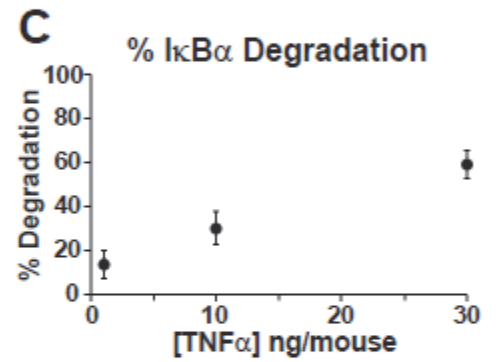
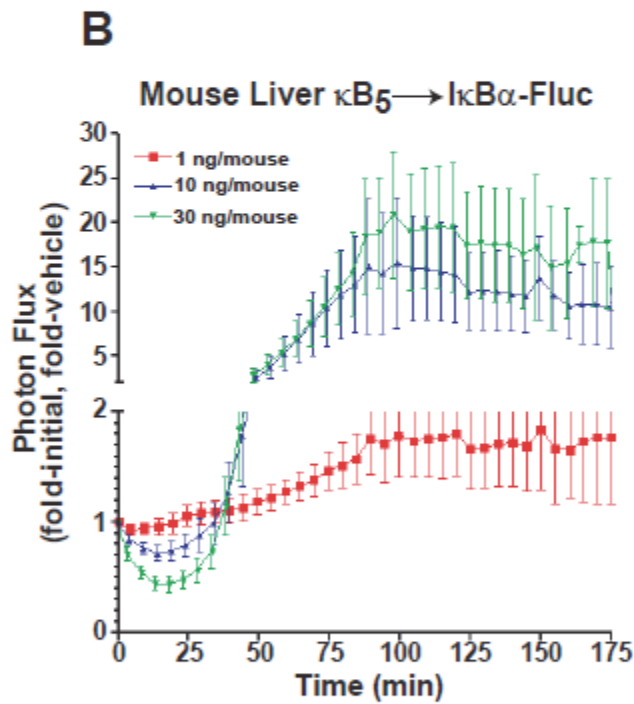
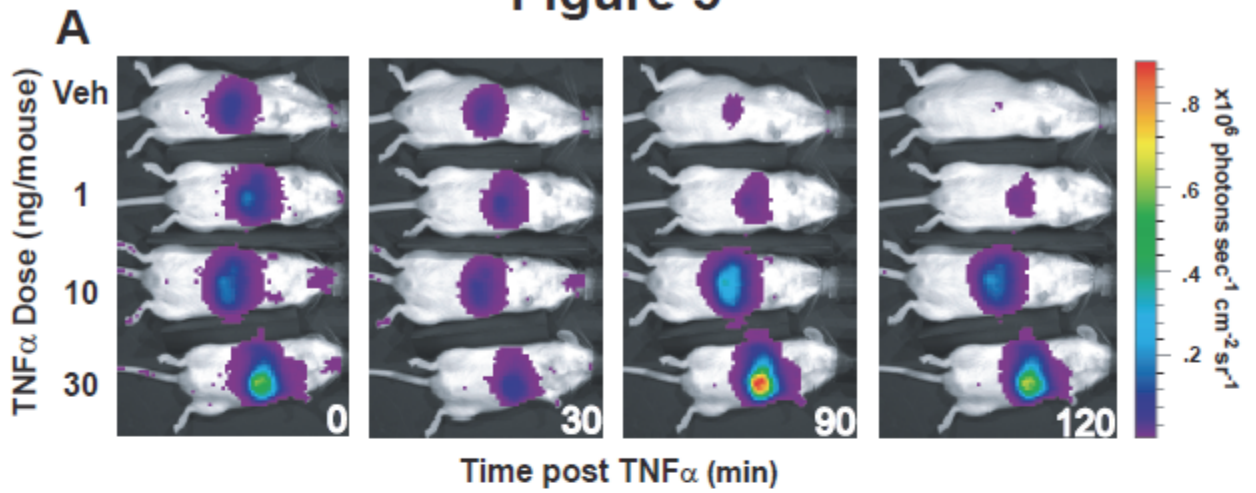


Figure 3.5: I κ B α Dynamics as a Function of TNF α Dose *In Vivo*. (A) *In vivo* transfection of mouse hepatocytes was performed using the hydrodynamic somatic gene transfer method. Mice were imaged in an IVIS 100 to obtain a pre-stimulation reading, followed by tail vein injection of 100 μ L of vehicle (sterile PBS) or TNF α (at the indicated doses), and then imaged at 5 min intervals for 3 hr. (B) Data from five independent experiments are plotted normalized to the pre-TNF α stimulation levels (fold-initial) and to a vehicle-treated animal (fold-untreated); error bars represent mean \pm SEM. (C-F) Quantitative analysis of *in vivo* measurements from that represent the extent of maximal I κ B α degradation (C) and re-synthesis (E), and the time of maximal I κ B α degradation (D) and re-synthesis (F), as functions of TNF α dose. All data are presented as mean \pm SEM; the x-axis is plotted on a linear scale. The 1 ng/mouse data point in (D) represents n = 3 because two animals showed no degradation at that dose and thus no degradation time could be calculated.

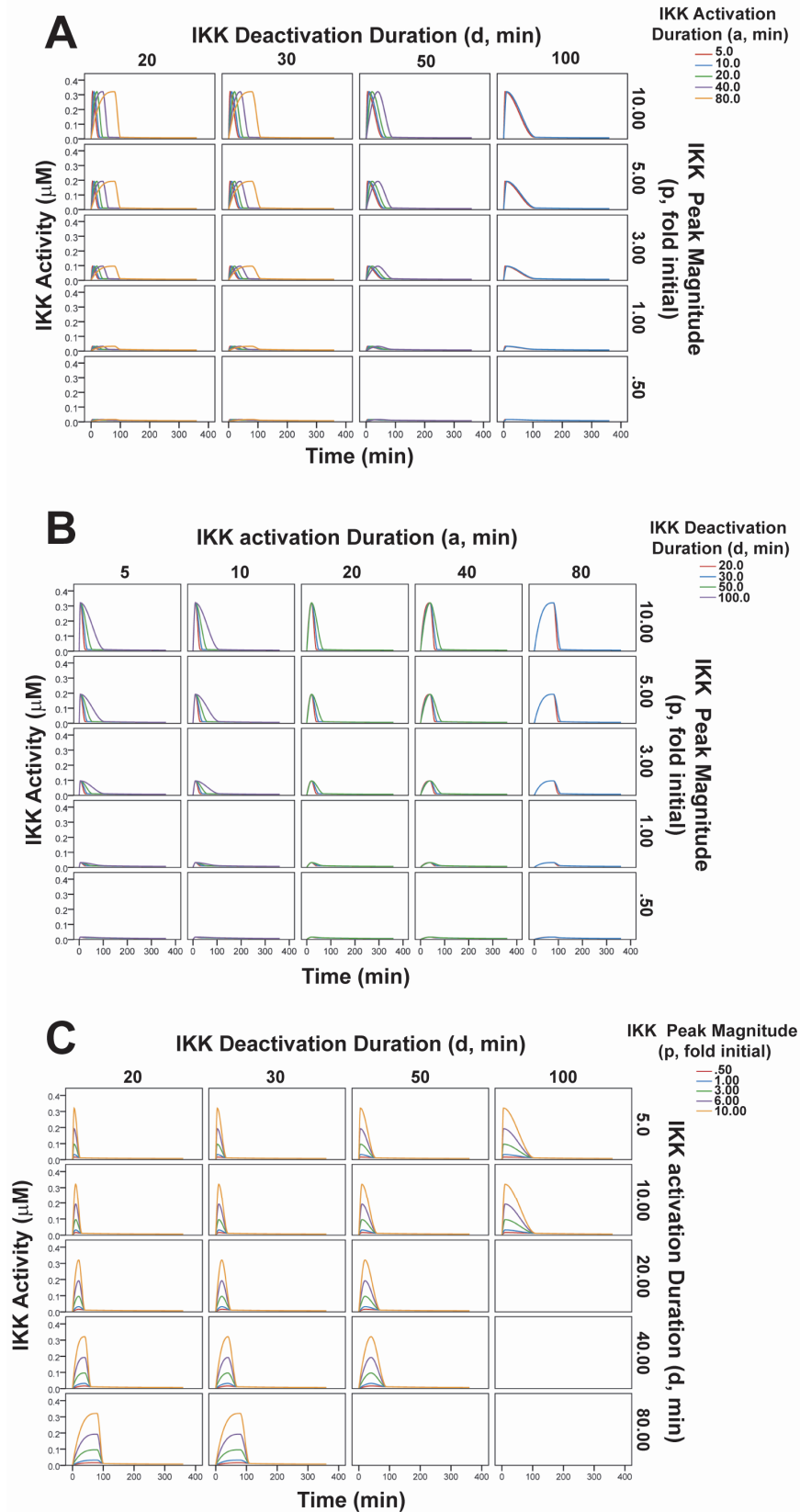
Figure 5



3.6 SUPPLEMENTARY FIGURES

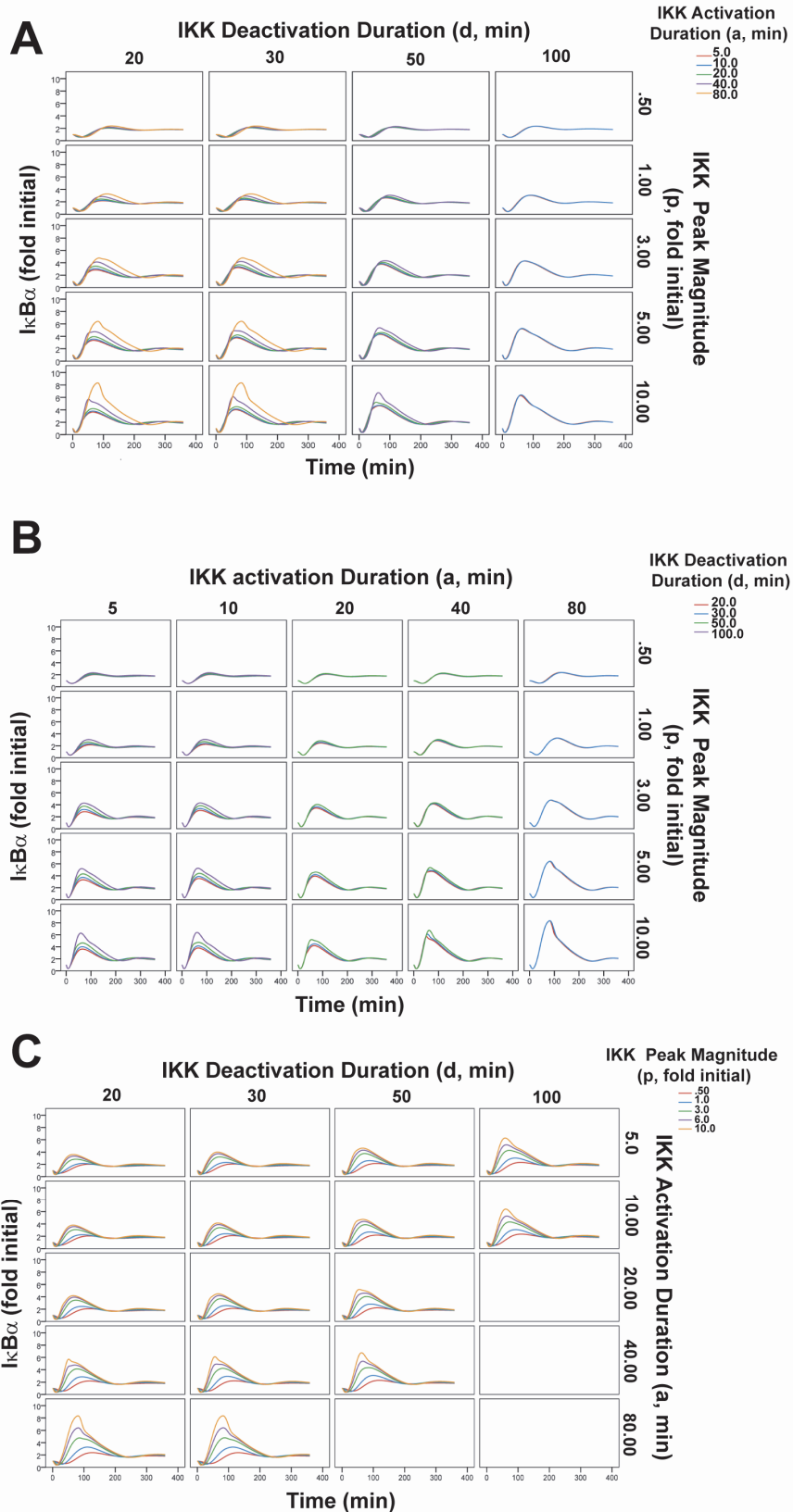
Supplemental Figure 3.1: Modified IKK Input Profiles. (A) The duration of the IKK deactivation phase and the IKK peak magnitude were held constant while the duration of the IKK activation phase was modulated. (B) The duration of the IKK activation phase and the IKK peak magnitude were held constant while the duration of the IKK deactivation phase was modulated. (C) The durations of the IKK activation and deactivation phases were held constant, while the IKK peak magnitude was modulated.

Supplemental Figure 1



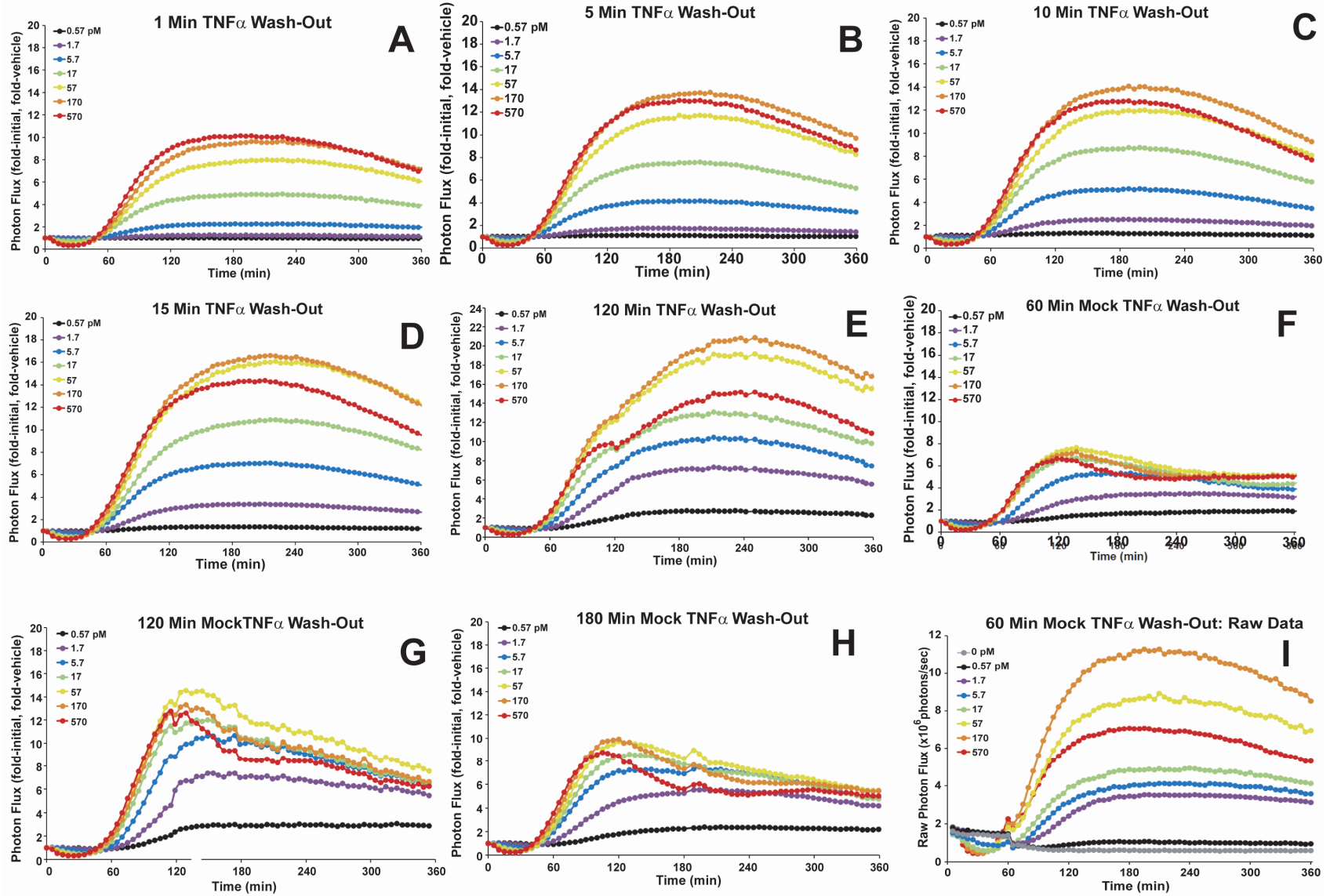
Supplemental Figure 3.2: Predicted I κ B α Dynamic Profiles in Response to Modulating IKK Activation, Deactivation, and Peak Magnitude. (A) The duration of the IKK deactivation phase and the IKK peak magnitude were held constant while the duration of the IKK activation phase was modulated. (B) The duration of the IKK activation phase and the IKK peak magnitude were held constant while the duration of the IKK deactivation phase was modulated. For a more detailed view, see Fig. 4B. (C) The durations of the IKK activation and deactivation phases were held constant, while the IKK peak magnitude was modulated. For a more detailed view, see Fig. 4C.

Supplemental Figure 2



Supplemental Figure 3.3: Representative Raw Data and Normalized Plots from Mock and TNF α Wash-Out Experiments. (A-H) HepG2 cells expressing $\kappa B_5 \rightarrow I\kappa B\alpha$ -FLuc were treated with the indicated TNF α concentrations or vehicle at $t = 0$ min. At the indicated time point, the cells were washed and replenished with fresh, TNF α -free media (wash-out conditions) or with media containing TNF α at the initial concentration (a mock wash-out). Images were taken every 5 min for 360 min; data were normalized as fold-initial and fold-vehicle, and the mean of three or four independent TNF α exposure experiments, each performed in triplicate and averaged, was plotted against time; the data in the mock wash-out plots represent a single experiment performed in triplicate. (I) The raw photon flux (photons/sec) from three wells each treated with the indicated concentration of TNF α were measured, averaged, and plotted as a function of time. A slight perturbation in signal is noted at 60 min when the cells were washed with PBS and placed back into TNF α - or vehicle-containing media; the perturbation also occurred in the vehicle-treated control (gray circles), and is thus accounted for when the data is normalized as fold-initial and fold-vehicle (Fig. S3F).

Supplemental Figure 3



3.7 REFERENCES

1. Kholodenko, B.N., *Cell-signalling dynamics in time and space*. Nat Rev Mol Cell Biol, 2006. **7**(3): p. 165-76.
2. Brandman, O. and T. Meyer, *Feedback loops shape cellular signals in space and time*. Science, 2008. **322**(5900): p. 390-5.
3. Cebecauer, M., et al., *Signalling complexes and clusters: functional advantages and methodological hurdles*. J Cell Sci, 2010. **123**(Pt 3): p. 309-20.
4. Perkins, N.D., *Integrating cell-signalling pathways with NF-kappaB and IKK function*. Nat Rev Mol Cell Biol, 2007. **8**(1): p. 49-62.
5. Moss, B.L., et al., *Identification of a ligand-induced transient refractory period in nuclear factor-kappaB signaling*. J Biol Chem, 2008. **283**(13): p. 8687-8698.
6. Werner, S.L., D. Barken, and A. Hoffmann, *Stimulus specificity of gene expression programs determined by temporal control of IKK activity*. Science, 2005. **309**(5742): p. 1857-61.
7. Werner, S.L., et al., *Encoding NF-kappaB temporal control in response to TNF: distinct roles for the negative regulators IkappaBalpha and A20*. Genes Dev, 2008. **22**(15): p. 2093-101.
8. Ashall, L., et al., *Pulsatile stimulation determines timing and specificity of NF-kappaB-dependent transcription*. Science, 2009. **324**(5924): p. 242-6.
9. Turner, D.A., et al., *Physiological levels of TNFalpha stimulation induce stochastic dynamics of NF-kappaB responses in single living cells*. J Cell Sci, 2010. **123**(Pt 16): p. 2834-43.
10. Tay, S., et al., *Single-cell NF-kappaB dynamics reveal digital activation and analogue information processing*. Nature, 2010. **466**(7303): p. 267-71.
11. Hayden, M.S., A.P. West, and S. Ghosh, *NF-kappaB and the immune response*. Oncogene, 2006. **25**(51): p. 6758-80.
12. Pasparakis, M., *Regulation of tissue homeostasis by NF-kappaB signalling: implications for inflammatory diseases*. Nat Rev Immunol, 2009. **9**(11): p. 778-88.
13. Lee, T.K., et al., *A noisy paracrine signal determines the cellular NF-kappaB response to lipopolysaccharide*. Sci Signal, 2009. **2**(93): p. ra65.
14. Janes, K.A., et al., *The response of human epithelial cells to TNF involves an inducible autocrine cascade*. Cell, 2006. **124**(6): p. 1225-39.
15. Ito, C.Y., A.G. Kazantsev, and A.S. Baldwin, Jr., *Three NF-kappa B sites in the I kappa B-alpha promoter are required for induction of gene expression by TNF alpha*. Nucleic Acids Res, 1994. **22**(18): p. 3787-92.
16. Hoffmann, A., et al., *The IkappaB-NF-kappaB signaling module: temporal control and selective gene activation*. Science, 2002. **298**(5596): p. 1241-5.
17. Karin, M., *NF-kappaB as a critical link between inflammation and cancer*. Cold Spring Harb Perspect Biol, 2009. **1**(5): p. a000141.
18. Elizur, A., A.T. Vacek, and A.J. Howells, *Cloning and characterization of the white and topaz eye color genes from the sheep blowfly Lucilia cuprina*. J Mol Evol, 1990. **30**(4): p. 347-58.
19. Berasain, C., et al., *Inflammation and liver cancer: new molecular links*. Ann N Y Acad Sci, 2009. **1155**: p. 206-21.
20. Vlantis, K. and M. Pasparakis, *Role of TNF in pathologies induced by nuclear factor kappaB deficiency*. Curr Dir Autoimmun, 2010. **11**: p. 80-93.
21. Wullaert, A., et al., *Hepatic tumor necrosis factor signaling and nuclear factor-kappaB: effects on liver homeostasis and beyond*. Endocr Rev, 2007. **28**(4): p. 365-86.

22. Chen, F., K. Beezhold, and V. Castranova, *Tumor promoting or tumor suppressing of NF-kappa B, a matter of cell context dependency*. *Int Rev Immunol*, 2008. **27**(4): p. 183-204.
23. Vainer, G.W., E. Pikarsky, and Y. Ben-Neriah, *Contradictory functions of NF-kappaB in liver physiology and cancer*. *Cancer Lett*, 2008. **267**(2): p. 182-8.
24. Nelson, D.E., et al., *Oscillations in NF-kappaB signaling control the dynamics of gene expression*. *Science*, 2004. **306**(5696): p. 704-8.
25. Kearns, J.D., et al., *IkappaBepsilon provides negative feedback to control NF-kappaB oscillations, signaling dynamics, and inflammatory gene expression*. *J Cell Biol*, 2006. **173**(5): p. 659-64.
26. Sung, M.H., et al., *Sustained oscillations of NF-kappaB produce distinct genome scanning and gene expression profiles*. *PLoS One*, 2009. **4**(9): p. e7163.
27. Tian, B., D.E. Nowak, and A.R. Brasier, *A TNF-induced gene expression program under oscillatory NF-kappaB control*. *BMC Genomics*, 2005. **6**: p. 137.
28. Cheong, R., et al., *Transient IkappaB kinase activity mediates temporal NF-kappaB dynamics in response to a wide range of tumor necrosis factor-alpha doses*. *J Biol Chem*, 2006. **281**(5): p. 2945-50.
29. Paszek, P., et al., *Population robustness arising from cellular heterogeneity*. *Proc Natl Acad Sci U S A*, 2010. **107**(25): p. 11644-9.
30. Spiller, D.G., et al., *Measurement of single-cell dynamics*. *Nature*, 2010. **465**(7299): p. 736-45.
31. Gross, S. and D. Piwnica-Worms, *Real-time imaging of ligand-induced IKK activation in intact cells and in living mice*. *Nat Methods*, 2005. **2**: p. 607-614.
32. Place, R.F., D. Haspeslagh, and C. Giardina, *Induced stabilization of IkappaBalpha can facilitate its re-synthesis and prevent sequential degradation*. *J Cell Physiol*, 2003. **195**(3): p. 470-8.
33. Place, R.F., et al., *Cytokine-induced stabilization of newly synthesized I(kappa)B-alpha*. *Biochem Biophys Res Commun*, 2001. **283**(4): p. 813-20.
34. Warrington, N.M., et al., *Cyclic AMP Suppression Is Sufficient to Induce Gliomagenesis in a Mouse Model of Neurofibromatosis-1*. *Cancer Research*, 2010. **70**(14): p. 5717-5727.
35. Villalobos, V., et al., *Dual-color click beetle luciferase heteroprotein fragment complementation assays*. *Chem Biol*, 2010. **17**: p. 1018-1029.
36. Pichler, A., et al., *Generation of a highly inducible Gal4->Fluc universal reporter mouse for in vivo bioluminescence imaging*. *Proc Natl Acad Sci U S A*, 2008. **105**(41): p. 15932-7.
37. Harper, C.V., et al., *Dynamic organisation of prolactin gene expression in living pituitary tissue*. *J Cell Sci*, 2010. **123**(Pt 3): p. 424-30.
38. Dothager, R., et al., *Advances in bioluminescence imaging of live animal models*. *Curr Opin Biotechnol*, 2009. **20**: p. 45-53.
39. Webb, A.B., et al., *Intrinsic, nondeterministic circadian rhythm generation in identified mammalian neurons*. *Proc Natl Acad Sci U S A*, 2009. **106**(38): p. 16493-8.
40. Nelson, G., et al., *Multi-parameter analysis of the kinetics of NF-kappaB signalling and transcription in single living cells*. *J Cell Sci*, 2002. **115**(Pt 6): p. 1137-48.
41. Shih, V.F., et al., *Kinetic control of negative feedback regulators of NF-kappaB/RelA determines their pathogen- and cytokine-receptor signaling specificity*. *Proc Natl Acad Sci U S A*, 2009. **106**(24): p. 9619-24.
42. Zandi, E., Y. Chen, and M. Karin, *Direct phosphorylation of IkappaB by IKKalpha and IKKbeta: discrimination between free and NF-kappaB-bound substrate*. *Science*, 1998. **281**(5381): p. 1360-3.
43. O'Dea, E.L., et al., *A homeostatic model of IkappaB metabolism to control constitutive NF-kappaB activity*. *Mol Syst Biol*, 2007. **3**: p. 111.

44. Liu, F., Y. Song, and D. Liu, *Hydrodynamics-based transfection in animals by systemic administration of plasmid DNA*. *Gene Ther*, 1999. **6**(7): p. 1258-1266.
45. Pichler, A., et al., *In vivo RNA interference-mediated ablation of MDR1 P-glycoprotein*. *Clin Cancer Res*, 2005. **11**(12): p. 4487-94.

CHAPTER FOUR

High-Throughput Phosphatase RNA Interference Screen Identifies Novel Regulators of TNF α -Induced IKK:I κ B α :NF- κ B Negative Feedback Loop Dynamics

4.1 INTRODUCTION

It is currently believed that activation/de-activation of IKK (and other members of the NF- κ B signaling cascade) is regulated by the opposing effects of kinases/phosphatases [1], and although a large body of literature exists on the mechanisms by which kinases act during NF- κ B signaling, much less is known about the role of phosphatases in regulating members of the NF- κ B signal cascade. A number of phosphatases have been implicated in negative regulation of IKK activity and in regulation of NF- κ B activity (including PP2C β , PP2A, PP1, PPM1A, PPM1B and WIP1), and they often operate to counteract the activity of a kinase. Study of these phosphatases has revealed differential activity dependent on stimulus and cell specificity, redundant or compensatory pathways, and positive and negative regulatory roles (occasionally based on conflicting evidence; for example, PP2A has been posited by some to be a positive regulator of IKK and others claim it to be a negative regulator) [2-11]. Furthermore, an RNAi phosphatase library was recently utilized to identify unknown phosphatase regulators of NF- κ B transcriptional activity in mouse astrocytes [9]. The authors identified 19 phosphatases that activate or suppress NF- κ B activity 6-8 hours post-TNF α stimulation; their work indicated that the PP2A catalytic subunit

interacts with and inactivates IKK β , however, this function was not conserved in the context of human cell lines [8]. Given that our $\kappa B_5 \rightarrow I\kappa B\alpha$ -FLuc reporter had enabled us to study the IKK-I $\kappa B\alpha$ -NF- κB negative feedback loop with high temporal resolution [12], and given that temporal control of this and other negative feedback loops has emerged as a critical regulatory component of the intensity and specificity of the NF- κB transcriptional program [13-16], we sought to perform an RNAi screen to identify novel regulators of IKK-I $\kappa B\alpha$ -NF- κB negative feedback loop dynamics.

4.2 RESULTS

Optimization of siRNA and $\kappa B_5 \rightarrow I\kappa B\alpha$ -FLuc co-transfection in 96 well plate format.

We initially intended to perform the high-throughput RNAi screen by transfecting siRNAs into HepG2 cells stably transfected with a bi-directional pBI Tet vector to simultaneously express $\kappa B_5 \rightarrow I\kappa B\alpha$ -CBR and a constitutive SV40 \rightarrow CBG (which could be used to normalize for cell number and non-specific effects induced by siRNA knockdown and/or other experimental conditions). The two-color imaging capabilities on the IVIS 100 bioluminescence imager, coupled with spectral un-mixing software, can allow deconvolution of the signals from each of these reporters [17]. Additionally, the Tet-inducible pBI plasmid system would have given us the ability to “dial-in” an optimal level of reporter expression (i.e., allow expression optimization for high signal-to-noise and effective dynamic range). Pilot transient transfection experiments with the pBI- $\kappa B_5 \rightarrow I\kappa B\alpha$ -CBR/SV40 \rightarrow CBG reporter revealed leaky expression of both reporters and

doxycycline-induction actually dampened the dynamic range (amount of I κ B α -CBR degradation and re-synthesis) of the κ B $_5$ →I κ B α -CBR reporter. Attempts at making stable HepG2 Tet-ON cells with the pBI- κ B $_5$ →I κ B α -CBR/SV40→CBG reporter were unsuccessful. Efforts were then focused towards employing HepG2 cells transiently expressing the pBI- κ B $_5$ →I κ B α -CBR/SV40→CBG reporter construct and making use of the fact that leaky expression gave reasonable dynamic range and TNF α dose responsiveness. After scaling down to 96 well plate format and testing a panel of plasmid/siRNA co-transfection reagents, X-TremeGENE (Roche) was chosen and co-transfections of siRNA and plasmid reporter were optimized. This was accomplished by using control siRNAs designed against either I κ B α or CBR; when these siRNAs are efficiently transfected they will knock-down bioluminescent signal from the κ B $_5$ →I κ B α -CBR portion of the reporter, a phenotype that is easily quantified by imaging cellular bioluminescence. It was found that optimal knock-down of luciferase signal was achieved using 50 ng/well reporter, 88 ng/well siRNA, and 0.8 μ L/well X-TremeGENE with a 48 hr transfection.

Using the optimized co-transfection protocol, we stimulated HepG2 cells with TNF α (20 ng/mL) and measured the effect of siRNA expression upon I κ B α dynamics. It became apparent that HepG2 cell expression levels of SV40→CBG in 96 well plate format were too low to reliably use for normalization purposes, and for that reason, taking a series of red, green, and open filtered images for each time point was adding unnecessary complexity. Therefore, the decision was made to abandon the pBI vector, and go back to our original κ B $_5$ →I κ B α -FLuc construct. Several unsuccessful attempts were made to develop HepG2 cells stably expressing the κ B $_5$ →I κ B α -FLuc, so we

subsequently began optimizing transient co-transfections of this plasmid reporter and siRNA. We were able to achieve robust knock-down using X-tremeGENE and to successfully perform real-time imaging of I κ B α -FLuc dynamics with high-temporal resolution, allowing us to investigate not only changes in the amplitude of I κ B α -FLuc degradation and re-synthesis (as typically measured in high-throughput screens), but also the effect of siRNAs on the kinetic aspects of the negative feedback loop (i.e., times of maximal degradation and re-synthesis, rate of re-synthesis, and re-synthesis lag time).

Optimization of a novel method by which high-throughput robotic screening strategies can be used to assay for alterations in the dynamics (both amplitude and kinetics) of the IKK:I κ B α :NF- κ B negative feedback loop.

Once the optimal conditions for bioluminescent reporter and siRNA co-transfection were determined, we sought to develop, optimize, and determine the robustness of a novel method for robotic high-throughput RNAi screening that would allow us to assay for phosphatases involved in regulating I κ B α dynamics. The Washington University High-Throughput Screening Robotics Core (HTC) has purchased an siRNA phosphatase library (consisting of 444 duplexes against 222 phosphatases and phosphatase-associated genes in the human genome; Qiagen, Inc.) as well as a Beckman-Coulter Biomek FX dual bridge liquid handler, bar-code printer and independent reader, a lid station capable of removing and replacing lids, a tip-lift, an ambient temperature carousel, a heated, humidified CO₂ incubator and a MultiDrop dispensing station. These instruments are controlled by the Sagian SAMI software and accessed by a Sagian ORCA robot.

A script was written to program the robot and liquid handler to perform triplicate co-transfections of $\kappa B_5 \rightarrow I\kappa B\alpha$ -FLuc reporter and siRNA from a library plate onto three 96 well plates pre-plated with HepG2 cells (see a detailed description of this protocol in the Methods Section). Each library plate contained 80 experimental siRNAs (two different duplexes/well towards the same target) arrayed in Columns 2-11, two negative control siRNAs (a scrambled negative control sequence and a sequence targeting GFP) in the last two wells of Column 12, and the remaining wells in Columns 1 and 12 were empty to allow addition of screen-relevant positive, negative, and transfection controls. The additional controls we added were: (1) siTNFR1 as a positive control for non-response to TNF α treatment, (2) siFLuc as a control of transfection efficiency, (3) Qiagen AllStars siNeg as a negative control, (4) siPPP2CA as a biological positive control given its known role as a regulator of IKK, and (5) no siRNA as a control for transfection toxicity (Figure 4.1).

Of critical importance to our screen was acquiring data with high temporal resolution that would enable evaluation of kinetic parameters of the IKK-I $\kappa B\alpha$ -NF- κB negative feedback loop. Due to the fast rate of photon flux change at certain times post TNF α stimulation, bioluminescence images must be taken at least every 5 min, with all wells of a 96 well plate being imaged simultaneously. The only instrument available to us with this capability is the aforementioned IVIS 100 bioluminescence imager (Caliper Life Sciences, Inc.), which also allows controlled temperature and CO₂ conditions.

A test transfection was carried using a test library plate and three plates of pre-plated HepG2 cells. Forty-eight hours post-transfection, cells were stimulated with TNF α and bioluminescence imaging was carried out for 6 hr on the IVIS to capture a set of full

dynamic I κ B α profiles. The knock-down efficiency, as measured by a decrease in luciferase signal in wells transfected with siFLuc, was 87.1 ± 0.3 % (mean \pm SD), indicating efficient siRNA transfection. Bioluminescent photon flux values (normalized as fold-initial) from each control well were graphed as a time course (Figure 4.2). The data showed good correlation of controls within plates during the I κ B α -FLuc degradation phase (with Plate 2 demonstrating more intra-plate variability). TNFR1 knock-down completely abolished responsiveness to TNF α stimulation while PPP2CA knock-down showed little effect on the degree of degradation when compared to no siRNA or siNeg controls. A higher degree of intra- and inter-plate variability was noticed during the I κ B α -FLuc re-synthesis phase, but siTNFR showed no evidence of re-synthesis, and siPPP2CA treatment resulted in slowed re-synthesis rate and decreased amplitude compared to negative controls. This gave us confidence that novel phosphatase siRNAs that impact I κ B α -FLuc dynamics could be readily discerned from negative control siRNAs during the subsequent screen.

Execution of phosphatase RNAi screen to identify novel regulators of I κ B α dynamics in the presence of TNF α -induced stimulation.

The screen was performed by co-transfecting the phosphatase siRNA library with the κ B β →I κ B α -FLuc reporter in HepG2 cells in 96 well plate format (Figure 4.3). The co-transfected cells were then stimulated with TNF α and imaged for luciferase bioluminescence under (for more details, see Methods section). This regimen provided a dynamic read-out with high-temporal resolution, allowing us to investigate not only

changes in the amplitude of degradation and re-synthesis (as typical high-throughput screens monitor), but also the effect of siRNAs on the kinetic aspects of the negative feedback loop (i.e., times of maximal I κ B α -FLuc degradation and re-synthesis, rates of re-synthesis, and re-synthesis lag times). Though other RNAi screens have been published looking for novel regulators (including phosphatases) of the NF- κ B pathway ([7, 9, 18]), most have examined down-stream NF- κ B transcriptional activity many hours-to-days following pathway stimulation and none have honed in specifically on the IKK-I κ B α -NF- κ B negative feedback loop or on the kinetic aspects of NF- κ B signaling.

The raw bioluminescence time course data was normalized as fold initial and then graphed as a first-pass examination of quality control (see example plate in Fig. 4.4). We noted that within a triplicate, the replicates were tight correlated in regard to I κ B α -FLuc degradation and re-synthesis rate, though more variability was observed in magnitude of peak re-synthesis. Of particular note was the variety of I κ B α -FLuc dynamic profiles observed, many with vastly different shapes than seen under control siRNA treatment. For example (Fig. 4.4) some wells exhibited very sharply defined re-synthesis peaks (row 5, column 6) and others had much broader peaks (row 7, column 5); some wells showed higher levels of re-synthesis (row 3, column 4) and others less re-synthesis (row 7, column). Surprisingly, when focusing on the I κ B α -FLuc degradation phase (Fig. 4.4) we observed that the experimental siRNAs did not greatly affect shape, degree, or kinetics of I κ B α -FLuc. The few exceptions were siRNAs that seemed to prolong the duration of the degradation phase (for example row 6, column 2).

While the controls within a given plate triplicate were very tightly correlated, we observed a minor degree of inter-plate (across the three siRNA library plates) control

well variability during screen run #1 and a larger degree during run #2. This variability may have stemmed from the fact that the screen inherently monitors a common stress-activated pathway with highly sensitive temporal and dynamic readouts. Thus, we chose to analyze the phosphatase screen data on a plate-by-plate basis rather than screen-wide. While this method makes it difficult to rank hits found on one plate against hits found on another, it does somewhat overcome the non-random alphabetic placement of siRNAs within library plates, an issue that can result in over-representation of hits from one plate. Additionally, hits from each plate can be ranked against each other during secondary screening analysis.

Rigorous statistical analysis of phosphatase screen data and identification of high-confidence hits.

The raw bioluminescent photon flux data was normalized as fold-initial as a means of intra-well normalization. The phosphatase screen was analyzed plate-by-plate due to high variability observed within internal controls between plates. Three different approaches were undertaken to analyze the screen data and determine hits. The first approach was a quartile-based method that is robust to outliers, true hits, and non-symmetrical data [21, 22] and that has been successfully used in previous high-throughput screens [19]. The second approach was to apply unbiased K-means clustering and Principal Component Analysis (PCA) for exploratory data analysis and to group siRNA treatments based on similarity of corresponding I κ B α -FLuc bioluminescent profiles. The third approach, cumulative log-likelihood analysis, was based on a

Gaussian probability density function and allowed us to rank the deviation of an experimental siRNA treatment from the negative controls screen wide (personal communication with Dr. Joshua Swamidass and Mr. Reece Goiffon).

In quartile-based analysis, both raw photon flux data and fold-initial normalized data from each run of the screen were analyzed plate-by-plate. A total of seven parameters were chosen for evaluation (Figure 4.5):

- (1) Initial Photon Flux Level (the raw photon flux signal at $t = 0$ min)
- (2) Degradation Level (i.e. the minimum flux or fold-initial signal detected during I κ B α -FLuc degradation)
- (3) Degradation Time (the time at which minimum occurred)
- (4) Re-Synthesis Level (the maximum flux or fold-initial signal achieved during I κ B α -FLuc re-synthesis)
- (5) Re-Synthesis Time (the time at which maximal re-synthesis occurred)
- (6) Re-Synthesis Rate (the slope of re-synthesis between the minimum and maximum)
- (7) Re-Synthesis Lag Time (the value of the x-intercept of the linear regression of the I κ B α -FLuc re-synthesis rate)

The first five parameters were determined by descriptive statistics methods and the last two parameters were defined and analyzed by linear regression of the I κ B α -FLuc re-synthesis phase. Hits were identified for each parameter using a quartile-based method that is robust to outliers, true hits, and non-symmetrical data [19, 20]; statistical analysis was completed using both low stringency (targeted error rate $\alpha = 0.05$) and high stringency (targeted error rate $\alpha = 0.0027$) cut-offs. The collections of hits from each independently-run screen were then compared and the common strong and weak hits for each parameter are listed in Supplemental Table 4.1; a summary of strong hits for fold-

initial analysis are presented in Table 4.1. The known IKK regulators PPP1CB, PPP2CA, and PPP2C (the catalytic subunits of protein phosphatase 1 and protein phosphatase 2) showed up as weak hits in re-synthesis rate and maximum, confirming the ability of this screening technique to identify known regulators of NF- κ B signaling [2, 3, 5, 6, 8-10].

However, this analytical technique was not ideal for our time course data for a number of reasons: (1) many of the I κ B α -FLuc profiles had shapes that made regression analysis and determination of peak re-synthesis parameters difficult or impossible, (2) rather than relying on single points on the curve (minimums, maximums, etc), we sought a method that would allow simultaneous analysis of many or all data points along the I κ B α -FLuc profile, and (3) we sought a means of quantifying differences/similarities in I κ B α -FLuc profiles that are qualitatively obvious. We attempted to address some of these issues by the use of data clustering approaches, specifically by using unbiased K-means clustering and Principal Component Analysis (PCA) for exploratory data analysis and to group siRNA treatments based on similarity of corresponding I κ B α -FLuc bioluminescent profiles. Unfortunately, we found that overall these techniques did not contribute greatly to our data analysis, mainly because the minor degree of control well inter-plate variability proved to be a more significant issue during clustering, and the resultant multi-dimensional clusters were often difficult to interpret and did not significantly contribute information that could not easily be validated qualitatively.

The third analytical method, cumulative log-likelihood, was undertaken to compensate for inter-plate variability and for the non-random array of siRNAs. This technique quantifies the degree of deviation for a given siRNA treatment from the

negative controls (Fig. 4.6). This method adjusts for confounding variance that otherwise prevents direct comparisons between plates. More specifically, we first made a Gaussian probability density function at each time point based on the mean and variance of the plate negative controls. We then input each siRNA measurement into this function to quantify the normalized deviation from the set of negative controls. To combine replicates, and to later make a cumulative sequence, we prevented computational rounding error by taking the negative logarithm of the likelihood (log-likelihood) and summing ($\log A + \log B = \log AB$). In general, the greater the difference from the negative controls the greater the log-likelihood value for a given siRNA. The siRNA were then ranked and visualized in a bar graph in which each division of the bar height represents the contribution of an individual time point to the cumulative log-likelihood value (Sup. Fig. 4.1). This rank-based method allows for approximate comparison between plates and precise comparison within each plate. In addition, the bars were colored-coded based on Directional Replicate Agreement, wherein a value of ± 3 means all plates within the triplicate agreed and were either above or below the negative controls, and a value of ± 1 means imperfect agreement, with one of the replicates deviating from the others because it registered differentially above or below the negative controls.

Table 4.2 lists the top 10 hits from each plate separated into degradation phase, re-synthesis phase, and cumulatively for both degradation and re-synthesis considered together. The degradation phase analysis (Sup. Fig. 4.1) had low log-likelihood values (indicating they were not strongly different than controls) and many of the siRNAs exhibited directional replicate disagreement (denoted by green and yellow shading).

While the known IKK regulators PPP1CB, PPP2CA and PPP2CB (the catalytic subunits of protein phosphatase 1 and protein phosphatase 2) were identified as weak hits (i.e. falling towards the center of rank graphs), the recently identified PPM1A frequently showed up as a medium strength hit (i.e., towards the left end of the rank graphs) when considering both degradation and re-synthesis, confirming the ability of this screening technique and analytical method to identify true regulators of NF- κ B signaling [2-11]. This confirmed that the log-likelihood means of analysis could be successfully applied to dynamic time course data from a high-throughput RNAi screen, and may represent a new paradigm for analysis of this type of data.

Execution of a focused secondary RNAi screen in the presence of TNF α or IL-1 β .

Next, a focused secondary screen was executed. Preparation for the secondary screen was initiated prior to the development of the log-likelihood analytical method; therefore, hits for the secondary screen (Figure 4.7) were chosen based on the strongest stringency hits from each parameter analyzed by the quartile-based method (the results of both resazurin normalized and un-normalized data analysis were included). This screen was performed with the purposes of (1) ranking the top hits from both runs across all plates, and (2) comparing TNF α - and IL-1 β -induced I κ B α -FLuc dynamics to determine whether any of the top hits from the primary screen exhibited a TNF α -specific phenotype (understanding of which could potentially expedite mechanism-of-action investigations for the top hits). The 39 top hits from quartile-based analysis, 5 siRNAs that did not show up as strong or weak hits, and scrambled negative control siRNAs were re-arrayed

into a 96 well master plate (Fig. 4.8). The secondary screen was carried out using the procedures described for the primary screen (see Methods), however one half each plate was stimulated with 20 ng/mL TNF α and the other half with 10 ng/mL IL-1 β . The raw bioluminescence time course data was normalized as fold-initial and then graphed (see example plate in Fig. 4.9). The I κ B α -FLuc re-synthesis phase of control siRNA wells under IL-1 β stimulation mostly resembled TNF α -treated controls, except that at “peak” re-synthesis the signal kept gradually drifting up rather than reaching plateau. Visual comparison of the TNF α -stimulated wells versus the identical IL-1 β -stimulated wells revealed no obvious strong differences between the two different ligands, indicating that these top hits are likely general regulators of the NF- κ B pathway rather than regulators of ligand-specific induction of the pathway.

Data were analyzed using the log-likelihood method described above given the limitations of quartile-based analysis mentioned previously, especially on a small data set. As was noted previously for the primary screen, the degradation phase analysis (Sup. Fig. 4.2) had low log-likelihood values (indicating they were not strongly different than controls) and many of the siRNAs exhibited directional replicate disagreement (denoted by green and yellow shading). Furthermore, a number of the non-hit and negative siRNA controls (denoted in bold) ranked high, giving further indication that the degradation phase did not significantly differ from negative controls. Log-likelihood analysis of the re-synthesis phase revealed a number of strong hits with large log-likelihood values and consistent directional replicate agreement (Sup. Fig. 4.2). Upon knock-down, CDNK3, PPFIA3, ENPP3, SKIP and PPP1R3D exhibit I κ B α -FLuc re-synthesis profiles with a faster rate of re-synthesis and higher or more pronounced peak re-synthesis (i.e., negative

regulators). Additionally, PTPN3, PTPRJ, and PTPRN were identified as possible positive regulators (i.e., knock-down produced $\text{I}\kappa\text{B}\alpha$ -FLuc re-synthesis profiles with slower rate of re-synthesis and lower or delayed peak re-synthesis). The top 15 log-likelihood hits for degradation, re-synthesis, and degradation combined with re-synthesis are listed in Table 4.3

Validation of PTPRJ as a Novel Regulator of IKK: $\text{I}\kappa\text{B}\alpha$:NF- κB Negative Feedback Loop Dynamics.

PTPRJ was chosen for validation as an interesting candidate positive regulator of IKK: $\text{I}\kappa\text{B}\alpha$:NF- κB negative feedback loop dynamics given that, (1) it had a very strong phenotype in the screen, (2) it is a receptor-type tyrosine phosphatases with no known function in NF- κB signaling, and (3) because researchers at Washington University in St. Louis had recently identified a novel mutation of PTPRJ through a DNA deep-sequencing screen of genome remodeling in basal-like breast cancer [21].

First, four siRNA sequences targeting PTPRJ were transiently co-transfected along with the $\kappa\text{B}_5 \rightarrow \text{I}\kappa\text{B}\alpha$ -FLuc reporter plasmid into HepG2 cells. Cells were stimulated with TNF α and imaged for 6 hr in the IVIS100 to capture full $\text{I}\kappa\text{B}\alpha$ -FLuc bioluminescent profiles. Interestingly, only one sequence showed a similar phenotype as observed in the primary and secondary screens (sequence #5; Fig. 4.10): prolonged $\text{I}\kappa\text{B}\alpha$ -FLuc degradation phase, decreased rate of $\text{I}\kappa\text{B}\alpha$ -FLuc re-synthesis, and lower $\text{I}\kappa\text{B}\alpha$ -FLuc re-synthesis peak that is not sharp peak but instead yields a gradually-rising plateau. This same siRNA was confirmed to knock-down endogenous PTPRJ expression (by 50%) in HepG2 cells (Fig. 4.10, inset).

Given that only one siPTPRJ sequence resulted in a phenotype similar to that seen in the screens, we next sought to use shRNA to more stably and thoroughly knock-down PTPRJ expression in HepG2 cells. Four different PTPRJ hairpin shRNAs (and a shGFP negative control) were packaged into lentivirus and used to infect HepG2 cells. Following selection, HepG2 cells expressing the shRNAs were transiently transfected with the $\kappa B_5 \rightarrow I\kappa B\alpha$ -FLuc reporter as previously described, stimulated with TNF α , and imaged. The strongest knock-down (as quantified by Western blot; Fig. 4.11, inset) was achieved with hairpins 21 and 22; the strongest I $\kappa B\alpha$ -FLuc phenotype was noted for hairpin 21. Even though several siRNA sequences and shRNA hairpins did not reproduce the PTPRJ phenotype observed in the screen, we felt that we had sufficient compelling evidence to proceed with further investigation of the potential role of PTPRJ in the NF- κB pathway.

We next tested the hypothesis that over-expression of PTPRJ should enhance TNF α -induced I $\kappa B\alpha$ -FLuc re-synthesis. Compared to empty vector control, PTPRJ over-expression yielded greater levels of I $\kappa B\alpha$ -FLuc degradation and greater re-synthesis (Fig. 4.12). A phosphatase-dead mutant form of PTPRJ (C1239S; [22]) was also tested and we found that it similarly enhanced I $\kappa B\alpha$ -FLuc degradation, but not re-synthesis. These same constructs were also tested in HepG2 cells against a simple NF- κB transcriptional activity reporter ($\kappa B_5 \rightarrow FLuc$) to assess the effect of PTPRJ over-expression on basal NF- κB activity and TNF α -induced transcriptional activity. We found that PTPRJ over-expression tended to give lower basal levels of bioluminescence from the $\kappa B_5 \rightarrow FLuc$ reporter when compared to either empty vector or the C1239S mutant (Fig. 4.13).

Furthermore, upon stimulation with $\text{TNF}\alpha$, cells over-expressing wild-type PTPRJ showed enhanced activation compared to either control.

Additional follow-up on hits from the phosphatase screen is ongoing. Of particular interest will be CDKN3 which strongly impacted $\text{I}\kappa\text{B}\alpha$ -FLuc re-synthesis levels, and PTPRN which phenocopies PTPRJ. Initial knock-down experiments have proven difficult, so future validation studies will utilize protein over-expression methodologies.

4.3 DISCUSSION

It is currently believed that activation/de-activation of IKK (and other members of the NF- κ B signaling cascade) is regulated by the opposing effects of kinases/phosphatases [1], and while much effort has been directed towards understanding the mechanisms by which kinases act during NF- κ B signaling, much less is known about the role of phosphatases in regulating members of the NF- κ B signal cascade. One of the critical regulatory nodes known to be regulated by kinases and phosphatases is the IKK- $\text{I}\kappa\text{B}\alpha$ -NF- κ B negative feedback loop [2-11]. Furthermore, this negative feedback loop plays a major role in regulating the strength and duration of NF- κ B transcriptional activity [13-16]. Therefore, we performed a high-throughput phosphatase RNAi screen to identify novel regulators of the dynamics of the IKK- $\text{I}\kappa\text{B}\alpha$ -NF- κ B negative feedback loop utilizing our $\kappa\text{B}_5 \rightarrow \text{I}\kappa\text{B}\alpha$ -FLuc reporter.

Our unique screen was carried out with high temporal resolution (taking images every 5 min for 6 hr) in order to fully capture both degradation and re-synthesis of the

$\kappa B_5 \rightarrow I\kappa B\alpha$ -FLuc reporter upon stimulation with TNF α , with the hope of identifying siRNA targets that might strongly impact kinetic aspects of feedback loop regulation. We observed many different $\kappa B_5 \rightarrow I\kappa B\alpha$ -FLuc profiles in the screen, some with vastly different shapes than seen under control siRNA treatment (Fig. 4.4). Surprisingly, when focusing on the I $\kappa B\alpha$ -FLuc degradation phase, we did not observe siRNAs that exhibited strong effects on I $\kappa B\alpha$ -FLuc shape, degree, or kinetic. It is possible that strong degradation phase hits were not observed because the degradation phase has a small dynamic range and is dependent on signal decrease, or because the screen was run using a saturating concentration of TNF α (20 ng/mL) that could have masked the effects of some weaker degradation regulators. In the future, it could prove useful to run similar screens under a range of TNF α concentrations to assess whether hits with weaker effects can be identified.

Because our phosphatase screen dataset contained I $\kappa B\alpha$ -FLuc dynamic profiles of a variety of shapes and sizes, we sought an analytical method that would allow us to quantify how different the overall profile (or select sections of the profile) was from negative controls. This led to the application and optimization of log-likelihood analysis, a method that was able to identify known pathway regulators (PPP1CB, PPP2CA, PPP2CB, and PPM1A; Sup. Fig. 4.1). This confirmed that the log-likelihood means of analysis could be successfully applied to dynamic time course data from a high-throughput RNAi screen, and may represent a new paradigm for analysis of this type of data. We then successfully applied this method to our secondary screen data and identified a number of novel hits (Sup. Fig. 4.2), including CDNK3, PPFIA3, ENPP3,

SKIP, PPP1R3D, PTPN3, PTPRJ, and PTPRN (Table 4.3). Many of these hits are part of ongoing validation studies in our lab, including PTPRJ.

The human receptor-type protein tyrosine phosphatase type J (PTPRJ, also known as DEP-1 and CD148) is a trans-membrane receptor that is involved in signal transduction in leukocytes, contributing to cellular differentiation processes, and is found on the surface of several epithelial cell types [23]. Additionally, as its name might imply, it was found in fibroblasts cell lines to become upregulated 10-fold in cultures grown at high-density [24], suggesting another role in sensing cell-contacts and in density-dependent growth inhibition. Additionally PTPRJ has emerged as a tumor suppressor capable of negatively regulating cell proliferation and motility [25, 26]. PTPRJ tends to negatively interfere with surface receptor signaling at several levels, including at the level of receptor tyrosine kinases (such as PDGFR, VEGFR2, and MET) and downstream mediators of cell signaling pathways (including PKB/Akt, SRC, p120 catenin, and ERK1/2) [22, 27-29]. Recently, a PTPRJ mutation was found to be highly enriched in both metastasis and xenograft in a DNA sequencing screen of genome remodeling in basal-like breast cancer [21], and missense polymorphisms of PTPRJ were found to influence susceptibility to a wide spectrum of cancers [30].

In our screen, PTPRJ emerged as a positive regulator of TNF α -induced I κ B α -FLuc dynamic profiles: knock-down of PTPRJ resulted in a prolonged I κ B α degradation phase and a dampened re-synthesis phase (Fig. 4.9). This phenotype was confirmed using siRNA and shRNA knock-down strategies (Fig. 4.10, 4.11). When we over-expressed PTPRJ in HepG2 cells, we found increased TNF α -induced I κ B α degradation and re-synthesis, as well as enhanced NF- κ B transcriptional activity (Fig. 4.12, 4.13).

This data would suggest that PTPRJ can act to enhance TNF α -induced activation of NF- κ B signaling (a pro-proliferative signal), and that loss of PTPRJ would result in delayed or decreased NF- κ B activation (a more anti-proliferative effect). Thus, in the context of NF- κ B signaling, and in contrast to its previously known roles, PTPRJ seems to be acting to positively regulate TNF α -induced activation of NF- κ B signaling. Further validation and investigation of the mechanism by which PTPRJ impinges upon the NF- κ B pathway will hopefully confirm this novel new role for PTPRJ and lead to investigation of the physiological and/or pathophysiological relevance of PTPRJ in NF- κ B signaling.

4.4 METHODS

High-throughput primary siRNA screen. siRNA screening was performed in black, clear-bottomed, 96-well culture plates (Corning 3904) using a Beckman-Coulter Core robotics system, including an FX liquid handler, controlled by the Sagian graphical method development tool (SAMI scheduling software). A day prior to transfection, we manually seeded 10,000 cells in complete medium (DMEM supplemented with 10% heat-inactivated fetal bovine serum (Δ FBS) and 1% glutamine) at 150 μ l/well into three plates. Plates were maintained in an environmentally controlled incubator until needed for operations, thereby optimizing health and uniform treatment of all plates. Prior to transfection, siRNA library plates were thawed from -80C and centrifuged to pool the siRNA in the bottom of the well. Experimental siRNA oligos were pre-arrayed in columns 2-11 of each plate and individual controls comprising mock-transfected wells, non-targeting AllStars Negative Control sequence (siNeg, Qiagen Inc.), Firefly luciferase-targeting PGL3 siRNA (Integrated DNA Technologies, Inc.), TNFR1 targeting sequences (siTNFR1, Integrated DNA Technologies, Inc.), and a PPP2CA siRNA (siPPP2Ca, Integrated DNA Technologies, Inc.) were placed manually in columns 1 and 12 (Figure 4.1).

Forward co-transfection of siRNA and plasmid reporter was performed in triplicate. First, κ B₅→I κ B α -FLuc reporter plasmid was diluted into serum-free media and transferred onto one siRNA library plate (containing enough siRNA to transfect three identical cell plates) with a 96 multichannel head on the FX liquid handler and allowed to incubate for 5 min at room temperature. Next, 50 uL of X-TremeGENE (Roche, Inc.) transfection reagent, diluted in serum-free media, was added to the plasmid/siRNA

mixture with a 96 multichannel head on the FX liquid handler, mixed, and allowed to incubate for 15 min at room temperature. Subsequently, 30 uL/well of this mixture was transferred to the three previously seeded cell plates to a final concentration of 50 ng/well reporter plasmid, 0.8 uL/well X-TremeGENE reagent, and 88 ng siRNA/well in a final volume of 180 uL. Plates were maintained in an incubator for 24 hrs, and then aspirated and 150 uL/well of fresh colorless full media was added using the FX liquid handler.

At 48 hours post-transfection, D-luciferin (Biosynth) was added using the FX liquid handler to a final concentration of 150 µg/mL bringing the final volume up to 180 uL/well. Cells were allowed to equilibrate in this media for 30-60 min before the addition 20 uL/well of TNFα (20 ng/mL final concentration; #210-TA-050, R&D Systems, Minneapolis, MN) or vehicle (D-luc imaging media). Bioluminescence measurements were acquired in an IVIS 100 imaging system (Caliper Life Sciences, Hopkinton, MA) at 37°C under 5% CO₂ flow for 6 hr. Typical acquisition parameters were as follows: acquisition time, 15-30 sec; binning, 4-8; FOV, 25 cm; f/stop, 1; filter, open; image-image interval, 5 min; total number of acquisitions, 73. Immediately post-IVIS imaging, phase contrast photographs were acquired on the InCell 1000 (three 10X fields of view per well). Cell viability was then determined with resazurin dye (Sigma R7017) (final conc., 44 µM after a 2 hr incubation at 37°C as monitored on a FLUOstar OPTIMA fluorescence reader (BMG Labtech); excitation, 544 nm, emission, 590 nm). This procedure was repeated twice for all three plates of the Qiagen Human Phosphatase siRNA Library 2.0.

Focused secondary siRNA screen. The top hits from the primary screen were re-arrayed onto a single master plate by the FX liquid handler using a cherry-picking script written by Jayne Marasa. The master plate (Fig. 4.8) was arrayed such that columns 1 and 12 were duplicates of control siRNAs: 3 Qiagen AllStars negative control sequences, 4 non-hit phosphatases selected at random from the library (PPP2R5C, ENpp1, and PTPN13), and 1 siFLuc transfection control. Columns 2-6 and 7-11 were duplicates of the 39 strong stringency hits from the primary screen plus 1 scrambled negative control from the phosphatase library plate. All subsequent transfections, incubations, media changes, and measurements were performed as previously described with the exception that one half of the plate was stimulated with TNF α (20 ng/mL final concentration) and the other half with IL-1 β (10 ng/mL final concentration).

Statistical analysis and “high confidence hit” selection. Data were analyzed using Living Image 3.2 for data acquisition and raw data capture, and PASW Statistics 18 and MatLab 2011a for data analysis, statistics, and graphing. Circular regions of interest (ROIs) were drawn around each well and the photon flux at every time point was measured using Living Image 3.2. This raw data was then imported into PASW and the data were normalized to the signal at the first timepoint (with or without normalization to resazurin viability measurements).

Quartile-based analysis method. Descriptive statistics were used to calculate five parameters describing properties of the amplitude and kinetics of the I κ B α -FLuc dynamic profile (Figure 4.5):

- (1) Initial Photon Flux Level (the raw photon flux signal at $t = 0$ min)
- (2) Degradation Level (i.e. the minimum flux or fold-initial signal reached during I κ B α -FLuc degradation)
- (3) Degradation Time (the time at which minimum occurred)
- (4) Re-Synthesis Level (the maximum flux or fold-initial signal achieved during I κ B α -FLuc re-synthesis)
- (5) Re-Synthesis Time (the time at which maximal re-synthesis occurred)

Two additional parameters were defined and analyzed by linear regression of the I κ B α -FLuc re-synthesis phase by considering all 3 replicates at once, but the center point (between time-of-min and time-of-max) is found for each individual curve.

- (6) Re-Synthesis Rate (the slope of re-synthesis between the minimum and maximum)
- (7) Re-Synthesis Lag Time (the value of the x-intercept of the linear regression of the I κ B α -FLuc re-synthesis rate)

For each parameter, the median (Q2), first (Q1) and third (Q3) quartile values were calculated for all fold-initialized values and subjected to plate-by-plate analysis. Upper and lower boundaries were calculated as $Q3 + 2c(Q3 - Q2)$ and $Q1 - 2c(Q2 - Q1)$, respectively, for $c = 1.7239$ corresponding to a high stringency targeted error rate ($\alpha = 0.0027$) and $c = 0.9826$ corresponding to a lower stringency targeted error rate ($\alpha = 0.046$) [19, 20, 31]. For each run of the screen, data were analyzed plate-by-plate. The collections of hits from each independently-run screen were then compared and the common strong (based on the high stringency error rates) for each parameter are listed in Table 4.1.

Log-likelihood analysis method. The cumulative log-likelihood approach quantifies the deviation of an experimental siRNA treatment from the negative controls (scrambled negative controls and siGFP). This was done by generating a Gaussian probability density function at each time point based on the mean and variance of the negative controls on within a given plate. We then input each siRNA measurement to this function to quantify the deviation from the set of negative controls. To combine replicates, and to later make a cumulative sequence, we prevented computational rounding error by taking the negative logarithm of the likelihood (log-likelihood) and summing ($\log A + \log B = \log AB$). The log-likelihood values were determined separately for the degradation phase (which was defined as from $t = 0$ min to the median time point of the minimum value of the negative controls) and the re-synthesis phase (defined between the end of the degradation phase to the median time of greatest downward inflection in the kinetic profile of the negative controls), or cumulatively for both degradation and re-synthesis. The individual siRNAs from a given plate triplicate were then ranked according to their negative log-likelihood value and presented as a bar graph in which each division of the bar height represents the contribution of an individual time point to the cumulative log-likelihood value (Figure 4.6). In addition, the bars were colored-coded based on directional replicate agreement, wherein a value of ± 3 means all plates within the triplicate agreed and were either above or below the negative controls, and a value of ± 1 means imperfect agreement with one of the replicates deviating from the others because it registered differentially above or below the negative controls. This rank-based method allows for approximate comparison between plates and precise comparison within each plate.

siRNA Transfection for Validation of Screen Hits

HepG2 cells were plated (8,000 or 10,000 cells/well) the day before transfection. Forward co-transfection of siRNA (Qiagen, Inc) and plasmid reporter was achieved using X-TremeGENE (Roche, Inc.) transfection reagent as per manufacturer recommendations. Subsequently, 30 uL/well of this mixture was transferred to the cell plates to a final concentration of 50 ng/well reporter plasmid, 0.8 uL/well X-TremeGENE reagent, and 88 ng siRNA/well in a final volume of 180 uL. Plates were maintained in an incubator for 24 hrs, and then aspirated and 150 uL/well of fresh colorless full media was added. At 48 hours post-transfection, D-luciferin (Biosynth) was added to a final concentration of 150 µg/mL bringing the final volume up to 180 uL/well. Cells were allowed to equilibrate in this media for 30-60 min before the addition 20 uL/well of TNF α (20 ng/mL final concentration) or vehicle (D-luc imaging media). Bioluminescence measurements were acquired in an IVIS 100 imaging system (Caliper Life Sciences, Hopkinton, MA) at 37°C under 5% CO₂ flow for 6 hr. Typical acquisition parameters were as follows: acquisition time, 15-30 sec; binning, 4-8; FOV, 25 cm; f/stop, 1; filter, open; image-image interval, 5 min; total number of acquisitions, 73. Data were analyzed using Living Image 3.2 for data acquisition and raw data capture, and Excel 2007 for analysis and graphing.

shRNA Infection for Validation of Screen Hits

Lentivirus expressing constructs (pLKO.1 puro) were obtained pre-synthesized from the Genome Sequencing Center at Washington University. The targeting sequences for the 4 shPTPRJ constructs and shGFP are as follows:

	Sequence	target
shGFP	GCCACAACATCGAGGACGGCA	
19	CCACACAAGCACGTATGACAA	exon 8 (2101-2121)
20	GCCATAGAGTTCAGGACAAAT	spans exon 6 & 7 (1430-1450)
21	CCGATACAATGCCACCGTTTA	exon 6 (1372-1392)
22	CCTACTGTGTCTTGGAAATCTA	exon 26 (4778-4798) specific to isoform 1

To generate lentivirus containing hairpins, 500,000 293T cells were pre-plated in 60 mm dishes and co-transfected the following day with 1 µg of hairpin construct, 900 ng packaging plasmid pCMV-ΔR8.2, and 100 ng of envelope plasmid pVSVG using Fugene 6. Two days after transfection, virus containing supernatant was collected from 293T cells and filtered through a 0.45 µm filter, mixed with 5ug/mL protamine sulfate, and added to HepG2 cells at 50% confluency in a 10cm² dish. Media was replenished 12 hrs post-transduction cells were subsequently maintained in media supplemented with 750 ng/mL puromycin hydrochloride to retain expression of the hairpins. Two days post-transduction, shPTPRJ or shGFP cells were plated in parallel for protein knockdown

confirmation (MAB1934) and transient transfection and subsequent imaging measurements with the $\kappa B_5 \rightarrow I\kappa B\alpha$ -FLuc reporter as previously described.

PTPRJ Over-Expression Studies

PTPRJ expression constructs were obtained from Dr. Len Maggi who had previously cloned wild-type PTPRJ cDNA (Open Biosystems) into the pDEST26 vector backbone to generate pDEST26-His-PTPRJ. The C1239S phosphatase-dead mutant of PTPRJ was made by site-directed mutagenesis.

HepG2 cells were plated (7,000 cells/well) in black 96 well plates the day before transfection. Co-transfection of PTPRJ or backbone control plasmid (75 ng/well), $\kappa B_5 \rightarrow I\kappa B\alpha$ -FLuc (50 ng/well) or $\kappa B_5 \rightarrow I\kappa B\alpha$ -FLuc (25 ng/well), and TK \rightarrow RLuc transfection control plasmid (5 ng/well) was achieved using Fugene 6 (Roche, Inc.) transfection reagent as per manufacturer recommendations. Media was replenished 24 hours post-transfection and imaging was carried out 48 hours post-transfection as described above for siRNA experiments.

4.5 FIGURES



	Qiagen Neg												no siRNA 
	IDT Fluc												Qia TNFRS F1A_5
	IDT Fluc												Qia PPP2C A_6
	no siRNA												Qiagen Neg
	Qia PPP2C A_6												Qiagen Neg
	Qia TNFRS F1A_5												Neg control
													siGFP

Figure 4.1: Schematic of the siRNA Phosphatase Master Plate with Added Controls

96 well plate grid denoting the location of each manually plated control siRNA duplex (white boxes), the phosphatase library controls (labeled gray boxes), and the experimental siRNAs (unlabeled gray boxes). The red symbols mark the two controls wells that were treated with vehicle in the screen.

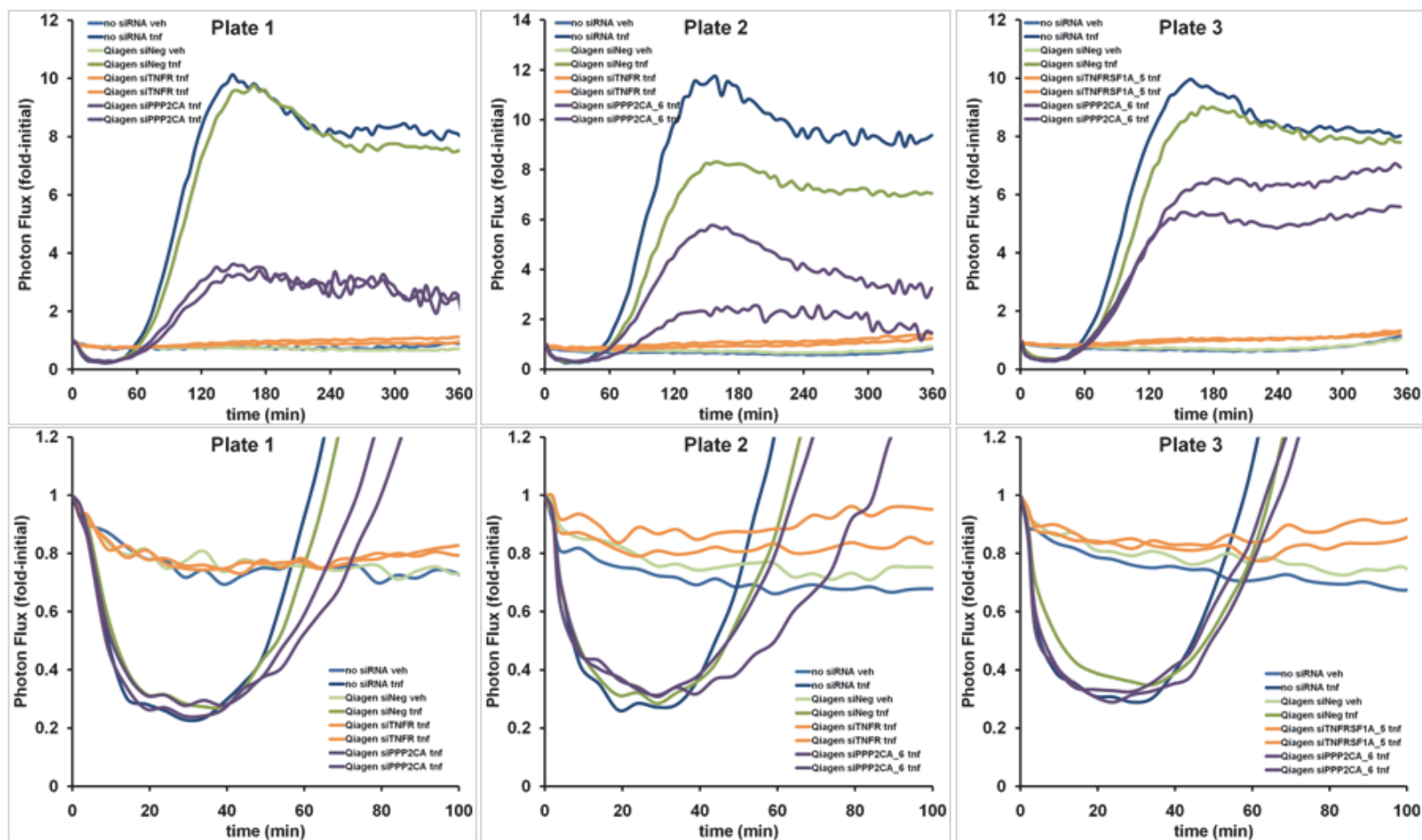


Figure 4.2: Schematic Efficient siRNA Transfection and Knock-Down of Luciferase Signal

A test transfection was carried using a test phosphatase siRNA library plate and three plates of pre-plated HepG2 cells. 48 hours post-transfection the cells were stimulated with TNF α or vehicle and bioluminescence imaging was carried out for 6 hr on the IVIS to capture a set of full dynamic $\text{I}\kappa\text{B}\alpha$. The photon flux from each control well was plotted as fold-initial versus time.

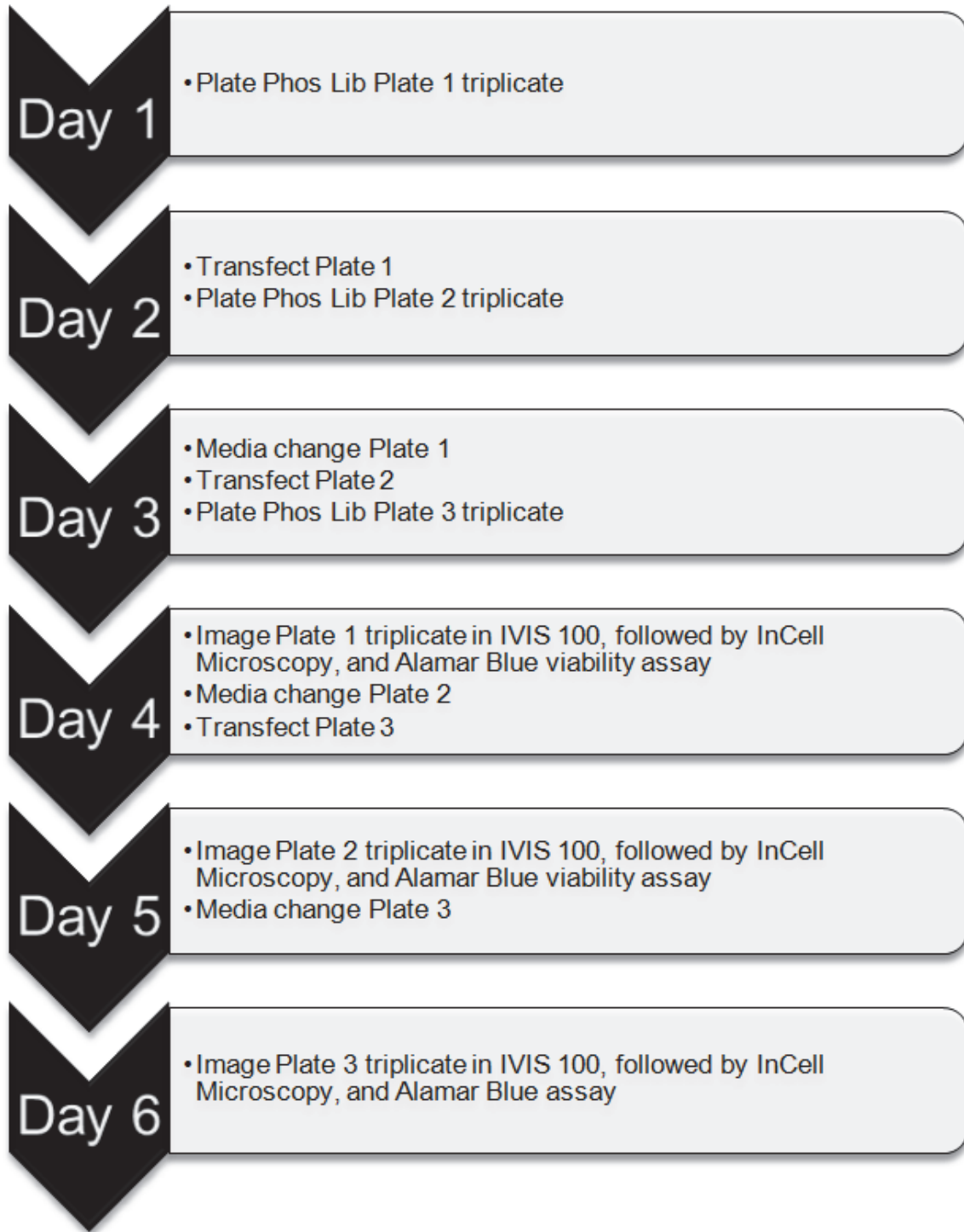
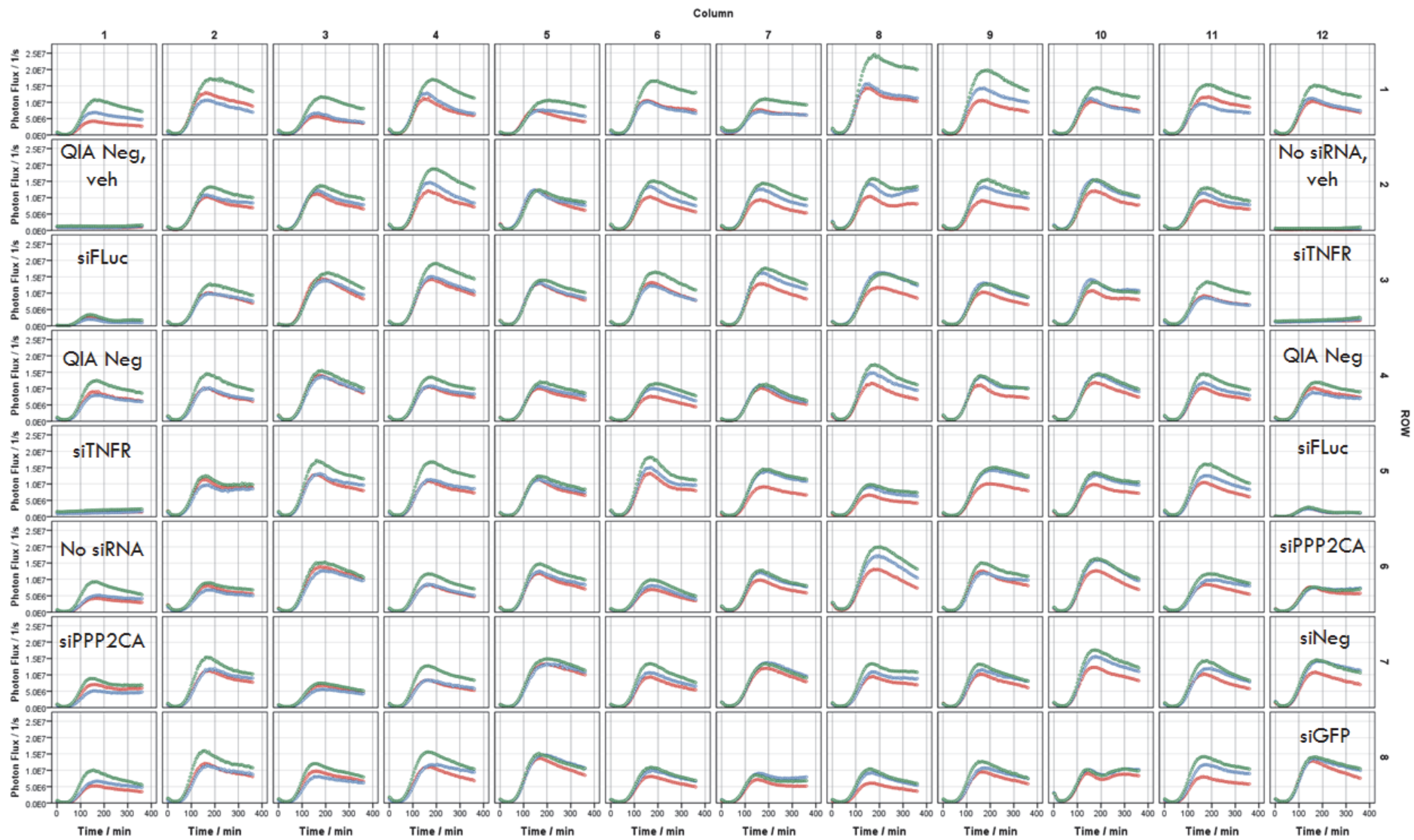


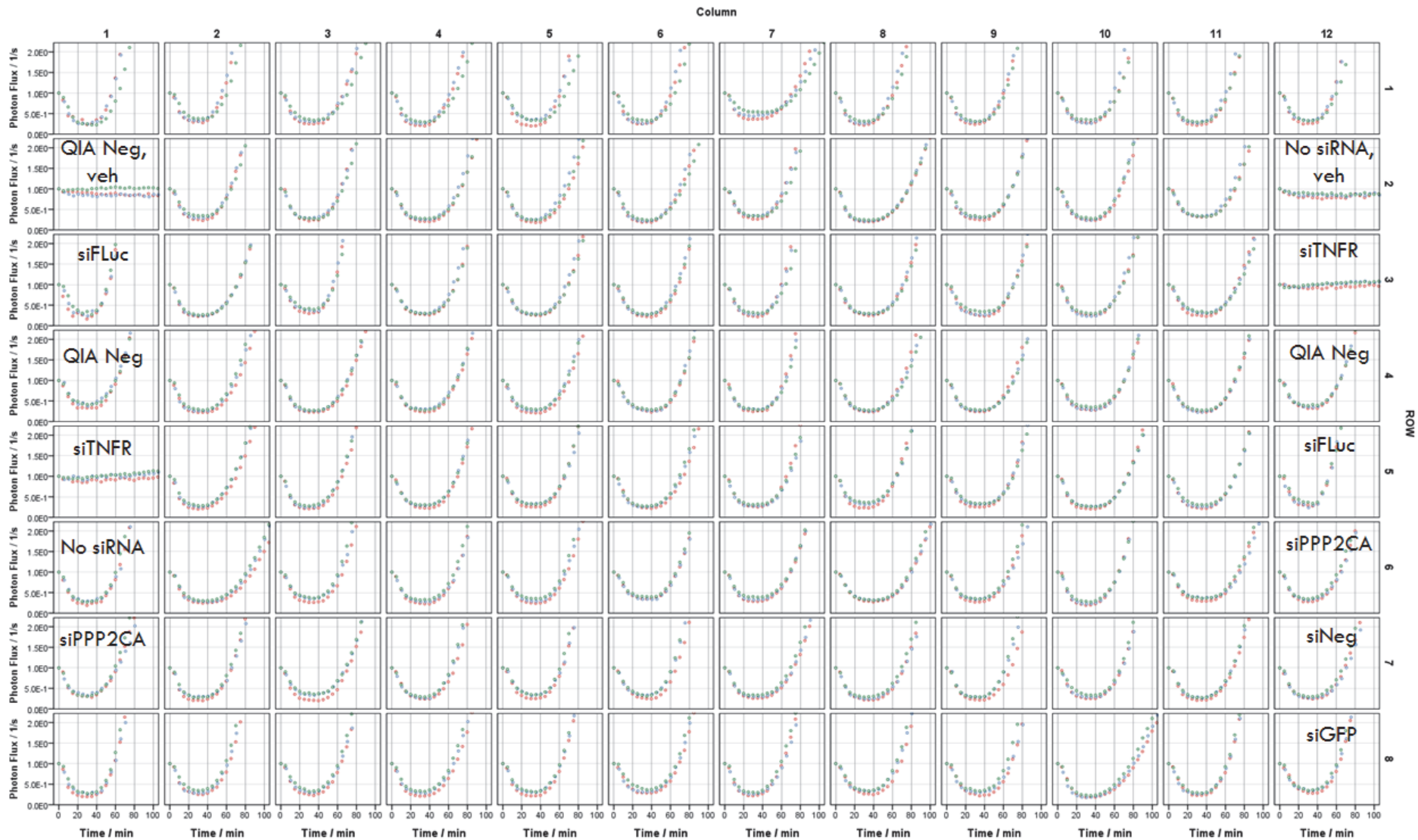
Figure 4.3: Timeline of High-Throughput Phosphatase siRNA Screening Procedure

By staggering transfections, the entire phosphatase siRNA library could be screened in 6 days.

Figure 4.4: Normalized photon flux data from the Qiagen Human Phosphatase Library 2.0 Plate 1 triplicate.

The raw photon fluxes for each well were normalized as fold-initial and then plotted against time. The first graph represents the full 6 hr profile; the second graph represents the degradation phase. The different colored symbols differentiate the data from each plate triplicate.





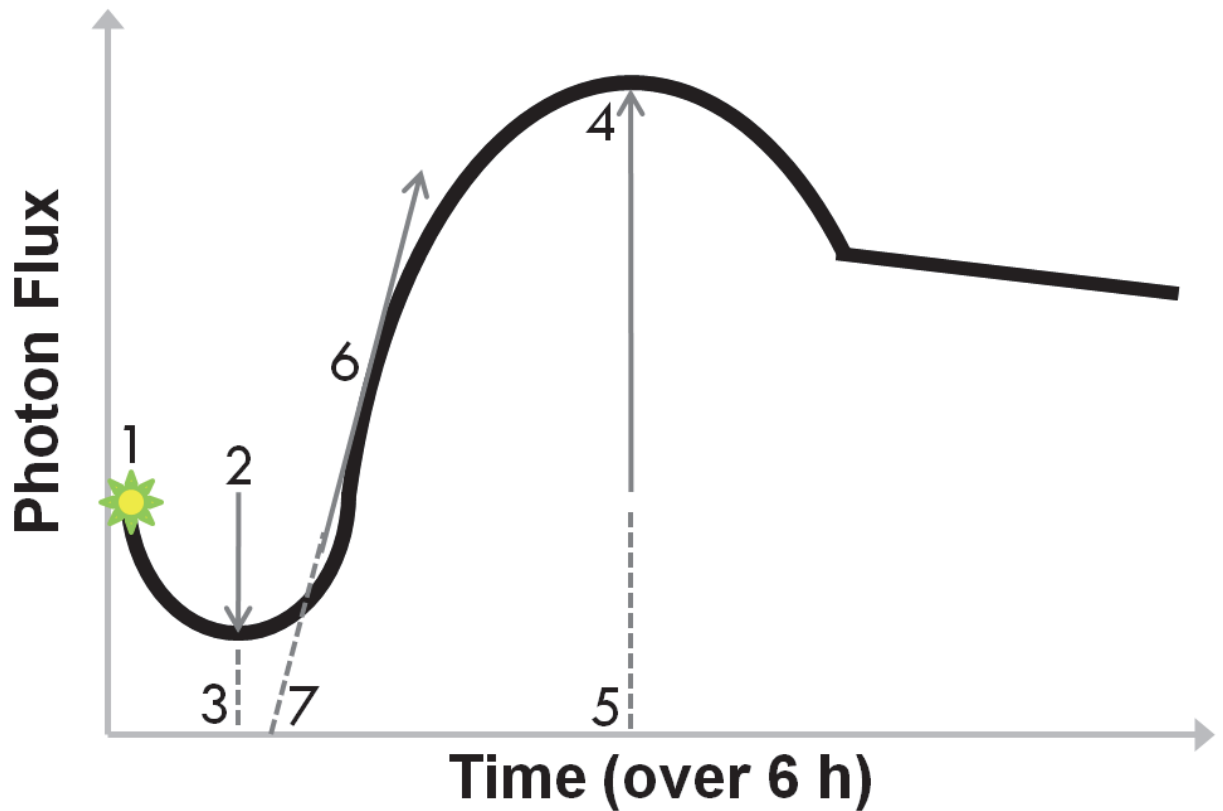


Figure 4.5: Definition of $\text{I}\kappa\text{B}\alpha$ -FLuc dynamic parameters that were evaluated for modulation by siRNA treatment.

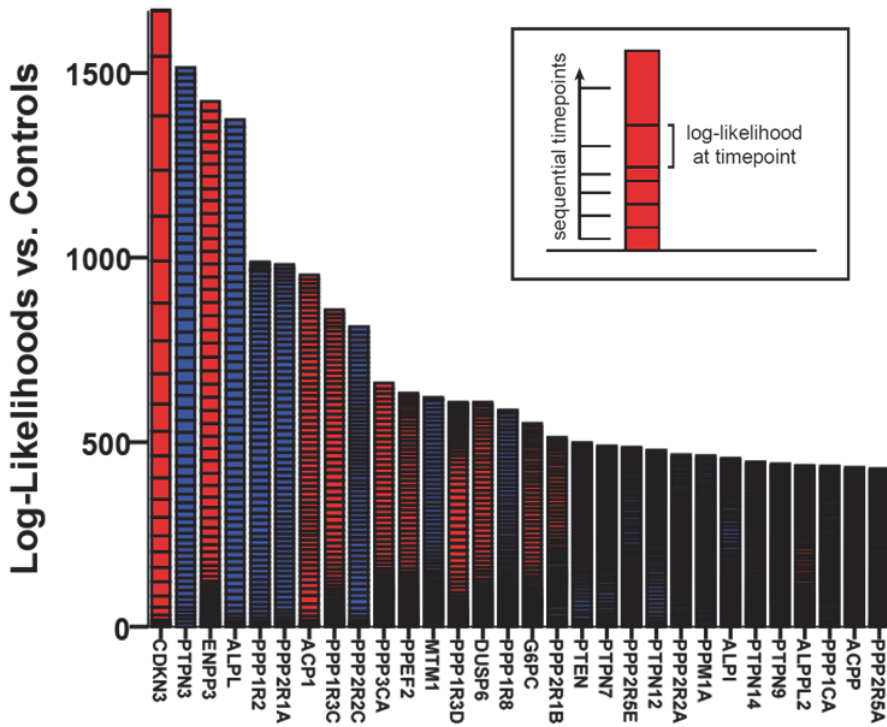
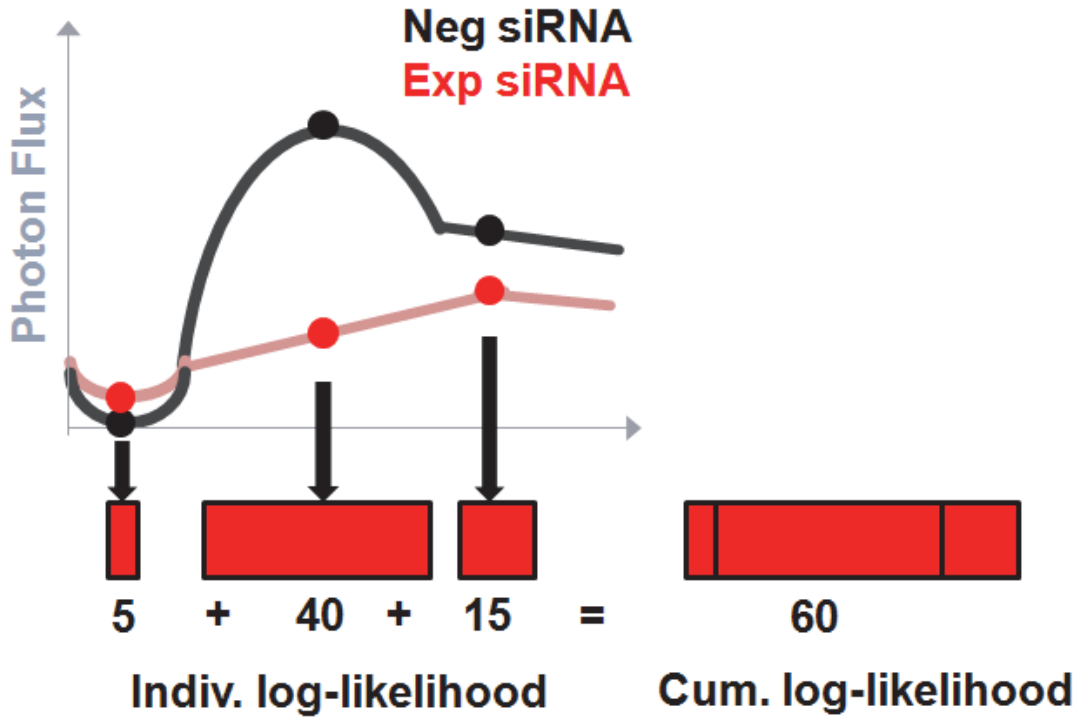
Example $\text{I}\kappa\text{B}\alpha$ -FLuc dynamic profile with corresponding visual representations of the seven parameters evaluated following the high-throughput siRNA screen.

- (1) Initial Photon Flux Level (the raw photon flux signal at $t = 0$ min)
- (2) Degradation Level (i.e. the minimum flux signal reached during $\text{I}\kappa\text{B}\alpha$ -FLuc degradation)
- (3) Degradation Time (the time at which minimum occurred)
- (4) Re-Synthesis Level (the maximum flux signal achieved during $\text{I}\kappa\text{B}\alpha$ -FLuc re-synthesis)
- (5) Re-Synthesis Time (the time at which maximal re-synthesis occurred)
- (6) Re-Synthesis Rate (the slope of re-synthesis between the minimum and maximum)
- (7) Re-Synthesis Lag Time (the value of the x-intercept of the linear regression of the $\text{I}\kappa\text{B}\alpha$ -FLuc re-synthesis rate)

Figure 4.6: Cumulative Log-Likelihood Normalization Procedure

The cumulative log-likelihood approach quantifies the deviation of an experimental siRNA treatment from the negative controls (scrambled negative controls and siGFP) by generating a Gaussian probability density function at each time point based on the mean and variance of the negative controls on a given plate. We then input each siRNA measurement to this function to quantify the deviation from the set of negative controls at each time point. To combine replicates, and to later make a cumulative sequence, we prevented computational rounding error by taking the negative logarithm of the likelihood (log-likelihood) and summing ($\log A + \log B = \log AB$). The individual siRNAs from a given plate triplicate were then ranked according to their cumulative log-likelihood value and presented as a bar graph in which each division of the bar height represents the contribution of an individual time point to the cumulative log-likelihood value. (modified from figure provided by Brandon Kocher)

'Cumulative log-likelihood'

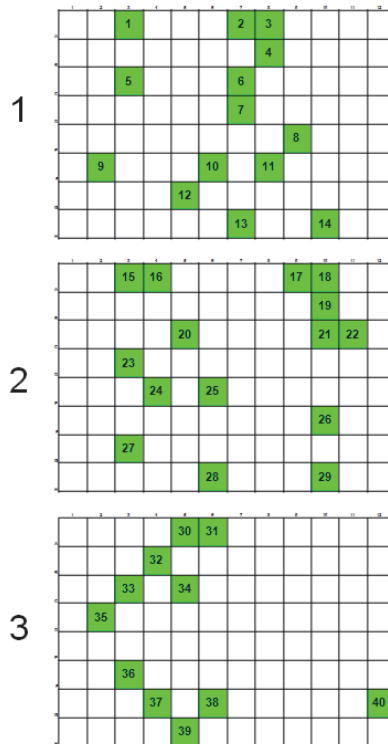


	w/ viability		w/out viability		common hits
1	ACPT	1	ACPT	1	ACPT
2	ALPL	2	ALPL	2	ALPL
3	CDC25B	3	CDC25B	3	CDC25B
4	CDKN3	4	CDKN3	4	CDKN3
5	DOLPP1	5	DOLPP1	5	DOLPP1
6	DUSP16	6	DUSP16	6	DUSP16
7	DUSP19	7	ENPP3	7	G6PC3
8	G6PC3	8	G6PC3	8	PHPT1
9	PHPT1	9	MTMR4	9	PIB5PA
10	PIB5PA	10	PHOSPHO1	10	PLIP
11	PLIP	11	PHPT1	11	PME-1
12	PME-1	12	PIB5PA	12	PPFIA3
13	PPFIA3	13	PLIP	13	PPP1CB
14	PPP1CB	14	PME-1	14	PPP1R12C
15	PPP1R12C	15	PPFIA3	15	PPP1R1B
16	PPP1R13B	16	PPP1CB	16	PPP1R2
17	PPP1R1B	17	PPP1R12C	17	PPP1R3C
18	PPP1R2	18	PPP1R1B	18	PPP2CA
19	PPP1R3C	19	PPP1R2	19	PPP2CB
20	PPP1R3D	20	PPP1R3C	20	PPP2R1A
21	PPP2CA	21	PPP2CA	21	PPP2R2C
22	PPP2CB	22	PPP2CB	22	PPP3CA
23	PPP2R1A	23	PPP2R1A	23	PR48
24	PPP2R2C	24	PPP2R2C	24	PSTPIP2
25	PPP3CA	25	PPP3CA	25	PTPN3
26	PR48	26	PR48	26	PTPRJ
27	PSTPIP2	27	PSTPIP2	27	PTPRN
28	PTPN3	28	PTP4A2	28	PTPRS
29	PTPRJ	29	PTPN3	29	SPAP1
30	PTPRN	30	PTPNS1	30	DUSP19
31	PTPRS	31	PTPRJ	31	PPP1R13B
32	SBF1	32	PTPRN	32	PPP1R3D
33	SPAP1	33	PTPRS	33	SBF1
		34	SKIP	34	ENPP3
		35	SPAP1	35	MTMR4
				36	PHOSPHO1
				37	PTP4A2
				38	PTPNS1
				39	SKIP

Figure 4.7: Primary Phosphatase Screen Hits Chosen for Secondary Screening

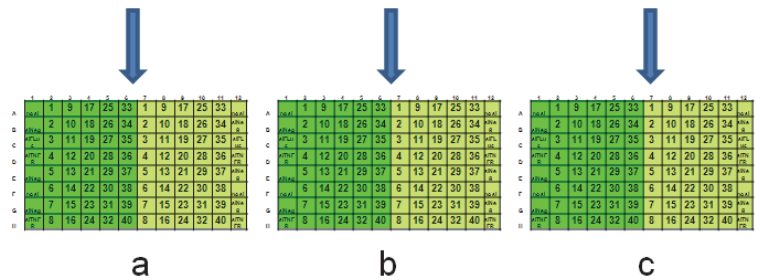
The highest stringency hits from each parameter analyzed in the quartile-based analysis of the primary phosphatase screen (with or without the inclusion of viability normalization) were combined to generate a master-list of common hits. This collection of hits was used as the basis for performing a secondary siRNA screen.

Phosphatase siRNA Library



3X Master Plate

	1	2	3	4	5	6	7	8	9	10	11	12
A	CDC25C	1	9	17	25	33	1	9	17	25	33	CDC25C
B	QIA Neg	2	10	18	26	34	2	10	18	26	34	QIA Neg
C	IDT Fluc	3	11	19	27	35	3	11	19	27	35	IDT Fluc
D	QIA Neg	4	12	20	28	36	4	12	20	28	36	QIA Neg
E	QIA Neg	5	13	21	29	37	5	13	21	29	37	QIA Neg
F	PPP2R5C	6	14	22	30	38	6	14	22	30	38	PPP2R5C
G	ENPP1	7	15	23	31	39	7	15	23	31	39	ENPP1
H	PTPN13	8	16	24	32	QIA Neg	8	16	24	32	QIA Neg	PTPN13



a

b

c

Cell Plate Triplicate

Figure 4.8: Re-Arraying Hits from the Phosphatase Library for Focused Secondary Screening

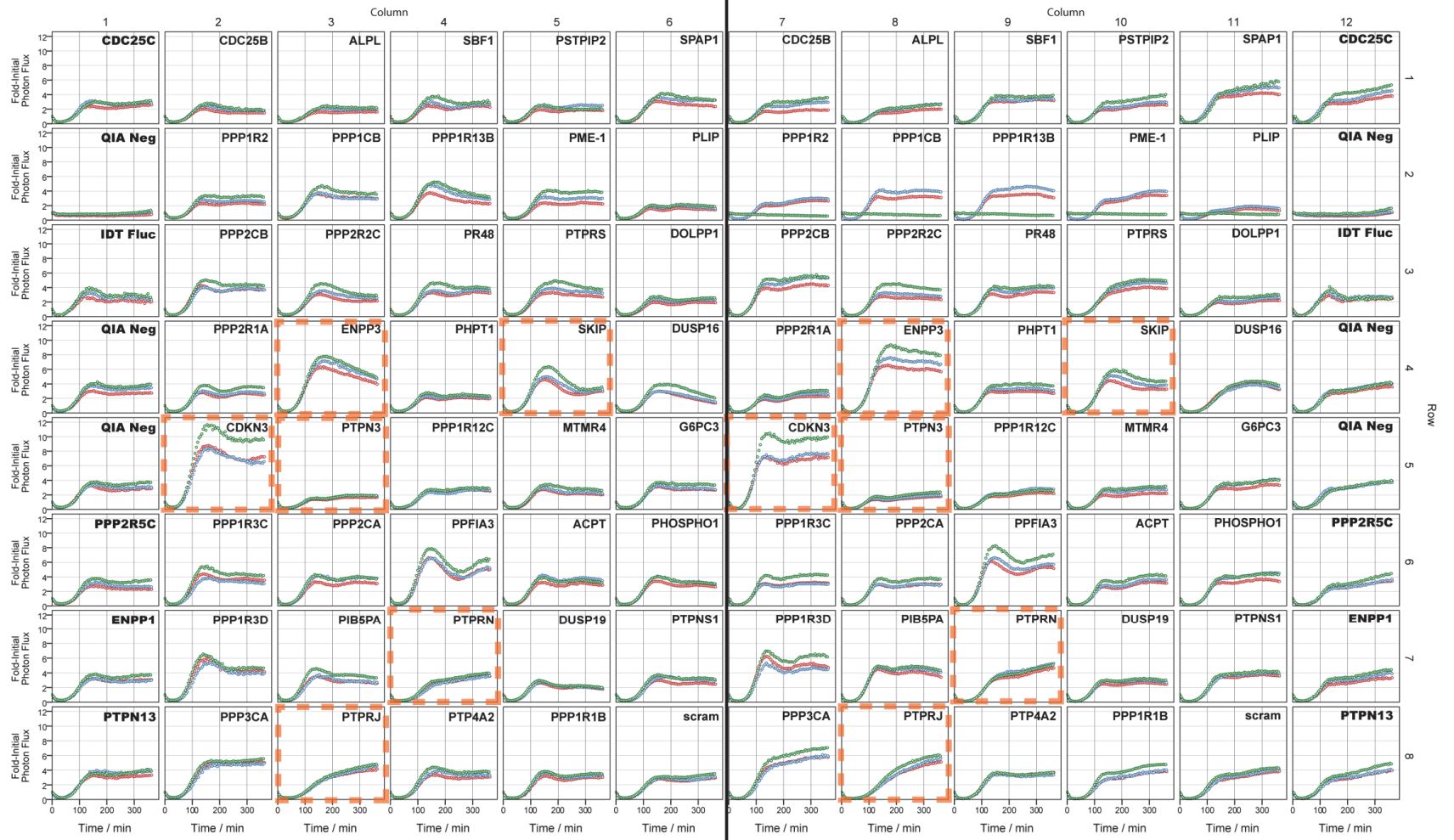
Top hits from the primary screen were re-arrayed from the primary phosphatase library onto a single master plate by the FX liquid handler using a cherry-picking script written by Jayne Marasa. It was arrayed such that columns 1 and 12 were duplicates of control siRNAs and Columns 2-6 and 7-11 were duplicates of the 39 strong stringency hits from the primary screen plus 1 scrambled negative control from the phosphatase library plate. This master plate was used to transfect 3 identical plates of HepG2 cells. One half of each cell plate was stimulated with TNF α (dark green) and the other half was stimulated with IL-1 β (light green).

Figure 4.9: Normalized Photon Flux Data From the Secondary Phosphatase Screen.

The raw photon fluxes for each well were normalized as fold-initial and then plotted against time. The first graph represents the full 6 hr profile; the second graph represents the degradation phase. The different colored symbols differentiate the data from each plate triplicate. Orange dashed boxes high-light top hits from the screen analysis.

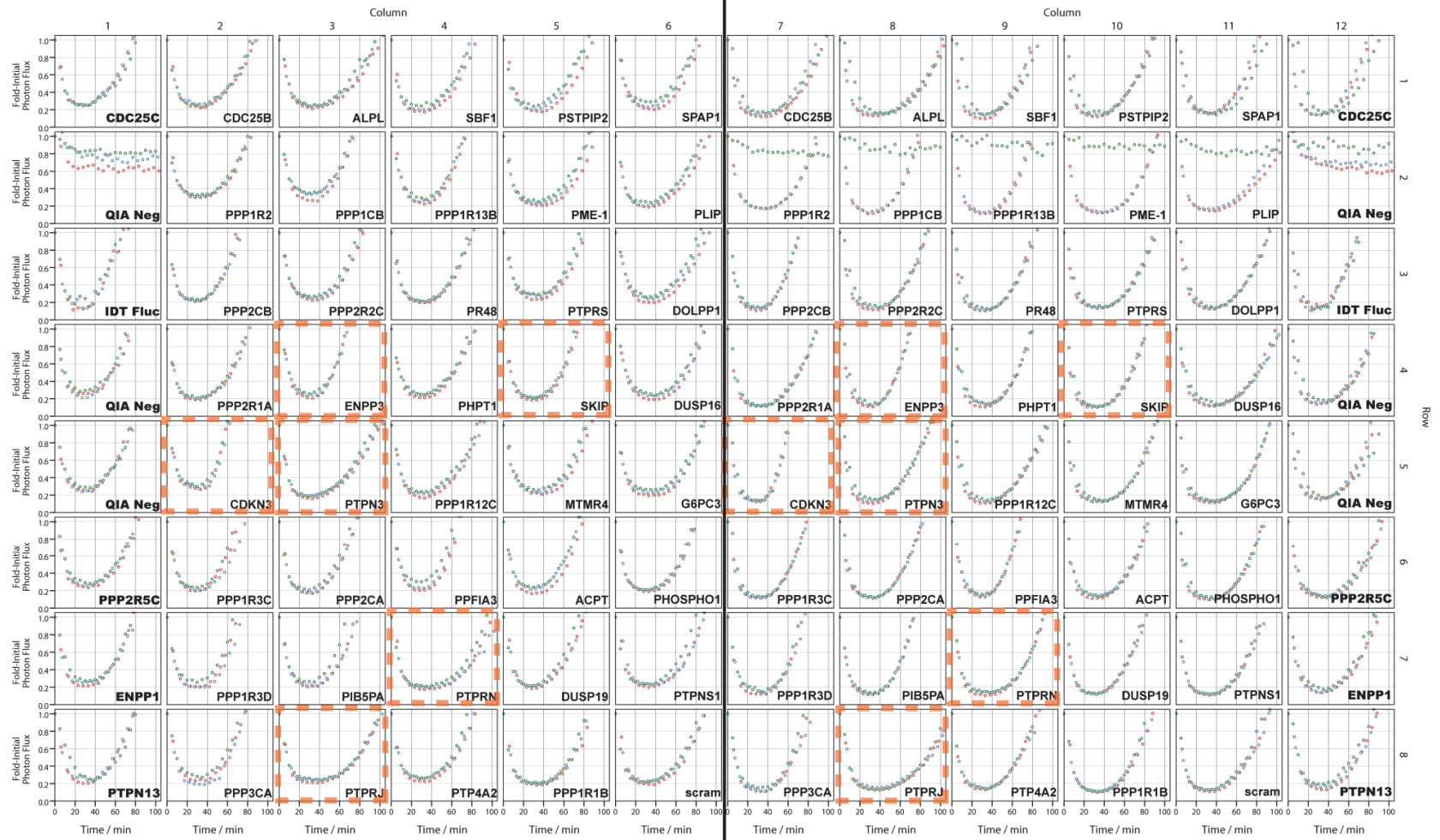
TNF α

IL-1 β



TNF α

IL-1 β



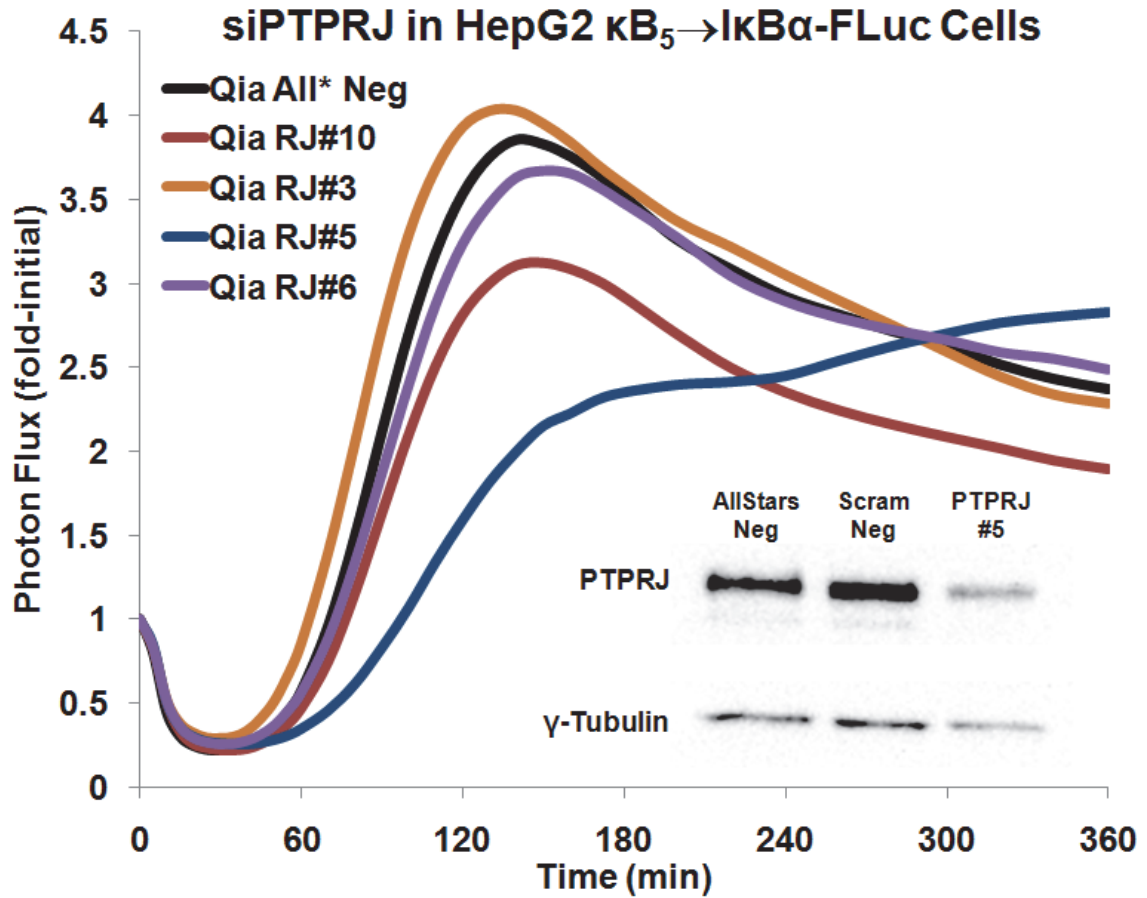


Figure 4.10: Validation of siPTPRJ Phenotype and Knock-Down

HepG2 cells were co-transfected with $\kappa B_5 \rightarrow I\kappa B\alpha$ -FLuc and siRNA targeting PTPRJ. Cells were then stimulated with $TNF\alpha$ and imaged for bioluminescence. The photon flux from each control well was plotted as fold-initial versus time. The inset confirms 50% knock-down of PTPRJ compared to negative control siRNAs.

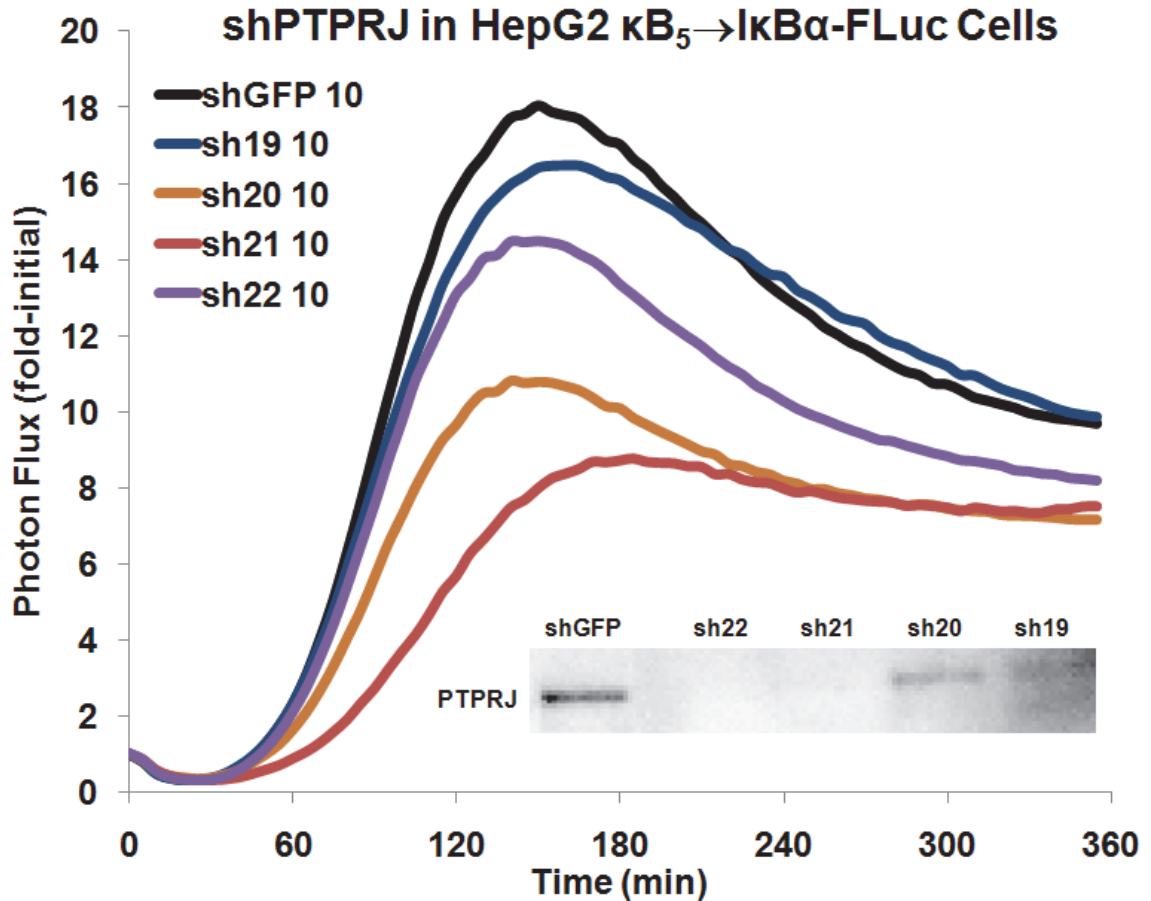


Figure 4.11: Validation of PTPRJ as a Regulator of $I\kappa B\alpha$ -FLuc Dynamics by shRNA-Mediated Knock-Down

HepG2 cells infected with shPTPRJ or control hairpins were transfected with $\kappa B_5 \rightarrow I\kappa B\alpha$ -FLuc. Cells were then stimulated with $TNF\alpha$ and imaged for bioluminescence. The photon flux from each control well was plotted as fold-initial versus time. While sh21 strongly reproduces the knock-down phenotype observed previously, the other hairpins only impact $I\kappa B\alpha$ -FLuc dynamics weakly if at all. The inset confirms nearly complete knock-down of PTPRJ with hairpin 21 and 22 and partial knock-down for sh19 and sh20, compared to negative control shGFP.

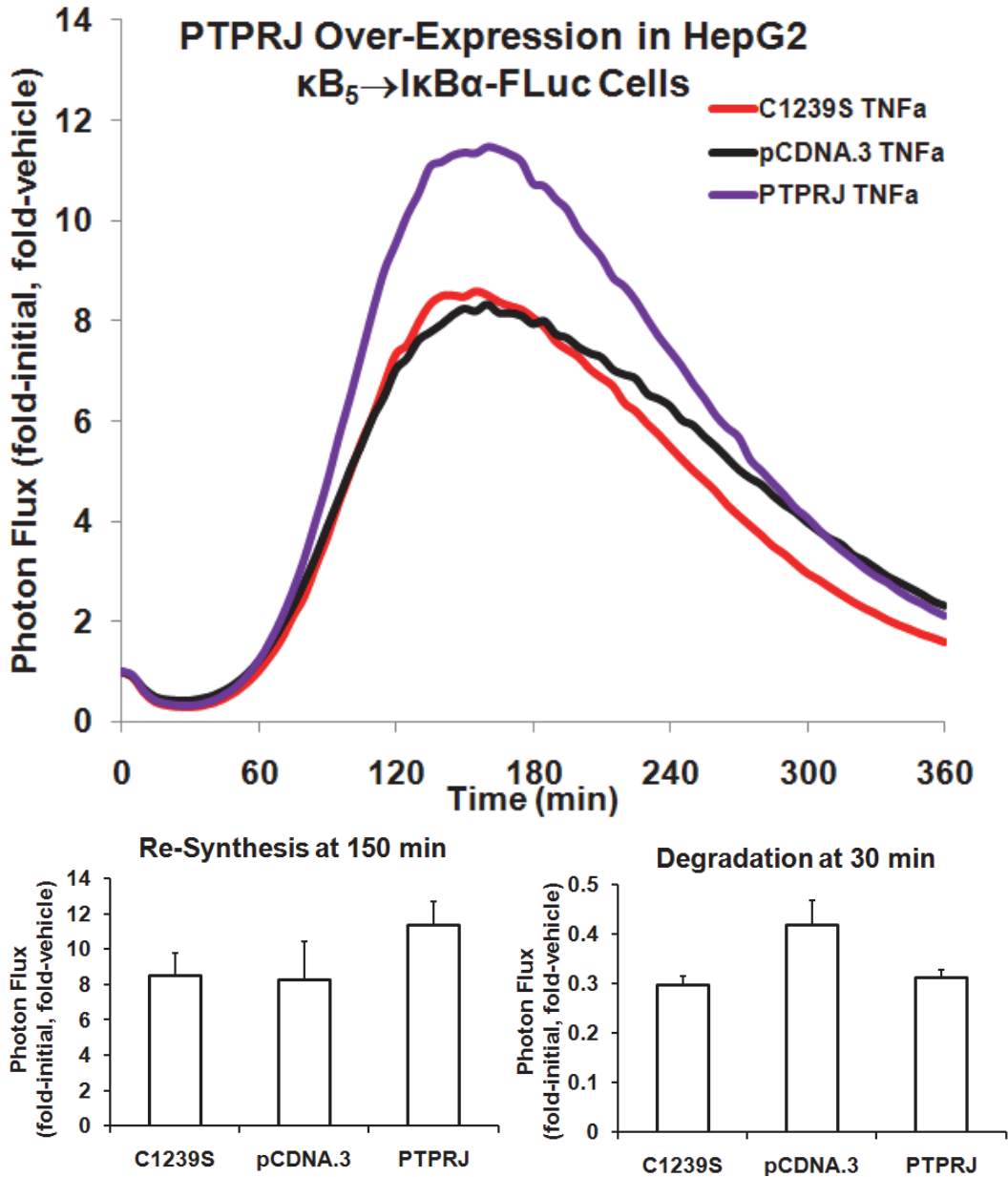


Figure 4.12: Over-Expression of PTPRJ Enhances $I\kappa B\alpha$ -FLuc Dynamics

HepG2 cells were co-transfected with $\kappa B_5 \rightarrow I\kappa B\alpha$ -FLuc and wild-type or phosphatase dead PTPRJ constructs (or vector control). Cells were then stimulated with TNF α and imaged for bioluminescence. The photon flux from each control well was plotted as fold-initial versus time. WT PTPRJ enhanced both $I\kappa B\alpha$ -FLuc degradation and re-synthesis, while the PTPRJ_{C1239S} mutant affected only degradation. Error bars represent propagated standard deviation.

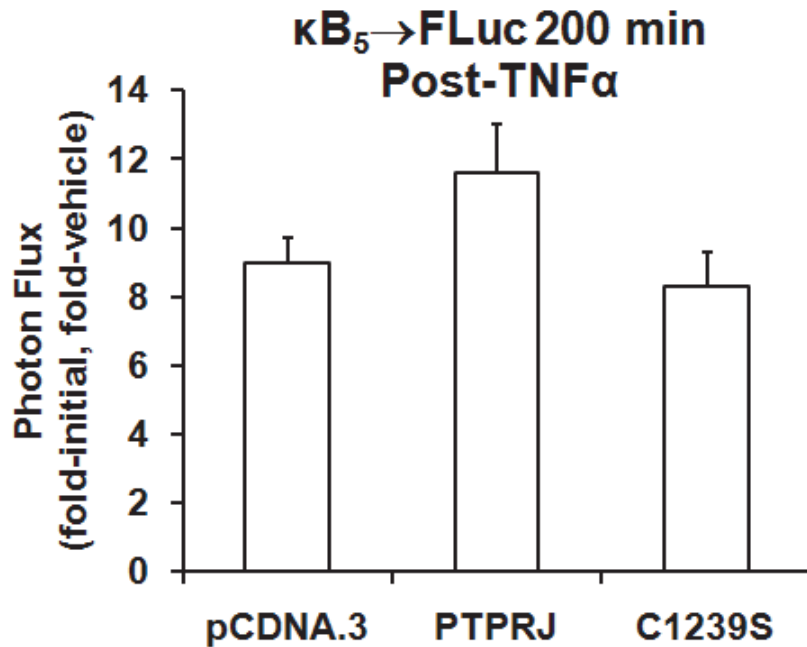
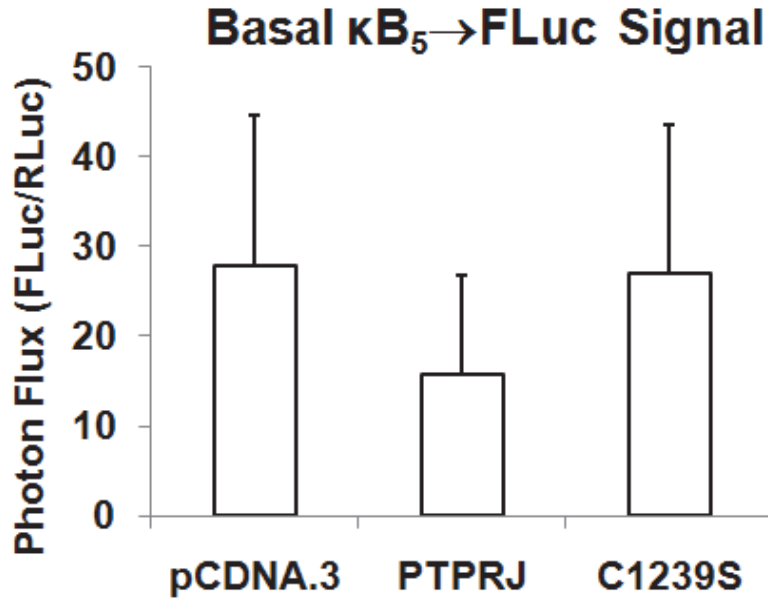


Figure 4.13: Over-Expression of PTPRJ Decreases Basal NF- κ B Transcriptional Activity, but sensitizes TNF α -Induced NF- κ B Activity

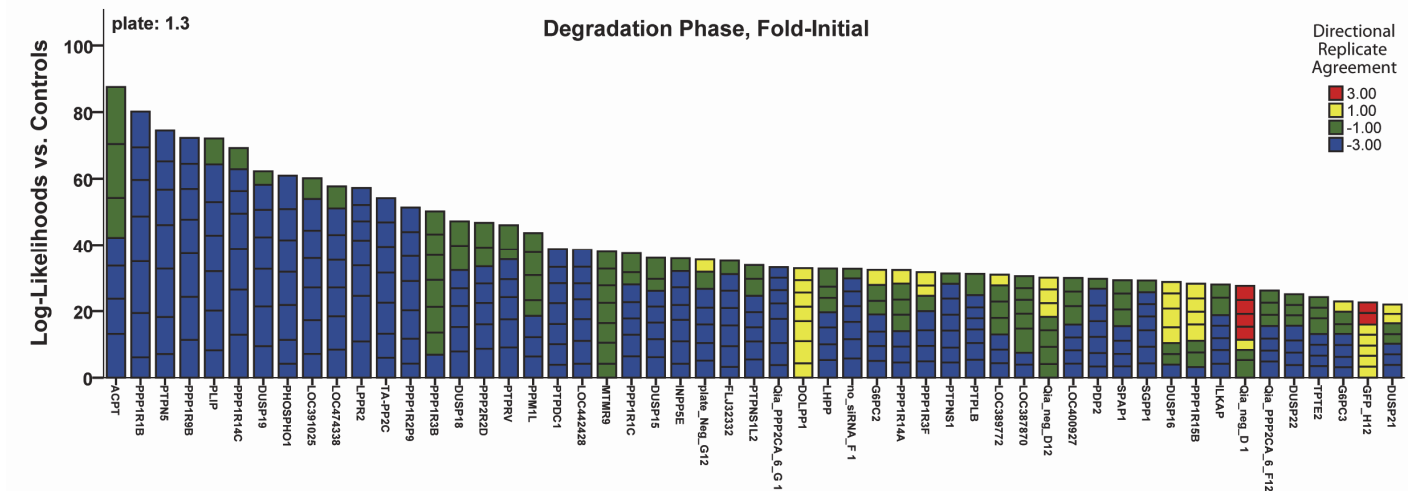
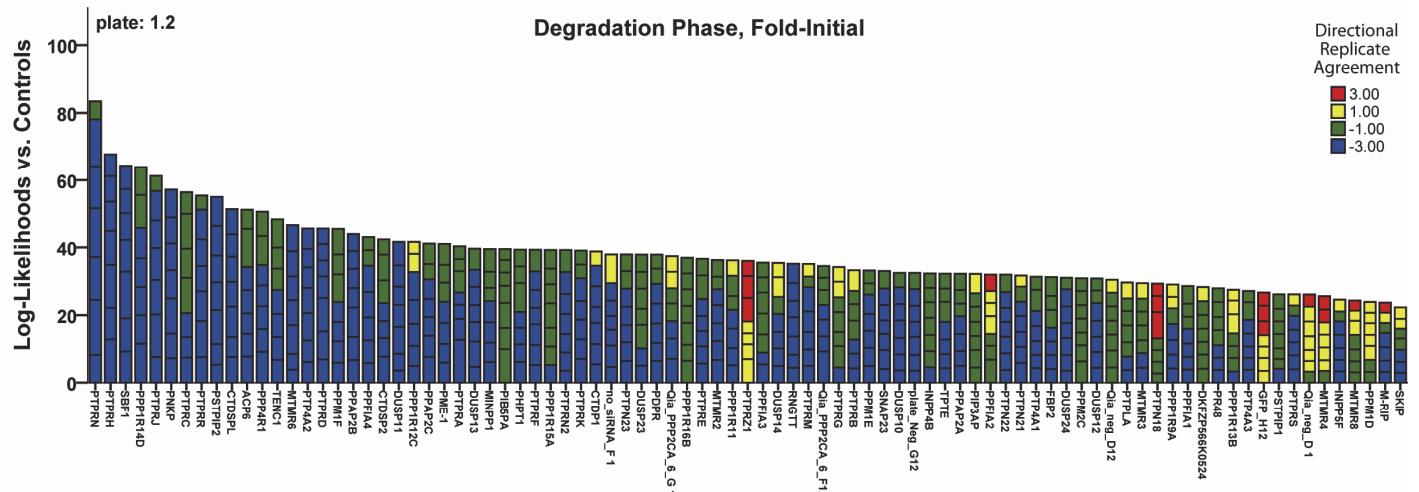
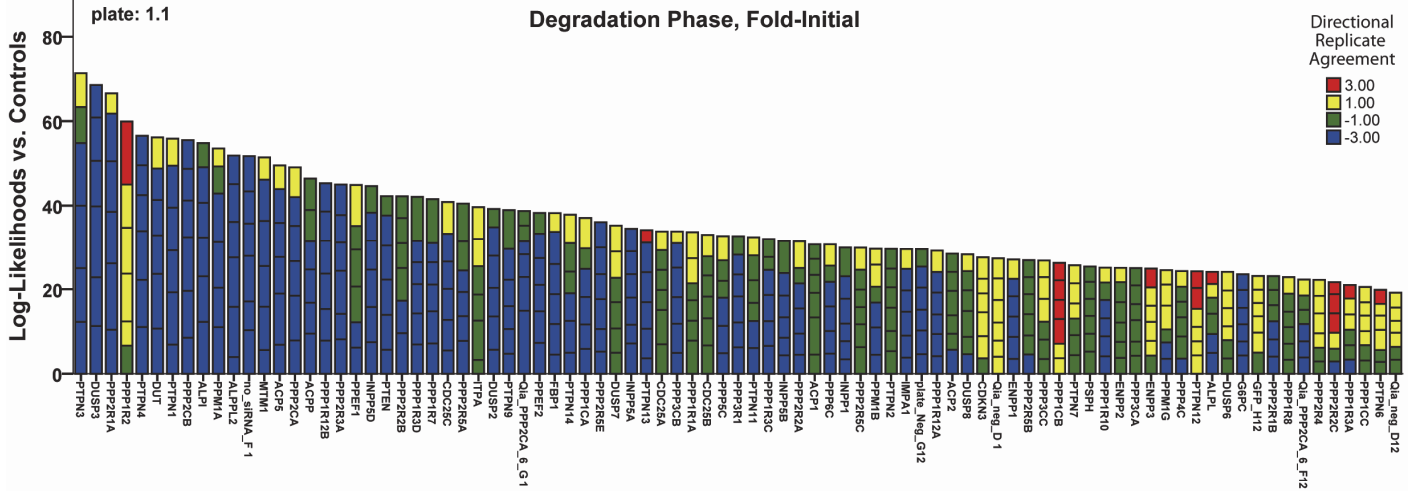
HepG2 cells were co-transfected with $\kappa B_5 \rightarrow FLuc$ reporter, TK \rightarrow RLuc transfection control reporter, and wild-type or phosphatase dead PTPRJ constructs (or vector control). Cells were then stimulated with TNF α and imaged for bioluminescence. The basal photon flux level was calculated as a ratio of FLuc signal over RLuc signal for a given treatment population. Error bars represent propagated standard deviation.

4.6 SUPPLEMENTAL FIGURES

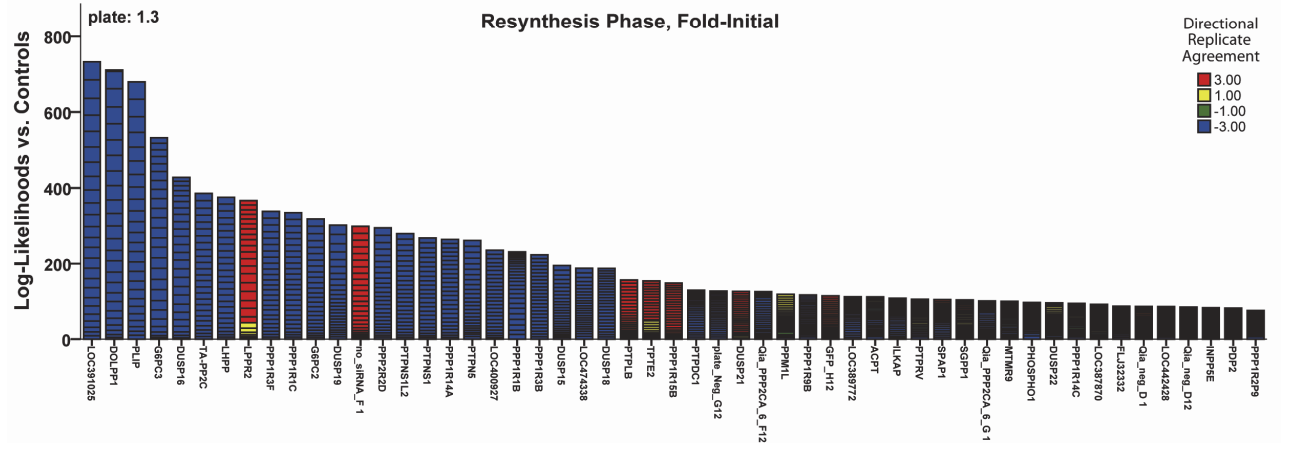
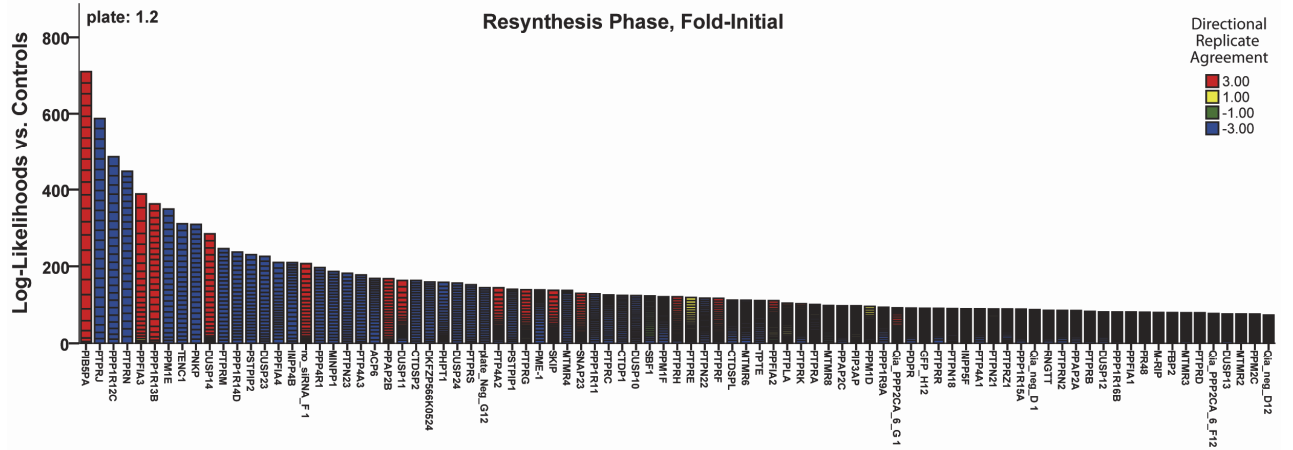
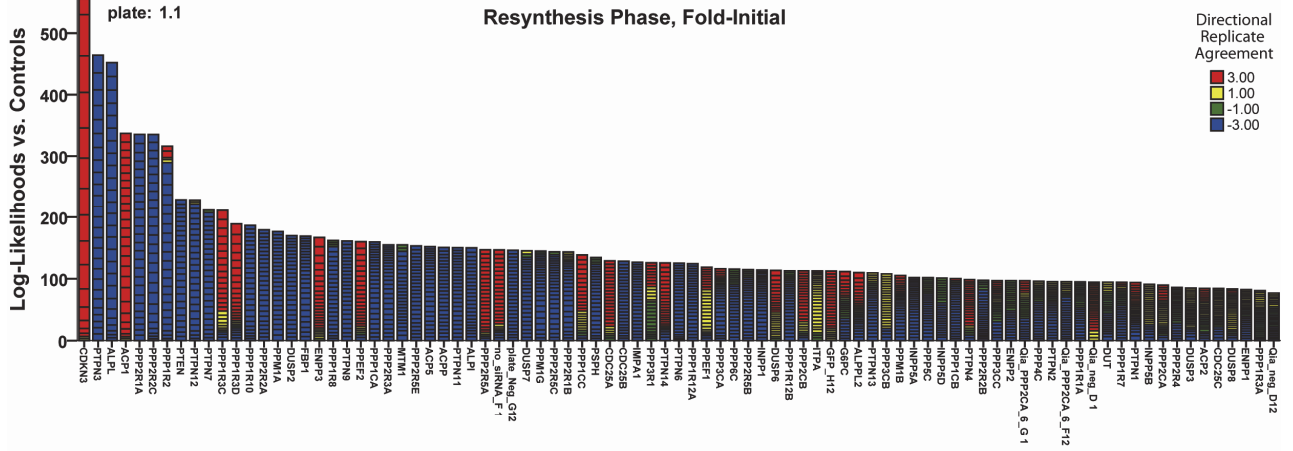
Supplemental Figure 4.1: Primary Phosphatase Screen Cumulative Log-Likelihood Plate-By-Plate Ranking

Each plate triplicate was analyzed separately for each run of the phosphatase screen. The cumulative log-likelihood value for each siRNA within that plate triplicate was then presented as a bar graph in which each division of the bar height represents the contribution of an individual time point to the cumulative log-likelihood value. This was done separately for each run of the screen, with each plate being denoted as 1.n or 2.n to represent the first and second screen runs. (A-C) Log-likelihood rank graphs from for plates 1.1, 1.2, and 1.3 considering just the degradation phase (A), just the re-synthesis phase (B), and both phases together (C). (D-F) Log-likelihood rank graphs from for plates 2.1, 2.2, and 2.3 considering just the degradation phase (D), just the re-synthesis phase (E), and both phases together (F).

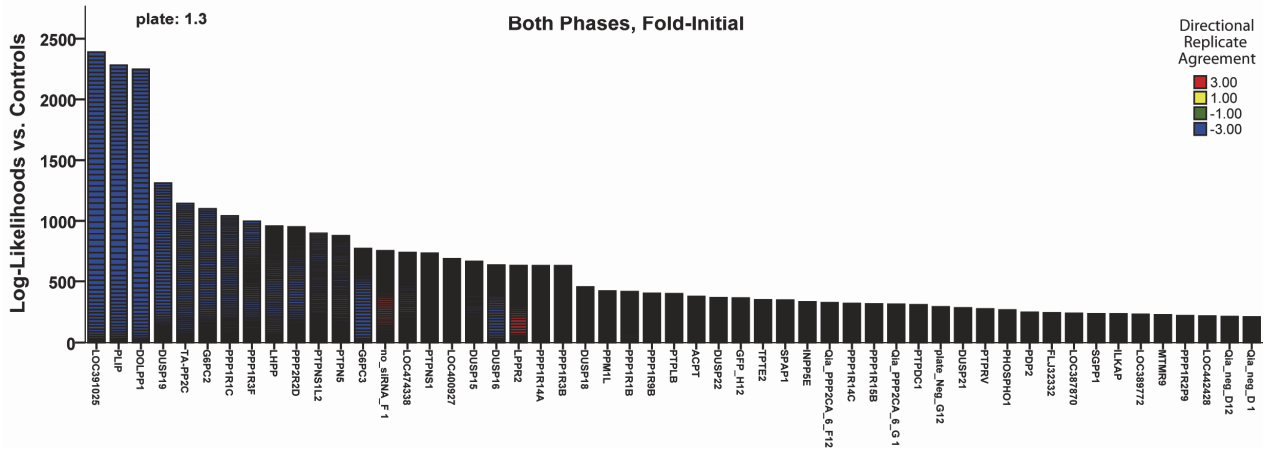
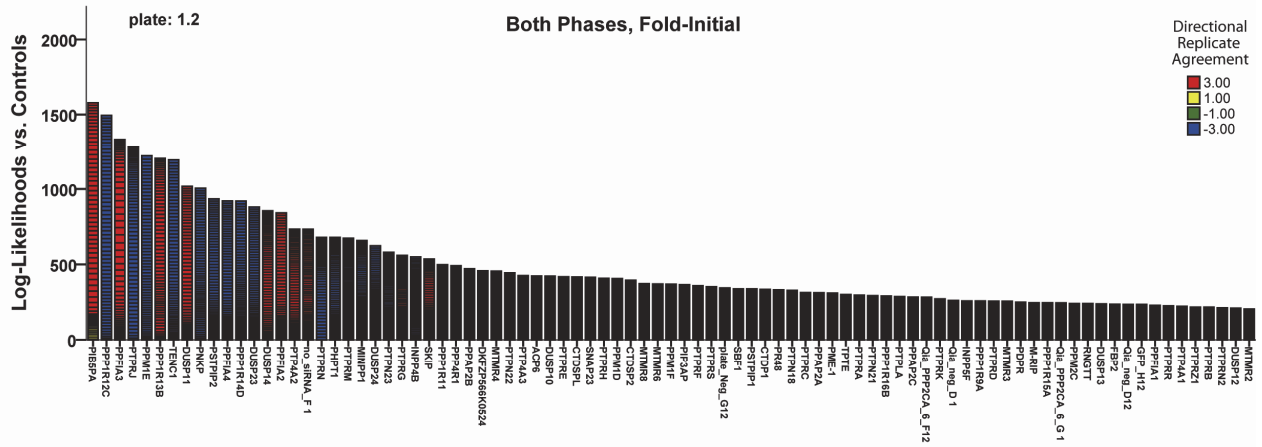
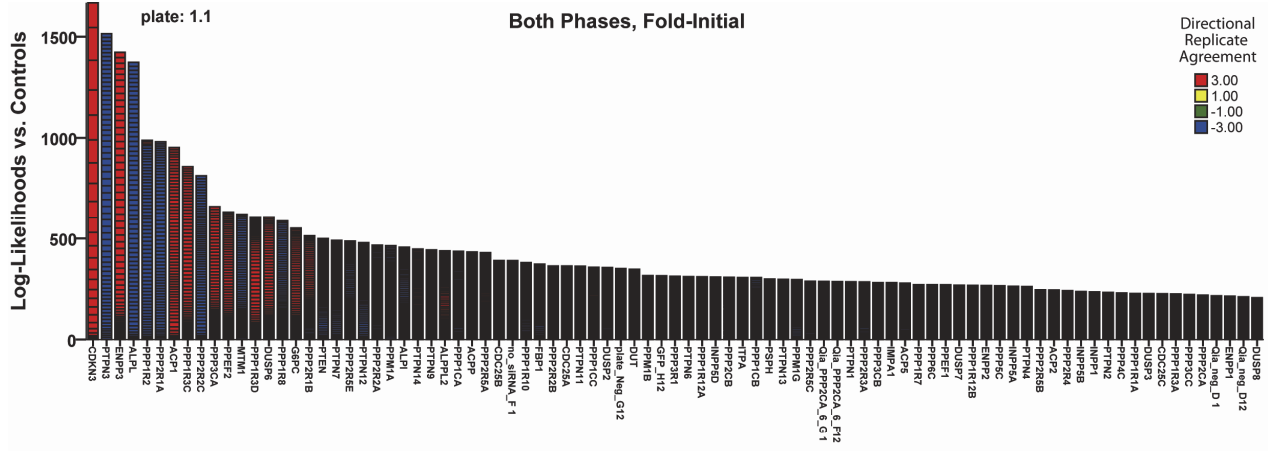
A



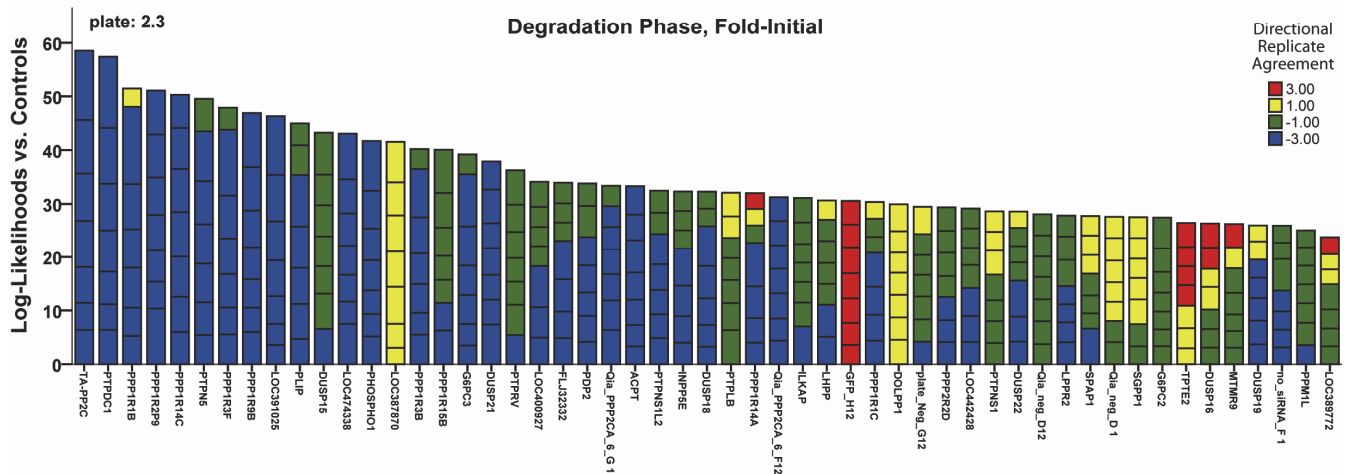
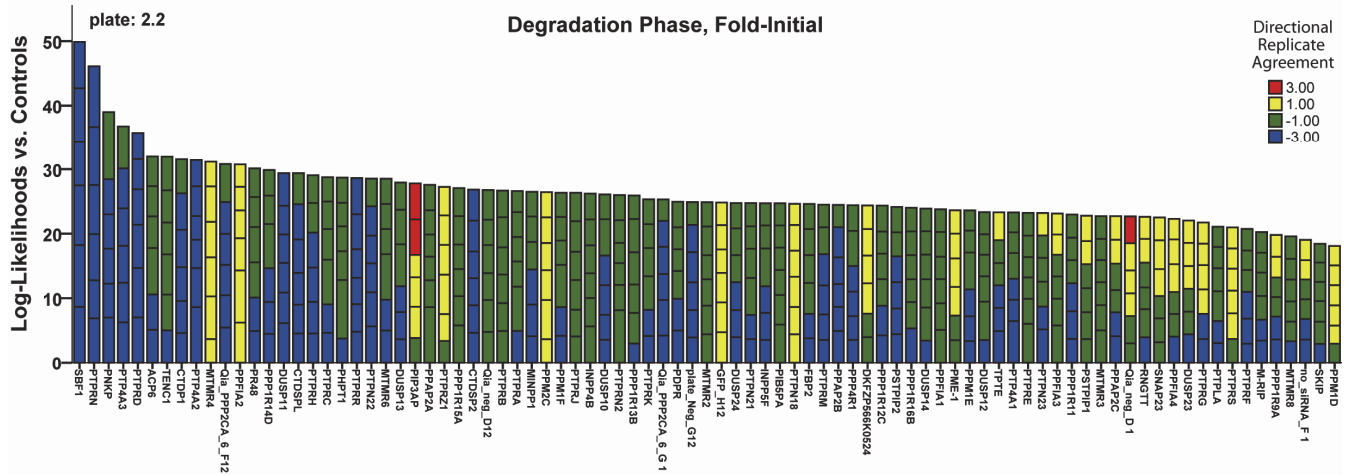
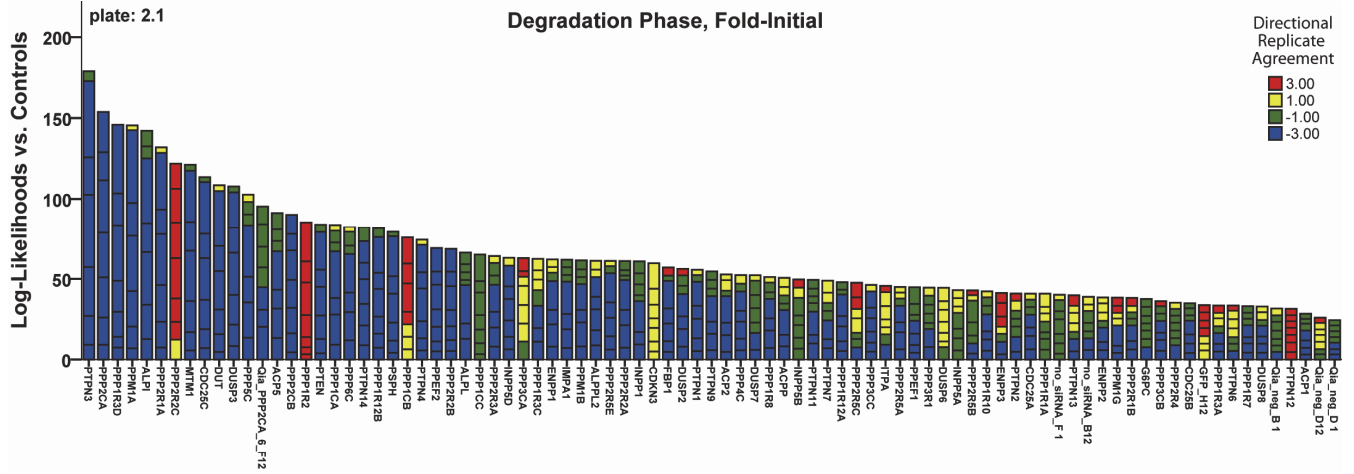
B



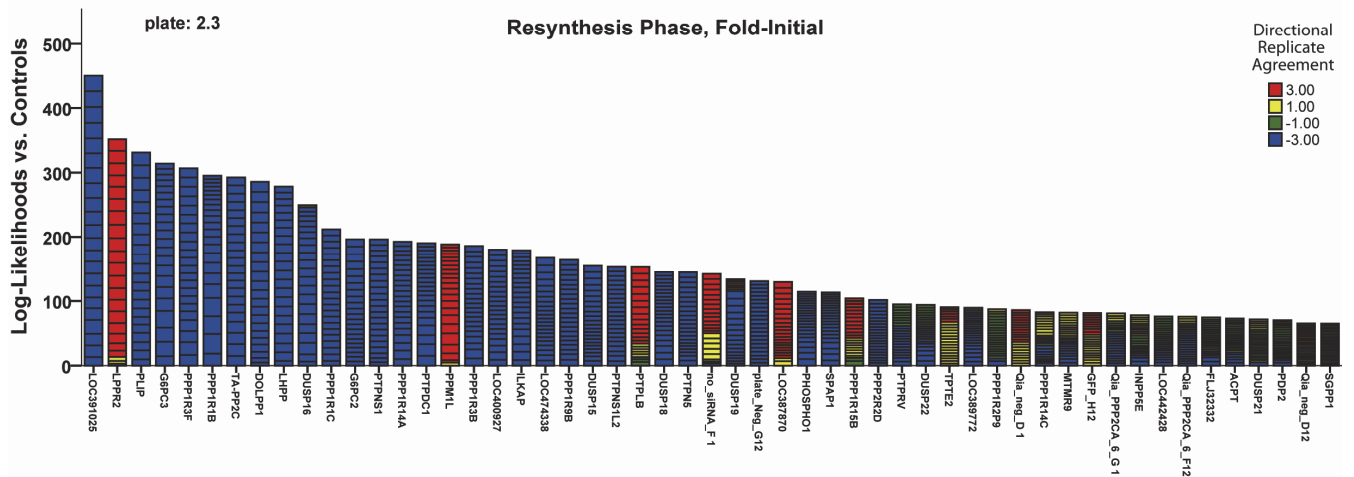
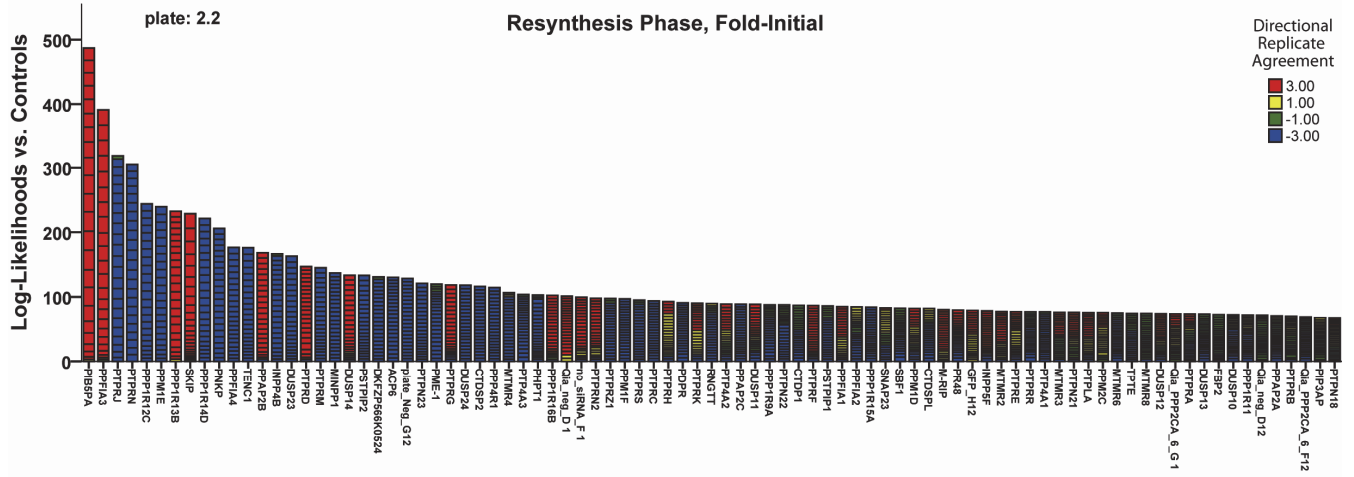
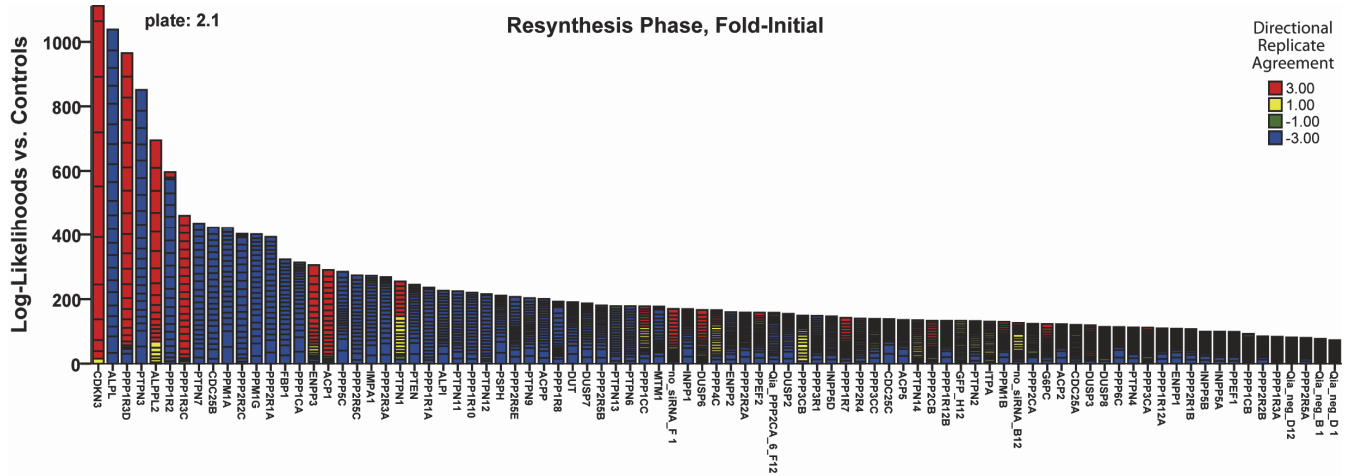
C



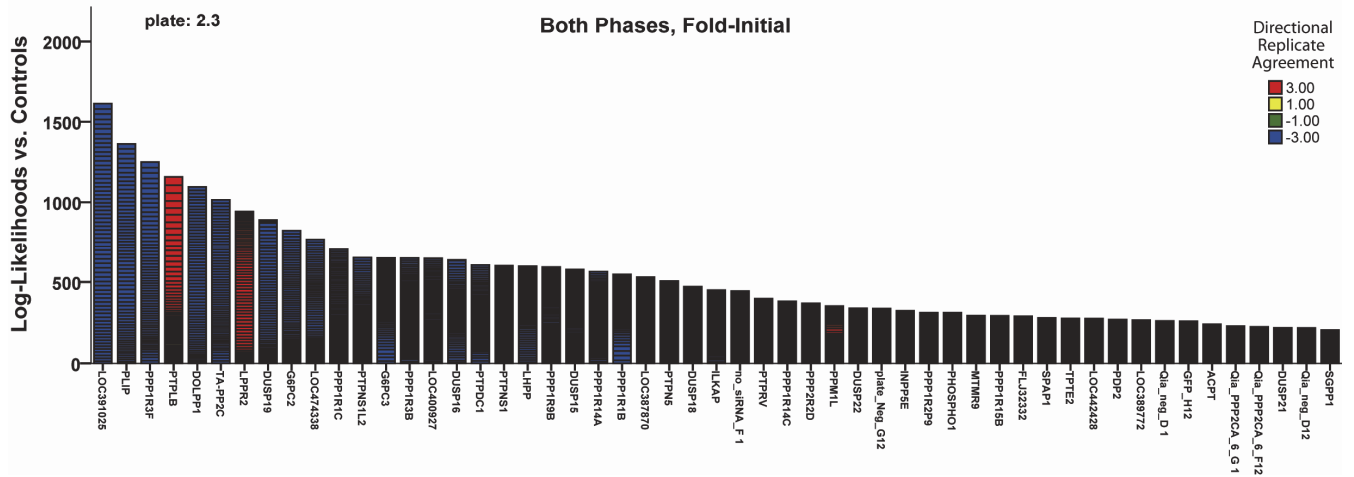
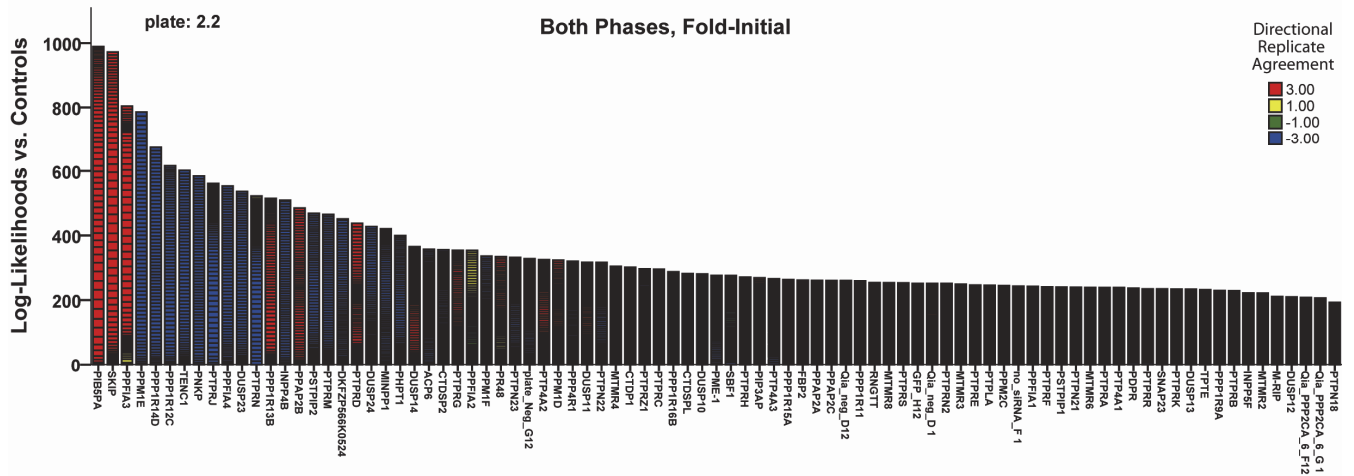
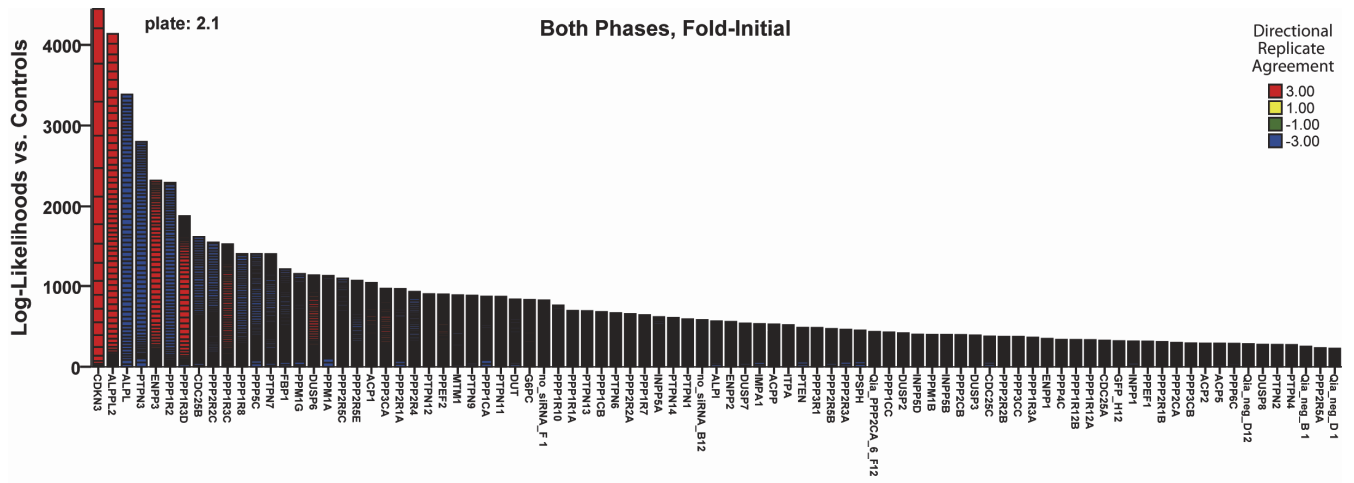
D



E

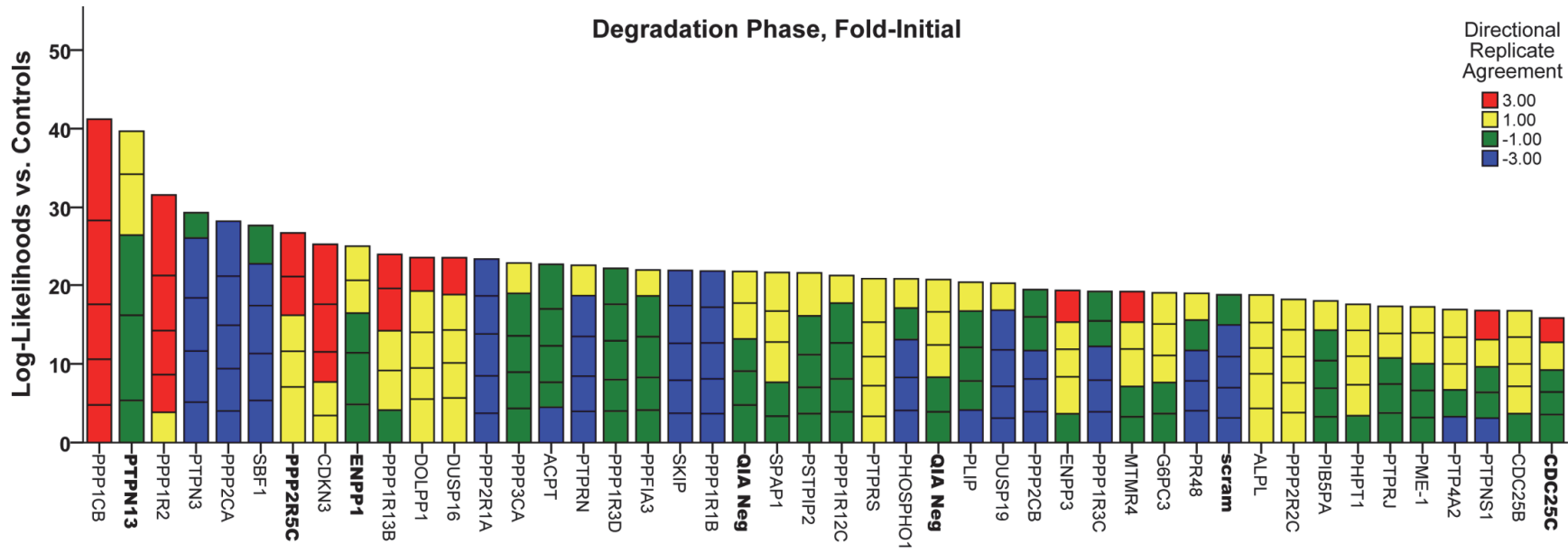


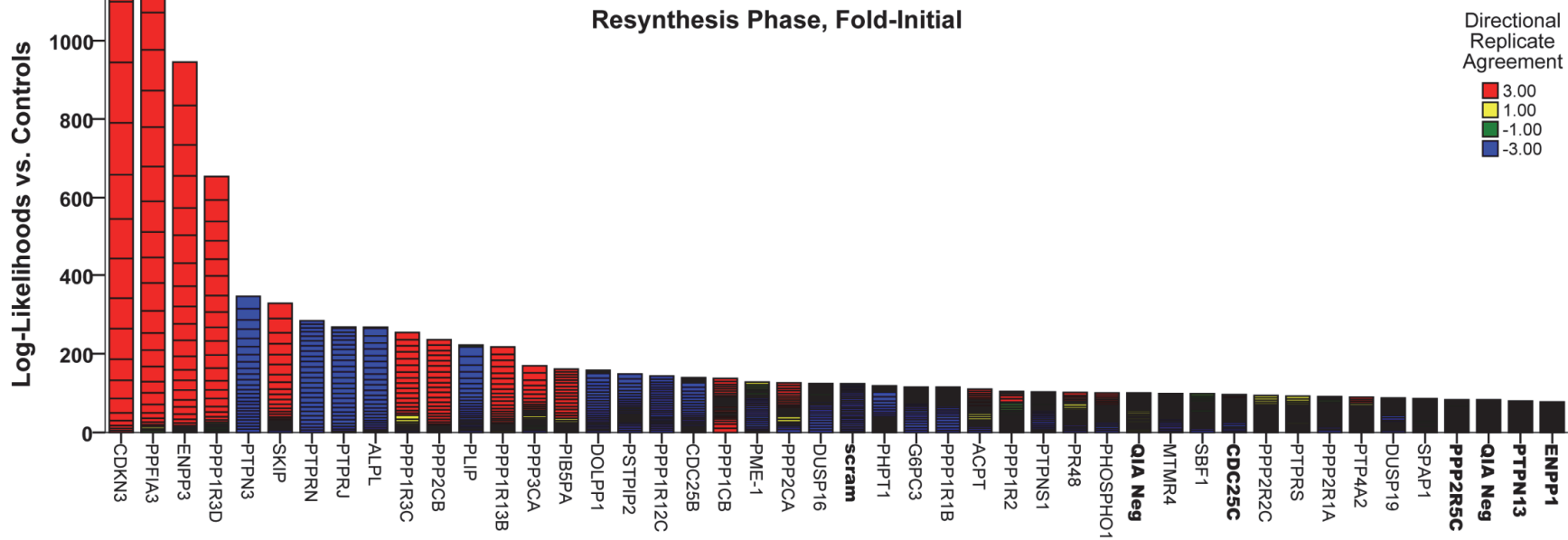
F

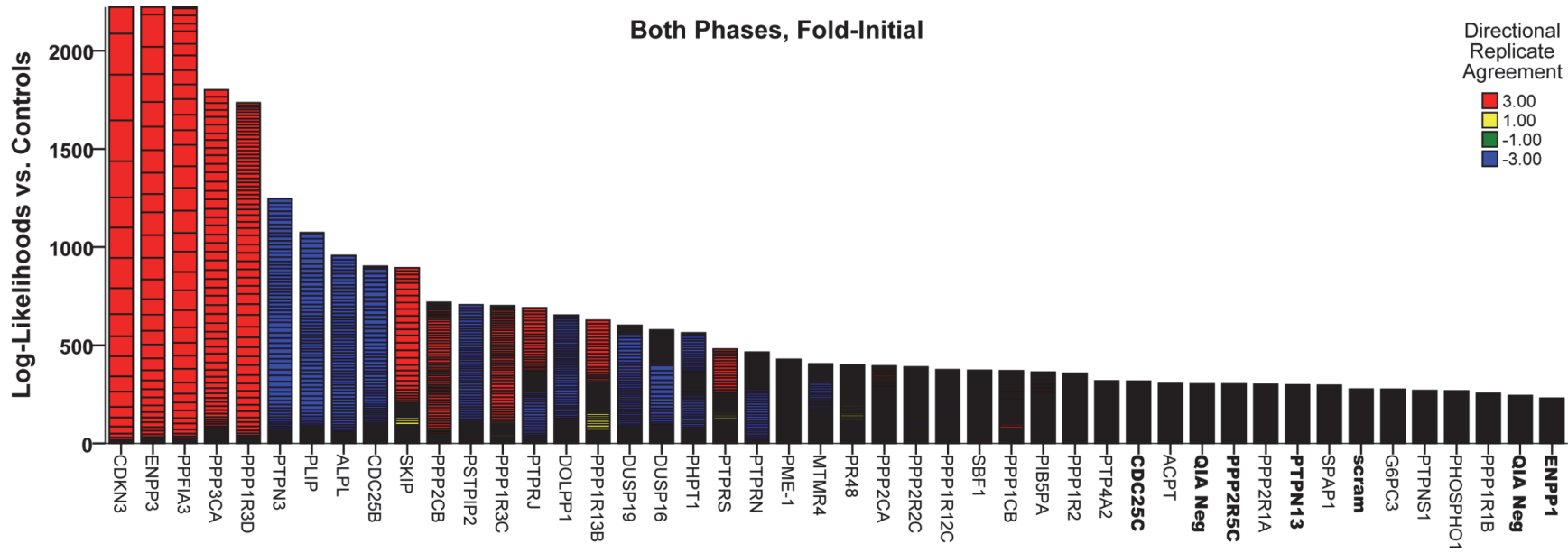


Supplemental Figure 4.2: Secondary Screen Cumulative Log-Likelihood Ranking

The cumulative log-likelihood value for each siRNA within the TNF α -stimulated plate triplicate is presented as a bar graph in which each division of the bar height represents the contribution of an individual time point to the cumulative log-likelihood value.







4.7 TABLES

Initial Flux	Degradation Minimum	Re-Synthesis Maximum	Time of Degradation Minimum	Time of Re-Synthesis Maximum	Re-Synthesis Rate	Re-Synthesis Lag Time
PTPN3 PPP2R2C PPP2R1A PPP1R12C PLIP DUSP19	SBF1 PTPRN PTPN3 PPP1R2 PPP1R13B CDKN3	PTPN3 PPP1R3D PPP1R3C PPP1R13B PPFIA3 PIB5PA CDKN3 ALPL	SPAP1 PPP1R1B DUSP16 DOLPP1 ACPT	PTPRS PTPRN PTPRJ PTPN3 PPP3CA PLIP	PTPRN PTPRJ PTPN3 PPP1R3D PPP1R3C PPP1R13B PPP1R12C PPFIA3 PIB5PA CDKN3 ALPL	PTPRN PTPRJ PTPN3 PSTPIP2 PPP1R1B PME-1 G6PC3
high low	less more	more less	later earlier	faster slower	longer shorter	

Table 4.1: Reproducible High Stringency Hits from the Phosphatase Screen

The strong hits (targeted error rate $\alpha = 0.0027$) calculated for each I κ B α -FLuc dynamic profile parameter using quartile-based analysis. The color indicates where the hit fell in relation to negative control siRNA treatment. The order of hits within each parameter does not indicate rank order, though rank order will be determined during secondary screening.

Table 4.2: Reproducible High Stringency Hits from the Phosphatase Screen

The strong hits (targeted error rate $\alpha = 0.0027$) calculated for each $\text{I}\kappa\text{B}\alpha$ -FLuc dynamic profile parameter using quartile-based analysis. The color indicates where the hit fell in relation to negative control siRNA treatment. The order of hits within each parameter does not indicate rank order, though rank order will be determined during secondary screening.

Degradation

	Plate 1.1	Plate 1.2	Plate 2.1	Plate 2.2	Plate 3.1	Plate 3.2
1	PTPN3	PTPN3	PTPRN	SBF1	ACPT	TA-PP2C
2	DUSP3	PPP2CA	PTPRH	PTPRN	PPP1R1B	PTPDC1
3	PPP2R1A	PPP1R3D	SBF1	PNKP	PTPN5	PPP1R1B
4	PPP1R2	PPM1A	PPP1R14D	PTP4A3	PPP1R9B	PPP1R14C
5	PTPN4	ALPI	PTPRJ	PTPRD	PLIP	PTPN5
6	DUT	PPP2R1A	PNKP	ACP6	PPP1R14C	PPP1R9B
7	PTPN1	PPP2R2C	PTPRC	TENC1	DUSP19	LOC391025
8	PPP2CB	MTM1	PTPRR	CTDP1	PHOSPHO1	PLIP
9	ALPI	CDC25C	PSTPIP2	PTP4A2	LOC391025	DUSP15
10	PPM1A	DUT	CTDSPL	MTMR4	LOC474338	LOC474338

Re-Synthesis

	Plate 1.1	Plate 1.2	Plate 2.1	Plate 2.2	Plate 3.1	Plate 3.2
1	CDKN3	CDKN3	PIB5PA	PIB5PA	LOC391025	LOC391025
2	PTPN3	ALPL	PTPRJ	PPFIA3	DOLPP1	LPPR2
3	ALPL	PPP1R3D	PPP1R12C	PTPRJ	PLIP	PLIP
4	ACP1	PTPN3	PTPRN	PTPRN	G6PC3	G6PC3
5	PPP2R1A	ALPPL2	PPFIA3	PPP1R12C	DUSP16	PPP1R3F
6	PPP2R2C	PPP1R2	PPP1R13B	PPM1E	TA-PP2C	PPP1R1B
7	PPP1R2	PPP1R3C	PPM1E	PPP1R13B	LHPP	TA-PP2C
8	PTEN	PTPN7	TNEC1	SKIP	LPPR2	DOLPP1
9	PTPN12	CDC25B	PNKP	PPP1R14D	PPP1R3F	LHPP
10	PTPN7	PPM1A	DUSP14	PNKP	PPP1R1C	DUSP16

Degradation + Re-Synthesis

	Plate 1.1	Plate 1.2	Plate 2.1	Plate 2.2	Plate 3.1	Plate 3.2
1	CDKN3	CDKN3	PIB5PA	PIB5PA	LOC391025	LOC391025
2	PTPN3	ALPPL2	PPP1R12C	SKIP	PLIP	PLIP
3	ENPP3	ALPL	PPFIA3	PPFIA3	DOLPP1	PPP1R3F
4	ALPL	PTPN3	PTPRJ	PPM1E	DUSP19	PTPLB
5	PPP1R2	ENPP3	PPM1E	PPP1R14D	TA-PP2C	DOLPP1
6	PPP2R1A	PPP1R12	PPP1R13B	PPP1R12C	G6PC2	TA-PP2C
7	ACP1	PPP1R3D	TENC1	TENC1	PPP1R1C	LPPR2
8	PPP1R3C	CDC25B	DUSP11	PNKP	PPP1R3F	DUSP19
9	PPP2R2C	PPP2R2C	PNKP	PTPRJ	LHPP	G6PC2
10	PPP3CA	PPP1R3C	PSTPIP2	PPFIA4	PPP2R2D	LOC474338

Table 4.3: Secondary Phosphatase Screen Top Hits

The top 15 hits from log-likelihood analysis of the secondary phosphatase screen; data were analyzed for hits within the I κ B α -FLuc reporter degradation phase alone, the re-synthesis phase alone, or both phases combined. PTPRJ is highlighted.

	Degradation	Re-Synthesis	Degradation + Re-Synthesis
	TNF	TNF	TNF
1	PPP1CB	CDKN3	CDKN3
2	PPP1R2	PPFIA3	ENPP3
3	PTPN3	ENPP3	PPFIA3
4	PPP2CA	PPP1R3D	PPP3CA
5	SBF1	PTPN3	PPP1R3D
6	CDKN3	SKIP	PTPN3
7	PPP1R13B	PTPRN	PLIP
8	DOLPP1	PTPRJ	ALPL
9	DUSP16	ALPL	CDC25B
10	PPP2R1A	PPP1R3C	SKIP
11	PPP3CA	PPP2CB	PPP2CB
12	ACPT	PLIP	PSTPIP2
13	PTPRN	PPP1R13B	PPP1R3C
14	PPP1R3D	PPP3CA	PTPRJ
15	PPFIA3	PIB5PA	DOLPP1

4.8 SUPPLEMENTAL TABLES

Initial Flux	Degradation Minimum (raw flux)	Degradation Minimum (fold initial)	Re-Synthesis Maximum (raw flux)	Re-Synthesis Maximum (fold initial)	<u>Time of Degradation Minimum</u>	<u>Time of Re-Synthesis Maximum</u>	<u>Re-Synthesis Rate (raw flux)</u>	<u>Re-Synthesis Rate (fold initial)</u>	<u>Re-Synthesis Lag Time (raw flux)</u>	<u>Re-Synthesis Lag Time (fold initial)</u>
PTPN3	PTPRS	PTPRN	SKIP	PTPN3	SPAP1	PTPRS	SKIP	PTPRJ	PTPRN	PTPRN
PPP2R2C	PTPNS1	PTPN3	PTPRS	PPP1R3D	PPP1R1B	PTPRN	PTPRN	PTPN3	PTPRJ	PTPRJ
PPP2R1A	PTPN3	PPP1R2	PR48	PPP1R3C	DUSP16	PTPRJ	PTPN3	PPP1R3D	PTPN3	PTPN3
PPP1R12C	PTP4A2	PPP1CB	PPP2CB	PPP1R2	DOLPP1	PTPN3	PR48	PPP1R3C	PME-1	PSTPIP2
PLIP	PPP2R2C	MTMR4	PPP2CA	PPFIA3	ACPT	PPP3CA	PPP2CB	PPP1R2	PHPT1	PPP1R1B
DUSP19	PPP2R1A	CDKN3	PHOSPHO1	PIB5PA		PLIP	PHOSPHO1	PPP1R12C	G6PC3	PME-1
CDKN3	PPP1R2		CDC25B	ENPP3			CDC25B	PPFIA3	DUSP16	G6PC3
	PPP1R12C		ALPL	CDKN3			ALPL	PIB5PA		DUSP16
	DOLPP1			ALPL				CDKN3		
	CDKN3							ALPL		
higher flux	less degradation		more re-synthesis		later degradation	later re-synthesis	faster rate		longer lag time	
lower flux	more degradation		less re-synthesis		earlier degradation	earlier re-synthesis	slower rate		shorter lag time	

Supplemental Table 4.1: Reproducible Strong & Weak Stringency Hits From the Phosphatase Screen

Black lettering indicates strong hits (targeted error rate $\alpha = 0.0027$), while white lettering denotes weaker hits (targeted error rate $\alpha = 0.05$) using quartile-based analysis. Black boxes indicate phosphatases that, for a given parameter, registered as hits in both raw photon flux data and fold-initial normalized data. The kinetic parameters are listed in bold, underlined text. The order of hits within each parameter does not indicate rank order, though rank order will be determined during secondary screening (see above text).

4.7 REFERENCES

1. Hacker, H. and M. Karin, *Regulation and function of IKK and IKK-related kinases*. Sci STKE, 2006. **2006**(357): p. re13.
2. Barisic, S., et al., *Identification of PP2A as a crucial regulator of the NF-kappaB feedback loop: its inhibition by UVB turns NF-kappaB into a pro-apoptotic factor*. Cell Death Differ, 2008. **15**(11): p. 1681-90.
3. Prajapati, S., et al., *Protein phosphatase 2Cbeta association with the IkappaB kinase complex is involved in regulating NF-kappaB activity*. J Biol Chem, 2004. **279**(3): p. 1739-46.
4. DiDonato, J.A., et al., *A cytokine-responsive IkappaB kinase that activates the transcription factor NF-kappaB*. Nature, 1997. **388**(6642): p. 548-54.
5. Kray, A.E., et al., *Positive regulation of IkappaB kinase signaling by protein serine/threonine phosphatase 2A*. J Biol Chem, 2005. **280**(43): p. 35974-82.
6. Witt, J., et al., *Mechanism of PP2A-mediated IKK beta dephosphorylation: a systems biological approach*. BMC Syst Biol, 2009. **3**: p. 71.
7. Chew, J., et al., *WIP1 phosphatase is a negative regulator of NF-kappaB signalling*. Nat Cell Biol, 2009. **11**(5): p. 659-66.
8. Li, H.Y., et al., *Deactivation of the kinase IKK by CUEDC2 through recruitment of the phosphatase PPI*. Nat Immunol, 2008. **9**(5): p. 533-41.
9. Li, S., et al., *RNAi screen in mouse astrocytes identifies phosphatases that regulate NF-kappaB signaling*. Mol Cell, 2006. **24**(4): p. 497-509.
10. Sun, W., et al., *Protein phosphatase 2A acts as a mitogen-activated protein kinase kinase kinase 3 (MEKK3) phosphatase to inhibit lysophosphatidic acid-induced IkappaB kinase beta /nuclear factor-kappaB activation*. J Biol Chem.
11. Sun, W., et al., *PPM1A and PPM1B act as IKKbeta phosphatases to terminate TNFalpha-induced IKKbeta-NF-kappaB activation*. Cell Signal, 2009. **21**(1): p. 95-102.
12. Moss, B.L., et al., *Identification of a ligand-induced transient refractory period in nuclear factor-kappaB signaling*. J Biol Chem, 2008. **283**(13): p. 8687-8698.
13. Werner, S.L., D. Barken, and A. Hoffmann, *Stimulus specificity of gene expression programs determined by temporal control of IKK activity*. Science, 2005. **309**(5742): p. 1857-61.
14. Werner, S.L., et al., *Encoding NF-kappaB temporal control in response to TNF: distinct roles for the negative regulators IkappaBalpha and A20*. Genes Dev, 2008. **22**(15): p. 2093-101.
15. Ashall, L., et al., *Pulsatile stimulation determines timing and specificity of NF-kappaB-dependent transcription*. Science, 2009. **324**(5924): p. 242-6.
16. Barken, D., et al., *Comment on "Oscillations in NF-kappaB signaling control the dynamics of gene expression"*. Science, 2005. **308**(5718): p. 52.
17. Gammon, S.T., et al., *Spectral unmixing of multicolored bioluminescence emitted from heterogeneous biological sources*. Anal Chem, 2006. **78**: p. 1520-1527.
18. Valanne, S., et al., *Genome-wide RNA interference in Drosophila cells identifies G protein-coupled receptor kinase 2 as a conserved regulator of NF-kappaB signaling*. J Immunol. **184**(11): p. 6188-98.
19. Naik, S., et al., *Vascular Endothelial Growth Factor Receptor-1 Is Synthetic Lethal to Aberrant {beta}-Catenin Activation in Colon Cancer*. Clin Cancer Res, 2009. **15**(24): p. 7529-7537.
20. Zhang, X.D., et al., *Robust statistical methods for hit selection in RNA interference high-throughput screening experiments*. Pharmacogenomics, 2006. **7**(3): p. 299-309.
21. Ding, L., et al., *Genome remodelling in a basal-like breast cancer metastasis and xenograft*. Nature, 2010. **464**(7291): p. 999-1005.

22. Sacco, F., et al., *Tumor suppressor density-enhanced phosphatase-1 (DEP-1) inhibits the RAS pathway by direct dephosphorylation of ERK1/2 kinases*. J Biol Chem, 2009. **284**(33): p. 22048-58.
23. Autschbach, F., et al., *Expression of the membrane protein tyrosine phosphatase CD148 in human tissues*. Tissue Antigens, 1999. **54**(5): p. 485-498.
24. Ostman, A., Q. Yang, and N.K. Tonks, *Expression of DEP-1, a receptor-like protein-tyrosine-phosphatase, is enhanced with increasing cell density*. Proc Natl Acad Sci U S A, 1994. **91**(21): p. 9680-4.
25. Petermann, A., et al., *Loss of the Protein-Tyrosine Phosphatase DEP-1/PTPRJ Drives Meningioma Cell Motility*. Brain Pathology. **21**(4): p. 405-418.
26. Toland, A.E., et al., *PTPRJ Haplotypes and Colorectal Cancer Risk*. Cancer Epidemiology Biomarkers & Prevention, 2008. **17**(10): p. 2782-2785.
27. Holsinger, L.J., et al., *The transmembrane receptor protein tyrosine phosphatase DEP1 interacts with p120(ctn)*. Oncogene, 2002. **21**(46): p. 7067-76.
28. Petermann, A., et al., *Loss of the protein-tyrosine phosphatase DEP-1/PTPRJ drives meningioma cell motility*. Brain Pathol, 2010. **21**(4): p. 405-18.
29. Omerovic, J., M.J. Clague, and I.A. Prior, *Phosphatome profiling reveals PTPN2, PTPRJ and PTEN as potent negative regulators of PKB/Akt activation in Ras-mutated cancer cells*. Biochem J, 2010. **426**(1): p. 65-72.
30. Mita, Y., et al., *Missense polymorphisms of <i>PTPRJ</i> and <i>PTPN13</i> genes affect susceptibility to a variety of human cancers*. Journal of Cancer Research and Clinical Oncology. **136**(2): p. 249-259.
31. Tukey, J.W., *Exploratory Data Analysis*. 1977, Reading, MA, USA: Addison-Wesley.

CHAPTER FIVE

High-Throughput Kinase RNA Interference Screen Identifies Novel Regulators of TNF α -Induced IKK:I κ B α :NF- κ B Negative Feedback Loop Dynamics

5.1 INTRODUCTION

In resting cells, NF- κ B dimers are sequestered in the cytoplasm through binding to isoforms of the I κ B family. Canonical activation of NF- κ B relies on ligand-dependent stimulation of IKK, a large heterotrimeric kinase complex containing two catalytic subunits (IKK α and IKK β) and a regulatory subunit (IKK γ , NEMO) [1, 2]. Many different surface receptors signal to IKK through multi-protein complexes containing TRAFs (TNF receptor associated factors which seem to serve as adaptors and may mediate K63-linked regulatory ubiquitination events) and a multitude of other adaptor proteins (with specific receptors interacting with specific subsets of TRAFs and other adaptors) that recruit and activate the IKK complex [1, 3]. Activation of IKK requires phosphorylation of T loop serines, however, the precise mechanism by which this occurs (trans-autophosphorylation or through phosphorylation by an upstream kinase) remains a major unanswered question, and adaptor protein mediated multimerization also seems to significantly contribute to IKK activation [3]. Upon activation, IKK phosphorylates I κ B α (on Ser 32/36), thus rendering I κ B α a substrate for poly-ubiquitination and proteasomal degradation. This series of events releases NF- κ B to freely translocate to the nucleus where it can modulate expression of its target genes, including I κ B α , thus

forming a transcriptionally-coupled negative feedback loop [4]. This newly synthesized I κ B α enters the nucleus and binds to NF- κ B which dissociates from the DNA and the complex translocates back to the cytoplasm [4-6], and, along with the activity of I κ B ϵ , drive NF- κ B nuclear:cytoplasmic oscillations [4, 7, 8]. Thus, this negative feedback loop plays a major role in regulating the strength and duration of NF- κ B transcriptional activity [9-12]. With respect to negative feedback, other transcriptionally-*independent* processes, aimed at auto-inhibition of NF- κ B activity, do exist. Such mechanisms down-regulate NF- κ B signaling on a much shorter timeframe (sec-min). These include homologous receptor desensitization [13, 14], asymmetric heterologous receptor desensitization [14, 15], autocatalytic C-terminal IKK hyperphosphorylation [16] and protein phosphatase 2 β (PP2 β)-dependent dephosphorylation of IKK [17].

Given that our κ B₅→I κ B α -FLuc reporter has enabled us to study the IKK-I κ B α -NF- κ B negative feedback loop with high temporal resolution [18], and given that temporal control of this and other negative feedback loops has emerged as a critical regulatory component of the intensity and specificity of the NF- κ B transcriptional program [9-12], we sought to perform an RNAi screen to identify novel kinase regulators of IKK-I κ B α -NF- κ B negative feedback loop dynamics. This information, coupled with the data acquired in our phosphatase RNAi screen, could add to our understanding of the opposing effects that kinases/phosphatases might play in activation/de-activation of IKK (and other members of the NF- κ B signaling cascade) [1].

5.2 RESULTS

Execution of kinase RNAi screen to identify novel regulators of I κ B α dynamics in the presence of TNF α -induced stimulation.

The screen was performed by co-transfecting the Qiagen Human Kinase siRNA Library 2.0 (which consists of nine 96 well plates with columns 1 & 12 empty for user-specified controls) with the κ B₅→I κ B α -FLuc reporter in HepG2 cells in 96 well plate format. A staggered schedule of transfection and imaging was rigorously followed as the IVIS 100 chamber can only accommodate three 96 well plates per session. The co-transfected cells were stimulated with TNF α and imaged for luciferase bioluminescence under the conditions described above (for more details, see Methods section). This regimen provided a dynamic read-out with high-temporal resolution, allowing us to investigate not only changes in the amplitude of degradation and re-synthesis (as typical high-throughput screens monitor), but also the effect of siRNAs on the kinetic aspects of the negative feedback loop (i.e. times of maximal degradation and re-synthesis, rate of re-synthesis, and re-synthesis lag time). Though other RNAi screens have been published looking for novel regulators of the NF- κ B pathway ([19-21]), most have examined downstream NF- κ B transcriptional activity many hours-to-days following pathway stimulation and none have honed in specifically on the IKK-I κ B α -NF- κ B negative feedback loop or on the kinetic aspects of NF- κ B signaling.

The kinase library was screened once in triplicate with negative and positive controls on each plate: Qiagen negative control siRNA and siGFP served as negative controls, siTNFR1 and siPPP2CB were used as biological positive controls as they have

been previously shown to positively and negatively regulate canonical NF- κ B, respectively.

Rigorous statistical analysis of kinase screen data and identification of high-confidence hits.

Raw photon flux data were normalized as fold initial and subsequently subjected to various types of statistical analysis in an attempt to utilize the entirety of the complex dataset. In one method, we characterized the dynamics of κ B₅→I κ B α -FLuc responses under each siRNA treatment and used linear regression to determine maximum reporter re-synthesis and degradation rates between signal minima and maxima. We then used quartile-based analysis to find outliers in these parameters. However, these parameters proved to be problematic as the assumptions behind the regression were not consistently met by the data. Additionally, quartile analysis was problematic for this experimental set up: the Qiagen siRNA library is arrayed by function and gene symbol, which results in clustering related kinases such as members of the MAPK family. Thus, quartile analysis led to false negative and positive hits based on which groups of kinases were on each plate.

The cumulative log-likelihood method was undertaken to compensate for inter-plate variability and the non-random array of siRNAs. This approach quantifies the deviation of a siRNA treatment from the negative controls and adjusts for confounding variance that otherwise prevents direct comparisons between plates. More specifically, we first made a Gaussian probability density function at each time point based on the

mean and variance of the plate negative controls. We then input each siRNA measurement into this function to quantify the normalized deviation from the set of negative controls. To combine replicates, and to later make a cumulative sequence, we prevented computational rounding error by taking the logarithm of the likelihood (log-likelihood) and summing ($\log A + \log B = \log AB$). In general, the greater the difference from the negative controls the greater the log-likelihood value for that siRNA. This value correlates with the deviation from negative controls and allowed us more direct comparison between siRNA plates. The siRNA were then ranked and visualized in a bar graph in which each division of the bar height represents the contribution of an individual time point to the cumulative log-likelihood value (Fig. 5.1). Each plate was analyzed for hits in the degradation phase (Sup. Fig. 5.1), the re-synthesis phase (Sup. Fig. 5.2), and cumulatively for both degradation and re-synthesis considered together (Sup. Fig. 5.3). This rank-based method allows for approximate comparison between plates and precise comparison within each plate. In addition, the bars were colored-coded based on Directional Replicate Agreement, wherein a value of ± 3 means all plates within the triplicate agreed and were either above or below the negative controls, and a value of ± 1 means imperfect agreement with one of the replicates deviating from the others because it registered differentially above or below the negative controls. Internal analysis showed that the top hits according to log-likelihood (highest log likelihood or lowest likelihood) analysis displayed no plate nor well position preference within plates.

Several known proteins involved in NF- κ B signaling were identified as top hits when considering degradation and re-synthesis together, including: NIK, JAK2, NLK, SPHK1, KSR2, ROCK2 and MK2 (Figure 5.2). This further confirmed that the log-

likelihood means of analysis could be successfully applied to dynamic time course data from a high-throughput RNAi screen, and may represent a new paradigm for analysis of this type of data. In contrast to the phosphatase siRNA screen, a number of strong hits impacting the I κ B α -FLuc degradation phase were identified (Sup. Fig. 5.1), including PRKACB and LIMK1 as positive regulators (i.e. upon knock-down *less* I κ B α -FLuc degradation is seen in comparison to controls, suggesting a role in positively regulating IKK activity), and GALK1, FER, and GAK as negative regulators (i.e. upon knock-down *greater* I κ B α -FLuc degradation is seen in comparison to controls, suggesting a role in negatively regulating IKK activity). PRKACB is especially interesting since it was also identified as positive regulator of I κ B α -FLuc re-synthesis (Sup. Fig. 5.2). Most of the strong hits identified for the re-synthesis phase were negative regulators, including JAK2, JAK3, and DAPK3.

Validation of DAPK3 as a novel regulator of TNF α -Induced NF- κ B Signaling.

Death associated protein kinase 3 (DAPK3/ ZIPK) was identified as a strong candidate regulator in the primary screen (Figure 5.2), acting as a negative regulator. Secondary validation experiments were carried out to confirm that stable knock-down of DAPK3 by lentivirus shRNA in HepG2 cells reproduced the same phenotype as that identified in the screen. We confirmed that two independent shRNA constructs targeting different sequences of the DAPK3 coding sequence showed robust knockdown (>90%) which correlated with increased κ B \rightarrow I κ B α -FLuc re-synthesis levels compared to

negative controls (~3.3 fold shGFP) upon TNF α treatment (Fig. 5.3), consistent with DAPK3 as a negative regulator of the NF- κ B pathway.

5.3 DISCUSSION

The transcription factor NF- κ B is a pivotal regulator of innate immunity and inflammation, and is active in both immune cells and non-immune tissues [22, 23]. In this capacity, the NF- κ B pathway must rapidly decode signals and integrate intracellular information to control individual cell fate decisions (proliferation, apoptosis, differentiation, etc.) and regulate the production and secretion of cytokines that can amplify and propagate the inflammatory response [24, 25]. NF- κ B dimers are typically sequestered and held inactive in the cytoplasm through binding to isoforms of the I κ B family, with I κ B α representing the prototypical member and major regulator of canonical NF- κ B activity. TNF α -induced stimulation of NF- κ B relies on activation of I κ B kinase complex (IKK), which phosphorylates I κ B α , marking it for subsequent ubiquitination and proteasomal degradation [2]. This series of events liberates NF- κ B, allowing it to undergo nuclear translocation and activation of target gene expression, including the I κ B α gene itself [26], thus establishing a critical transcriptionally-coupled negative feedback loop [4]. Furthermore, this negative feedback loop plays a major role in regulating the strength and duration of NF- κ B transcriptional activity [9-12]. Given that temporal control of this negative feedback loops has emerged as a critical regulatory component of the intensity and specificity of the NF- κ B transcriptional program and that our κ B $_5$ →I κ B α -FLuc reporter has previously enabled us to study the IKK-I κ B α -NF- κ B

negative feedback loop with high temporal resolution [18] and to run a *phosphatase* RNAi screen for novel regulators the feedback loop, we sought to perform an additional RNAi screen to identify novel *kinase* regulators of IKK-I κ B α -NF- κ B negative feedback loop dynamics.

Recently, NF- κ B has emerged as a mechanistic link between inflammation and cancer [27, 28]. This has been extensively studied in the liver where hepatocellular carcinoma (HCC) slowly unfolds on a background of chronic inflammation (often triggered by exposure to infectious agents or toxic compounds) [29]. TNF α -induced activation of NF- κ B signaling plays a pivotal role in liver homeostasis and pathophysiology due to its capacity to induce both hepatocyte cell death and proliferation [30, 31]. In the liver, NF- κ B signaling can have both tumor promoting and tumor suppressing effects that are dependent upon the type of cells (i.e., liver resident macrophages vs. hepatocytes), the stimuli, and cell context [29, 32, 33]. Thus, a more in-depth understanding of the complexities and intricacies of NF- κ B signaling in the liver is required to appropriately translate the use of NF- κ B-targeted therapeutics to liver pathologies.

Death associated protein kinase 3 (DAPK3/ ZIPK) was identified as a strong candidate regulator in the primary screen (Figure 5.2; Fig. 5.1), acting as a negative regulator of I κ B α -FLuc dynamics (i.e. showing higher I κ B α degradation and higher re-synthesis upon knock-down; Sup. Fig. 5.3). DAPK3 was validated as a true hit in work carried out by Brandon Kocher in our lab (Fig. 5.3). DAPK3 is a member of the death-associated protein (DAPK) serine/threonine kinase family which consists of several

kinases originally identified in the context of apoptosis [34]. DAPK3 shares 83% amino acid conservation in its kinase domain with that of DAPK, and is unique among the DAPK family as it contains a leucine zipper domain and several putative nuclear localization signals. Orthologues of DAPK3 have been identified in several lower eukaryotes such as *D. rerio* and *X. laevis*.

Unlike DAPK, there is limited evidence to support a pro-apoptotic role for DAPK3. Over expression of DAPK3 causes morphological characteristics of autophagy-like apoptosis (membrane blebbing, nuclear condensation) that are lost upon mutation of DAPK phosphorylation sites [35]. DAPK3 is phosphorylated on over 12 serines and threonines by several kinases most notably DAPK at T299. T299D DAPK3 mutants display cytoplasmic localization and increased cell death, whereas T299A mutants display nuclear localization and no significant effects on cell death compared to WT [35, 36]. This suggests that DAPK antagonizes nuclear DAPK3 functions by maintaining it in the cytoplasm. A larger body of literature suggests that DAPK3 participates in the positive and negative regulation of gene expression at various levels. In the cytoplasm, the DAPK-DAPK3 cascade negatively regulates IFN- γ induced inflammatory selective mRNA translation through activation of an inhibitory RNA binding protein complex [37]. DAPK3 also facilitates STAT3 and AR transcriptional activation through direct or indirect interactions [38, 39]. DAPK3 localizes to promyelocytic leukemia protein (PML) nuclear bodies, chromatin, centrosomes, mitotic centrosomes and the contractile ring during cytokinesis [34]. It is unclear as to how DAPK3 may be regulating NF- κ B as it was identified as a negative regulator of NF- κ B, which contrasts with its previously established role as a transcriptional co-activator. Overall, our preliminary data suggests

that DAPK3 may play a repressive role in the context of NF- κ B transcription/translation and/or that its transcriptional role is more complex than originally appreciated.

Intriguingly, DAPK is overwhelmingly down-regulated in many primary tumor tissues as reported by many groups (hepatocellular, non-small cell lung carcinomas, renal, leukemia, head and neck, colon, gastric, ovarian cancers and brain metastases) which correlates with disease reoccurrence and unfavorable prognosis [40-47]. Loss of DAPK therefore seems to facilitate tumorigenesis, and in part may be explained by a loss of cytoplasmic-apoptotic DAPK3 and a gain in DAPK3 nuclear activities. This would be advantageous to a cancer cell as DAPK3 facilitates activation of several HCC oncogenic transcriptional programs (STAT3 and AR) and DAPK exerts its tumor suppressive function by presumably preventing DAPK3-mediated activation of these pathways. Indeed, activation of the IL-6/JAK/STAT3 pathway is hepatoprotective, promotes compensatory proliferation of hepatocytes and is tumor promoting in carcinogen-induced mouse models of HCC [48]. Hepatocyte deletion of AR delays the development of carcinogen-induced HCC indicating that active AR is HCC promoting [49]. In the context of the screen conditions, TNF α induces NF- κ B activation which is associated with cytostatic effects in HepG2 cells [50]. Given that DAPK3 inhibits TNF α -mediated NF- κ B activation; this suggests that DAPK3 antagonizes these cytostatic effects thereby maintaining a proliferative signaling environment in conjunction with STAT3 and AR pathways. Thus, a better mechanistic understanding of the role of DAPK3 in the NF- κ B, STAT3 and AR pathways is needed as they may represent novel therapeutic targets for a variety of human cancers. Brandon Kocher, a graduate student in our lab is currently pursuing further study of DAPK3 and its role in NF- κ B pathway regulation.

Additionally, we are continuing to validate other hits from the kinase screen. Of particular interest for further study are PRKACB and LIMK1; knock-down of either results in decreased levels of I κ B α -FLuc degradation, a rarely observed phenotype in either the phosphatase or kinase screens. These proteins may play a role in positively regulating IKK activity, and thus directly impact the degree of I κ B α degradation upon ligand stimulation. Furthermore, it will be interesting to merge the data from the phosphatase and kinase screens into a single dataset for analysis in an effort to identify potentially novel pairs of phosphatases/kinases that similarly regulate the dynamics of the IKK-I κ B α -NF- κ B negative feedback loop.

5.4 METHODS

High-throughput primary siRNA screen. siRNA screening was performed in black, clear-bottomed, 96-well culture plates (Corning 3904) using a Beckman-Coulter Core robotics system, including an FX liquid handler, controlled by the Sagian graphical method development tool (SAMI scheduling software). A day prior to transfection, we manually seeded 10,000 cells in complete medium (DMEM supplemented with 10% heat-inactivated fetal bovine serum (Δ FBS) and 1% glutamine) at 150 μ l/well into three plates. Plates were maintained in an environmentally controlled incubator until needed for operations, thereby optimizing health and uniform treatment of all plates. Prior to transfection, siRNA library plates were thawed from -80C and centrifuged to collect all liquid into the bottom of the well. Experimental siRNA oligos were pre-arrayed in columns 2-11 of each plate and individual controls comprising mock-transfected wells, non-targeting AllStars Negative Control sequence (siNeg, Qiagen Inc.), Firefly luciferase-targeting PGL3 siRNA (Integrated DNA Technologies, Inc.), TNFR1 targeting sequences (siTNFR1, Integrated DNA Technologies, Inc.), and a PPP2CA siRNA (siPPP2CA, Integrated DNA Technologies, Inc.) were placed manually in columns 1 and 12.

Forward co-transfection of siRNA and plasmid reporter was performed in triplicate. First, κ B₅→I κ B α -FLuc reporter plasmid was diluted into serum-free media and transferred onto one siRNA library plate (containing enough siRNA to transfect three identical cell plates) with a 96 multichannel head on the FX liquid handler and allowed to incubate for 5 min at room temperature. Next, 50 uL of X-TremeGENE (Roche, Inc.) transfection reagent, diluted in serum-free media, was added to the plasmid/siRNA

mixture with a 96 multichannel head on the FX liquid handler, mixed, and allowed to incubate for 15 min at room temperature. Subsequently, 30 uL/well of this mixture was transferred to the three previously seeded cell plates to a final concentration of 50 ng/well reporter plasmid, 0.8 uL/well X-TremeGENE reagent, and 88 ng siRNA/well in a final volume of 180 uL. Plates were maintained in an incubator for 24 hrs, and then aspirated and 150 uL/well of fresh colorless full media was added using the FX liquid handler.

At 48 hours post-transfection, D-luciferin (Biosynth) was added using the FX liquid handler to a final concentration of 150 µg/mL bringing the final volume up to 180 uL/well. Cells were allowed to equilibrate in this media for 30-60 min before the addition 20 uL/well of TNFα (20 ng/mL final concentration) or vehicle (D-luc imaging media). Bioluminescence measurements were acquired in an IVIS 100 imaging system (Caliper Life Sciences, Hopkinton, MA) at 37°C under 5% CO₂ flow for 6 hr. Typical acquisition parameters were as follows: acquisition time, 15-30 sec; binning, 4-8; FOV, 25 cm; f/stop, 1; filter, open; image-image interval, 5 min; total number of acquisitions, 73. Immediately post-IVIS imaging, phase contrast photographs were acquired on the InCell 1000 (three 10X fields of view per well). Cell viability was then determined with resazurin dye (Sigma R7017) (final conc., 44 µM after a 2 hr incubation at 37°C as monitored on a FLUOstar OPTIMA fluorescence reader (BMG Labtech); excitation, 544 nm, emission, 590 nm). This procedure was repeated once for all nine plates of the Qiagen Human Kinase siRNA Library 2.0.

Statistical analysis and “high confidence hit” selection. Data were analyzed using Living Image 3.2 for data acquisition and raw data capture, and PASW Statistics 18 and MatLab 2011a for data analysis, statistics, and graphing. Circular regions of interest (ROIs) were drawn around each well and the photon flux at every time point was measured using Living Image 3.2. This raw data was then imported into PASW and the data were normalized to the signal at the first timepoint (without normalization to resazurin viability measurements).

Log-likelihood analysis method. The cumulative log-likelihood approach quantifies the deviation of an experimental siRNA treatment from the negative controls (scrambled negative controls and siGFP). This was done by generating a Gaussian probability density function at each time point based on the mean and variance of the negative controls on within a given plate. We then input each siRNA measurement to this function to quantify the deviation from the set of negative controls. To combine replicates, and to later make a cumulative sequence, we prevented computational rounding error by taking the negative logarithm of the likelihood (log-likelihood) and summing ($\log A + \log B = \log AB$). The log-likelihood values were determined separately for the degradation phase (which was defined as from $t = 0$ min to the median time point of the minimum value of the negative controls) and the re-synthesis phase (defined between the end of the degradation phase to the median time of greatest downward inflection in the kinetic profile of the negative controls), or cumulatively for both degradation and re-synthesis. The individual siRNAs from a given plate triplicate were then ranked according to their negative log-likelihood value and presented as a bar graph in which each division of the bar height represents the contribution of an individual

time point to the cumulative log-likelihood value (Figure 4.6). In addition, the bars were colored-coded based on directional replicate agreement, wherein a value of ± 3 means all plates within the triplicate agreed and were either above or below the negative controls, and a value of ± 1 means imperfect agreement with one of the replicates deviating from the others because it registered differentially above or below the negative controls. This rank-based method allows for approximate comparison between plates and precise comparison within each plate.

DAPK3 Validation Studies

Lentivirus expressing constructs (pLKO.1 puro) were obtained pre-synthesized from the Genome Sequencing Center at Washington University. The targeting sequences for the 4 shDAPK3 constructs and shGFP are as follows:

#1 - 5' CGTTCACTACCTGCACTCTAA

#3 - 5' CATCGCACACTTTGACCTGAA

#5 - 5' GAAGGAGTACACCATCAAGTC

#7 - 5' CGTTCACTACCTGCACTCTAA

shGFP - 5' CGGGATCACTCTCGGCATGGA

To generate lentivirus containing hairpins, 500,000 293T cells were pre-plated in 60 mm dishes and co-transfected the following day with 1 μ g of hairpin construct, 900 ng packaging plasmid pCMV- Δ R8.2, and 100 ng of envelope plasmid pVSVG using Fugene 6. Two days after transfection, virus containing supernatant was collected from 293T cells and filtered through a 0.45 μ m filter, mixed with 5 μ g/mL protamine sulfate, and added to HepG2 cells at 50% confluency in a 10cm² dish. Media was replenished 12 hrs

post-transduction cells were subsequently maintained in media supplemented with 750ng/mL puromycin hydrochloride to retain expression of the hairpins. Two days post-transduction, shDAPK3 or shGFP cells were plated in parallel for protein knockdown confirmation (Abcam, #ab2057) and transient transfection and subsequent imaging measurements with the $\kappa B_5 \rightarrow I\kappa B\alpha$ -FLuc reporter as previously described.

5.5 FIGURES

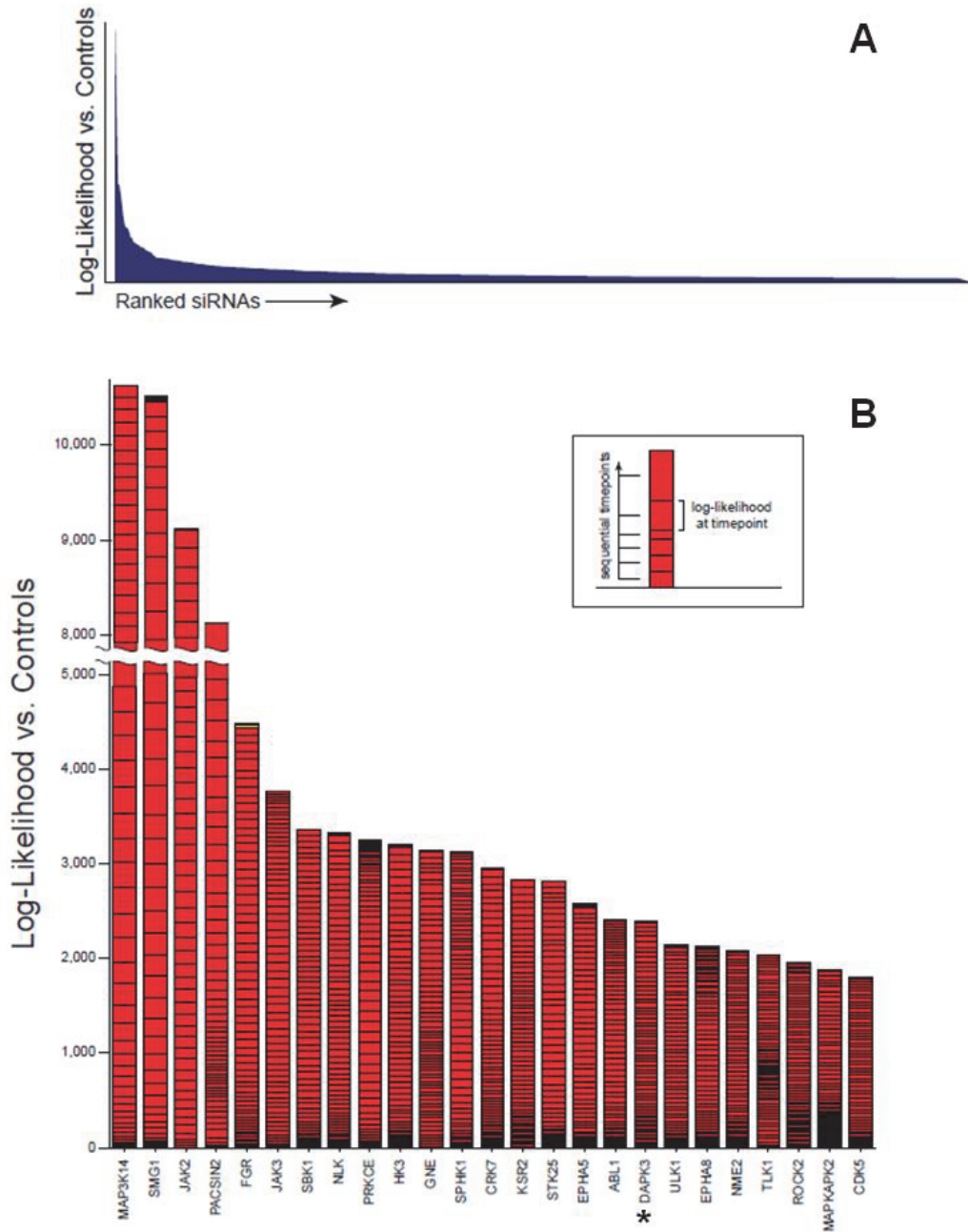


Figure 5.1: Cumulative Log-Likelihood Normalization Procedure

A) Representative image of rank based bar graph with cumulative-log likelihood values for all kinase siRNAs. Hits are arranged in descending cumulative log-likelihood values from left to right. **B)** Enlarged plot for top 25 rank based hits, including DAPK3*. Legend indicates a simple representation of time directionality and time point contribution to cumulative log-likelihood. Note the y-axis is truncated to allow visualization of high hit values.

A

Kinase	Known Impact on NFκB
1. NIK	Canonical & non-canonical activator
2. SMG1	Unknown
3. JAK2	Canonical activator
4. PACSIN2	Unknown
5. SRC2	Putative NEMO interaction
6. JAK3	Unknown
7. SBK1	Unknown
8. NLK	Activates TAK1
9. PKCε	Canonical Activator via MAPK pathways
10. HK3	Unknown
11. GNE	Unknown
12. SPHK1	Activator of PI3K/Akt/NF-κB pathway
13. CRK7/CDK12	Unknown
14. KSR2	Negative regulator of MAP3K3 activation of NF-κB pathway
15. STK25	Unknown
16. EPHA5	Unknown
17. ABL1	Inhibits proteasomal activity
18.* DAPK3	Unknown
19. ATG1	Unknown
20. EPHA8	Unknown
21. NME2	Unknown
22. TLK1	Unknown
23. ROCK2	Activating RelA phosphorylation (S536)
24. MK2	Maintains nuclear RelA
25. CDK5	Unknown

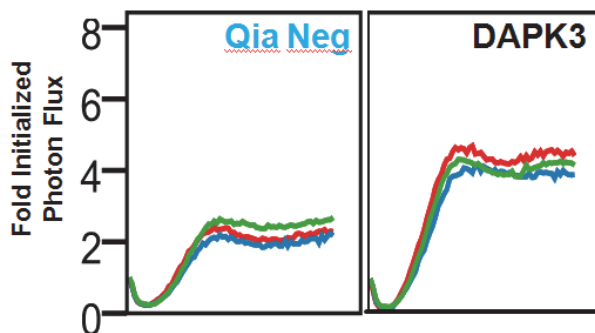
B

Figure 5.2: Top Kinase Hits from Cumulative Log-Likelihood Analysis of IκBα-FLuc Degradation and Re-Synthesis

A) List of top ranked hits and a description of the known mechanisms by which they influence the NF-κB pathway. DAPK3 (*) was chosen for secondary validation and further investigation. **(B)** siDAPK3 IκBα-FLuc dynamic profile from the primary kinase screen compared to Qiagen negative control siRNA.

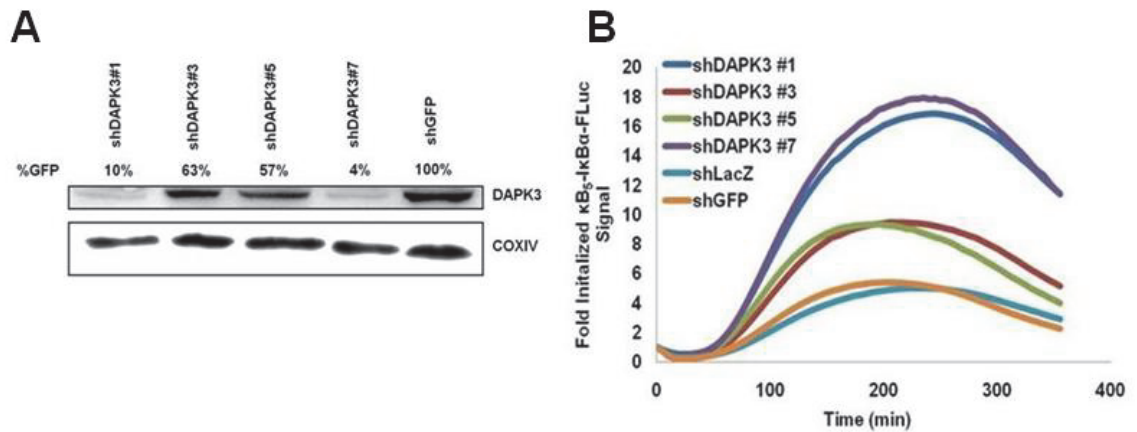


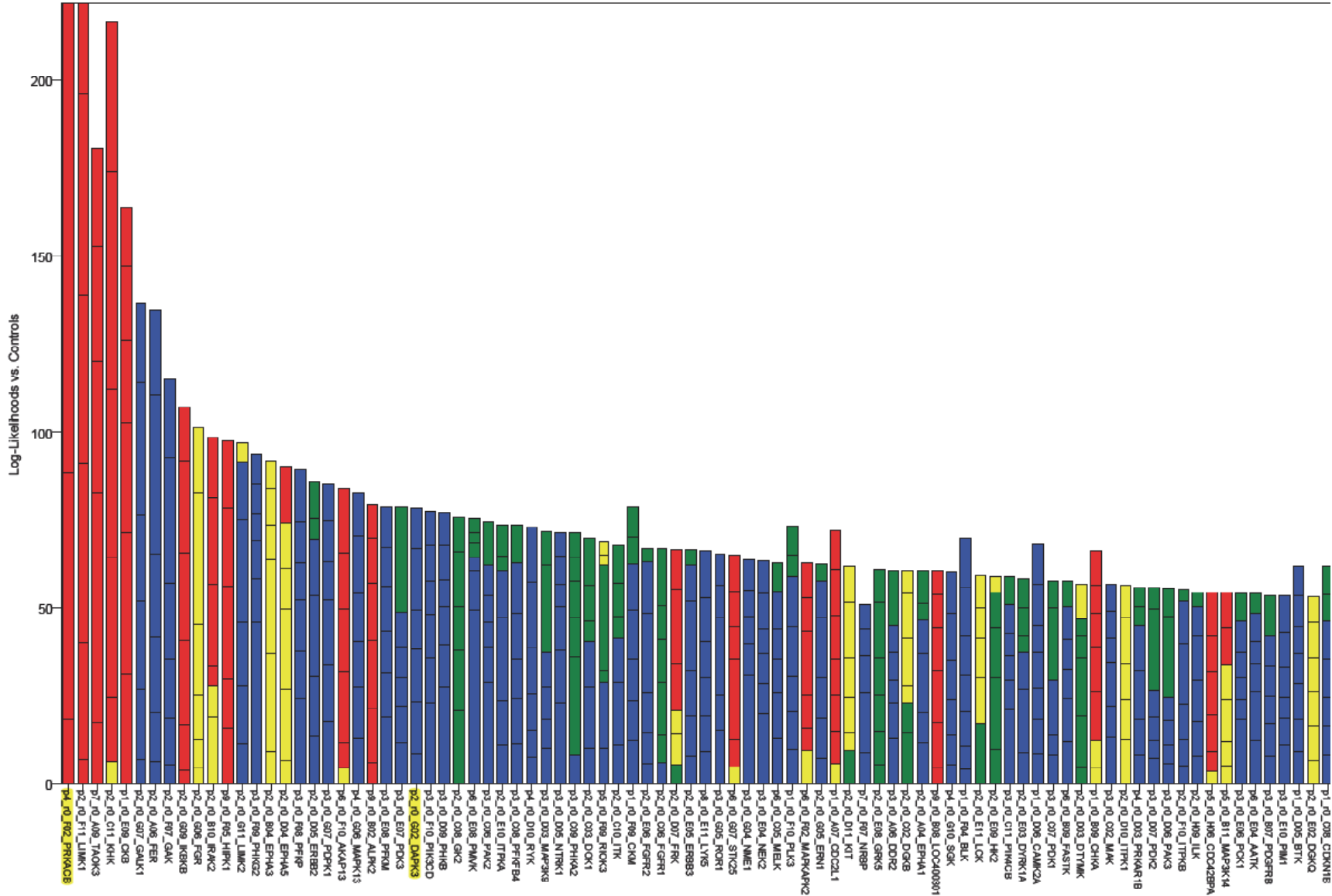
Figure 5.3: Validation of DAPK3 as a Negative Regulator of TNF α -Induced I κ B α Dynamics

A) Western blot of shRNA knockdown (%GFP = shRNA/COXIV/ shGFP/COXIV) of DAPK3 in HepG2 cells 3 days post transduction. COXIV protein levels were used for a loading control. **B)** Bioluminescence imaging sequence of lentivirus mediated DAPK3 knockdown in HepG2 cells transiently transfected with κ B₅- I κ B α -FLuc at 2 days post transduction. 24 hours post transfection cells were pre-incubated with 150 μ g/mL D-luciferin and subsequently treated with 10ng/mL of TNF α and imaged using the IVIS 50 system at 37 $^{\circ}$ C under 5%CO₂ and atmospheric oxygen. Data provided by Brandon Kocher.

5.6 SUPPLEMENTAL FIGURES

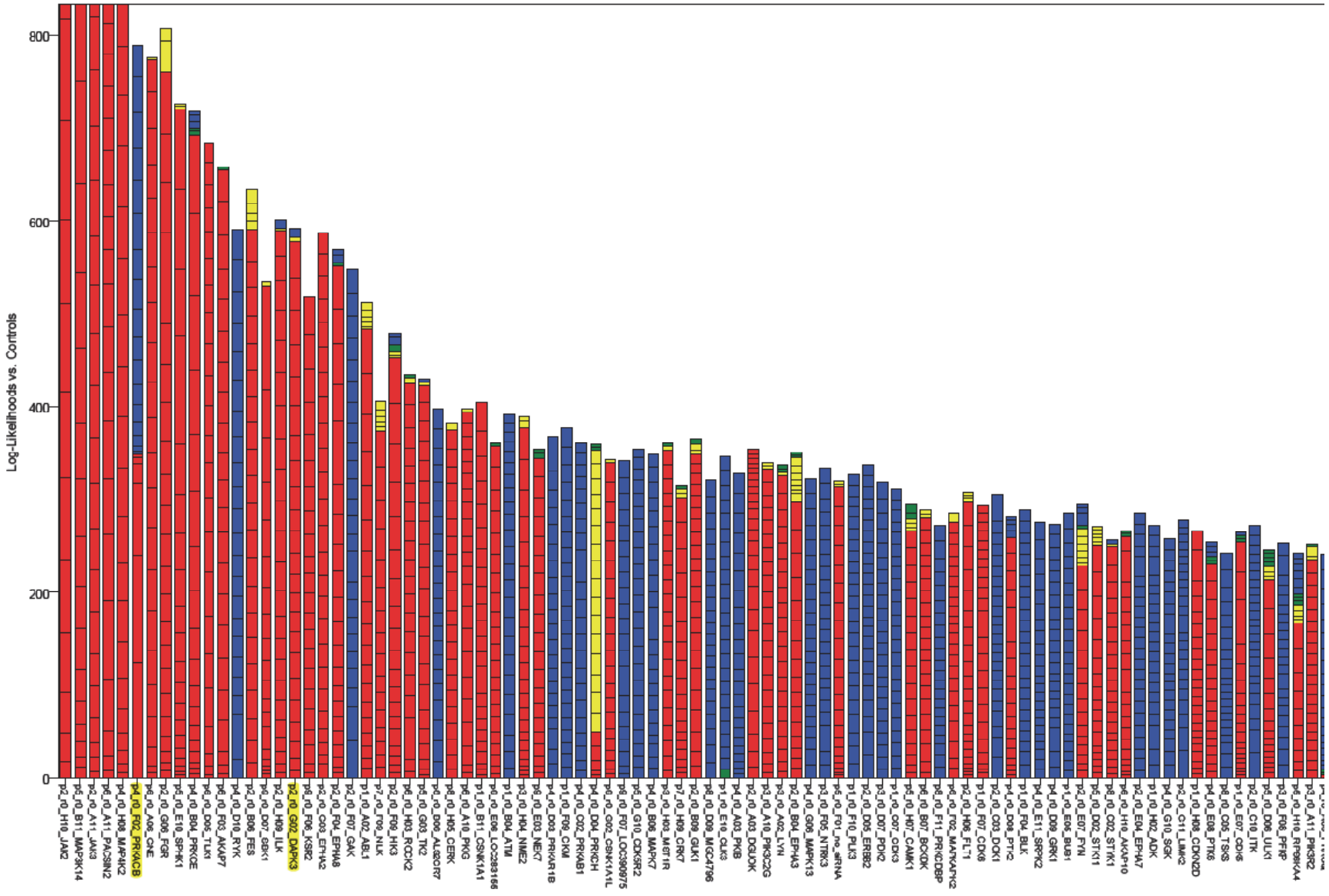
Supplemental Figure 5.1 Cumulative Log-Likelihood Ranking of Degradation Phase Hits from the Kinase Screen

Screen-wide analysis of the top hits identified for the $\text{I}\kappa\text{B}\alpha$ -FLuc degradation phase. The cumulative log-likelihood value for each siRNA is presented as a bar graph in which each division of the bar height represents the contribution of an individual time point to the cumulative log-likelihood value. Data shown represent the hits that differed the most from negative controls (i.e. have the largest log-likelihood values). Yellow highlighting denotes two hits discussed in the text, PRKACB and DAPK3.



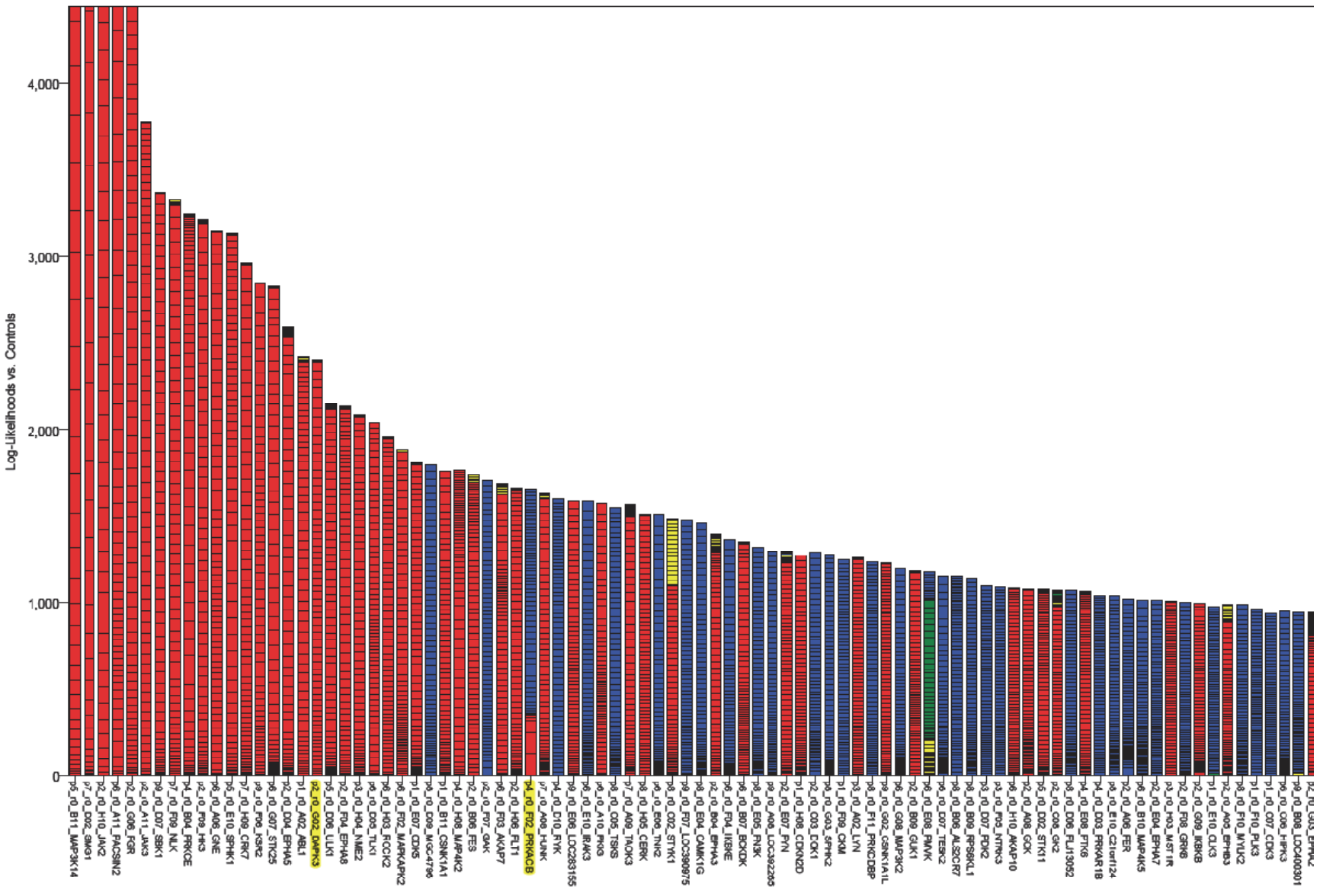
Supplemental Figure 5.2 Cumulative Log-Likelihood Ranking of Re-Synthesis Phase Hits from the Kinase Screen

Screen-wide analysis of the top hits identified for the I κ B α -FLuc re-synthesis phase. The cumulative log-likelihood value for each siRNA is presented as a bar graph in which each division of the bar height represents the contribution of an individual time point to the cumulative log-likelihood value. Data shown represent the hits that differed the most from negative controls (i.e. have the largest log-likelihood values). Yellow highlighting denotes two hits discussed in the text, PRKACB and DAPK3.



Supplemental Figure 5.3 Cumulative Log-Likelihood Ranking of Combined Degradation and Re-Synthesis Phase Hits from the Kinase Screen

Screen-wide analysis of the top hits identified for the I κ B α -FLuc degradation and re-synthesis phases combined. The cumulative log-likelihood value for each siRNA is presented as a bar graph in which each division of the bar height represents the contribution of an individual time point to the cumulative log-likelihood value. Data shown represent the hits that differed the most from negative controls (i.e. have the largest log-likelihood values). Yellow highlighting denotes two hits discussed in the text, PRKACB and DAPK3.



5.7 REFERENCES

1. Hacker, H. and M. Karin, *Regulation and function of IKK and IKK-related kinases*. Sci STKE, 2006. **2006**(357): p. re13.
2. Perkins, N.D., *Integrating cell-signalling pathways with NF-kappaB and IKK function*. Nat Rev Mol Cell Biol, 2007. **8**(1): p. 49-62.
3. Hayden, M.S. and S. Ghosh, *Shared principles in NF-kappaB signaling*. Cell, 2008. **132**(3): p. 344-62.
4. Hoffmann, A., et al., *The IkappaB-NF-kappaB signaling module: temporal control and selective gene activation*. Science, 2002. **298**(5596): p. 1241-5.
5. Arenzana-Seisdedos, F., et al., *Nuclear localization of I kappa B alpha promotes active transport of NF-kappa B from the nucleus to the cytoplasm*. Journal of Cell Science, 1997. **110**(3): p. 369-378.
6. Bergqvist, S., et al., *Kinetic enhancement of NF- κ B-DNA dissociation by I κ B \pm* . Proceedings of the National Academy of Sciences, 2009. **106**(46): p. 19328-19333.
7. Nelson, D.E., et al., *Oscillations in NF-kappaB signaling control the dynamics of gene expression*. Science, 2004. **306**(5696): p. 704-8.
8. Kearns, J.D., et al., *IkappaBepsilon provides negative feedback to control NF-kappaB oscillations, signaling dynamics, and inflammatory gene expression*. J Cell Biol, 2006. **173**(5): p. 659-64.
9. Werner, S.L., D. Barken, and A. Hoffmann, *Stimulus specificity of gene expression programs determined by temporal control of IKK activity*. Science, 2005. **309**(5742): p. 1857-61.
10. Werner, S.L., et al., *Encoding NF-kappaB temporal control in response to TNF: distinct roles for the negative regulators IkappaBalpha and A20*. Genes Dev, 2008. **22**(15): p. 2093-101.
11. Ashall, L., et al., *Pulsatile stimulation determines timing and specificity of NF-kappaB-dependent transcription*. Science, 2009. **324**(5924): p. 242-6.
12. Barken, D., et al., *Comment on "Oscillations in NF-kappaB signaling control the dynamics of gene expression"*. Science, 2005. **308**(5718): p. 52.
13. Karmann, K., et al., *Activation and homologous desensitization of human endothelial cells by CD40 ligand, tumor necrosis factor, and interleukin 1*. J Exp Med, 1996. **184**(1): p. 173-82.
14. Alberts, B., Bray, D., Lewis, J., Raff, M., Roberts, K. and Watson, J.D., *Target-Cell Adaptation*, in *Molecular Biology of the Cell*. 1994, Garland Publishing: New-York. p. 771-785.
15. Holtmann, H. and D. Wallach, *Down regulation of the receptors for tumor necrosis factor by interleukin 1 and 4 beta-phorbol-12-myristate-13-acetate*. J Immunol, 1987. **139**(4): p. 1161-7.
16. Delhase, M., et al., *Positive and negative regulation of IkappaB kinase activity through IKKbeta subunit phosphorylation*. Science, 1999. **284**(5412): p. 309-13.
17. Prajapati, S., et al., *Protein phosphatase 2Cbeta association with the IkappaB kinase complex is involved in regulating NF-kappaB activity*. J Biol Chem, 2004. **279**(3): p. 1739-46.
18. Moss, B.L., et al., *Identification of a ligand-induced transient refractory period in nuclear factor-kappaB signaling*. J Biol Chem, 2008. **283**(13): p. 8687-8698.
19. Valanne, S., et al., *Genome-wide RNA interference in Drosophila cells identifies G protein-coupled receptor kinase 2 as a conserved regulator of NF-kappaB signaling*. J Immunol. **184**(11): p. 6188-98.

20. Chew, J., et al., *WIP1 phosphatase is a negative regulator of NF-kappaB signalling*. Nat Cell Biol, 2009. **11**(5): p. 659-66.
21. Li, S., et al., *RNAi screen in mouse astrocytes identifies phosphatases that regulate NF-kappaB signaling*. Mol Cell, 2006. **24**(4): p. 497-509.
22. Hayden, M.S., A.P. West, and S. Ghosh, *NF-kappaB and the immune response*. Oncogene, 2006. **25**(51): p. 6758-80.
23. Pasparakis, M., *Regulation of tissue homeostasis by NF-kappaB signalling: implications for inflammatory diseases*. Nat Rev Immunol, 2009. **9**(11): p. 778-88.
24. Lee, T.K., et al., *A noisy paracrine signal determines the cellular NF-kappaB response to lipopolysaccharide*. Sci Signal, 2009. **2**(93): p. ra65.
25. Janes, K.A., et al., *The response of human epithelial cells to TNF involves an inducible autocrine cascade*. Cell, 2006. **124**(6): p. 1225-39.
26. Ito, C.Y., A.G. Kazantsev, and A.S. Baldwin, Jr., *Three NF-kappa B sites in the I kappa B-alpha promoter are required for induction of gene expression by TNF alpha*. Nucleic Acids Res, 1994. **22**(18): p. 3787-92.
27. Karin, M., *NF-kappaB as a critical link between inflammation and cancer*. Cold Spring Harb Perspect Biol, 2009. **1**(5): p. a000141.
28. Elizur, A., A.T. Vacek, and A.J. Howells, *Cloning and characterization of the white and topaz eye color genes from the sheep blowfly Lucilia cuprina*. J Mol Evol, 1990. **30**(4): p. 347-58.
29. Berasain, C., et al., *Inflammation and liver cancer: new molecular links*. Ann N Y Acad Sci, 2009. **1155**: p. 206-21.
30. Vlantis, K. and M. Pasparakis, *Role of TNF in pathologies induced by nuclear factor kappaB deficiency*. Curr Dir Autoimmun, 2010. **11**: p. 80-93.
31. Wullaert, A., et al., *Hepatic tumor necrosis factor signaling and nuclear factor-kappaB: effects on liver homeostasis and beyond*. Endocr Rev, 2007. **28**(4): p. 365-86.
32. Chen, F., K. Beezhold, and V. Castranova, *Tumor promoting or tumor suppressing of NF-kappa B, a matter of cell context dependency*. Int Rev Immunol, 2008. **27**(4): p. 183-204.
33. Vainer, G.W., E. Pikarsky, and Y. Ben-Neriah, *Contradictory functions of NF-kappaB in liver physiology and cancer*. Cancer Lett, 2008. **267**(2): p. 182-8.
34. Bialik, S. and A. Kimchi, *The death-associated protein kinases: structure, function, and beyond*. Annu Rev Biochem, 2006. **75**: p. 189-210.
35. Shani, G., et al., *Death-associated protein kinase phosphorylates ZIP kinase, forming a unique kinase hierarchy to activate its cell death functions*. Mol Cell Biol, 2004. **24**(19): p. 8611-26.
36. Graves, P.R., K.M. Winkfield, and T.A. Haystead, *Regulation of zipper-interacting protein kinase activity in vitro and in vivo by multisite phosphorylation*. J Biol Chem, 2005. **280**(10): p. 9363-74.
37. Mukhopadhyay, R., et al., *DAPK-ZIPK-L13a axis constitutes a negative-feedback module regulating inflammatory gene expression*. Mol Cell, 2008. **32**(3): p. 371-82.
38. Sato, N., et al., *Physical and functional interactions between STAT3 and ZIP kinase*. Int Immunol, 2005. **17**(12): p. 1543-52.
39. Leister, P., et al., *ZIP kinase plays a crucial role in androgen receptor-mediated transcription*. Oncogene, 2008. **27**(23): p. 3292-300.
40. Matsumoto, H., et al., *Prognostic significance of death-associated protein-kinase expression in hepatocellular carcinomas*. Anticancer Res, 2003. **23**(2B): p. 1333-41.
41. Niklinska, W., et al., *Prognostic significance of DAPK and RASSF1A promoter hypermethylation in non-small cell lung cancer (NSCLC)*. Folia Histochem Cytobiol, 2009. **47**(2): p. 275-80.

42. Christoph, F., et al., *Promoter hypermethylation profile of kidney cancer with new proapoptotic p53 target genes and clinical implications*. Clin Cancer Res, 2006. **12**(17): p. 5040-6.
43. Voso, M.T., et al., *Aberrant methylation of DAP-kinase in therapy-related acute myeloid leukemia and myelodysplastic syndromes*. Blood, 2004. **103**(2): p. 698-700.
44. Kim, J.C., et al., *Promoter methylation of specific genes is associated with the phenotype and progression of colorectal adenocarcinomas*. Ann Surg Oncol. **17**(7): p. 1767-76.
45. Hasegawa, M., et al., *Patterns of gene promoter methylation in squamous cell cancer of the head and neck*. Oncogene, 2002. **21**(27): p. 4231-6.
46. Tahara, T., et al., *Association between cyclin D1 polymorphism with CpG island promoter methylation status of tumor suppressor genes in gastric cancer*. Dig Dis Sci. **55**(12): p. 3449-57.
47. Gonzalez-Gomez, P., et al., *Frequent death-associated protein-kinase promoter hypermethylation in brain metastases of solid tumors*. Oncol Rep, 2003. **10**(4): p. 1031-3.
48. He, G. and M. Karin, *NF-kappaB and STAT3 - key players in liver inflammation and cancer*. Cell Res. **21**(1): p. 159-68.
49. Ma, W.L., et al., *Androgen receptor is a new potential therapeutic target for the treatment of hepatocellular carcinoma*. Gastroenterology, 2008. **135**(3): p. 947-55, 955 e1-5.
50. Chapekar, M.S., A.C. Huggett, and S.S. Thorgeirsson, *Growth modulatory effects of a liver-derived growth inhibitor, transforming growth factor beta 1, and recombinant tumor necrosis factor alpha, in normal and neoplastic cells*. Exp Cell Res, 1989. **185**(1): p. 247-57.

CHAPTER SIX

Conclusions and Future Directions

The transcription factor NF- κ B is a pivotal regulator of mammalian cell function, modulating genes implicated in cellular stress responses, proliferation, differentiation, cell survival and apoptosis, as well as immune and inflammatory responses [1]. Improper regulation of NF- κ B signaling has been implicated in a myriad of human pathological disorders, including cardiovascular and neurodegenerative diseases, chronic inflammation, and various cancers [2, 3]. A key regulatory node within canonical NF- κ B signaling is the IKK:NF- κ B:I κ B α negative feedback loop that plays a major role in regulating the strength and duration of NF- κ B transcriptional activity [29-32]. In recent years, bioluminescence imaging has proven an invaluable tool to probe the complex dynamics of NF- κ B signaling both *in cellulo* and *in vivo*. Our work utilizing the unique κ B₅→I κ B α -FLuc bioluminescent reporter has focused on understanding how diverse stimuli (i.e., ligand type, duration, concentration, sequential stimulation, etc.) impact the IKK:NF- κ B:I κ B α negative feedback loop *in cellulo* and *in vivo*, providing insights into a key cellular regulatory loop that controls NF- κ B nuclear localization dynamics and transcriptional responses.

6.1 Identification of a Ligand-Induced Transient Refractory Period in Nuclear Factor- κ B Signaling

Adequate resolution of an inflammatory reaction is as equally important as initiation. Persistent or fulminant responses can cause detrimental consequences both locally and systemically [4], and resolution of inflammation is important for both termination of an acute response as well as for prevention of destructive chronic responses. In this regard, recent studies have shown that nuclear factor- κ B (NF- κ B) signaling plays a critical role in both initiation and resolution of inflammation [5, 6]. The transcription factor NF- κ B is a key regulator of innate and adaptive immune responses, as well as a mediator of cell survival and proliferation [7]. Improper regulation of NF- κ B contributes to induction and progression of a wide range of human disorders, including a variety of pathological inflammatory conditions, neurodegenerative diseases, and many types of cancer [3, 8]. Considering the complex nature of the inflammatory milieu, one would expect that stationary tissue-residing cells are exposed to a myriad of temporally-distinct NF- κ B-stimulating cues. Central to any signaling desensitization mechanism is a refractory period during which cells cannot fully respond to a second insult (autologous or heterologous desensitization). Therefore, consideration of the dynamic pattern of stimulus exposure described above begs the immediate question of whether cells can instantly initiate an NF- κ B response to a second activating stimulus, and if not, when will such cells be able to remount a full response again? Specifically, are ligand-preconditioned cells capable of eliciting NF- κ B activation to the same extent as naïve cells?

To study in real time the temporal regulation of NF- κ B and its major regulator, inhibitor of NF- κ B α (I κ B α), we developed, characterized, and utilized a novel transcriptionally-coupled I κ B α -firefly luciferase fusion reporter (κ B $_5$ →I κ B α -FLuc) that recapitulated the activity of the endogenous IKK:NF- κ B:I κ B α negative feedback loop. We then utilized this reporter to characterize the dynamics and responsiveness of I κ B α processing upon a short 30 sec pulse of tumor necrosis factor α (TNF α) or a continuous challenge of TNF α following a 30 sec preconditioning pulse. Strikingly, a 30 sec pulse of TNF α robustly activated inhibitor of NF- κ B kinase (IKK), leading to I κ B α degradation, NF- κ B nuclear translocation, and strong transcriptional up-regulation of I κ B α . Furthermore, we identified a transient refractory period (lasting up to 120 min) following preconditioning, during which the cells were not able to fully degrade I κ B α upon a second TNF α challenge. Kinase assays of IKK activity revealed that regulation of IKK activity correlated in part with this transient refractory period. In contrast, experiments involving sequential exposure to TNF α and interleukin-1 β (IL-1 β) indicated that receptor dynamics could not explain this phenomenon. Utilizing a well-accepted computational model of NF- κ B dynamics, we further identified an additional layer of regulation, downstream of IKK, that may govern the temporal capacity of cells to respond to a second pro-inflammatory insult. Overall, the data suggested that nuclear export of NF- κ B:I κ B α complexes represented another rate-limiting step that may impact this refractory period, thereby providing an additional regulatory mechanism. Since completion of this work [9], the existence of this transient TNF α -induced refractory period has been confirmed by others [10, 11].

Our study highlights the multifaceted regulation of NF- κ B signaling and sheds light on the refractory nature of I κ B α processing as a route to transiently desensitize NF- κ B activity upon subsequent rounds of stimulation. Rapid and transient deactivation of IKK activity as well as temporal reduction in its capacity to respond to a subsequent challenge (IKK responsiveness) seems to play a crucial role in this process. Previous studies indicated that both the amplitude and the timing of IKK activation affect not only the intensity of NF- κ B-dependent transcription, but also the specificity of the transcriptional response [12, 13]. This indicated that besides resolution of the inflammatory response and induction of a refractory period (temporally preventing subsequent rounds of I κ B α degradation upon re-stimulation), rapid down-regulation of IKK activity [14] plays a pivotal role in determining the type of elicited transcriptional program. In the present and previous studies [15], we demonstrated that dynamic bioluminescence imaging of I κ B α -FLuc reporters in live cells provides robust and accurate readouts of ligand-induced I κ B α dynamics. In effect, real time bioluminescence imaging was equivalent to performing continuous on-line Western blots of I κ B α at five minute intervals.

6.2 Synchronicity of the I κ B α :NF- κ B Negative Feedback Loop *In Cellulo* and *In Vivo*

Cells have evolved complex signaling networks that sense cues from the environment and transduce this information to elicit appropriate biological responses [16]. These networks equip cells with sensitive, reversible, regulated, and robust responses to a variety of signaling activators; in particular, these networks can confer on cells the ability to distinguish weak signals from background noise with high precision

and selectivity [17, 18]. The NF- κ B signaling pathway and its downstream transcriptional targets are responsive to a large number of different stimuli [7], and recent work has focused on NF- κ B pathway responsiveness to the *mode* of stimulation (i.e., stimulus concentration, pulse duration, or pulse interval). Particularly relevant during cellular responses are inflammatory cytokines, such as TNF α , which are likely perceived as transient pulses or waves of TNF α occurring over a wide range of concentrations [9, 10, 12, 19-21]. Recent studies have shown that continuous stimulation or sequential pulsing of TNF α can induce oscillations in NF- κ B nuclear translocation that are dependent upon cycles of degradation and re-synthesis of I κ B proteins (i.e., negative feedback loops), and that the frequency of these NF- κ B oscillations encode distinct gene expression profiles [10, 22-25]. Additionally, the amplitude of NF- κ B activity, but not the temporal profile, is particularly sensitive to changes in TNF α concentration and is crucially dependent on the transient nature of IKK activity [14]. Single cell imaging of NF- κ B nuclear localization (as monitored by nuclear:cytoplasmic shuttling of NF- κ B proteins fused to fluorescent protein reporters) and computational modeling have suggested that single cells exhibit stochastic, heterogeneous, and paracrine NF- κ B responses, especially in response to low concentrations of TNF α [20, 21, 26, 27]. A key unresolved issue in the field relates to how biological robustness is achieved within cell populations displaying heterogeneous and dynamic single-cell behavior [26-28], and the physiologic relevancy of these single-cell phenomena to tissue- and organ-level biological responses *in vivo*.

We exploited the unique characteristics of the κ B₅→I κ B α -FLuc negative feedback loop reporter to rigorously characterize dynamic I κ B α responses in single cells, populations of cell, and *in vivo* upon stimulation with a range of TNF α concentrations

and pulses. Remarkably, modulation of either TNF α pulse duration or concentration produced highly complex and reproducible patterns in I κ B α -FLuc dynamics that did not change significantly when measured in single cells versus cell populations. Single cell responses were highly synchronous upon stimulation with TNF α pulses or medium-to-high range TNF α concentrations. Individual cells exhibited synchronized I κ B α -FLuc degradation and re-synthesis kinetics, even though the amplitudes of degradation and re-synthesis varied greatly. Of particular note was the observation in cell populations that pulses of TNF α tended to elicit very broadly shaped I κ B α -FLuc re-synthesis peaks, whereas continuous TNF α stimulation elicited a more defined peak that occurred earlier. These same trends were observed for single cell I κ B α -FLuc dynamic profiles, indicating that broad re-synthesis peaks and complex kinetics are inherent properties of single cells rather than the sum of heterogeneous single cell behaviors. Furthermore, we discovered that these complex I κ B α re-synthesis patterns resulted from the continuous presence of TNF α initiating re-activation of IKK and driving secondary rounds of I κ B α degradation.

After rigorous characterization of the TNF α -induced response patterns of the κ B α →I κ B α -FLuc reporter in single cells and cell populations in culture, we took advantage of the amenability of luciferase reporter imaging *in vivo* to interrogate TNF α -induced activation of the I κ B α :NF- κ B negative feedback loop within mouse livers. Our data indicated that circulating TNF α , administered at varying doses, produced I κ B α dynamic behaviors *in vivo* with synchronized kinetics and very high levels of I κ B α re-synthesis and broad re-synthesis peaks, patterns that were consistent with *in cellulo* experiments in which TNF α pulse duration was varied. Thus, even though TNF α was

administered at varying doses *in vivo*, this data strongly suggested that circulating TNF α is perceived by hepatocytes *in vivo* as a pulse.

Thus, while several *in silico* and *in vitro* studies have demonstrated highly heterogeneous and/or asynchronous NF- κ B responses to TNF α at the single cell level that are largely masked when individual cells are averaged together into populations [10, 20-22, 24, 27], our single cell, cell population, and *in vivo* data indicated that I κ B α degradation and re-synthesis is surprisingly robust and synchronous. These data, coupled with the low frequency at which we observed I κ B α -FLuc oscillatory behavior, place reservations on the physiologic relevance of the highly heterogeneous and oscillatory NF- κ B behaviors observed during *continuous* TNF α stimulation of single cells. On the other hand, our data do support the relevancy of the synchronous NF- κ B oscillatory behaviors that are observed upon sequential TNF α *pulsing* and that drive frequency-encoded transcriptional programs [10, 21].

Thus, our work revealed that the NF- κ B:I κ B α negative feedback loop exhibits differential and reproducible dynamic patterns in response to modulating TNF α concentration or pulse duration, and that responses to TNF α exhibited a remarkable degree of synchronicity at the level of single cells, cell populations, and *in vivo*.

6.3 High-Throughput Phosphatase and Kinase RNA Interference Screens Identify Novel Regulators of TNF α -Induced IKK:I κ B α :NF- κ B Negative Feedback Loop Dynamics

It is currently believed that activation/de-activation of IKK (and other members of the NF- κ B signaling cascade) is regulated by the opposing effects of

kinases/phosphatases [29], and although more is known about the mechanisms by which kinases act during NF- κ B signaling, much less is known about the role of phosphatases in regulating members of the NF- κ B signal cascade. A number of phosphatases have been implicated in negative regulation of IKK activity and in regulation of NF- κ B activity (including PP2C β , PP2A, PP1, PPM1A, PPM1B and WIP1), and they often operate to counteract the activity of a kinase. Study of these phosphatases has revealed differential activity dependent on stimulus and cell specificity, redundant or compensatory pathways, and positive and negative regulatory roles (occasionally based on conflicting evidence; for example, PP2A has been posited by some to be a positive regulator of IKK and others claim it to be a negative regulator) [30-39]. Furthermore, an RNAi phosphatase library was recently utilized to identify unknown phosphatase regulators of NF- κ B transcriptional activity in mouse astrocytes [37]. The authors identified 19 phosphatases that activate or suppress NF- κ B activity 6-8 hours post-TNF α stimulation; their work indicated that the PP2A catalytic subunit interacts with and inactivates IKK β , however, this function was not conserved in the context of human cell lines [36].

Given that our κ B₅→IkB α -FLuc reporter has enabled us to study the IKK-IkB α -NF- κ B negative feedback loop with high temporal resolution [9], and given that temporal control of this and other negative feedback loops has emerged as a critical regulatory component of the intensity and specificity of the NF- κ B transcriptional program [10, 12, 19, 40], we sought to perform ambitious phosphatase and kinase RNAi screens to identify novel regulators of IKK-IkB α -NF- κ B negative feedback loop dynamics, and possibly new pairs of phosphatases/kinases that act in concert [29]. In addition to developing a novel method by which high-throughput robotic RNAi screening strategies can be used to

assay for alterations in the dynamics (both amplitude and kinetics) of the IKK:I κ B α :NF- κ B negative feedback loop, we concurrently developed an analytical method, cumulative log-likelihood analysis, capable of simultaneously analyzing many or all data points along the I κ B α -FLuc profiles and that afforded us the ability to rigorously evaluate and identify hits within these complex datasets.

We observed many different κ B $_5$ →I κ B α -FLuc profiles in the screens, some with vastly different shapes than seen under control siRNA treatment (Fig. 4.4), highlighting the large number and diverse activities of kinases and phosphatases regulating the NF- κ B pathway. Separate analysis of the phosphatase and kinase siRNA screens identified a number of novel regulators whose knock-down either attenuated (phosphatases PTPN3, PTPRJ, and PTPRN; kinases PRKACB and LIMK1) or enhanced (phosphatases CDNK3, PPFIA3, ENPP3, SKIP and PPP1R3D; kinases GALK1, FER, GAK, JAK2, JAK3, and DAPK3) TNF α -induced activation of the IKK-I κ B α -NF- κ B negative feedback loop. Both PTPRJ and DAPK3 have been validated and are the subjects of current investigations to understand the physiological and/or pathophysiological relevance in NF- κ B, especially in the context of TNF α signaling during cancer and inflammation in the liver.

Additionally, we are continuing to validate other hits from the screens. Of particular interest for further study are the kinases PRKACB and LIMK1; knock-down of either resulted in decreased levels of I κ B α -FLuc degradation, a rarely observed phenotype in either the phosphatase or kinase screens. These proteins may play a role in positively regulating IKK activity, and thus directly impact the degree of I κ B α degradation upon ligand stimulation. Furthermore, it will be interesting to merge the data

from the phosphatase and kinase screens into a single dataset in an effort to identify potentially novel pairs of phosphatases/kinases that similarly regulate the dynamics of the IKK-I κ B α -NF- κ B negative feedback loop.

In conclusion, our studies using dynamic, real-time bioluminescence imaging have demonstrated the utility of employing bioluminescent reporters alongside traditional biochemical assays, *in silico* modeling, and cell/molecular biology techniques to rigorously interrogate how diverse stimuli (i.e., ligand type, duration, concentration, sequential stimulation, etc.) impact the IKK:NF- κ B:I κ B α negative feedback loop in single cells, cell populations, and at the organ- and tissue-level *in vivo*.

6.4 REFERENCES

1. Li, Q. and I.M. Verma, *NF-kappaB regulation in the immune system*. Nat Rev Immunol, 2002. **2**(10): p. 725-34.
2. Karin, M., et al., *NF-kappaB in cancer: from innocent bystander to major culprit*. Nat Rev Cancer, 2002. **2**: p. 301-310.
3. Karin, M., *Nuclear factor-kappaB in cancer development and progression*. Nature, 2006. **441**(7092): p. 431-6.
4. Han, J. and R.J. Ulevitch, *Limiting inflammatory responses during activation of innate immunity*. Nat Immunol, 2005. **6**(12): p. 1198-205.
5. Winsauer, G. and R. de Martin, *Resolution of inflammation: intracellular feedback loops in the endothelium*. Thromb Haemost, 2007. **97**(3): p. 364-9.
6. Hoffmann, A. and D. Baltimore, *Circuitry of nuclear factor kappaB signaling*. Immunol Rev, 2006. **210**: p. 171-86.
7. Perkins, N.D., *Integrating cell-signalling pathways with NF-kappaB and IKK function*. Nat Rev Mol Cell Biol, 2007. **8**(1): p. 49-62.
8. Karin, M. and F.R. Greten, *NF-kappaB: linking inflammation and immunity to cancer development and progression*. Nat Rev Immunol, 2005. **5**(10): p. 749-59.
9. Moss, B.L., et al., *Identification of a ligand-induced transient refractory period in nuclear factor-kappaB signaling*. J Biol Chem, 2008. **283**(13): p. 8687-8698.
10. Ashall, L., et al., *Pulsatile stimulation determines timing and specificity of NF-kappaB-dependent transcription*. Science, 2009. **324**(5924): p. 242-6.
11. Shih, V.F., et al., *Kinetic control of negative feedback regulators of NF-kappaB/RelA determines their pathogen- and cytokine-receptor signaling specificity*. Proc Natl Acad Sci U S A, 2009. **106**(24): p. 9619-24.
12. Werner, S.L., D. Barken, and A. Hoffmann, *Stimulus specificity of gene expression programs determined by temporal control of IKK activity*. Science, 2005. **309**(5742): p. 1857-61.
13. Covert, M.W., et al., *Achieving stability of lipopolysaccharide-induced NF-kappaB activation*. Science, 2005. **309**(5742): p. 1854-7.
14. Cheong, R., et al., *Transient IkappaB kinase activity mediates temporal NF-kappaB dynamics in response to a wide range of tumor necrosis factor-alpha doses*. J Biol Chem, 2006. **281**(5): p. 2945-50.
15. Gross, S. and D. Piwnica-Worms, *Real-time imaging of ligand-induced IKK activation in intact cells and in living mice*. Nat Methods, 2005. **2**: p. 607-614.
16. Kholodenko, B.N., *Cell-signalling dynamics in time and space*. Nat Rev Mol Cell Biol, 2006. **7**(3): p. 165-76.
17. Brandman, O. and T. Meyer, *Feedback loops shape cellular signals in space and time*. Science, 2008. **322**(5900): p. 390-5.
18. Cebecauer, M., et al., *Signalling complexes and clusters: functional advantages and methodological hurdles*. J Cell Sci, 2010. **123**(Pt 3): p. 309-20.
19. Werner, S.L., et al., *Encoding NF-kappaB temporal control in response to TNF: distinct roles for the negative regulators IkappaBalpha and A20*. Genes Dev, 2008. **22**(15): p. 2093-101.
20. Turner, D.A., et al., *Physiological levels of TNFalpha stimulation induce stochastic dynamics of NF-kappaB responses in single living cells*. J Cell Sci, 2010. **123**(Pt 16): p. 2834-43.
21. Tay, S., et al., *Single-cell NF-kappaB dynamics reveal digital activation and analogue information processing*. Nature, 2010. **466**(7303): p. 267-71.
22. Nelson, D.E., et al., *Oscillations in NF-kappaB signaling control the dynamics of gene expression*. Science, 2004. **306**(5696): p. 704-8.

23. Kearns, J.D., et al., *IkappaBepsilon provides negative feedback to control NF-kappaB oscillations, signaling dynamics, and inflammatory gene expression*. J Cell Biol, 2006. **173**(5): p. 659-64.
24. Sung, M.H., et al., *Sustained oscillations of NF-kappaB produce distinct genome scanning and gene expression profiles*. PLoS One, 2009. **4**(9): p. e7163.
25. Tian, B., D.E. Nowak, and A.R. Brasier, *A TNF-induced gene expression program under oscillatory NF-kappaB control*. BMC Genomics, 2005. **6**: p. 137.
26. Lee, T.K., et al., *A noisy paracrine signal determines the cellular NF-kappaB response to lipopolysaccharide*. Sci Signal, 2009. **2**(93): p. ra65.
27. Paszek, P., et al., *Population robustness arising from cellular heterogeneity*. Proc Natl Acad Sci U S A, 2010. **107**(25): p. 11644-9.
28. Spiller, D.G., et al., *Measurement of single-cell dynamics*. Nature, 2010. **465**(7299): p. 736-45.
29. Hacker, H. and M. Karin, *Regulation and function of IKK and IKK-related kinases*. Sci STKE, 2006. **2006**(357): p. re13.
30. Barisic, S., et al., *Identification of PP2A as a crucial regulator of the NF-kappaB feedback loop: its inhibition by UVB turns NF-kappaB into a pro-apoptotic factor*. Cell Death Differ, 2008. **15**(11): p. 1681-90.
31. Prajapati, S., et al., *Protein phosphatase 2Cbeta association with the IkappaB kinase complex is involved in regulating NF-kappaB activity*. J Biol Chem, 2004. **279**(3): p. 1739-46.
32. DiDonato, J.A., et al., *A cytokine-responsive IkappaB kinase that activates the transcription factor NF-kappaB*. Nature, 1997. **388**(6642): p. 548-54.
33. Kray, A.E., et al., *Positive regulation of IkappaB kinase signaling by protein serine/threonine phosphatase 2A*. J Biol Chem, 2005. **280**(43): p. 35974-82.
34. Witt, J., et al., *Mechanism of PP2A-mediated IKK beta dephosphorylation: a systems biological approach*. BMC Syst Biol, 2009. **3**: p. 71.
35. Chew, J., et al., *WIP1 phosphatase is a negative regulator of NF-kappaB signalling*. Nat Cell Biol, 2009. **11**(5): p. 659-66.
36. Li, H.Y., et al., *Deactivation of the kinase IKK by CUEDC2 through recruitment of the phosphatase PPI*. Nat Immunol, 2008. **9**(5): p. 533-41.
37. Li, S., et al., *RNAi screen in mouse astrocytes identifies phosphatases that regulate NF-kappaB signaling*. Mol Cell, 2006. **24**(4): p. 497-509.
38. Sun, W., et al., *Protein phosphatase 2A acts as a mitogen-activated protein kinase kinase kinase 3 (MEKK3) phosphatase to inhibit lysophosphatidic acid-induced IkappaB kinase beta /nuclear factor-kappaB activation*. J Biol Chem.
39. Sun, W., et al., *PPM1A and PPM1B act as IKKbeta phosphatases to terminate TNFalpha-induced IKKbeta-NF-kappaB activation*. Cell Signal, 2009. **21**(1): p. 95-102.
40. Barken, D., et al., *Comment on "Oscillations in NF-kappaB signaling control the dynamics of gene expression"*. Science, 2005. **308**(5718): p. 52.